THE MEASUREMENT AND ANALYSIS OF ACCELERATIONS IN ROCK SLOPES

A thesis submitted to the University of London
(Imperial College of Science and Technology)
for the degree of Doctor of Philosophy
in the Faculty of Engineering.

by

Peter Alan Cundall, B.Sc.(Eng.), A.C.G.I.

February 1971

ABSTRACT

Most of this Thesis deals with an investigation into the response of an open-pit mine in an elastic homogeneous solid, due to excitation by blasting. The following ways of dealing with the problem were used: existing solutions to similar problems were examined and relevant conclusions drawn; a three-dimensional model study was conducted using a transparent silicone rubber; computer simulations using Dynamic Relaxation were carried out on two- and three-dimensional systems. In addition, full-scale tests were carried out on a large open-pit using a specially-developed borehole accelerometer device to monitor motion due to blasting. The general conclusion was that the geometrical shape of the pit plays very little part in the levels and frequencies of motion, compared to the effects due to other factors.

A number of other topics were investigated: the static stress distribution of a number of structures was determined; progressively failing joints were introduced into the static Dynamic Relaxation analysis; a new computer programme was developed to simulate the large-scale progressive failure of a number of discrete rectangular blocks, incorporating realistic friction laws.

ACKNOWLEDGMENTS

The author would like to acknowledge his gratitude to all those people and organisations who made this work possible. In particular, thanks are due to:

All members of the Rock Mechanics Project at Imperial College for the stimulation provided by constant discussions, and especially to Professor E. Hoek, the author's supervisor, for encouraging a unique atmosphere of free debate and co-operation;

The Rio Tinto Zinc Corporation Ltd., for their generous support, together with Anglo American International (U.K.) Ltd., Bougainville Copper Pty., Ltd., Consolidated Gold Fields Ltd., English China Clays Ltd., Iranian Selection Trust Ltd., National Coal Board Opencast Executive, Palabora Mining Co., Ltd., Rio Tinto Espanola, S.A., Roan Selection Trust, Ltd., and seven member companies of the Australian Mineral Industries Research Association, Ltd.;

Dr. J.W. Bray for many enlightening discussions;

Dr. A.C. Cassell and Dr. R.E. Hobbs of the Civil Engineering Department at Imperial College for their help with Dynamic Relaxation;

Mr. David Hinds and Mr. R.C. Sidey for their enthusiastic help both in the field and laboratory;

Mr. L.D. Wilson who managed to come up with an answer to the knottiest problem;

Mr. J. Sullivan and his team for unmatched workshop facilities;

Mr. Barry Holt for his swift and efficient help with the production of the thesis;

Finally the writer's wife and daughter for their patience and understanding during the final traumatic months.

GENERAL INDEX

/continued....

Chapter 1

Chapter 1: INTRODUCTION

Blasting

Earthquakes

A. LIMITATIONS OF CONVENTIONAL STABILITY CALCULATIONS

Earthquake Response of Dams

B. RELEVANCE OF ELASTIC ANALYSIS

C. METHODS OF SOLUTION

Analytical Studies

Full-Scale Field Tests

Model Studies

Computer Simulation

Failure Considerations

In the design of open-pit mines from a stability point of view, it is recognised that the occurrence of dynamic ground motion must decrease the stability of the slopes to some extent.

Blasting

In the case of blasting due to normal mining operations, it is only very rarely that large-scale rock failure has been observed to occur immediately following a blast, such reports as there are being mainly by word of mouth. It might be argued that even in those cases, the factor of safety was so low as to render even static failure imminent, and that blasting only brought forward the time of failure by a few days. Even if no immediate effects are noticed after a blast, it may be that significant reductions in the strength of rock joints are caused by slight ground movements, and that in the long-term, the stability of the rock slopes will gradually be reduced. It is only by knowing the magnitudes and ditribution of movements around a pit that an assessment of the cumulative effects of regular blasting can be made. A knowledge of the overall movements induced by blasting is also necessary in order to assess whether heavier blasting can be safely undertaken at a particular mine.

Earthquakes

As the Earth's resources get scarcer, it will become necessary to locate mines in increasingly more inhospitable places, for instance in strong earthquake regions. To give some idea of the magnitude of the problem, consider a horizontal acceleration of 0.1 g (which is not at all uncommon in strong earthquakes) acting upon a slope of 45 degrees. This additional acceleration can be regarded as instantaneously causing gravity to act at an angle to the vertical; in this case, the change in the apparent direction of gravity is 6 degrees. In other words, in order to maintain the factor of safety of the slope under the additional acceleration, it must be mined at a 6 degree flatter angle, i.e. at 39 degrees. This calculation has obvious gross simplifications but it shows that the effect of even a moderate earthquake can be significant in terms of slope angle, and hence in its economics. In fact in contrast to blasting effects, there are numerous records of earthquakes causing landslides, earth slumps and rock falls (see Richter, ref 1).

A. LIMITATIONS OF CONVENTIONAL STABILITY CALCULATIONS

In order to make some allowance for the extra forces imposed by earthquakes or large blasts conventional slope design has regarded an earthquake as equivalent to a static acceleration acting in a given direction on a slope, the magnitude of the assumed acceleration be set to the peak reached by the previous largest recorded earthquake in the area. Several deficiencies of this approach are evident:

(i) Any geometry deviating from that of a flat half-space will have a non-uniform spacial distribution of motion when excited by a dynamic source. This effect could be important, for instance, if an area of high acceleration were concentrated largely within a potential sliding mass.

(ii) Another important factor is the characteristic of certain geometries to amplify the applied motion at particular frequencies. It seems intuitively obvious that a "positive" structure such as a dam can have modes of resonance, but not so obvious that "negative structure" (such as pits, underground cavities etc) possess this characteristic. However, such is in fact the case, as will be shown in the chapters following.

(iii) A further limitation to the "static approach" is that under dynamic conditions, the stresses and accelerations at any point vary with time. This fact of oscillating accelerations may in fact lead to more stable slopes, since the inertia of any failing block may prevent it from moving in response to the many reversals of force. However, this observation ignores any non-linearity of the shear-stress vs. displacement curve and also the reduction of dynamic friction over static. Both these effects can tend to lower the apparent static friction under dynamic conditions.

(iv) Variations in bulk material properties are further complicating factors under dynamic motion. It is well known that the particle motions of waves from a stiff, dense material can be amplified on passing to a soft, light material. This fact has a particular bearing on the location used to monitor earthquakes, the records of which are subsequently used in a failure analysis.

Having established that it is unrealistic to regard an earthquake, for design purposes, as an equivalent static acceleration it might be argued that the errors arising from such an assumption are negligible. However at the present time it as not possible to know what these errors are; it was with the hope of remedying this situation that the present research was undertaken.

Earthquake Response of Dams

A large volume of work has been carried out to find the dynamic response of earth- and rock-fill dams to earthquakes. As far as is known, all work to date has been concerned with determining the elastic dynamic response, which in most cases takes the form of finding the frequency and shape of

each mode of vibration that might be excited by an earthquake. The work has been carried out by three main methods: models, analytical solutions and finite element computer simulations (refs 2,3,4). These methods will be discussed more fully in Chapter 2. Any failure analysis performed subsequently to the elastic analysis regards the peak dynamic accelerations as static for the purposes of, say, a limit equilibrium calculation. This may seem a retrograde step, but in fact the resonance magnification has been taken into account, as well as the distribution of acceleration within the dam, representing a significant increase in accuracy over using solely the ground acceleration. In the present work it is hoped to carry out a similar analysis for open-pit mines, but to take it one step further - to incorporate a failure mechanism in the dynamic analysis.

B. RELEVANCE OF ELASTIC ANALYSES

An important point to be examined at this stage is the relevance of an elastic analysis to the solution of a stability problem. It is true that several factors combine to make a *static* elastic analysis an exercise of dubious validity:

(i) Unknown pre-stressing due to previous tectonic movements.

(ii) Non-linear properties of the material comprising the structure.

(iii) Irreversible and hysteretic effects in the material, causing the final stress in a structure to be largely dependent on the sequence of loading.

(iv) Creep effects, causing the stresses to change slowly with time.

(v) Partial slippage along planes of weakness, resulting in a state of stress different from that before slip.

Bearing in mind these difficulties, it is surprising that in some case an elastic analysis can give accurate results in a static case (ref 5). The success is probably due to a set of unusually favourable circumstances. In fact there are several reasons why these circumstances do not apply in the case of an open-pit excavation; these factors are considered more fully in Chapter 6.

However, in the dynamic case, an elastic solution can be a good approximation to reality when *small* motions are considered. No matter what pre-stressing exists, or how non-linear the stressing curve may be, or that slow, irreversible effects are taking place, the dynamic motion will

be superimposed upon all these. Providing that the motion is small enough, any curve can be approximated by a straight line, so that a linear elastic analysis must give a good solution to any small-signal dynamic problem. Of course, when large motions are considered, the approximation breaks down, but at least the solution is asymptotic to the linear case at one extreme.

The practical outcome of the above considerations is that it is meaningful to pursue the dynamic linear elastic analysis of an open-pit in the hope that it will give an accurate estimate of the response to fairly small motions, before failure or other irreversible processes take place. Even if the analysis breaks down at the time of failure, it should yield a good estimate of the conditions *causing* failure; this assumption has shown to be false in the case of some static elastic analyses (ref 6).

C. METHODS OF SOLUTION

Analytical Studies

A good argument in favour of an analytical approach is that it gives insight into the mechanisms of the problem, as well as predicting the outcome of a change in the parameters relating to the problem. This cannot be said of an experimental approach, where observations can be recorded without an understanding of the mechanisms, and extrapolation of results may or may not be meaningful. However in the present research an analytic method was considered too difficult and was not undertaken. The difficulties were believed to lie mostly in the following: asymmetric excitation; presence of free surface; the fact that the system is non-conservative (i.e. continuously radiates energy which is then lost to the system).

There are however several physical problems, similar in some respects to an open-pit, for which exact solutions have been obtained. These include: bubble oscillation, borehole and tunnel waves, cavity resonances and Moon crater effects. Due note has been taken of these solutions in Chapter 2, and conclusions drawn which may have some relevance to the present problem.

Full Scale Field Tests

This method has been approached with some caution since it is all too easy to take hundreds of arbitrary measurements in the field, many of which may have dubious relevance to the problem in hand. There is also the difficulty of excitation,

since an open-pit vibrating represents a considerable quantity of stored energy, due to the large volume of material in motion. An associated difficulty is that of measuring the vibration, the amplitude of which is likely to be rather small. Chapter 4 gives an account of tests performed on the large Atalya pit in Southern Spain, using the daily blasting as excitation.

Model Studies

Physical models offer potentially more information than field tests since, ideally, the experimental conditions are under the control of the experimenter, or at least known to him if not controllable. Models also offer the facility for many detailed measurements in the comfort of the laboratory, with the magnitudes of motion and excitation amenable to measurement and production respectively.

Foremost amongst the drawbacks is the fact that it may be difficult to reproduce every physical property of the prototype in the model. In the case of open-pit vibrations it is also difficult to simulate the existance of an infinite half-space, since the model must have boundaries. The simulation of earthquake excitation also creates difficulties due to the near-impossibility of organising the boundary displacements to be in the form of a travelling-wave. Also awkward is the need to measure values of vibration *within* the material itself, in order to define the areas of acceleration for stability purposes.

An important requirement for the model is that it will give an immediate visual picture of the nature of the vibration of an open-pit. This need is occasioned by the practical nature of the mining industry; far more notice is likely to be taken of results if they can actually be demonstrated in a physical model, rather than if they exist merely in a set of equations, or in a computer.

Chapter 3 gives an account of a large transparent rubber model which was constructed to satisfy at least some of the requirements noted above.

Computer Simulations

No Thesis seems complete nowadays without some computer programs, and this one is no exception. Whilst computers can be extremely valuable in solving complex problems, there are notorious pitfalls, such as placing too much reliance on the output, when the input is of dubious value. Also, with computer programs it is easy to make a programming error which goes un-noticed; it is essential to check all programs initially against known solutions, before attempting to solve a new problem.

In Chapter 5 a description is given of the

attempt to solve numerically the three-dimensional elastic dynamic equations of a half-space with an open-pit embedded in the surface. As in the case of the model it is difficult to arrange that the boundaries imposed upon the calculations do not influence the response of the open-pit. However the advantages lie in the extreme facility with which the pit geometry and elastic properties can be changed, as well as the ease with which solutions can be automatically plotted in many different ways. In fact the abundance of data generated by the computer can present real problems in deciding how best to make available the information for use by engineers.

The computing techniques used in the present research were of an elementary nature; there is a strong tendency to become more involved in the mechanics of computing than in the original problem to be solved. In view of this, simpler, perhaps longer, procedures were used in preference to more sophisticated methods.

In the case of open-pit dynamics, the use of computers may be carried a stage further than elastic calculations, to simulate failure by incorporating laws describing irreversible effects. The particular method of numerical analysis used (Dynamic Relaxation) was chosen with this possibility in mind.

Failure Considerations

The bulk of the present research has been concerned with establishing the linear elastic response of an open-pit. But, as was pointed out earlier, there is reason to believe that dynamic elastic solutions will come closer to reality than static elastic solutions. In Chapter 6, several simple cases of slope failure are considered and the elastic results of the previous chapters used to estimate the magnitude of any change in stability, what parts of the pit are most likely to be affected and whether the shape of open-pits could usefully be changed in view of the dynamic loadings involved. Also considered are the results of incorporating failure laws into the existing numerical calculations.

REFERENCES

Chapter 1

1. RICHTER, C.F. "Elementary Seismology" W.H. Freeman & Co., Ltd., San Francisco, 1958.
2. OKAMOTO, S., TAMURA, C., KATO, K., OTAWA, M. "Dynamic Behaviour of Earth Dam During Earthquakes" Report of the Institute of Industrial Science, University of Tokyo. 1966.
3. AMBRASEYS, N.N., SARMA, S.K. "The Response of Earth Dams to Strong Earthquakes" Geotechnique V17 No 3, 1967.
4. CLOUGH, R.W., CHOPRA, A.K. "Earthquake Stress Analysis in Earth Dams" Soil Mech. & Bit. Mat. Res Lab., University of California. November 1965.
5. WILSON, J.W., MORE-O'FERRALL, R.C. "Application of the Electrical Resistance Analogue to Mining Operations" Transactions, Section A, V79, Jan 1970, Institution of Mining & Metallurgy.
6. St.JOHN, C.M. PhD. Thesis (to be published) London University (Imperial College) 1971.

* * * * * *

Chapter 2

Chapter 2: GENERAL ELASTIC CONSIDERATIONS

A. SUMMARY OF DYNAMIC ELASTIC EQUATIONS

B. PROPAGATION OF WAVES

- Body Waves
- Effect of Poisson's Ratio on Body Waves
- Other Types of Wave - The Rayleigh Wave
- Effect of Poisson's Ratio on Rayleigh Waves

C. DAMPING

- Radiation Damping
- Internal Damping

D. A STUDY OF PROBLEMS SIMILAR TO THAT OF A OPEN-PIT VIBRATING

- Conservative/Non-Conservative Systems
- Characteristic Response of Conservative Systems
- Non-Conservative Systems
- Oscillations of the Surface of a Half-Space
- Lunar Crater Effect
- Spherical Cavity: *radial oscillations*
- Bar Propagation: *reflection effects*
- Bar Propagation: *dispersion effects*
- Tunnel Waves: *resonance?*
- Tunnel Oscillations: *field observations*
- Tunnel Oscillations: *asymmetric oscillations*

E. CONCLUSIONS TO BE DRAWN

- Open-Pit Vabration
- Implications for Rubber Model
- Boundaries
- Analytical Solutions
- Some Remarks Concerning Procedures for Obtaining Dynamic Constants

---

Whatever the method used to obtain the full elastic dynamic response of an open-pit, it is in essence a specific solution of the three-dimensional stress-strain and equilibrium equations subject to given boundary conditions. For convenience, these are reproduced below; they can be found in most textbooks on elastic theory (e.g. Love, ref 1).

A. SUMMARY OF DYNAMIC ELASTIC EQUATIONS

The stress-strain equations for a homogeneous, isotropic linear elastic medium are as follows:

Cartesian co-ordinates.

$$\sigma_{xx} = \lambda\left(\frac{\partial u}{\partial x}+\frac{\partial v}{\partial y}+\frac{\partial \omega}{\partial z}\right)+2\mu\frac{\partial u}{\partial x} \quad (1)$$

$$\sigma_{yy} = \lambda\left(\frac{\partial u}{\partial x}+\frac{\partial v}{\partial y}+\frac{\partial \omega}{\partial z}\right)+2\mu\frac{\partial v}{\partial y} \quad (2)$$

$$\sigma_{zz} = \lambda\left(\frac{\partial u}{\partial x}+\frac{\partial v}{\partial y}+\frac{\partial \omega}{\partial z}\right)+2\mu\frac{\partial \omega}{\partial z} \quad (3)$$

$$\sigma_{xy} = \mu\left[\frac{\partial v}{\partial x}+\frac{\partial u}{\partial y}\right] \quad (4)$$

$$\sigma_{yz} = \mu\left[\frac{\partial \omega}{\partial y}+\frac{\partial v}{\partial z}\right] \quad (5)$$

$$\sigma_{zx} = \mu\left[\frac{\partial u}{\partial z}+\frac{\partial \omega}{\partial x}\right] \quad (6)$$

Cylindrical Polar co-ordinates.

$$\sigma_{rr} = (\lambda+2\mu)\frac{\partial u_r}{\partial r}+\lambda\left(\frac{u_r}{r}+\frac{1}{r}\frac{\partial u_\theta}{\partial \theta}+\frac{\partial u_z}{\partial z}\right) \quad (7)$$

$$\sigma_{\theta\theta} = (\lambda+2\mu)\left(\frac{u_r}{r}+\frac{1}{r}\frac{\partial u_\theta}{\partial \theta}\right)+\lambda\left(\frac{\partial u_r}{\partial r}+\frac{\partial u_z}{\partial z}\right) \quad (8)$$

$$\sigma_{zz} = (\lambda+2\mu)\frac{\partial u_z}{\partial z}+\lambda\left(\frac{\partial u_r}{\partial r}+\frac{u_r}{r}+\frac{1}{r}\frac{\partial u_\theta}{\partial \theta}\right) \quad (9)$$

$$\sigma_{r\theta} = \mu\left[\frac{1}{r}\frac{\partial u_r}{\partial \theta}-\frac{u_\theta}{r}+\frac{\partial u_\theta}{\partial r}\right] \quad (10)$$

$$\sigma_{\theta z} = \mu\left[\frac{\partial u_\theta}{\partial z}+\frac{1}{r}\frac{\partial u_z}{\partial \theta}\right] \quad (11)$$

$$\sigma_{zr} = \mu\left[\frac{\partial u_r}{\partial z}+\frac{\partial u_z}{\partial r}\right] \quad (12)$$

The symbols have the meanings given in Appendix I

The dynamic equilibrium equations are as follows:

Cartesian.

$$\rho\frac{\partial^2 u}{\partial t^2}+k\frac{\partial u}{\partial t} = \frac{\partial \sigma_{xx}}{\partial x}+\frac{\partial \sigma_{xy}}{\partial y}+\frac{\partial \sigma_{zx}}{\partial z} \quad (13)$$

$$\rho\frac{\partial^2 v}{\partial t^2}+k\frac{\partial v}{\partial t} = \frac{\partial \sigma_{xy}}{\partial x}+\frac{\partial \sigma_{yy}}{\partial y}+\frac{\partial \sigma_{yz}}{\partial z} \quad (14)$$

$$\rho\frac{\partial^2 \omega}{\partial t^2}+k\frac{\partial \omega}{\partial t} = \frac{\partial \sigma_{zx}}{\partial x}+\frac{\partial \sigma_{yz}}{\partial y}+\frac{\partial \sigma_{zz}}{\partial z} \quad (15)$$

Cylindrical polar.

$$\rho\frac{\partial^2 u_r}{\partial t^2}+k\frac{\partial u_r}{\partial t} = \frac{\partial \sigma_{rr}}{\partial r}+\frac{1}{r}\frac{\partial \sigma_{r\theta}}{\partial \theta}+\frac{\sigma_{rr}-\sigma_{\theta\theta}}{r} \quad (16)$$

$$\rho\frac{\partial^2 u_\theta}{\partial t^2}+k\frac{\partial u_\theta}{\partial t} = \frac{\partial \sigma_{r\theta}}{\partial r}+\frac{1}{r}\frac{\partial \sigma_{\theta\theta}}{\partial \theta}+\frac{\partial \sigma_{\theta z}}{\partial z}+\frac{2\sigma_{r\theta}}{r} \quad (17)$$

$$\rho\frac{\partial^2 u_z}{\partial t^2}+k\frac{\partial u_z}{\partial t} = \frac{\partial \sigma_{rz}}{\partial r}+\frac{1}{r}\frac{\partial \sigma_{\theta z}}{\partial \theta}+\frac{\partial \sigma_{zz}}{\partial z}+\frac{\sigma_{rz}}{r} \quad (18)$$

It will be noted that the left-hand sides of the above equations are of the form:

$$\rho\frac{\partial^2 u}{\partial t^2} + k\frac{\partial u}{\partial t} =$$

inertial term. *viscous damping term.*

The second, viscous damping term is rarely included in analytical solutions, but is sometimes useful to describe the "lossy" nature of a solid, in which the energy of waves is attenuated by some dissipation mechanism. It is true that such mechanisms are probably not of a viscous nature, but provided that the magnitude of the loss is small, a viscous dashpot can be a reasonable approximation. A fuller discussion of damping mechanisms is given in Section C of this Chapter.

The above equations have been written down in the "separated" form; that is to say, the elastic equations have been given separately from the equilibrium equations. Each set of equations contains both stress and displacement terms. It is possible to combine the two sets to produce one set which is a function of, say, only displacement. The resultant equations are as follows:

$$\rho\frac{\partial^2 u}{\partial t^2} = (\lambda+\mu)\frac{\partial \Delta}{\partial x} + \mu\nabla^2 u \quad (19)$$

$$\rho\frac{\partial^2 v}{\partial t^2} = (\lambda+\mu)\frac{\partial \Delta}{\partial y} + \mu\nabla^2 v \quad (20)$$

$$\rho\frac{\partial^2 \omega}{\partial t^2} = (\lambda+\mu)\frac{\partial \Delta}{\partial z} + \mu\nabla^2 \omega \quad (21)$$

(Cartesian co-ordinates)

Where Δ, *the dilation* = $\frac{\partial u}{\partial x}+\frac{\partial v}{\partial y}+\frac{\partial \omega}{\partial z}$

and ∇^2 *is the differential operation:*

$$\left(\frac{\partial^2}{\partial x^2}+\frac{\partial^2}{\partial y^2}+\frac{\partial^2}{\partial z^2}\right)$$

Of course a similar operation could be performed in the case of stress, in this case eliminating displacement.

The preceding equations have been written in terms of Lame's constants. In order to write them in terms of other elastic constants, the following relations are useful.

$$E = \frac{\mu(3\lambda+2\mu)}{\lambda+\mu} \quad (22) \qquad \mu = \frac{E}{2(1+\nu)} \quad (25) \qquad \mu = \frac{\lambda(1-2\nu)}{2\nu} \quad (28)$$

$$\nu = \frac{\lambda}{2(\lambda+\mu)} \quad (23) \qquad \lambda = \frac{E\nu}{(1+\nu)(1-2\nu)} \quad (26) \qquad \mu = \frac{3k(1-2\nu)}{2(1+\nu)} \quad (29)$$

$$k = \lambda + \frac{2\mu}{3} \quad (24) \qquad \lambda = \frac{2\mu\nu}{1-2\nu} \quad (27) \qquad \lambda = \frac{3k\nu}{1+\nu} \quad (30)$$

E = *Young's Modulus,* ν = *Poisson's ratio*
k = *Bulk Modulus,* μ,λ = *Lame's constants*

B. PROPAGATION OF WAVES

Body Waves

In an unbounded, homogeneous, isotropic solid, integration of the above equations (Love, ref. 1, Kolsky, ref. 2) shows that only two types of wave (body waves) may be propagated through the interior of a solid - longitudinal waves and transverse waves. Longitudinal waves, which have variously been called compressional, dilatation, P, irrotational or pressure waves, are characterised by having their particle motion parallel to the direction of propagation of the wave. The progression of the wave-train involves alternate compression and dilation of the material as the wave passes.

Transverse waves, which have variously been called shear, S, equivoluminal, or distortion waves, propagate by means of a shearing action in which the particle motion is perpendicular to the direction of propagation. No change of volume is involved as a wave-train passes through a material (hence the name equivoluminal).

Both types of wave propagate at characteristic speeds, which are independent of the frequency of the wave-trains (i.e. no dispersion). The transverse wave speed is always less than the longitudinal wave speed, and in rock-like materials (Poisson's ratios from 0.2 to 0.3) the ratio of their speeds is around $\frac{3}{4}$. This difference in speeds is made use of in analysing earthquake records, since the waves from a distant earthquake arrive in two distinct groups - first the Primary (P) group, consisting of compressional-type waves, and then the Secondary (S) group, made up of transverse-type waves. The difference in arrival times of the two groups can be made use of to estimate the distance from the hypocentre of the earthquake.

The velocities of the two body waves are given by:

$$V_L = \sqrt{\frac{\lambda + 2\mu}{\rho}} \qquad (31)$$

Longitudinal

$$V_T = \sqrt{\frac{\mu}{\rho}} \qquad (32)$$

Transverse

Effects of Poisson's Ratio on Body Waves

It is interesting to consider the effects of Poisson's ratio on the two velocities, particularly from the point of view of rubber models, in which the Poisson's ratio approaches 0.5.

Rewriting equations (31) and (32) using the relations (25), (26)

$$V_L = \sqrt{\frac{E(1-\nu)}{(1+\nu)(1-2\nu)\rho}} \qquad V_T = \sqrt{\frac{E}{2(1+\nu)\rho}}$$

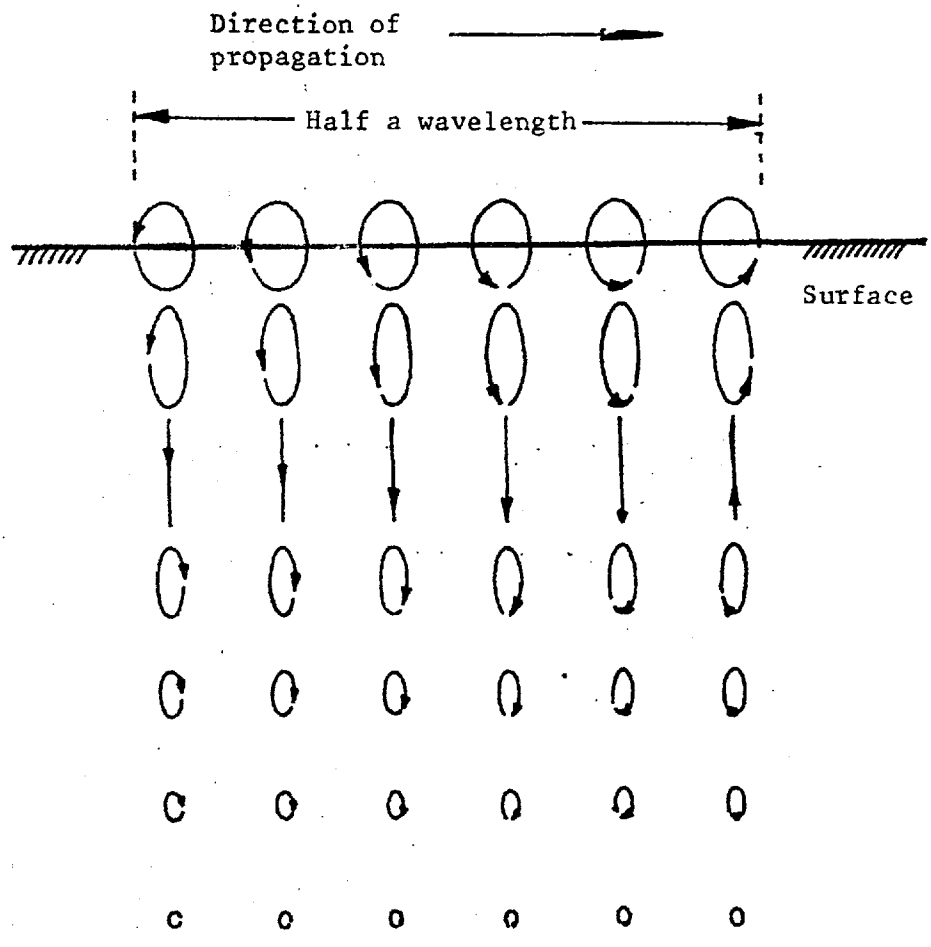

FIG. 3 PARTICLE MOTION IN
A RAYLEIGH WAVE
(Greatly exaggerated)

It can be seen that as Poisson's ratio nears 0·5, the longitudinal speed approaches infinity, which is clearly absurd. The fallacy lies in the fact that Young's modulus, E, itself approaches zero* as ν approaches 0·5, in which case the velocity V_L is undefined. It is more meaningful to express the velocities in terms of the bulk modulus, k, which remains finite even for materials with a Poisson's ratio equal to 0·5 (e.g. water):

$$V_L = \sqrt{\frac{3k(1-\nu)}{\rho(1+\nu)}} \qquad V_T = \sqrt{\frac{3k(1-2\nu)}{2\rho(1+\nu)}}$$

As Poisson's ratio approaches 0·5 the longitudinal velocity drops slightly, but the transverse (shear) velocity approaches zero. This means that in a rubber-like material the shear-wave speed will be considerably less than the dilatation-wave speed, typically, $V_T = \frac{V_L}{20}$

Other Types of Wave: *The Rayleigh Wave*

The two types of wave that have been discussed are the only ones that can be propagated through the interior of a solid, so long as the solid is unbounded, isotropic, homogeneous and linearly elastic. If any one of these conditions is not satisfied, other types of wave may exist. For instance if a material is layered, each layer having different elastic properties, Love waves can be propagated within a layer. More important to the present work are surface waves, which propagate along the free surface of a solid, their amplitude decreasing rapidly with depth. One such is the Rayleigh wave. The theoretical derivation of this wave is performed in many text-books (e.g. Love or Kolsky). Its main characteristic is that its components of displacement and stress decrease exponentially with depth, so that it is confined to a very small distance beneath the surface of a solid. In view of this, it might be expected that the Rayleigh wave would play a large part in dynamic phenomena occuring at or near the surface of the earth. This is confirmed by a theoretical analysis by Miller & Pursey (ref. 3) who show that 67·4% of the energy radiated by a vertically vibrating plate on the surface is in the form of Rayleigh waves, whilst shear and dilatation waves represent 25·8% and 6·9% respectively.

The Rayleigh wave propagates slower than both dilatation and shear waves, its speed being just below that of shear waves. The ratio of the Rayleigh speed to the shear speed varies slightly with Poisson's ratio, as shown by Fig. 1. (This graph, and Fig. 2 were calculated using the equations from Kolsky, ref. 2).

The particle motion in a Rayleigh wave is in the form of an ellipse, the direction of motion being such that when a particle

---

* Young's modulus is, by definition, the stiffness of a sample of material stressed in one direction, but unconfined in the other directions. Such a test performed on a $\nu = 0.5$ material, like water, causes the sample to continuously deform laterally, so that no stress is built up in the axial direction; i.e. E=0.

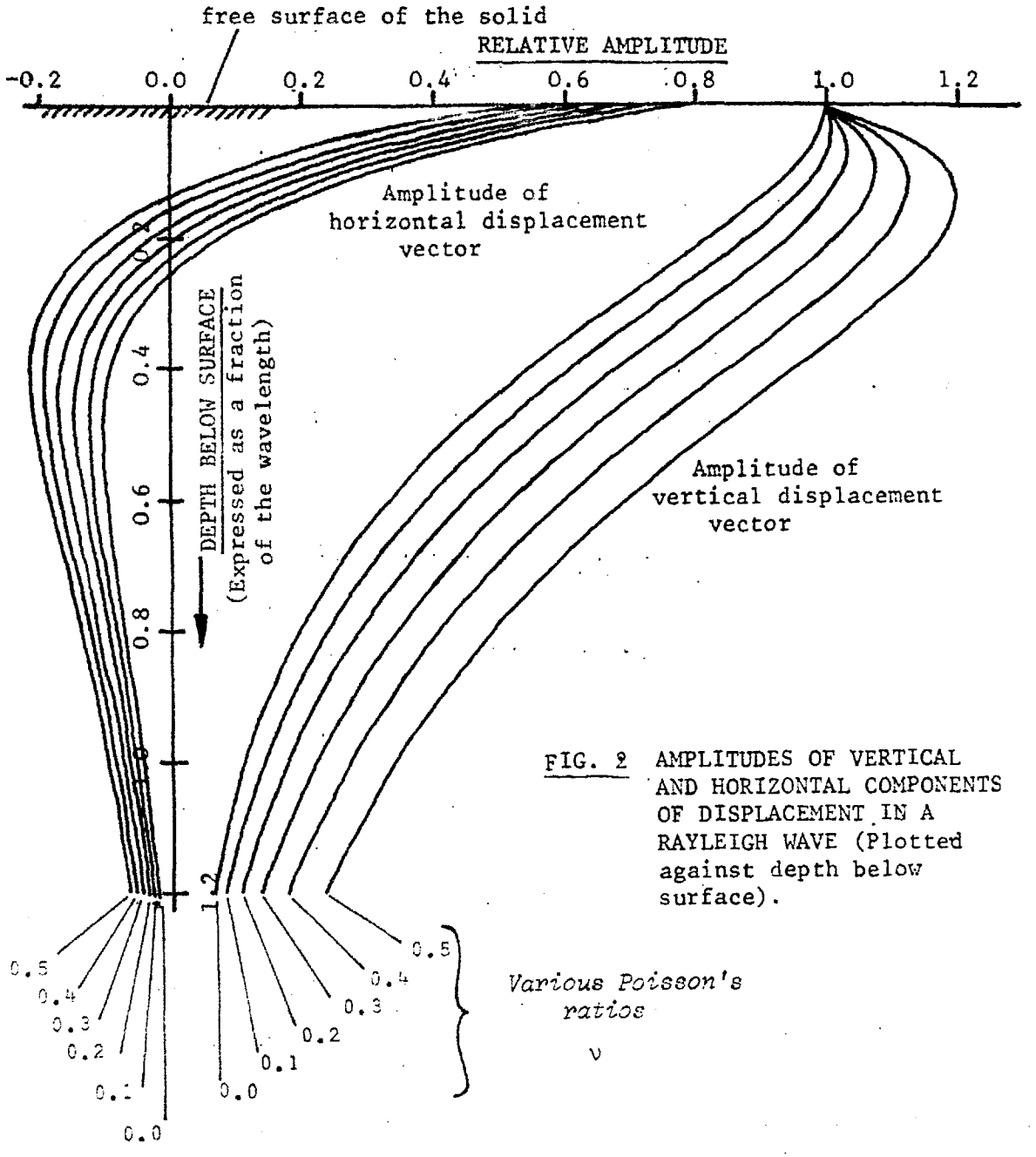

FIG. 2 AMPLITUDES OF VERTICAL AND HORIZONTAL COMPONENTS OF DISPLACEMENT IN A RAYLEIGH WAVE (Plotted against depth below surface).

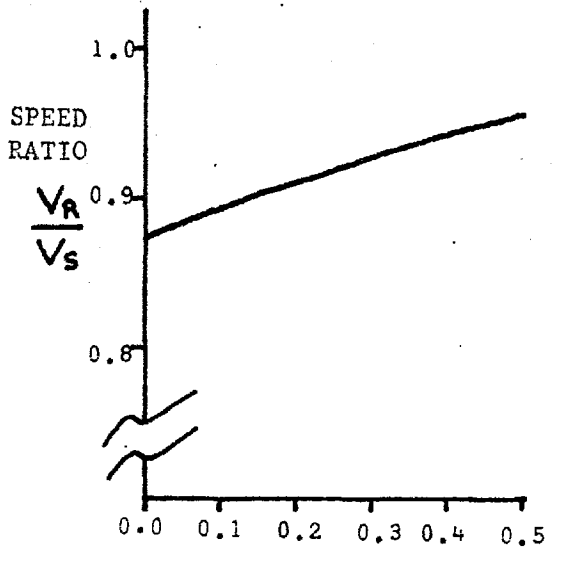

FIG. 1 RAYLEIGH WAVE SPEED (Expressed as a fraction of the Shear speed)

is at the top of its ellipse, the motion is opposite to the direction of propagation of the wave (the reverse of a water wave in fact). The major axis of the ellipse is vertical. The rate at which the particle motions attenuate with depth is directly dependent on the wavelength of the travelling wave. Figure 2 shows how the vertical and horizontal components of displacement vary with depth, the depth scale being non-dimensional - actual depth being divided by wavelength. The curves also show the effects of Poisson's ratio. An interesting point is that the horizontal motion vanishes at one particular depth (about 0·2 of a wavelength down, for $\nu = 0{\cdot}2$), then reverses direction.

Effect of Poisson's Ratio on Rayleigh waves

Figure 2 shows that variations in Poisson's ratio make very little difference to the components of displacement associated with Rayleigh waves. Even with the limiting ν of 0·5, the distribution of displacements with depth is similar to those for $\nu = 0{\cdot}2$ to 0·3, corresponding to rock-like materials.

The velocity of Rayleigh waves, expressed as a fraction of the shear speed, also changes very little with Poisson's ratio as shown in Figure 1.

The implications of a high Poisson's ratio for a model using a rubberlike material will be examined later on in this Chapter, since the effects of other factors (such as dispersion) will need to be considered.

C. DAMPING

All forms of dynamic motion are subject to damping. It is important to distinguish between two distinct forms of energy dissipation:

(i) Internal friction or viscous mechanisms a material causing energy to be lost from the vibrations, and converted into heat, or other irreversible forms.

(ii) Radiation from a vibrating system in the form of waves which carry away the energy from the system.

The first type will be called "internal damping", and the second "radiation damping".

Radiation Damping

The energy radiated away from a vibrating system is a critical function of its geometry: for instance, a structure such as a chimney built on the surface of the ground has very little radiation damping, since only a small part of its geometry (the base) can radiate energy into the ground. More radiation damping occurs in an earth-dam, which has a large area of its surface in contact with the ground. Of course the ultimate case of radiation damping is a single point oscillating within an infinite solid. Here, any external energy supplied to the point is immediately radiated away, so that it can perform no natural oscillations; i.e. it is heavily damped.

The response of an open-pit lies somewhere between the two extremes: a large part of its vibrational energy will be radiated in the form of waves, but it may be possible for it to exhibit natural oscillations at various frequencies, even though these must decay rapidly. Due to the existence of such high radiation damping in the case of an open-pit, the internal damping of the rock material may play only a small part in the dynamic response.

Internal Damping

As dynamic waves propagate through a solid, they are damped by various forms of internal energy dissipation which convert the vibrational energy into heat. There are many ways of quantifying internal damping, the most direct being the "specific loss", which is: $\frac{\Delta W}{W}$, where ΔW is the energy dissipated in one cycle of oscillation, and W is the total vibrational energy of the system, in both kinetic and strain forms. This definition makes no assumptions about the nature of the energy-absorbing mechanisms. If the mechanism is assumed to be viscous, the oscillations of a free, bounded system will die away exponentially, and the amplitude of each oscillation peak will bear a constant ratio to the preceding one. The damping factor in this case can be described by the logarithmic decrement, which is defined as:

$$\delta = \log_e \frac{a_2}{a_1} \qquad 33$$

where δ is the logarithmic decrement
and a_2, a_1 are successive excursions of the waveform on the same side of the equilibrium position.

If the damping is low, the specific loss can be related to the logarithmic decrement:

$$2\delta \approx \frac{\Delta W}{W} \qquad 34$$

A viscous damping mechanism implies that the logarithmic decrement will increase as the frequency of oscillation rises. However, there is a considerable body of evidence to show that very many rock types exhibit constant decrement over a considerable range of frequency (Gemant & Jackson, ref 4, Wegel & Walter, ref 5). In view of this, it must be concluded that the major cause of dynamic damping in rock is associated simply with the static hysteresis loop of the material, which causes a constant amount of energy to be lost per cycle, irrespective of the rate at which the cycle is traversed.

Although "static" hysteresis loss may be the most correct physical model for internal damping, it is almost impossible to treat analytically. Almost invariably analytical solutions to dynamic problems incorporate damping in the form of some arrangement of viscous forces (i.e. force proportional to particle velocity). This approach is valid only for a small frequency range, and if the magnitude of damping is low.

D. A STUDY OF PROBLEMS SIMILAR TO THAT OF AN OPEN-PIT VIBRATING

Whilst, at the present time, there does not appear to be any analytic, numerical or experimental solution to the problem of elastic open-pit vibrations, there are many related problems, some of the characteristics of which may have a direct bearing on the present problem. It is useful to examine these similar problems in the hope of formulating some general statements about the dynamic response of an open-pit.

Conservative/Non-Conservative Systems

The most prominent feature of an open-pit is that, being embedded in the surface of a solid, it is obliged to radiate large proportions of its vibrational energy into the surrounding half-space; i.e. it is non-conservative (energy is not conserved within the system). Strictly speaking, no system is conservative, since some form of friction is always present to dissipate energy. But it is true that in many cases the loss is so small that for most purposes the system can be treated as a conservative one. Such a system is a tall structure, such as a large block of flats, which radiates only a very small proportion of vibrational energy through its base into the surrounding ground material; it can be approximated to a conservative system. An earth- or rock-fill dam has also been treated as a conservative system many times (e.g. Clough & Chopra, ref 6), but the approach would seem to be a dubious one, in view of the large area of the dam in contact with the surface of the ground. Perhaps the saving grace is that the difference in elastic properties between the dam fill and the ground material will cause transfer of energy across the interface to be inefficient.

In the case of the open-pit, no possibility exists of approximating it to a conservative system; its response will be dominated by radiation into the solid half-space, since it is itself part of the half-space.

Characteristic Response of Conservative Systems

A vibrating system without energy loss would behave in the following manner: at certain frequencies the amplitude of oscillation would build up to infinity, in response to an exciting force of that frequency ("forcing function"). At other frequencies, the amplitude would be vanishingly small in comparison with the particular "resonance" frequencies, or "normal modes". A description of normal modes is given in Love (ref 1). Each normal mode corresponds to a characteristic shape of oscillation: for instance the first mode of a stretched string is as follows:

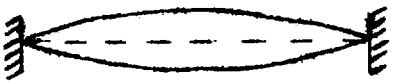

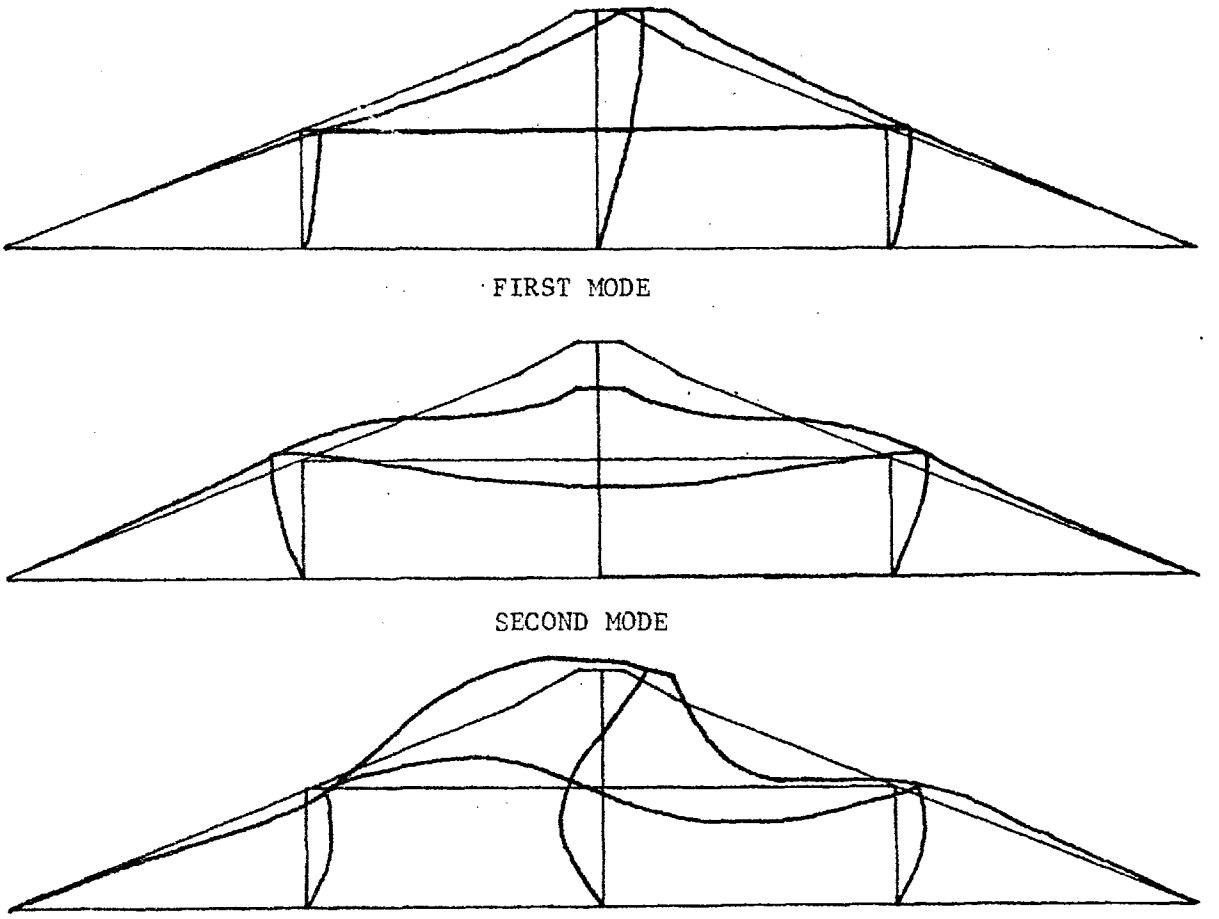

FIG. 4 THE FIRST 3 MODES OF RESONANCE OF AN ELASTIC DAM (After Martin & Seed, 1966)

and the second mode:

The two lines on each diagram represent the positions of the string at the extremes of its displacement, and the dotted line the rest position.

Another prominent characteristic of conservative systems is the fact that all parts of the body have the same phase; i.e. all parts go through the zero position together and all parts reach their maxima together. This means that the locus of any point, over the cycle, is a straight line. A two-dimensional example of a conservative system is shown in the diagram opposite, reproduced from a paper by Martin & Seed (1966, ref 7). The first three modes (= three lowest resonant frequencies) of an elastic dam with rigid base are shown in exaggerated form. An important point to note here is that the diagrams contain all the information necessary to completely specify the motion: at any other time in the cycle, the diagrams will be similar, with only the amplitudes of deflections changed. This will not apply in the case of non-conservative systems.

Since a conservative system has a negligible response to excitation that is not at its mode frequencies, it follows that the response of the system to an arbitrary input waveform will be a linear sum of its response at the mode frequencies.

Non-Conservative Systems

None of the simplifications possible with a conservative system are applicable to a non-conservative system. A finite response occurs at all frequencies, the graph of frequency response being a continuous curve, instead of a number of discrete "spikes" at particular frequencies. Every point in the system has, in general, a different phase when excited by a continuous sine wave. Even the horizontal and vertical components of displacement at one point have different phases, so that the locus of motion of any point becomes an ellipse. Following from this, it can be seen that at no stage in a cycle of oscillation will any particle pass through its rest position. It is apparent that a diagram such as Fig 4 cannot uniquely define the motion, since the phase needs to be specified at each point in addition to the displacements.

Although a non-conservative system may have a characteristic shape of response at a particular frequency, it is meaningless to speak of "normal modes". A classic normal mode analysis cannot be used.

Oscillations of the Surface of a Half-Space

Before considering the effects of various geometries, it is interesting to note the characteristics of the flat surface of a half-space, with no excavations etc. Awojobi and Grootenhuis (ref 8) developed the theory of the vibration of a rigid body in contact with the surface. When the body has a large

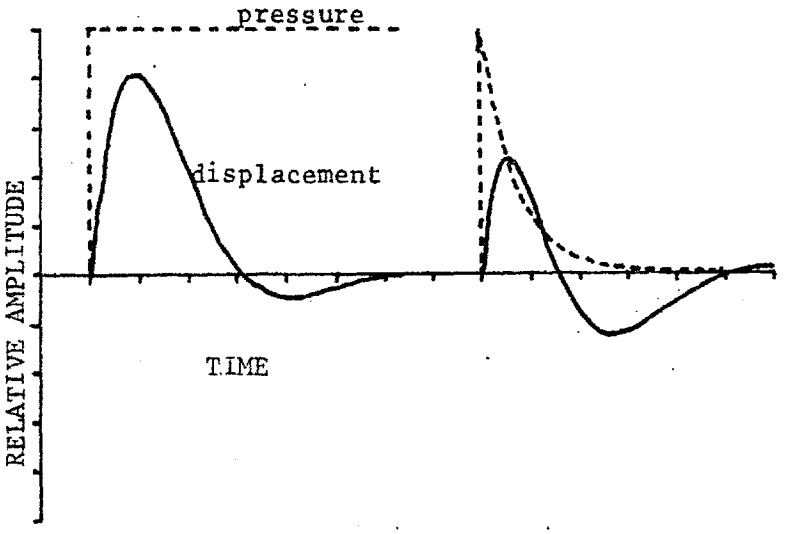

FIG. 5 RADIAL DISPLACEMENTS (solid lines) DUE TO TWO FORMS OF PRESSURE PULSE (dotted lines) IN A SPHERICAL CAVITY (After Sharpe, 1942).

mass, it can be set into damped resonance at a particular frequency. However when the mass is reduced to zero, no resonance is possible. It is a commonly-held belief that when the surface of the ground is struck by something, it responds with a characteristic frequency. This is not true in the case of flat, homogeneous ground. Any discrete frequencies observed must be due to other phenomena, such as discontinuities, mass irregularities, boundaries, etc.

Lunar Crater Effect

An interesting effect has been proposed to explain the prolonged "ringing" of the Moon after being hit by the Appolo 12 lunar module. Steg & Klemens (ref 9) consider theoretically the scattering of Rayleigh waves by surface irregularities, both of positive mass and negative mass (craters). Due to the storage of vibrational energy by the craters, the surface waves spread outwards much slower than if the surface were smooth. The analysis, as such, is not applicable to open-pit vibrations, since it deals with the gross scattering of a continuum of mass defects. However it serves to show that a pit in the surface of a solid can store vibrational energy. The analysis in fact only considers a continuum of point mass inclusions or defects, so that it cannot possibly include oscillation effects which are due to the shape of a pit.

Spherical Cavity: radial oscillations

Atheoretical result which has some bearing on the present problem was presented by Sharpe (1942, ref 10), who considered the dynamic displacement field produced by an arbitrary pressure waveform in a spherical cavity. In this case, the cavity was embedded in an infinite solid, with no free-surface effects considered. Furthermore, the only mode of response considered was axi-symmetric i.e. the cavity is assumed to deform radially. However even though the problem may seem remote from an open-pit vibrating, an idea of the frequencies and damping factors involved may be obtained. Two of the curves given by Sharpe are shown opposite (fig 5). They show the distant resonse of the solid to two input pressure waveforms (shown dotted) in the cavity. The response is seen to be a heavily-damped oscillation; the equation of motion at the cavity surface is:

$$u = \frac{a p_0}{4\mu}\left[1 - \frac{\sqrt{3}}{2} e^{-\frac{\omega t}{\sqrt{2}}} \sin(\omega t + \tan^{-1}\sqrt{2}) + \sqrt{2}\, e^{-\frac{\omega t}{\sqrt{2}}} \sin \omega t\right] \qquad 35$$

for a step input pressure of P_0 with
Poisson's ratio = 0.25 ($\lambda=\mu$)
a = radius of cavity
$\omega = \frac{2\sqrt{2}\, V_L}{3a}$ where V_L = dilation velocity $\frac{dt}{\lambda} \sqrt{\frac{\lambda+2\mu}{\rho}}$

For a cavity of a similar size to a large open-pit, radius 1000 feet, the frequency of oscillation is 1.5 to 3 cycles per second (for dilation wave speeds of 10,000 to 20,000 feet/sec). These frequencies must be modified in the case of a real open-pit, since the presence of the ground surface will cause an apparent reduction in the stiffness of the material (see next section: dispersion) causing the above frequencies to be lowered. Of course it must be remembered that

the type of motion considered here is rather strange (all parts of the pit moving either outwards or inwards together), and may not be excited under normal conditions.

The decay of the oscillations is very rapid, as can be seen from Figure 5. In the case of the impulsive excitation the amplitudes of successive oscillations are in the ratio of approximately 9 to 1, giving a logarithmic decrement of 2·2.

Bar Propagation: reflection effects

At low frequencies, dilation waves travel down a long solid bar at a fixed speed, $\sqrt{\frac{E}{\rho}}$ where E is the Young's modulus, and ρ the density. In later Chapters (the Model chapter and Numerical chapter) it will be necessary to consider the effects of terminating the half-space with particular types of boundaries. It is instructive to examine here what happens to a wave travelling down a bar, when the bar is abruptly terminated.

There are two limiting cases: the bar could have a free end, or a fixed end.

In the case of the free end, the end must be free of stress so an equal and opposite stress to that contained in the stress wave needs to exist at the end, in order to satisfy the boundary conditions. This equal and opposite stress is a "mirror image" of the incident wave and in fact gives rise to a reflected wave which propagates back down the bar. In other words, there is no energy loss at a free end, all the incident energy being reflected back along the bar.

The case of a fixed end is very similar, but here no *displacement* can exist at the end of the bar, so the displacement components of the wave need to be matched at every instant in time by an equal and opposite displacement in order that the net displacement at the end be zero. As in the previous case, a reflected wave is generated but now the *displacement* components are reversed compared with the *stress* components previously. There is no energy loss at a fixed end, all incident energy being returned along the bar.

At any intermediate boundary condition, between those of a fixed end and free end, energy loss occurs and not all the incident energy is reflected. The amount of energy loss depends on the nature of the boundary conditions, but there is one particular condition in which all the energy contained in the wave is absorbed by the boundary. The bar itself has a "characteristic impedance" which is the ratio of stress to particle velocity at a point. This ratio is constant (for low frequencies) and has the value ρC_p, where ρ is the density and C_p the velocity of dilation waves. If the bar is terminated with this impedance, complete absorption of energy occurs. The physical meaning of the termination is a viscous dashpot, in which the ratio of stress to velocity is ρC_p

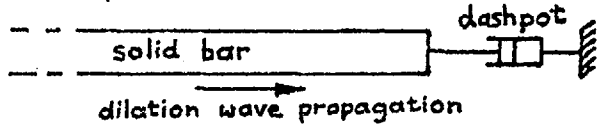

Similar arguments may be employed for shear waves propagating down the bar, but in this case reflections can be eliminated by a dashpot termination of ρC_s where C_s is the shear wave speed.

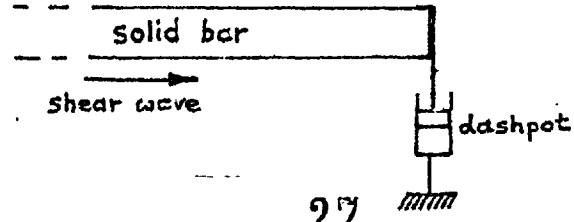

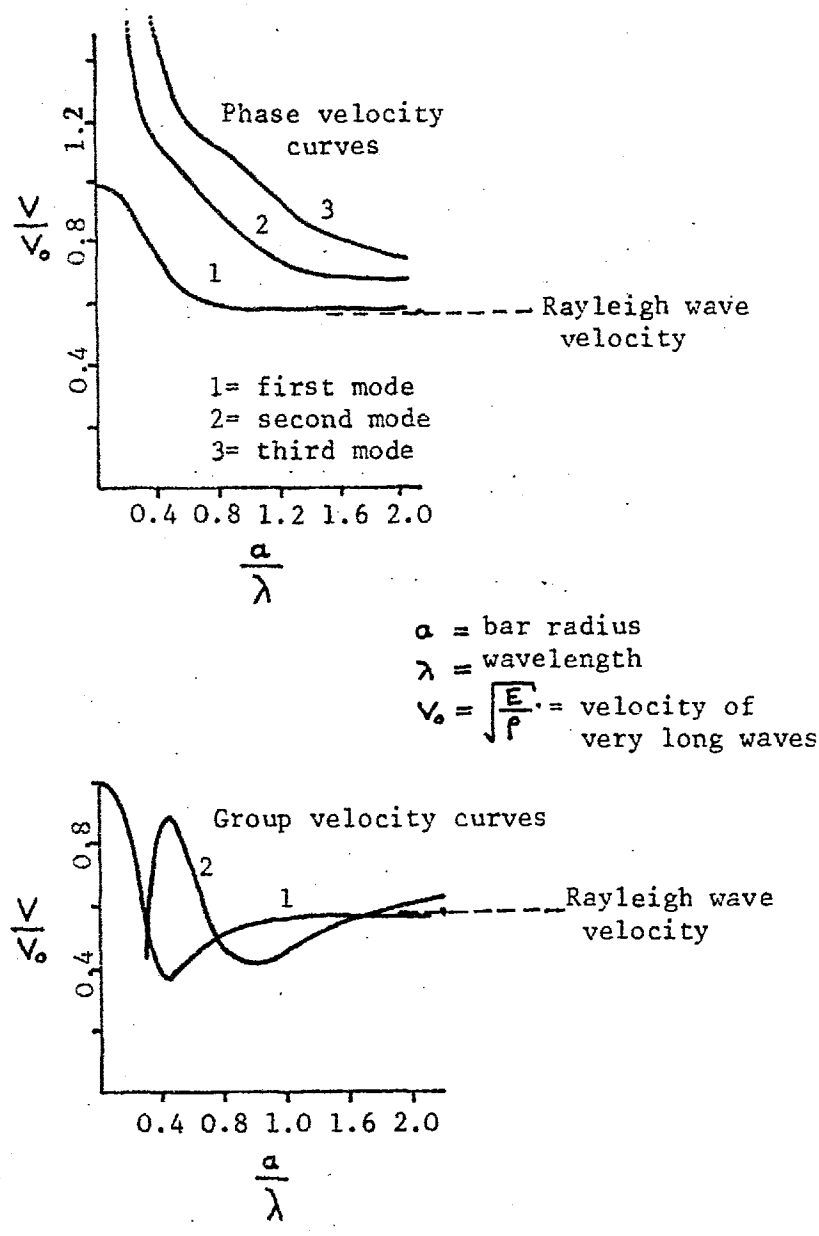

FIG 6. PHASE AND GROUP VELOCITY CURVES FOR LONGITUDINAL WAVES IN A CYLINDRICAL BAR, PLOTTED AGAINST RADIUS OF THE BAR (After Kolsky, 1953)

In the two and three-dimensional cases, fully absorbing boundaries cannot be met by single-element dashpots, but this point will be fully examined in the chapter about numerical methods.

Bar Propagation: dispersion effects

The simple theory predicts that dilatational waves of any frequency travel down a long circular bar at a fixed speed. However, there are a number of factors which cause the velocity to vary markedly with frequency. At very low frequences, the wavelengths are long compared with the diameter of the bar, so that the bar is under essentially static load. In this case, the static gross stiffness of the bar (Young's modulus E) governs the motion, the velocity is given by:

$$v = \sqrt{\frac{E}{\rho}}$$

It will be noted that this velocity is less than the dilatational speed through an infinite solid. This is because the bar appears to be less stiff in compression than the infinite solid, since it is unconfined in the lateral direction. This fact has great relevance for a material with a Poisson's ratio approaching 0.5, since the unconfined stiffness of a bar, E, is very much less than the confined stiffness. Hence, the dilation speed when a free surface is involved will be much less than if no surface existed.

As the frequency rises, and the wavelengths become smaller, the surface of the bar begins to look like a plane surface (in comparison with the small lengths of waves) this effect of changing velocity is called *dispersion*.

Another effect is the mode in which the wave propagates, depending on the geometrical distribution of the longitudinal displacement along a radius, the relation between wave velocity and frequency can follow any one of a number of curves. Three of these curves for a circular bar are shown opposite (Fig. 6) (from Kolsky, ref. 2).

As a general observation, it can be postulated that dispersion effects occur when the wavelength is of the same order as the principal dimensions of the body through which the wave is being propagated. This idea is reinforced by the next section of this Chapter (e.g. tunnel waves).

Tunnel waves: resonance?

Biot (ref. 11) considered the propagation of elastic waves along a long empty cylindrical bore within an elastic solid. At all frequencies above a certain value, waves can propagate along the surface of the bore, without losing energy due to radiation into the surrounding solid. As with the bar, at high frequencies the wave speed approaches that of Rayleigh waves. However, as the frequency is reduced, a stage is reached when waves are radiated into the interior of the solid. This effect forms a "cut-off" frequency below which wave cannot propagate along the bore without severe attenuation. The phase and group velocity curves are shown

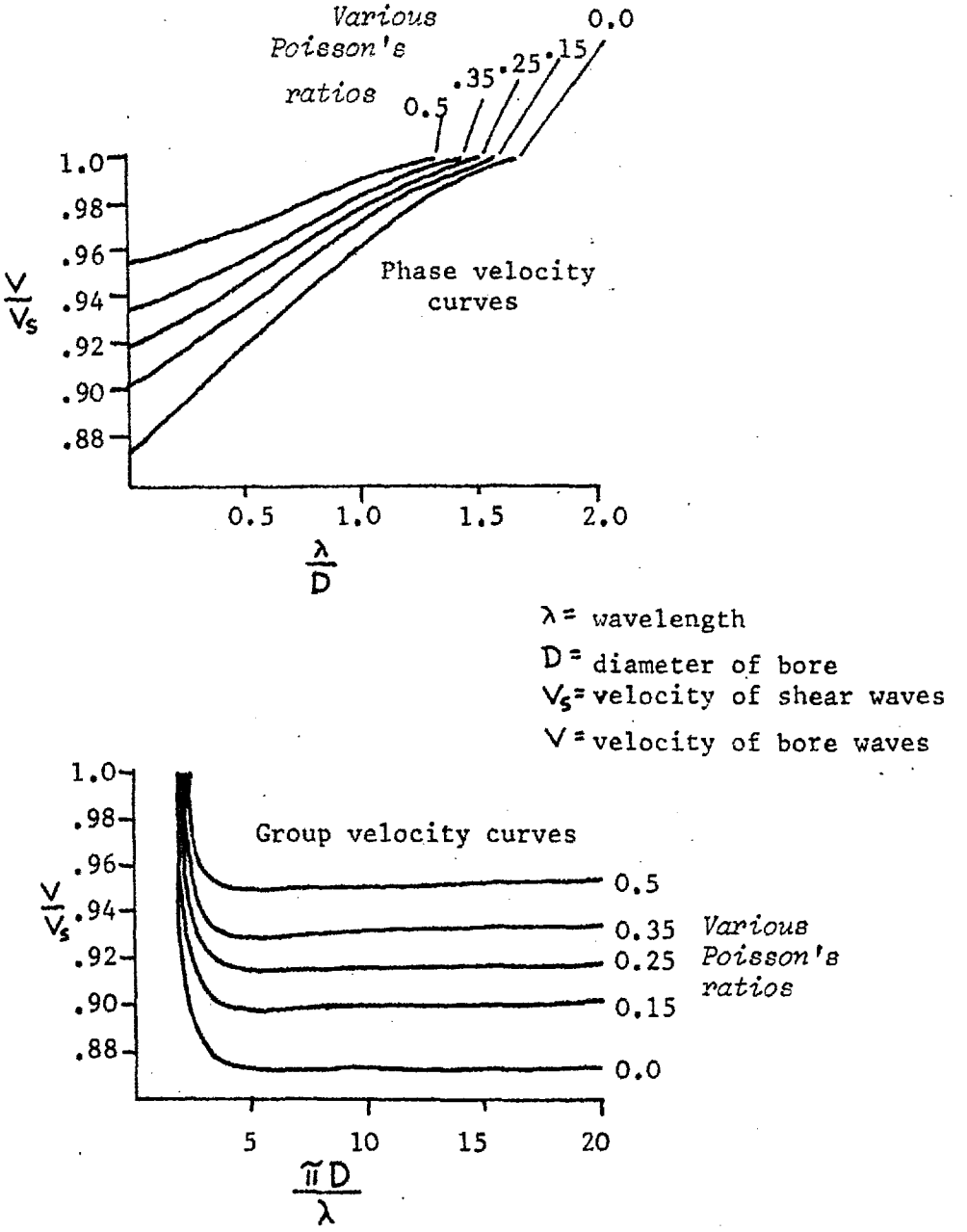

FIG. 7 PHASE AND GROUP VELOCITY CURVES FOR WAVES ALONG A CYLINDRICAL BORE (After Biot, 1952)

in Fig. 7. It should be mentioned that Biot only considered waves with axial symmetry (similar to radial oscillations of the spherical cavity). The interesting point about the group-velocity curves is that there exists a shallow minimum at a particular frequency. Hence waves of this frequency should propagate with the slowest speed, and will predominate in the trailing edge of a pulse propagated down the bore. Another consideration is that the bore acts like a filter, with a fairly sharp cut-off frequency. It is a property of sharp cut-off filters that ringing (oscillation) is produced in response to a step input pulse. The ringing frequency is approximately equal to the cut-off frequency of the filter.

The outcome of the preceding observations is that a tunnel may seem to exhibit resonance-like effects, appearing to oscillate at a particular frequency. However, the following points must be borne in mind:

(i) The "resonant" frequency will only manifest itself after the wave has been travelling down the bar for some distance.

(ii) The decay rate of the oscillations is likely to be rapid, in view of the shallowness of the minimum in the group velocity curves.

(iii) The foregoing arguments apply only to radial type oscillations. There may be other oscillation modes which are far more powerful.

Tunnel Oscillations: *field observations*

A report prepared for the U.S. Space Agency NASA (ref. 12) gives some results for tests performed in the field to detect near-surface tunnels and cavities by trying to pick up their natural oscillation frequencies, when excited by a surface explosion. The authors' use Biot's results for tunnel waves (see previous section) in an attempt to predict the cavity dimensions from the observed "ringing" frequency of the tunnel. In two cases considered, the dimensions thus obtained differ by some 300% from the known dimensions (the frequencies observed were far lower than those expected). The authors conclude that the oscillations observed "are probably radial oscillations of the cavity walls". This statement would seem open to severe doubt in view of the very large difference between the calculated and known dimensions of the tunnels.

Furthermore, the geophone traces given show a much smaller decay envelope than that expected from radial tunnel waves*. Also, the location of the shot point (Fig. 8) would seem to be directly unfavourable to the production of the looked-for oscillations. It was mentioned in the previous section that the development of a discrete frequency only became apparent when a wave had travelled some distance down the bore. In the case in question, the measurements were taken at precisely that point at which the bore wave originated: hence it is unlikely that any frequency-selective filtering could take place in the manner postulated.

× × × = Geophone locations

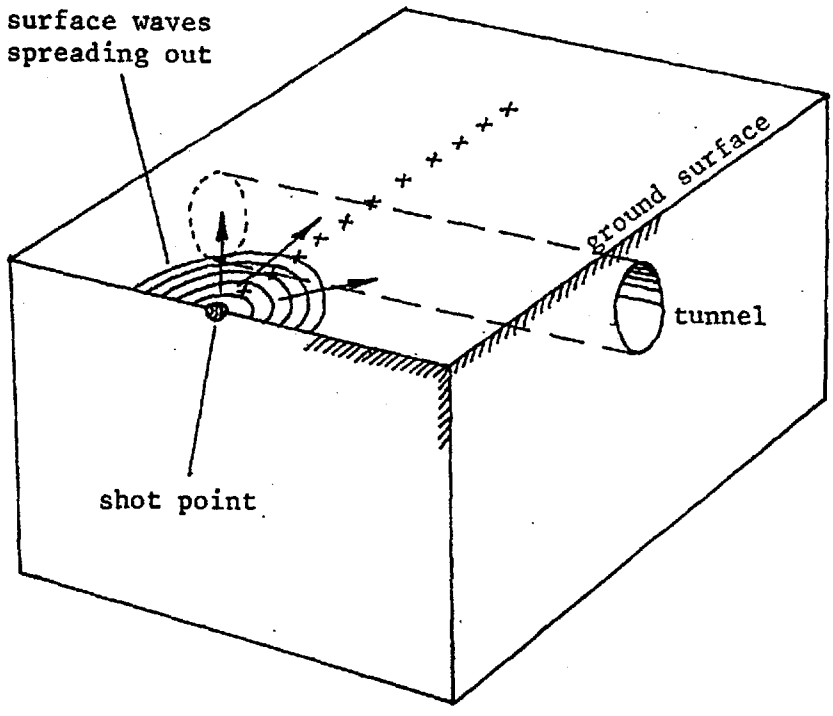

FIG. 8 DIAGRAM SHOWING LOCATION OF SHOT POINT AND GEOPHONES IN RELATION TO THE TUNNEL (see text)

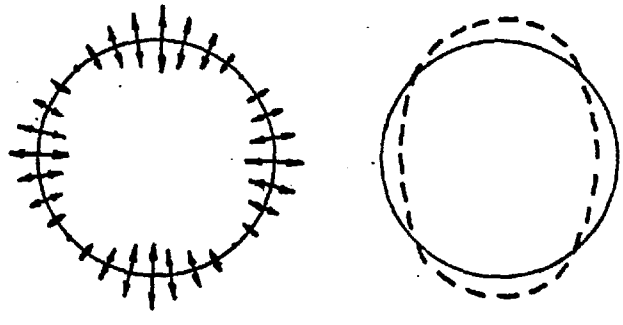

Locii of particles, over a period of one cycle.

Instantaneous deformation profile.

FIG. 9 POSTULATED SHEAR MODE FOR OSCILLATION OF A TWO-DIMENSIONAL HOLE

Tunnel Oscillations: *Asymmetric Oscillations*

A possible explanation for the anomalous results referred to above is that the tunnel may be stimulated to oscillate in an *asymmetric* fashion about its axis. A simple shear mode such as that shown opposite (Fig. 9) is probably not the answer, since a a great deal of energy would be radiated into the solid and the decay of oscillations would be severe (c.f. "Spherical Cavity" - this Chapter). Also, assuming no dispersion effects, and that the tunnel oscillates in the first shear mode, the calculated frequency would still be far higher than the observed frequency.

A much more attractive possibility lies with the Rayleigh wave. Consider a circular hole in an infinite two-dimensional solid. By analogy with the plane-surface case, it should be possible to propagate Rayleigh waves around the surface of the hole. If the waves are of high frequency, with wavelengths much smaller than the hole radius, the wave speed should appraoch that of plane Rayleigh waves, since the curvature of the surface becomes negligible in comparison with the small wavelengths. However as the wavelengths become comparable with the hole radius, it is reasonable to assume that dispersion will occur, causing the wave speed to be a function of wavelength. Indeed, there may be a cut-off wavelength beyond which propagation might be impossible without energy being radiated into the interior (by analogy with the bore waves discussed earlier).

If the above assumptions are correct, the implications are far-reaching. It is a rare example of the trapping of vibrational energy within an infinite medium, with no loss of energy through radiation. This is due to the surface wave being confined to a narrow skin around the surface of the hole. If the frequency of the circulating wave were such that an integral number of wavelengths could fit around the circumference, then that frequency would represent a strong resonance, damped only by the internal friction of the material. If the first mode exists, it should take this form:

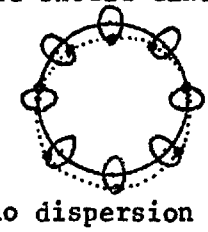

Assuming no dispersion at this frequency, the oscillation frequency is given by

$$f = \frac{C_R}{2\pi r} \qquad 36$$

C_R = Rayleigh speed
r = radius of hole

Substituting the figures given in the NASA report, the frequency obtained is within 5% of the measured frequency in both cases. Furthermore, the low damping factor is consistent with the above model, since in a three-dimensional tunnel, energy would be lost in only one dimension - along the bore. Also the type of excitation used in the experiment would favour the stimulation of a Rayleigh mode: the plane Rayleigh wave generated by the explosion would travel along the ground surface, and interact with the top of the near-surface tunnel. Thus an asymmetric excitation is provided, which is exactly that needed to excite circulating Rayleigh waves in the tunnel.

It was mentioned above that the radiational energy loss from a circulating Rayleigh wave in a bore should be only one-dimensional. The same arguments should hold for an open-pit. Here a circulating wave set up at some horizontal section through the pit would radiate energy both upwards and downwards, but not outwards. In fact if the circulating wave is near the surface of the ground, the radiation may only be downwards, so that the damping in this case would be unusually low.

The lowest resonant frequency in a 2000 foot diameter pit with realistic elastic constants should be of the order of 1 c.p.s.

Due to the low damping factor involved, circulating Rayleigh waves may play a large part in the dynamic response of open-pits. The whole subject is investigated more fully in Appendix II.

E. CONCLUSIONS TO BE DRAWN

Open-Pit Vibration

Drawing on the various analytical and experimental work examined in this Chapter, certain predictions may be made about the general characteristics which govern the dynamic response of an open-pit.

The primary characteristic will be that sharp resonances as understood in the case of finite, bounded bodies, will not exist. The frequency response graph of an open-pit will be a smooth curve; whilst it may have maxima resembling resonances, these will always be of a shallow nature due to the irrecoverable radiation of dynamic energy into the solid. A "normal-mode" method of analysis would seem inappropriate for a non-conservative system. As a direct consequence, "mode-shapes" as commonly understood will not exist: the motion of any point, at a particular frequency, will be an ellipse. The geometric pattern of ellipses will change smoothly as the frequency is varied.

The characteristic frequencies of an open-pit are liable to be of the order of cycles per second, for a large pit. Since shallow earthquakes yield similar frequencies, open-pits located in earthquake regions may have a stability problem which would be underestimated by a psuedo-static analysis.

The damping factors of several geometries considered in this chapter are very high, and if similar factors were to pertain in open-pits, there would be little cause for concern. However, as mentioned in the previous section, there may be certain wave modes, peculiar to near-circular geometries, that have lower damping factors.

Implications for Rubber Model

Since a future Chapter will describe tests made on a rubber model, it is pertinent to enquire what effect the Rubber's high Poisson's ratio will have on the response. It has been shown that those modes of response which involve shear- or Rayleigh-waves should be little affected provided that the correct (very low) values of velocities are taken note of. On the other hand, any mode involving dilation (P) waves is likely to be drastically altered, since, in the bulk of the rubber the velocity could typically be 1000ft/sec, whilst near a free surface the speed could drop to 50 ft/sec. Dilation waves will also exhibit heavy dispersion (velocity varying with frequency).

Boundaries

In both a physical model and in numerical analysis, due note and allowance must be made for boundaries, since it has been shown that all the incident energy is reflected back from both a free and a fixed boundary. Standing waves between boundaries could completely mask the response characteristics of the open-pit being analysed.

Analytical Solutions

From the analytical solutions considered here it is apparent that only the simplest geometries (generally two-dimensional) have been easy enough to solve. The possibility seems remote that an analytical solution may be found for a three-dimensional open-pit vibrating in asymmetric mode.

Some Remarks on Procedures for Obtaining Dynamic Constants

The results of any calculation are only as good as the input information. The field of Dynamics seems to suffer more than most from a number of obscure and arbitrary tests intended to furnish values for parameters such as velocity of sound, dynamic modulii etc. One classic case is an expensive commercially available instrument which is intended to measure the compressional wave velocity in a small rod of material. It uses a quartz transducer to produce a short burst of high frequency oscillation applied to one end of the rod, and a similar transducer at the other to receive the delayed signal. The transit time is measured (which quantity varies with the gain setting on the instrument). However the frequency of oscillation used is such that the wave-length is nearly equal to the diameter of the rod. It was pointed out earlier in this Chapter that under that condition, maximum dispersion occurs, so that the velocity of sound can take on any value between wide extremes. In fact, depending on the precise mode of propagation, a literally infinite velocity range is possible. It is little wonder that dynamic testing results are not generally taken seriously. Similar errors can be made in large-scale field dynamic tests where the measured velocities are critically dependent on the type of wave propagated, dispersion characteristics, geometry etc.

REFERENCES

Chapter 2

1. LOVE, A.E.H. "A Treatise on the Mathematical Theory of Elasticity" Cambridge University Press 1892.

2. KOLSKY, H. "Stress Waves in Solids" Clarendon Press oxforD 1953

3. MILLER, G.F., PURSEY, H. "On the Partition of Energy Between Elastic Waves in a semi-Infinite Solid" Proc. Roy. Soc. Series A, V233, 1955.

4. GEMANT, A., JACKSON, W. Phil. Mag. V23, pp960, 1937.

5. WEGEL, R.L., WALTHER, H. Physics V6, pp141, 1935.

6. CLOUGH, R.W., CHOPRA, A.K. "Earthquake Stress Analysis in Earth Dams" Soil. Mech. & Bit. Mat. Lab. University of California, November 1965.

7. MARTIN, G.R., SEED, H.B., "An Investigation of the Dynamic Response Characteristics of Bon Tempe Dam, California" Soil Mech. & Bit. Mat. Res. Lab. University of California, Feb. 1966.

8. AWOJOBI, A.O., GROOTENHUIS, P. "Vibration of Rigid Bodies on Semi-Infinite Media" Proc. Roy. Soc. Series A, V287, 1965.

9. STEG, R.G., KLEMENS, P.G., "Scattering of Rayleigh Waves by Surface Irregularities" Physical Review Letters, V24, N° 8, Feb. 1970.

10. SHARPE, J.A. "The Production of Elastic Waves by Explosion Pressures" Geophysics, V7, N° 2, 1942.

11. BIOT, M.A. "Propagation of Elastic Waves in a Cylindrical Bore Containing a Fluid" Jour. Appl. Phys. V23 N° 9, Sept. 1952.

12. WATKINS, J.S., GODSON, R.H., WAISON, K. "Seismic Detection of Near-Surface Cavities" Geological Survey Professional Paper N° 599-A, U.S. Government 1967.

* * * * * *

Chapter 3

Chapter 3: MODEL

A. CONSIDERATION OF THE MODEL MATERIAL
   - Ideal Model Material
   - Practical Model Material

B. DESCRIPTION AND PROPERTIES OF THE RUBBER

C. BOUNDARY CONDITIONS AND EXCITATION
   - Boundaries
   - Excitation

D. PROVISION WITHIN THE MODEL FOR DEFINING INTERNAL DEFLECTIONS
   - Suspended Particles
   - Stretched Bands
   - Attachment of Bands

E. OPTICAL CONSIDERATIONS
   - Optical Distortion Through Interfaces
   - Viewing and Measurement System

F. CASTING PROCEDURE
   - General Observations
   - Method of Casting

G. IN SITU STATIC AND DYNAMIC PROPERTIES OF THE RUBBER AND TANK
   - Plate Load Test
   - Dynamic Tests
     - *Damping*
     - *Velocity of Propagation*
     - *Frequency Response of Box*

H. RESULTS OF TESTS
   - Method
   - Conclusions

A. CONSIDERATION OF THE MODEL MATERIAL

Ideal Model Material

It is instructive to consider the attributes of an ideal material to model the dynamic elastic response of an open-pit mine. It should of course be perfectly elastic, and have the same Poisson's ratio and dynamic damping factor as the prototype material. It should be cheap and easy to work with, and must lend itself to easy measurement of the amplitude and phase of vibrations in three dimensions, both on the surface, and within the bulk of the material surrounding the excavation. The latter requirement implies that the frequency and amplitude of vibrations set up in the model pit must be well within the range of conventional instruments to measure accurately, and also within the range of conventional vibrators to produce. The ideal material must also exhibit constant properties with respect to time, temperature, atmospheric pressure and humidity, as well as having no shrinkage, expansion or undue evolution of heat when cast or otherwise manufactured.

Practical Model Material

The factor of overriding importance in the present research is the need to measure the vibration amplitude and phase *within* the mass of material surrounding the excavation. This requirement is occasioned by the need, in any subsequent simple failure analysis to be able to delineate any region accelerating in a given direction at a given time. A severe difficulty exists in proposing a means to measure the internal dynamic deflections of a mass of material in three dimensions. If electrical means are used, this involves implanting, within the material as it is cast, some form of active device (i.e. transducers, such as strain-gauges or accelerometers), and leading the wires out to some measuring device. This method seems excessively tedious and expensive, when it is considered that hundreds of transducers would be needed for adequate definition of the wave patterns (especially for the high-frequency modes). There is also the possibility of the transducers themselves interfering with the wave patterns, if they are large and rigid.

It is possible to imagine using some form of passive device embedded in the material, with a system of external read-out. The problem then arises of how the read-out system can locate an individual device and uniquely distinguish it from all the others. This may be relatively simple in the two-dimensional case: for example, X-ray shadow images of metal particles (Roscoe, ref 1), or acoustic doppler-effect sensor used to detect the foetal heart in pregnant women. The problem is greatly eased of course if the model material is transparent, when the vibrations of internal suspended particles can be observed optically. However, in the three-dimensional case, the *only* method open appears to be the latter one, using a transparent material; it is only by optical means that it is possible to observe, with precision, a particle lying behind several others.

Having settled for a transparent model material, it remains to decide whether to use a rigid substance (Perspex, glass) or a soft substance (organic gel, rubber). The rigid substance would have a high resonant frequency (tens or hundreds of kilocycles) and extremely small displacements (0.0001"), so that the read-out system would need to be some form of interferometric device in order to be sensitive enough. The system is experimentally feasible, but expensive, delicate and does not give an immediate visual picture of the motion of the model. The soft transparent material, on the other hand, could be observed directly with a conventional travelling telescope, and in fact the motion may be of a sufficiently large amplitude to be seen by the un-aided eye (using a stroboscope to "freeze" the motion).

Another factor to be considered at this stage is Poisson's ratio. Whilst rigid transparent substances can be found with Poisson's ratios approximating to that of rock (0.2 to 0.3), soft transparent materials have the unfortunate tendency to exhibit Poisson's ratios approaching 0.5 . However, this may not be as serious a drawback as it is with static models, since the velocity and form of surface waves change very little with Poisson's ratio. This topic is examined more closely in Chapter 2, Section B .

The choice now lies between various soft transparent materials. Organic, water-based gels have been used in the past for both static and dynamic models. Gelatin is a common material for self-weight photo-elastic models (ref 2) and agar-agar has been used to determine the dynamic response of a gravity dam (ref 3). In this case, the deflections were measured only at the surface, by strands of cotton lying along the surface. The water-based gels have a fair drawback, in that the water evaporates with time, giving the model only a limited life, and causing the mechanical properties to alter with time. The mechanical properties are also largely affected by temperature. The problem of internal deflection measurements presents difficulties, since the gels have such low modulii of elasticity that any body suspended within the material is likely to have a large effect on the vibration modes, since it may be stiff compared with the gel.

Several experimenters have used non-transparent rubber (refs 2 & 4) for static models. However in recent years there has become available a synthetic transparent rubber intended in fact for incapsulating electronic circuitry. This rubber cold-cures by the addition of a small quantity of catalyst, is extremely transparent (similar to pure water), has a low internal damping factor, seems little affected by time and is insensitive to both temperature and humidity. However, it is very expensive (£1·75 per pound weight), bonds poorly to most other substances, has a high Poisson's ratio and a low tensile strength.

However, the advantages were thought to outweigh the disadvantages, and it was chosen for use in the present experiment.

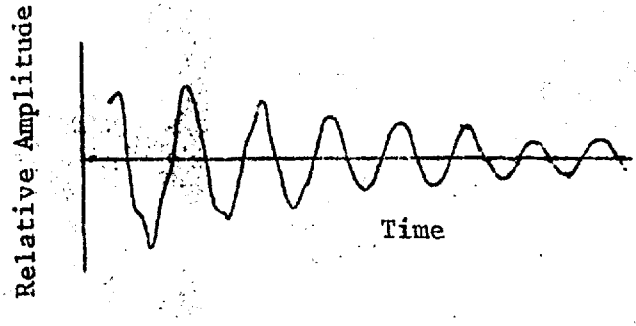

FIG. 3: FREE OSCILLATION OF RUBBER ROD, DUE TO IMPULSIVE EXCITATION.

B. DESCRIPTION AND PROPERTIES OF THE RUBBER

Type of Rubber: DP2628, made by Midland Silicones Ltd., of Reading, Berkshire, England. It is cured with catalyst DP2629. Imperial Chemical Industries Ltd. make a similar rubber, type EP411, but this was found unsuitable, since it became cloudy when cast, and also set more rapidly towards its surface due to water vapour in the air. The cost of the rubber used was, in 1968, £1·8 per pound weight for an 850 pound batch.

Curing: The curing time is dependent upon the proportion of catalyst in the mix. In the present case the recommended minimum quantity was used (1%) in order to prolong the setting as long as possible. With this proportion of catalyst it was found that after two hours a significant increase in viscosity had occurred, with the formation of "strings" of partially set rubber, which made pouring difficult. After five hours the mix could not be poured, but was still very soft. It was found that almost a week was needed before the final elastic properties were reached.

Shrinkage, Heat Evolution: The manufacturers state that about 1% shrinkage can be expected on casting, but fortunately nothing like this was observed in the large model. This may be due to the presence of large gravity stresses. No significant heat evolution or absorption could be detected. Surprisingly the reaction is not speeded-up by heating the mix.

Bond Strength, Tensile Strength: The strength of the bond when the rubber is cast in contact with some surface is generally very low, in the order of a few p.s.i. The bond can be increased beyond the tensile strength of the rubber itself by coating the surface to be bonded with Midland Silicones resin, type MS840. The The tensile strength of the rubber alone is very low - around 30 p.si., the failure being characteristic of a brittle material. A small sample of the rubber can in fact be crumbled to dust by rubbing between the fingers.

Density: The density of the cured rubber is 0·98 that of water.

Young's Modulus: In an unconfined compression test, the Young's modulus was found to be 133 p.s.i., with negligible non-linearity or hysteresis up to 2% strain.

Poisson's Ratio: This was assumed to be 0·5.

Internal Damping factor: This was measured by exciting a rod of the rubber with an impulsive force, and noting the envelope of the decaying oscillations (one end of the rod was fixed, the other free). The oscillation amplitude was found to decay by a factor of roughly 0·75 per cycle (see Fig. 3). Thus the energy ratio between cycles is $0{\cdot}75^2 = 0{\cdot}56$. The specific loss (see Chap. 2) is

$$\frac{\Delta W}{W} = 0{\cdot}44$$

Velocity of Propagation: A rod of the rubber was vibrated at one end, and the other, free, end was monitored with a dynamic capacitive displacement transducer (a copper-foil electrode was glued to the end of the rubber for that purpose). The phase difference between the vibrator drive voltage and the displacement signal was then plotted against frequency. After allowing for the

vibrator phase lag (which was known), the phase plot was found to be a straight line above about 300 c.p.s. The slope was $2\pi/160$c.p.s., which means that one more wavelength was added to those already existing along the length of the sample every time the frequency increased by 160 c.p.s.

Using $c = \lambda f$,

$$c = \frac{1}{4}.160 \qquad \text{(length of bar = 3")}$$

$$= \underline{40 \text{ ft/sec}}$$

$$= \underline{12 \text{ m/sec}}$$

This velocity is probably that of Rayleigh waves, since, at high frequencies, the longitudinal wave speed along a bar is asymptotic to the Rayleigh speed (see Chapter 2).

C. BOUNDARY CONDITIONS AND EXCITATION

Boundaries

In order that the model may accurately represent an open-pit excavated in an infinite half-plane, the existence of the model boundaries must not influence the response of the pit to any significant extent. Initially it was thought that it might be possible to eliminate boundary reflections by surrounding the rubber by some form of damping material. However a suitable material could not be found which satisfied a number of incompatible requirements such as: complete transparency, good damping of both P and S, and Rayleigh waves. The only other alternative was to make the boundaries far enough away from the pit so that any reflected waves would be sufficiently reduced in amplitude by the natural damping of the rubber. In order to calculate the damping of the reflected waves, it is necessary to know the approximate wavelengths associated with the open-pit. If the pit diameter is d then the wavelengths must be of the same order as d. Let D be the distance from the pit to the boundary. It is assumed that all the waves emitted by the pit are reflected back to the pit; i.e. there is no radiation damping. Thus internal damping operates over a distance of 2D. The number of cycles of oscillation in that distance

$$= \frac{2D}{\lambda}$$

Now, from Section B, the rubber was found to cause successive oscillations to have an amplitude ratio of 0·75. It was decided that the reflected waves should have amplitudes of no more than one tenth of the emitted wave amplitude. In this case the necessary number of wavelengths occurring along the reflection path can be calculated:

$$(0{\cdot}75)^n = 0{\cdot}1$$

$$n \simeq 8$$

i.e. eight wavelengths are necessary for the amplitude to decrease to one tenth.

$$\frac{2D}{\lambda} = 8$$

$$D = 4\lambda$$

If the wavelengths are assumed to be of the same order as the dimensions of the pit,

$$D = 4d \text{ , where } d = \text{dia. of pit.}$$

A reasonable experimental size for the pit is six inches, which allows access to the vibrator.

$$\underline{D = 2 \text{ feet}}$$

The box was made 4 ft. square. The depth of the bottom boundary was made only one foot away from the pit since it was shown in Chapter 2 that nearly 70% of the energy from vibrating vertical force was radiated in surface waves.

In the case of a six inch pit, the frequencies that might be expected are:

$$f = \frac{c}{\lambda}$$

$$= \frac{40}{0{\cdot}5} = 80 \text{ c.p.s.}$$

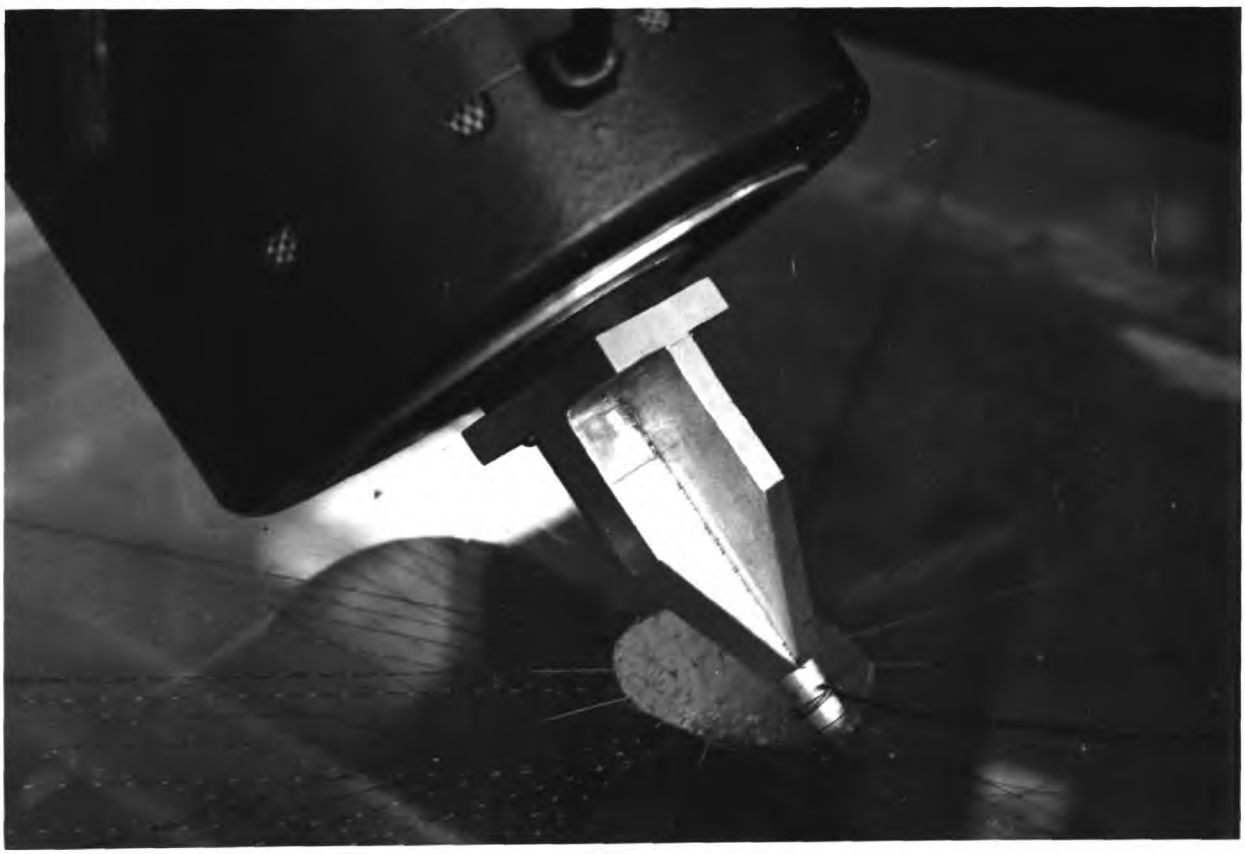

THE VIBRATOR IN CONTACT WITH A SMALL PIT IN THE SURFACE OF THE RUBBER. The small cylinder at the end of the vibrator extension is a piezo-electric force transducer.

Obviously the frequencies will vary considerably from this figure, but it is representative of the order of magnitude. This order of frequency is ideal from the experimental point of view, being well within the capabilities of the various instruments such as vibrators, stroboscopes and displacement-measuring instruments.

Excitation

Blasting can be simulated quite well with a mechanical vibrator, arranged to excite a small part of the surface of the pit. Impulsive forces can also be applied if desired.

Earthquake excitation would appear to be out of the question since the very nature of the interaction between earthquake wave and pit depends on the travelling nature of the wave. It is difficult to see how the boundaries of the model could be excited so that the phase variations of travelling wave would be simulated. Rigidly vibrating the box as a whole would only confuse the issue.

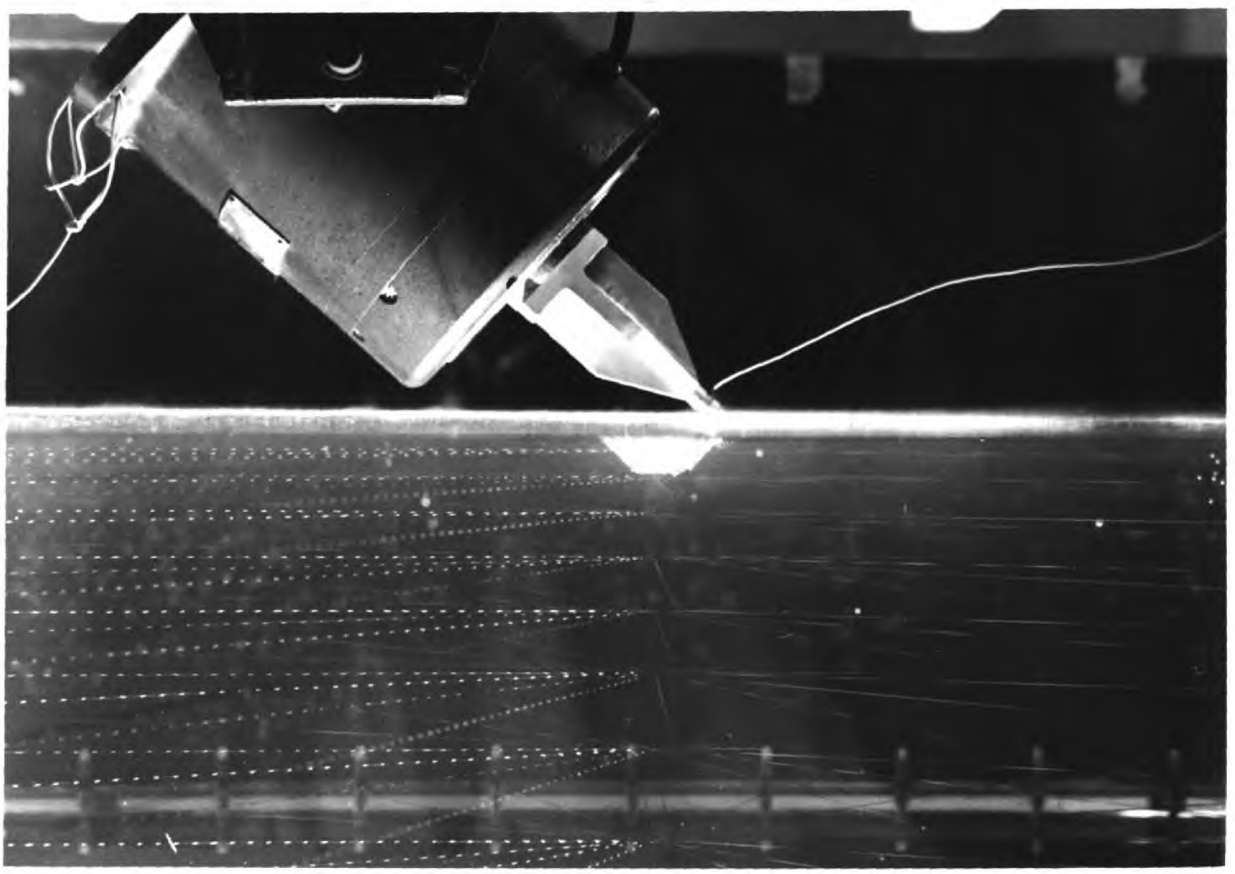

SIDE VIEW OF THE TANK OF RUBBER, WITH VIBRATOR IN POSITION.
The stretched rubber bands, with marking spots, can be clearly seen.

D. PROVISION WITHIN THE MODEL FOR DEFINING INTERNAL DEFLECTIONS

A travelling telescope (described in the next Section) was used to measure ~~the~~ internal deflections. However it was necessary to have something embedded within the rubber to focus upon.

Suspended Particles

The possibility of using a random distribution of very small balls within the rubber was considered, the actual location of the balls in space being determined by the travelling telescope scale. However after a few experiments, it was found that if a sufficient density of balls for good resolution of vibration patterns was used, then it became difficult to view through a large distance of rubber due to a "snowstorm" effect.

As a matter of interest, it was found that neutral-density balls could be made by using non-expanded polystyrene granules, and expanding them in a controlled fashion by immersing them in hot water of a particular temperature for a set time. By varying the temperature and time, balls of any density from 0·04 to 0·94 could be manufactured. In fact, the granules are normally expanded in steam, when they enlarge to nearly thirty times their original volume. Since the density of the silicon rubber was 0.98, it was possible to make polystyrene balls with a density very close to this figure, so that on setting the rubber, the balls would neither rise to the surface, nor sink to the bottom. The minimum size of ball that could be obtained ~~was~~ was 0·04" (1m.m.).

A means of overcoming the "snowstorm" effect would be to cast the rubber in layers, and arrange the balls so that the maximum density would occur near the open-pit, where high definition is required, whilst towards the outer boundaries the density could fall off rapidly. A severe drawback here is that pronounced optical distortion is noticeable when viewing along the interface between two separately-cast layers of rubber.

Stretched Bands

As with the balls, a network of thin bands within the rubber could be arranged to give a high density near the open-pit, dropping off towards the boundaries. In view of the low modulus of elasticity of the rubber, it is undesirable to use rigid wires or strings (such as cotton or copper wire) due to the strengthening effect on the rubber, and the modification of its elastic properties in the vicinity of the band. It was found that even 40 s.w.g. copper wire had a marked effect on the modulus of elasticity of a sample of rubber. Accordingly, thin rubber bands (0·04", 1 m.m.) were used in the present model.

A rectangular network of bands was considered, but it is difficult to achieve a high density in the centre, without producing areas of high density elswhere, since all the central bands must pass through the rest of the model in order to be attached to the boundary. A more logical scheme is to employ a

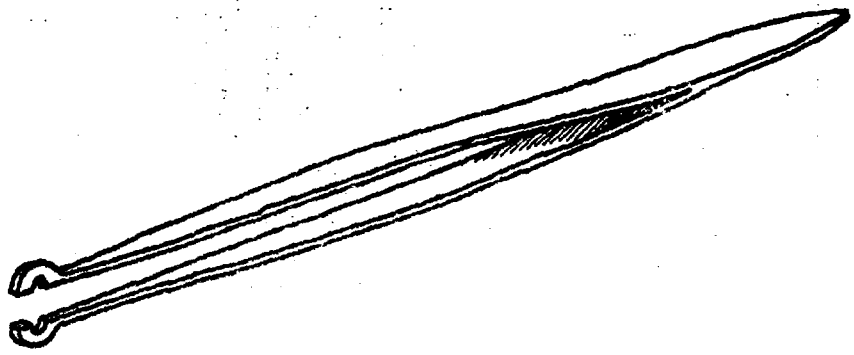

FIG. 1 SPECIAL TWEEZERS USED TO APPLY PAINT TO BANDS

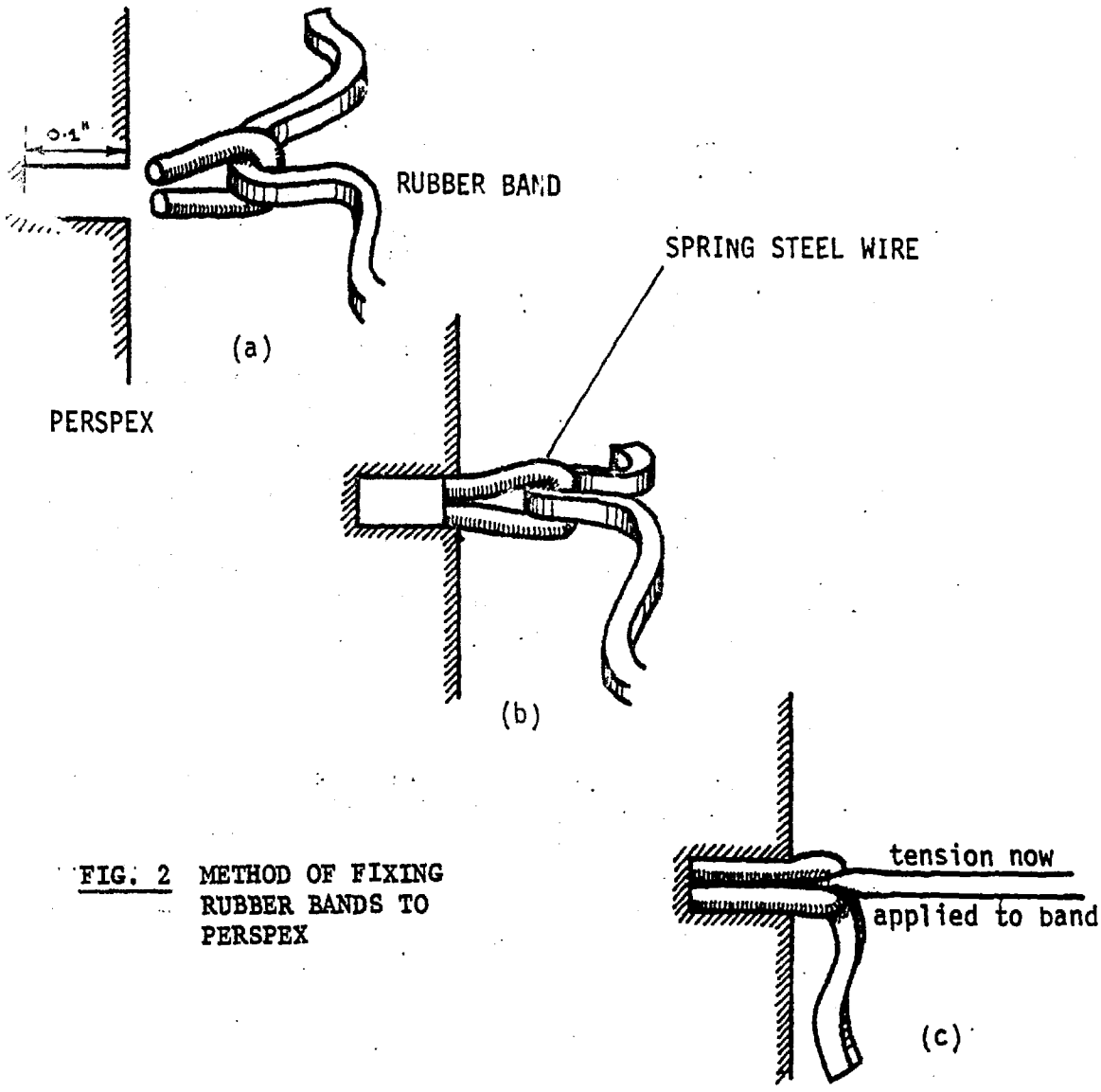

FIG. 2 METHOD OF FIXING RUBBER BANDS TO PERSPEX

radial net: this geometry automatically gives a linear gradation of band density proceeding from the centre outwards. There would seem to be a case for also providing circumferential bands, in the manner of a spider's web, but this is no easy task to realise experimentally as the tension in each band would influence the location of others close to it. Even if it were possible to adjust the tension in each band to the correct value, the original pattern would be lost within a few days due to the "creep" that rubber bands exhibit. However it was decided that a sufficient number of observation points would be provided if the bands were marked all along their length at, say, one centimetre intervals.

The markings were of various colours of paint, the colour used on each band being decided by the requirement that in any one traverse of the model, either horizontally or vertically, no colour must be repeated. This allows a particular band to be identified uniquely by its colour on viewing through the telescope. The paint markings were placed only approximately, since the accurate position could be determined from the telescope's travelling scale. It was found convenient to apply the paint by means of a pair of specially-constructed tweezers, shown opposite.

Attachment of Bands

The box containing the rubber was made from 1 inch thick Perspex. It was found to be very difficult to drill small holes right through this depth of Perspex, in order to provide attachment for the rubber bands. A more practical method was to drill short holes (0.1 to 0.2" long) from the interior of the box, and attach the bands to the holes by means of simple clips made from 0·005" spring steel wire. The series of diagrams on the opposite page shows the method in sequence.

The method provided a neat, almost invisible, way of attaching the bands, with the added advantage that there was no leakage path for the liquid rubber, as would have been the case with holes drilled right through the Perspex.

The bands were all given a pre-tension corresponding to 100% strain; this was to ensure that they would return quickly to their equilibrium positions after the dynamic drag caused by pouring had subsided. In fact, after the rubber had been cast, it was found that some of the bands had displaced permanently up to 2 m.m., so perhaps even more tension might have been desirable.

E. OPTICAL CONSIDERATIONS

Optical Distortion Through Interfaces

Since the model is a dynamic one, any free surface will acquire local curvatures dependent on the mode of vibration excited. If any observation is attempted through the free surface, the dynamic curvatures will act as moving lenses, distorting the true image of an internal point. In fact even a stationary internal point may appear to be vibrating,due to the oscillatory nature of the surface. In view of this all observations must be made through the sides or bottom of the Perspex box.

Of course the preceding arguments presuppose that the rubber is in good contact with the Perspex. In fact the rubber/Perspex bond is not very strong, and in addition the rubber contracts slightly on setting. The rubber may be bonded to the box by means of the resin described earlier. However it was found to be impossible to apply a uniform coating of the resin without ripples or bubbles being formed. The presence of these of course destroyed the good optical properties of the interface. It was finally decided to dispense with a bonding agent and rely on the inherent bond strength as cast.

Viewing and Measurement System

In order to define the dynamic motion exactly it must be possible to measure, at each point within the model, the maximum dynamic excursion in three dimensions, together with the three corresponding phases with respect to the phase of the exciting sinusoid. Phase measurement is facilitated by illuminating the model with a stroboscopic light source synchronised to the exciting frequency, but having a variable calibrated phase delay. The peak amplitude of the particle motion can also be found by varying the strobe phase through its full range, and measuring the maximum excursions of the particle either side of the mean position.

The requirement for the travelling telescope was for an instrument with a small depth of focus and good rejection of objects between it and the point of focus. The focal distance was to be between three feet and a few inches. These requirements were met by the combination of a large-aperture camera lens and a conventional monocular microscope. The camera lens forms a real image in space, and the microscope focusses on this and enlarges it to any reasonable degree of magnification.

The telescope system was mounted on an optical bench having two mutually perpendicular directions of movement, both of which could be adjusted and read to 0·001 inches. In this way, the deflection of an internal point could be measured in two dimension. The motion in the third dimension could be measured by viewing through another face of the box.

STIRRING THE CATALYST INTO THE RUBBER. Four of the twelve dustbins are shown.

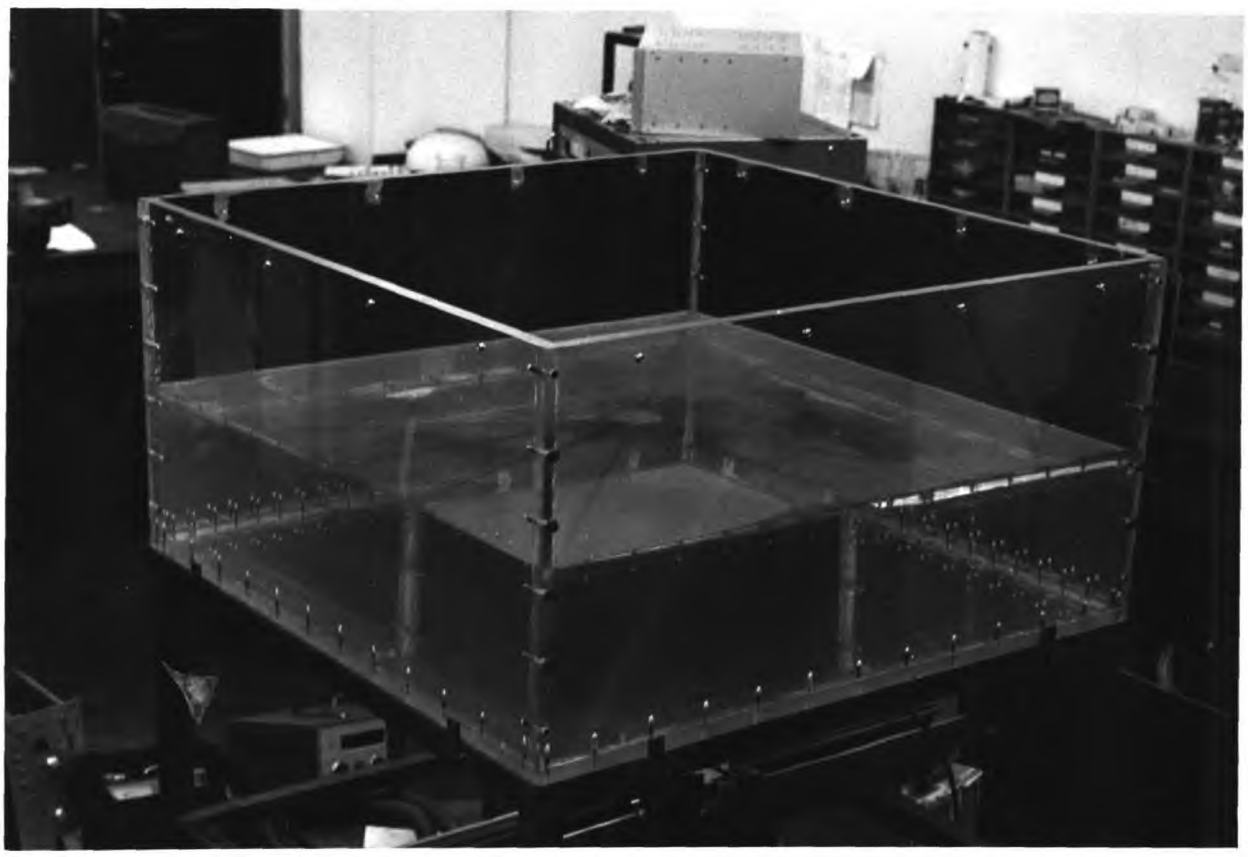

GENERAL VIEW OF THE TANK CONTAINING THE RUBBER. The optical bench can just be seen underneath.

F. CASTING PROCEDURE

General Observations

Great care must be taken when casting the rubber, as several (sometimes conflicting) conditions need to be observed.

The primary difficulty is that the rubber must be cast in one mix (of 850 pounds) in order that the model will be homogeneous, devoid of optical distortion. If the rubber were to be cast in successive layers, the slight differences in densities would be negligible from the vibration point of view, but optically a severe distortion would exist when viewing along an interface.

Secondly the action of mixing in the catalyst introduces myriads of bubbles. The only way to remove these before the rubber sets is to apply a mild vacuum to the mix. The effect of the vacuum is to enlarge the bubbles to a greater size, so that they become more buoyant, and rise rapidly to the surface. The optimum vacuum for this purpose was found to be about 0·5 atmospheres. If more vacuum is applied, the mix seems to "boil" and the froth can overflow the container, and probably cause more bubbles than were present initially. If less vacuum is used the bubbles are not enlarged sufficiently to rise before the rubber starts to set. After all the bubbles have been removed great care must be used to ensure that no more are introduced by pouring etc. The length of time spent in the vacuum must be kept as short as possible, otherwise the catalyst evaporates away. About one or two minutes was found to be ideal.

An overriding consideration is the curing time, as this governs the speed with which operations need to be performed. It was found that about 1½ hours after the catalyst had been added the viscosity had increased sufficiently to render pouring difficult. A major problem is that "strings" of partially-set rubber can form; these may possibly be caused by the neat catalyst being left too long in contact with the rubber during the mixing stage.

Method of Casting

In view of the short length of permitted handling time it was decided to split up the total quantity of rubber into easily-manageable quantities. In this way many operations could be performed in parallel. The 850 pounds of rubber was divided into twelve lots, and contained in plastic dustbins. Each dustbin could be placed inside a steel vessel for evacuation. In fact the evacuation process governed the timing of the whole operation, since only one dustbin could be accommodated in the vacuum vessel at a time. The overall evacuation process for one dustbin took four minutes. After evacuation each dustbin was allowed to stand for 30 minutes, after which time all the bubbles had risen to the surface. The rubber was poured into the tank down a 45° ramp made of semi-circular section plastic, with rounded ends. In this way the rubber had very little distance to fall, minimising turbulence and bubbles. The whole process of casting, from the catalyst being introduced into the first dustbin, to the last dustbin being poured, took 1½ hours.

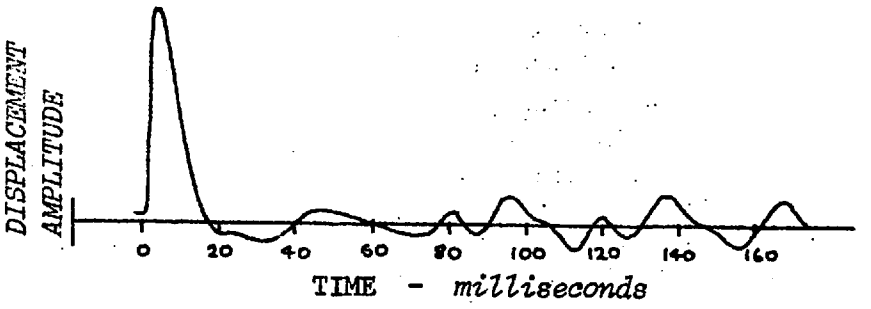

FIG. 4: DISPLACEMENT OF RUBBER SURFACE 2·5 cm FROM THE EXCITATION POINT.
Impulse excitation.

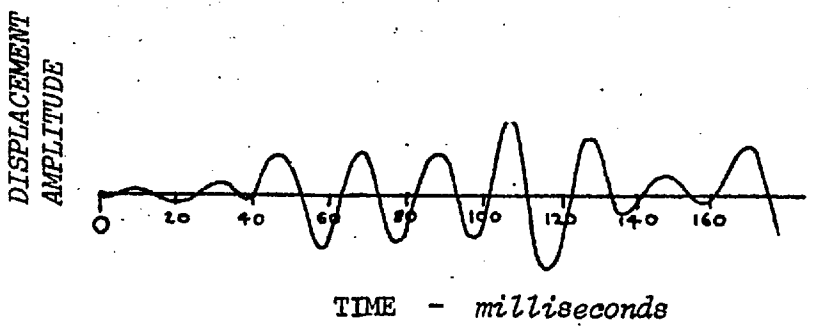

FIG. 5: DISPLACEMENT OF RUBBER SURFACE 10 cm FROM THE EDGE OF THE BOX.
Impulse excitation

G. IN SITU STATIC AND DYNAMIC PROPERTIES OF THE RUBBER & TANK

Plate Load Test

A steel plate of 8cm diameter was placed in the middle of the rubber surface, and loaded with weights. The vertical deflection for various loads was then measured by means of a travelling telescope. There was found to be negligible hysteresis; i.e. the unloading curve corresponded closely with the loading curve. The curve was also essentially linear, with a slope of 8·6 Kg/mm. To ascertain the effects of the boundaries, the test was also performed halfway between the side of the box and the centre. The slope in this case was 10 Kg/mm.

Using the formula $E = \frac{P(1 - \nu^2)}{2r\delta}$, where P=load
δ=deflection
r=radius
ν=Poisson's ratio

$$\text{Young's modulus, } E = \frac{8{\cdot}6 \;.\; 0{\cdot}75}{2 \;.\; 4 \;.\; 10^{-1}}$$

$$= \underline{8{\cdot}1 \text{ Kg/cm}^2}$$

$$= \underline{115 \text{ p.s.i.}}$$

This is somewhat lower than that derived from the test on a sample. The low value might be explained by the fact that the rubber was seen to deform away from the centre of the plate:

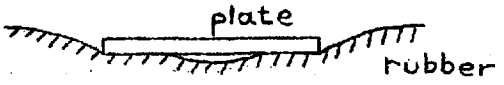

In this case, the deflection would tend to be greater than if the contact were good all over the plate.

Dynamic Tests

Damping

In order to verify if the boundary reflections were of the expected order, a vibrator was set up vertically above the centre of the rubber surface. The vibrator was set to be just clear of the surface, and fed with a short pulse of current. The vertical displacement of the surface of the rubber was measured at a point 2·5cm away from the vibrator application point. The measuring instrument* was of the capacitive type, and had no contact with the rubber (a very thin foil electrode was glued to the surface). The type of trace obtained is shown in Figure 4. The outgoing wave can be seen, as well as numerous subsequent reflected waves. The ratio of the peak amplitude of the outgoing wave to the peak amplitude of the reflected waves is about 7·5. This is rather lower than that calculated previously. The reason for this is probably that the low frequencies generated by box resonances are less damped than those (higher) frequencies which are associated with pit vibrations. This question will be discussed further in the paragraph about frequency response of the box.

* Wayne Kerr. Distance Meter type DM 100 B.

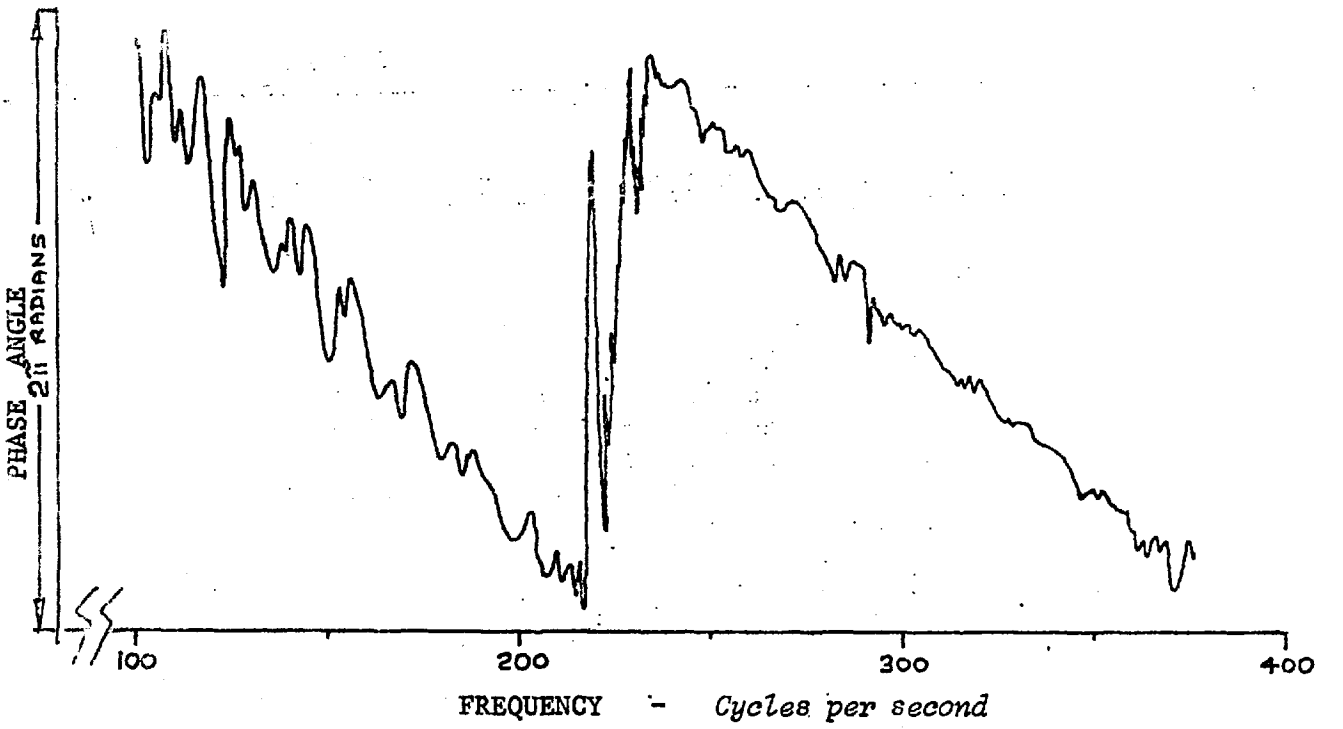

FIG. 6: PHASE VARIATION AT THE RUBBER SURFACE 9·6 cm FROM THE EXCITATION POINT.

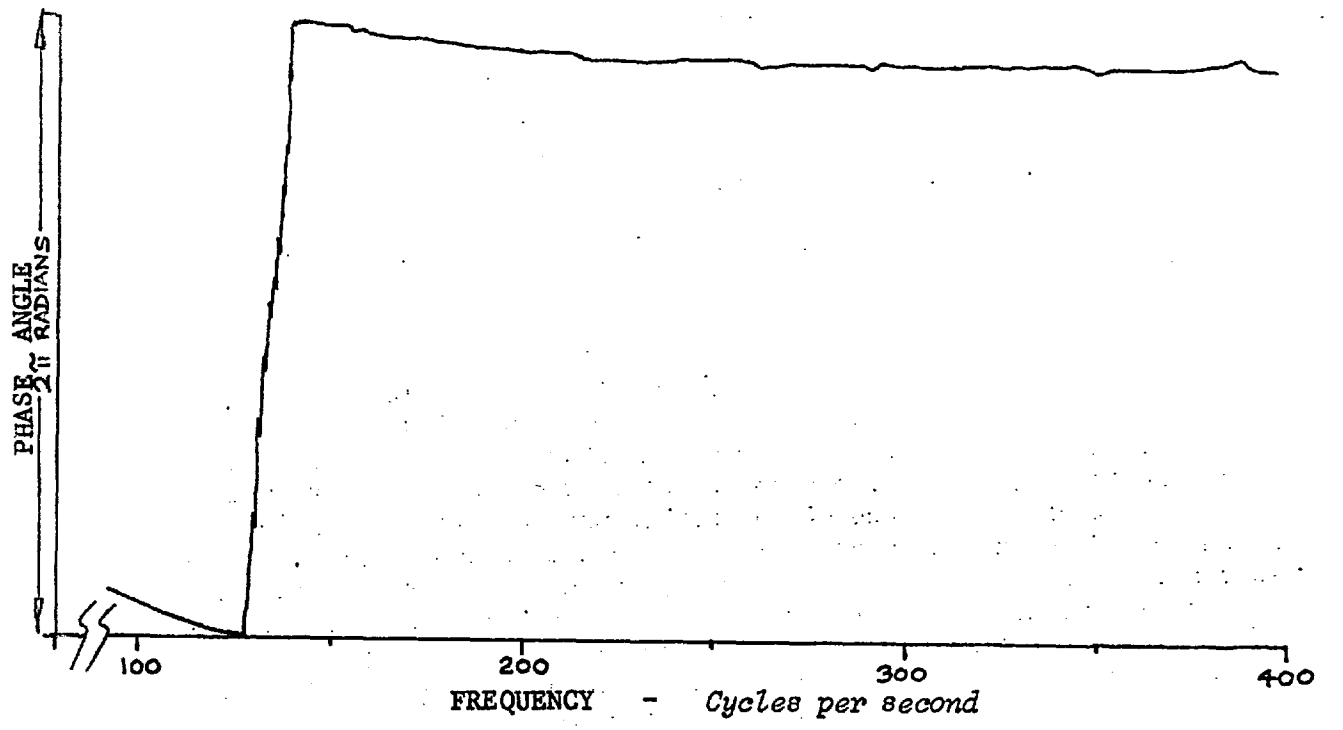

FIG. 7: PHASE VARIATION OF THE VIBRATOR.

Velocity of Propagation

The most common means of measuring the wave speed is to time the interval between a wave leaving one point and it arriving at another some distance away. However in practice the experiment is not so easy to interpret, especially in a situation where dispersion occurs, which means that different frequencies arrive at different time instants. This fact is relevant in the case of the model.

The rubber was again excited by a vertical impulse in the centre, but the displacement was monitored 10cm from the edge of the box. The trace shown in Figure 5 gives the record of displacement. The start of the trace corresponds to the leading edge of the vibrator pulse. It is clearly fruitless to try to deduce an "arrival time" from this trace.

A more practical approach is to measure the phase velocity directly - by measuring the phase difference between source and measuring point. Clearly, if the source is a large distance from the pickup, the phase will change rapidly with frequency. Conversely if the pickup is very close to the source the pickup signal will hardly alter its phase as the frequency is varied. Figure 6 shows the variation of phase with frequency of a point 9.6cm from the vibrator. The phase was measured relative to the vibrator drive voltage. In order to obtain the true phase difference between source and pickup, the phase of the vibrator was measured relative to its own drive voltage, and the curve is shown in Figure 7. It can be seen that the vibrator phase is nearly constant above about 200 c.p.s. The average slope of the phase plot in Fig. 6 is about:

170 c.p.s. for 2π radians phase change

Thus, an increase in frequency of this amount corresponds to the insertion of an additional complete wavelength in the 9·6cm between source and pickup.

$$c = \lambda f$$

$$c = 9{\cdot}6 \;.\; 170 \quad \text{cm/sec}$$

$$= \underline{16{\cdot}3 \text{ m/sec}}$$

$$= \underline{53{\cdot}5 \text{ ft/sec}}$$

This is undoubtedly the velocity of surface Rayleigh waves. It is interesting to note that the peaks and troughs in the phase plot (Fig. 6) represent changes in the velocity of propagation due mainly to resonance effects in the box. In other words, there is significant *dispersion* which accounts for the difficulty in interpreting the transit-time measurements shown in Figure 4. The method used above may be employed to determine the true phase velocity curve in any material that exhibits dispersion.

The velocity of Rayleigh waves may also be calculated from the elastic constants mentioned earlier.

$$E = 133 \text{ p.s.i.}$$

$$\rho = 0{\cdot}98 \;.\; 62.4 \text{ lb/ft}^3$$

The shear modulus, $\mu = \dfrac{E}{2(1 + \nu)}$

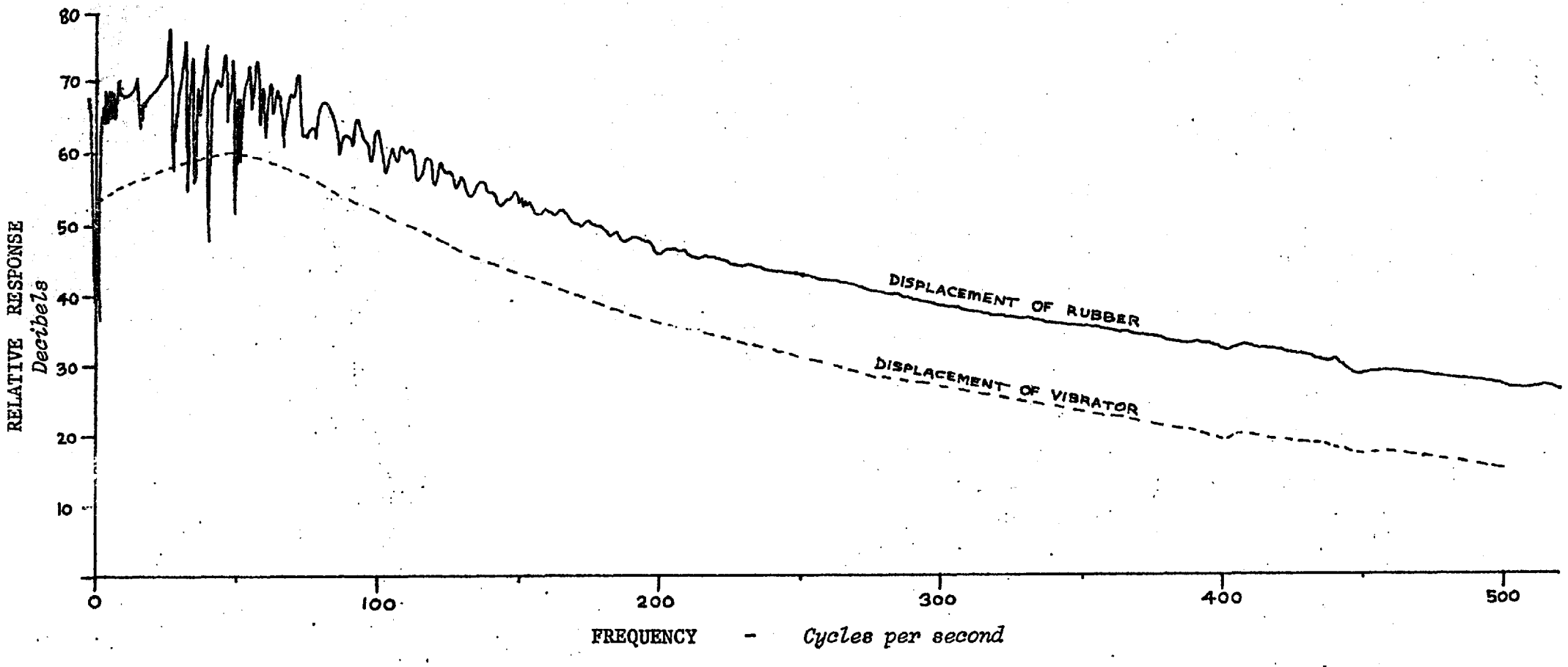

FIG. 8: DISPLACEMENT RESPONSE OF THE RUBBER CONTAINED IN THE BOX.

$$\mu = \frac{133}{2(1.5)}$$

$$= 44.3 \text{ p.s.i.}$$

Velocity of Rayleigh waves

$$= 0.955\sqrt{\frac{\mu}{\rho}} \quad \text{(see Chapter 2)}$$

$$= \underline{55.1 \text{ ft/sec}}$$

$$= \underline{16.8 \text{ m/sec}}$$

This agrees well with the figure derived from the phase velocity tests.

Frequency response of Box

The displacement transducer was positioned 2.5cm from the centre of the surface of the rubber, the vibrator being arranged so as to excite the centre point with a vertical oscillating force. The vibrator was in fact driven by a scanning Wave Analyser*, and the transducer output fed back into the analyser which then acted as a selective filter (bandwidth = 3 c.p.s.). The filter centre frequency was locked to the vibrator drive frequency, so that excellent noise rejection could be obtained.

The output of the displacement transducer as a function of frequency is shown in Figure 8 (upper curve), as well as the displacement characteristics of the vibrator (lower curve) under the same conditions. The two curves should be subtracted to obtain the true response of the rubber block. It should be noted that the vertical scale is logarithmic, being expressed in decibels.

$$1 \text{ decibel} = 20\log_{10}\left(\frac{u_1}{u_2}\right)$$

where $\frac{u_1}{u_2}$ is the ratio of two amplitudes.

The peaks and troughs of the upper curve in Figure 8 correspond to various resonances of the box. A peak in the curve shows that reflected waves are in phase with the exciting waveform, and are adding their amplitudes to it, giving an increased total response. The amplitude of the reflected wave can be found as follows:

$$H = 20\log\left(\frac{u + u_r}{u}\right) \quad \text{where} \quad H = \text{height of peak above mean level in dB.}$$

$$= 20\log\left(1 + \frac{u_r}{u}\right) \qquad u = \text{mean response amplitude}$$

$$\therefore \quad \frac{u_r}{u} = \text{antilog}\left(\frac{H}{20}\right) - 1 \qquad u_r = \text{reflection amplitude}$$

This relation is plotted on the next page:

* General Radio Wave Analyser type 1900.

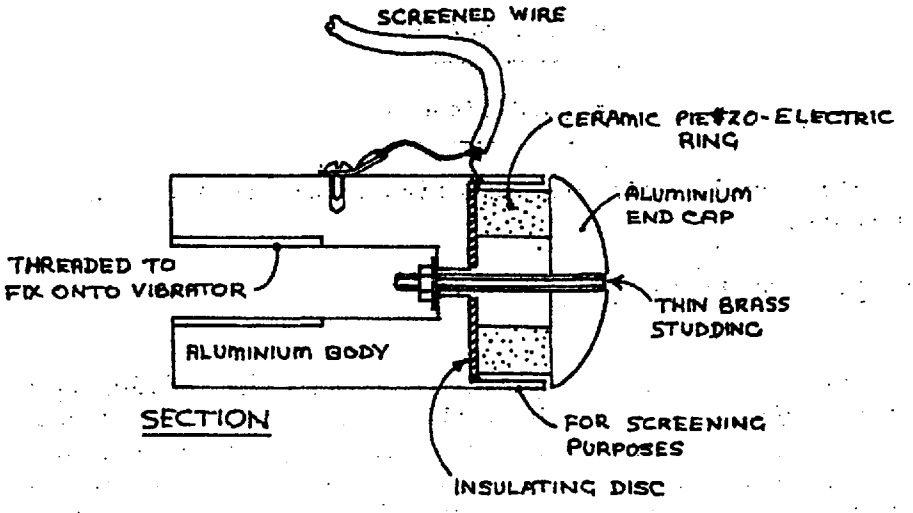

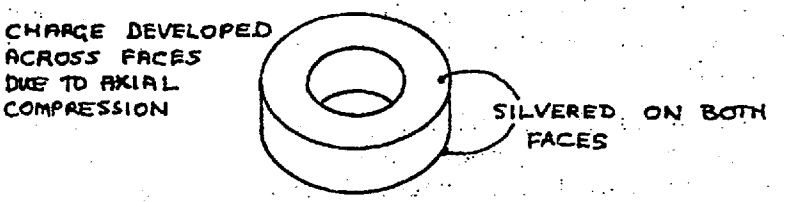

NOTE: the operation of the transducer is based on the fact that the ceramic disc is much stiffer than the brass studding. Thus most of the force is transmitted through the disc.

FIG. 9: TO SHOW THE CONSTRUCTION OF THE FORCE TRANSDUCER

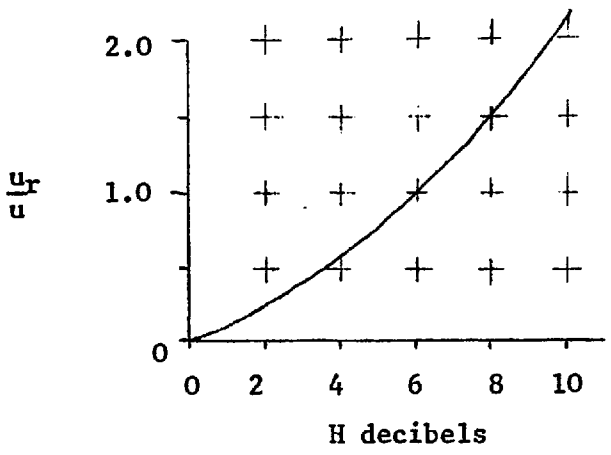

Around 80 c.p.s., the design frequency, the excursions about the mean curve are about ± 2 dB, which implies that the reflections are 0.25 of the outgoing wave. This figure is rather higher than that calculated previously (0.1), but still should enable a reasonable estimate to be made of the pit response, as distinct from the box response. Figure 8 shows clearly how the amplitudes of the reflections decrease with increasing frequency. This is due to more and more complete oscillation cycles being incorporated into the return journey to the reflection surface.

H. RESULTS OF TESTS

Method

A pit of diameter 15cm, base diameter 5cm and slope angle 45° was cut out in the centre of the rubber surface. If a smaller pit was used, the deflections were rather too small to observe easily. It was excited by a point load applied at the pit crest, vibrating at 45° to the horizontal since the dimensions of the vibrator prevented further lowering. The force imparted to the pit by the vibrator was measured by a small force transducer. This was designed so that it contained the very minimum of "dead-mass" - i.e. the mass of the active part of the device, which would cause an output to be given even with no load applied. It is shown in Figure 9. The diameter of the device was 0.5 inches, and it was designed to screw onto the end of the vibrator extension, as shown in several of the previous photographs. The object of using the force transducer was to enable the "magnification factor" of the particular mode of vibration to be found. If, for a given displacement, the force required dropped to, say, one half for a particular frequency, then the displacement magnification factor for a given force would be two.

As the rubber was being vibrated, it was illuminated with stroboscopic light of a slightly different frequency from that of the vibrator. In this way a slow motion image of the movements could be seen.

As the frequency was varied throughout a wide range a surprising fact became evident: there were *no* magnification factors greater than those attributable to box resonances (i.e 1.2 to 1.3). Clearly these factors are of no engineering significance in a mining environment, bearing in mind the variability of other factors involved (e.g. geology, layering, weathering). The dynamic deformation of the rubber surface in fact gave the appearance of distinct modes of oscillation, but could be explained by the diffraction of waves around the surface of the pit. Thus if, at a particular frequency, one side of the pit was moving outwards at the same time as the opposite side, this was an indication of the fact that a phase difference of 360° existed between the two points, and not necessarily that a resonance was found.

In view of the lack of distinct modes to measure, only a short series of measurements were made. The following observations are in order of frequency, the only criterion for inclusion being a visual identification of some identifiable shape of motion, or a force minimum. The arrows show the direction of displacement at one extreme of motion, and the figure give the peak displacements in thousanths of an inch.

47.0 c.p.s. - slight minimum force (less than 5%)

41.9 c.p.s.

Distinct minimum - 10% - probably box resonance, since large displacement extended to the edges.

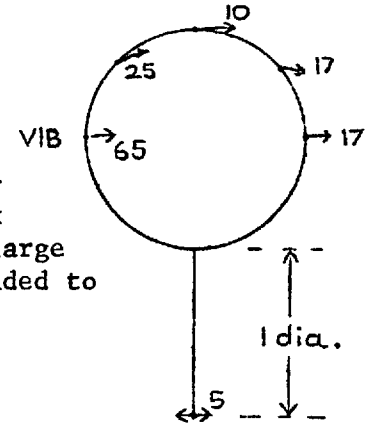

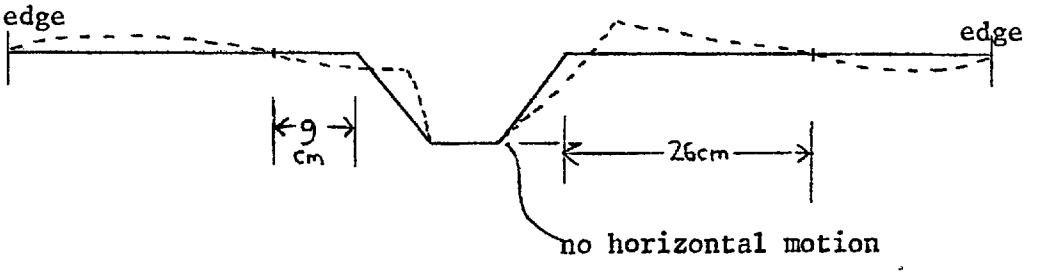

21 ← 5cm from the base

43.2 c.p.s. - no measurable force change

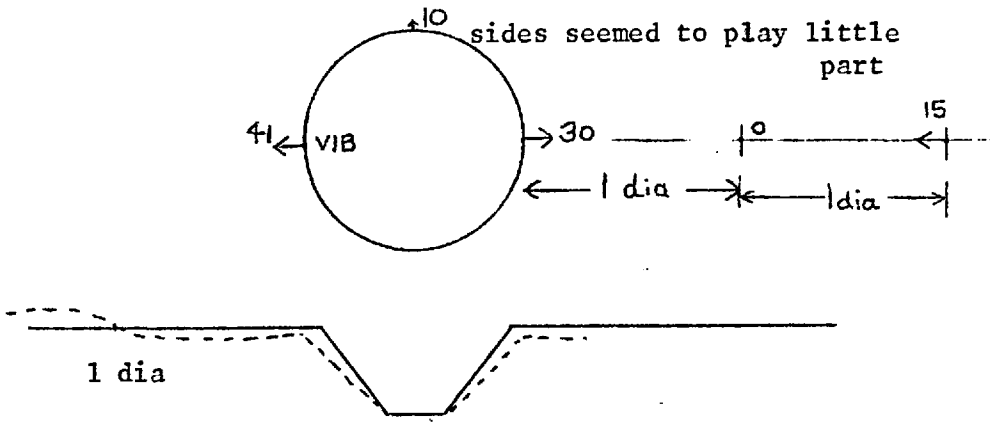

34.6 c.p.s. - strong mode of whole box rocking

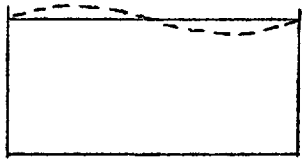

27.8 cps - appeared to be circulating wave fundamental

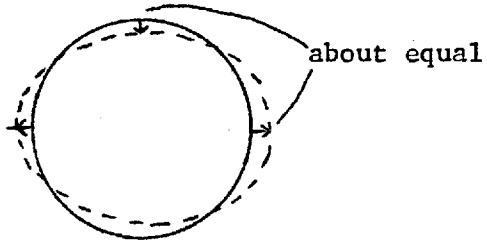

23.4 c.p.s. - uniform translation of whole rubber surface.

Conclusions

The main outcome of the model tests is the fact that no strong modes of oscillation are attributable to the geometry of the open-pit. Had this fact been obvious beforehand, a different approach might have been made with regard to the boundaries, since the boundary reflections were clearly strong compared to the weak pit response. Another fact revealed subsequent to constructing the model was that the components of circulating waves extend to a considerable distance from the source, causing the boundary effects to be increased beyond that calculated from simple reflection considerations. This phenomenon is discussed in Chapter 5 and Appendix II.

There have been several secondary outcomes which may prove of use: a relatively new model material has been tested and evaluated; a means for accurately measuring phase velocity has been demonstrated, and may have application in full-scale tests; a sensitive force transducer has been designed.

REFERENCES

Chapter 3

1. ROSCOE, K.H. "Soils and Model Tests" Journal of Strain Analysis A. V 3, N° 1. Jan 1968.

2. STIMPSON, B. "Modelling Materials for Engineering Rock Mechanics" Int. Jour. Rock Mech. Min. Sci. V. 7. N° 1. 1970.

3. OKAMOTO, S., TAMURA, C., KATO, K., OTAWA, M. "Dynamic Behaviour of Earth Dam During Earthquakes" Report of the Institute of Industrial Science, University of Tokyo. 1966.

4. SEVERN, R.T., SMITH, N.A.F., TAYLOR, P.R. "Theoretical and Rubber Model Studies on Design Shape 1 Arch Dam Under Hydrostatic Load. CERA, TR/AD/4 1965.

Chapter 4

Chapter 4: FIELD TESTS

A. OBJECTS & GENERAL DISCUSSION

B. FREQUENCIES OF INTEREST

C. NATURE OF EXCITATION CAUSED BY BLASTING

D. BOREHOLE ACCELEROMETER UNIT
- The Accelerometer Used
- The Complete Instrument
- The Remote Read-Out Compass
- Frequency Response

E. EXPERIMENTAL SETUP
- Mobile Laboratory
- Power Supplies
- Recording Equipment
- Location of Accelerometers
- Geology

F. RESULTS
- Nature of Blasting at Atalya
- Frequency Analyses and Integration of Records
  - *On The Interpretation of Spectrum Plots*
- The Blast Records
- Interpretation of Results
  - *General Remarks*
  - *Speed of Waves*
  - *Frequencies*
  - *Reflections*
  - *Amplitudes of Motion*
  - *Decay Factors*
- Conclusions

FIG. 1: VIEW ACROSS ATALYA PIT LOOKING EAST FROM THE PORPHYRY TOWARDS THE SLATE. Note the area at the left of the picture consisting of back-fill left by the underground mining.

A. OBJECTS AND GENERAL DISCUSSION

The Mining Industry is a highly practical concern. Ideas generated by Rock Mechanics engineers are likely to be viewed with suspicion unless they can be shown valid in a realistic mining environment. The objects behind the present tests were to determine, both quantitatively and qualitatively, the response characteristics of a large open-pit, to see if the observed characteristics were consistent with the conclusions drawn from the numerical analyses and model studies. By virtue of the sheer size of the pit, and the problems involved in exciting any measurable vibration, the tests performed were not comprehensive enough to give a complete description of all modes of response. The aim was to carry out several representative tests in the hope of verifying some of the major characteristics predicted by the other methods, so that some degree of confidence could be felt when using the methods.

The mine chosen for the experiments was Rio Tinto Espanola's Atalya pit in Southern Spain. The pit is large (700m diameter, 270m deep at the deepest point) and of nearly circular shape, with steep slopes (40 to 50 degrees). In these respects it is almost ideal. There is daily blasting of up to 20,000 cu. metres of rock from the benches: this was used as the excitation, the response of the pit being measured in several places. The instruments used for measuring the dynamic motion were accelerometers, chosen because acceleration is of more use in stability calculations than velocity or displacement. The instruments were specially constructed to lower down boreholes, so that surface effects (such as wind and machinery noise, broken nature of surface rock, air shocks, etc.) could be eliminated. A down-hole pneumatic fixing device was used.

B. FREQUENCIES OF INTEREST

If a large potentially failing mass is considered, it is clear that for the greatest adverse effect, the dynamic accelerations throughout the mass must all act in similar directions, otherwise cancellation would occur and reduce the total force. This implies that the wavelength of the dynamic wave should be of the same order as, or longer than, the dimensions of the failing mass. Assuming dimensions of the failing mass of between 100 and 500 feet, the maximum frequencies turn out as 20 to 100 c.p.s. (for wave speed = 10,000 ft/sec) or 4 to 20 c.p.s. (for wave speed = 2,000 ft/sec).

Another consideration is the time the failing mass will take to respond to the acceleration: if the pulse is too short, the mass will move hardly at all, which may be insufficient to mobilise the peak strength of the failure surface. As an example, consider a block given a pulse of acceleration of "a". The displacement is given by

$$d = \tfrac{1}{2}at^2$$

The time duration of the pulse will be inversely proportional to the frequency of the wave, i.e. $t = \frac{k}{f}$

$$\therefore d = \frac{mak^2}{2f^2}$$

In view of this, the lower frequencies will be much more likely to cause failure than the higher ones, other things being equal.

Hence the frequencies which might be expected to cause large-scale failure should lie in the range below, say, 30 c.p.s. The investigation of the response of the Atalya open-pit was limited to that range. It is true that blasting generates a good deal of energy at high frequencies (100 to 1000 c.p.s.), but this is severely attenuated by the rock, and should only cause fairly local failure inview of the above arguments.

C. NATURE OF EXCITATION CAUSED BY BLASTING

On the face of it, a blast is a complex stimulus, with separate wave-trains spreading out from each shot hole and often complicated by millisecond delays between shots. It may be possible to evaluate the contribution of all the waves, and sum them to give the total dynamic flux released into the rock as a function of time. However, it is much simpler to consider, not the waves propagated into the body of the pit, but to assess the momentum given to the rock blocks thrown off the pit face. The mass of rock blasted off is accurately known from the shot hole geometry, and the average velocity which is given to it can be assigned a reasonable value from measurements taken from cine-films, etc. Thus the momentum, MV, is known.

However, MOMENTUM = IMPULSE
MV = Pt

The average force, P, is required, so that an estimate of the time, t, needs to be made. This can be taken as the total duration of the blast (i.e. the total delay period). In other words, a reasonable estimate of the force imparted to the rock can be made. In many instances only the Impulse needs to be known, so that the time duration of the blast is immaterial.

Due to the fact that the effective force due to blasting is generally of short duration compared with the frequencies associated with the response of the whole pit, the blast may be treated as an impulse with zero time duration. The maximum total delay period used at Atalya pit was about 0.1 sec for a very large blast (i.e. the separate shots were spread over a period of 0.1 sec.). Thus, compared with frequencies of around 1 c.p.s., the blasting force would appear to be a short impulse, but with frequencies of 10 c.p.s., the time duration of the pulse would need to be taken into account. However, most of the blasts had much shorter total delays, especially the small 'tidying-up" shots fired by Cordite, which were instantaneous.

It should be noted that if a frequency analysis is performed on an infinitely sharp impulse, it is found to contain all frequencies from zero to infinity with equal amplitudes. In a less-sharp impulse, the higher frequencies in the spectrum are attenuated. A blast can be seen as an efficient means of exciting a large number of response modes.

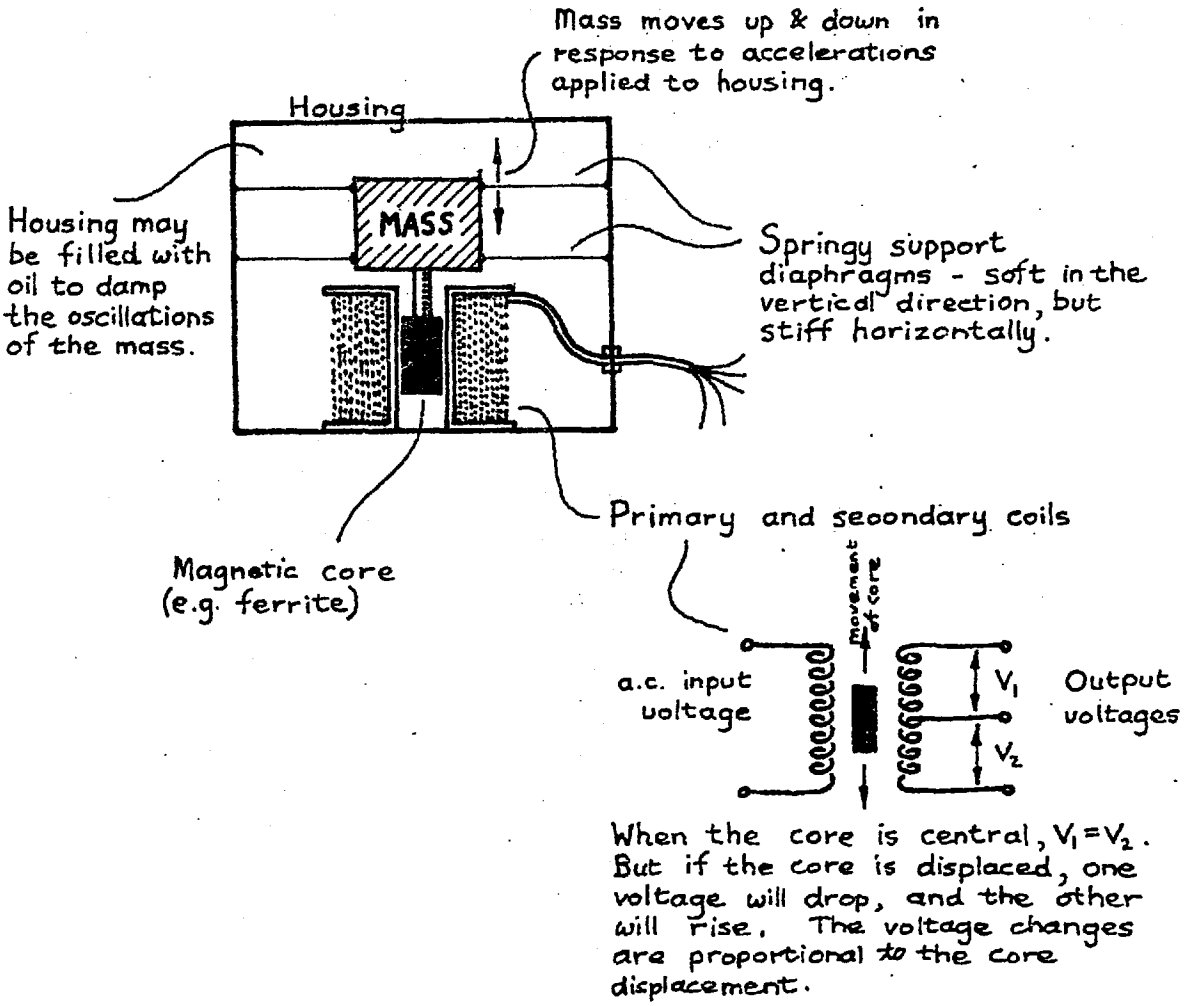

NOTE: If the frequency of acceleration applied to the housing is well below the resonant frequency of the mass/spring system, then the displacement of the mass will be proportional to the acceleration. Used in this mode, it is a true accelerometer.

FIG. 2 TO EXPLAIN THE ACTION OF A TYPICAL L.V.D.T. ACCELEROMETER.

D. BOREHOLE ACCELEROMETER UNIT

As mentioned previously, the object in placing the vibration detecting device down a borehole was to eliminate:

(i) the effects of a weak, broken surface layer,
(ii) the air-bourne noise of machinery, wind, rain,
(iii) the air pressure-wave from the blast, which can confuse the record, if the blast is close.

An earlier experiment, with a surface-mounted accelerometer had indicated the need for a borehole device.

The instrument housing was initially designed to be capable of measuring the high frequencies found very close to a blast, so that the construction was exceptionally rigid, and in fact had a flat response to at least 2.5 Kc/s. In this application ceramic piezo-electric accelerometers were used, with resonant frequencies of 35 Kc/s*. These devices are extremely rugged, and permit accurate measurements of accelerations below 0.001 g, using suitable amplifiers.

The Accelerometer Used

In the present application however, the need was for a device to measure accelerations in the range 0 to 30 c.p.s. The piezo-electric transducer can be made to respond to these frequencies simply by connecting it to a very high resistance amplifier. With an input resistance of 10,000 MΩ (easy to obtain, using field-effect transistors), the typical lower cut-off frequency is 0.01 c.p.s. However, they are exceptionally sensitive to changes in temperature, which register as an equivalent acceleration. The output drift, even when the device is thermally insulated, turned out to be unacceptable when measuring low accelerations (0.001 g). Consequently an L.V.D.T. (Linear Variable Differential Transformer) accelerometer was used. These have a true zero frequency response, in that they can measure the static acceleration due to gravity. The essence of the construction is shown in fig 2 . The particular model used** had a resonant frequency of 35 c.p.s. so that its response was essentially flat up to 25 c.p.s. The device needs a driving oscillator and demodulator to provide a voltage output proportional to acceleration: a commercially available unit was used†, specially modified to operate from a 24 volt power supply so that it could conveniently be used in the field. With this setup, and with realistic lengths of cable, it was found that the overall noise level was equivalent to about 0.001 g, so that 0.005 g could be detected with confidence.

---

* Enviromental Equipments Ltd. Type AQ40
** Electro-Mechanisms Ltd. Type MEM 3G
† Electro-Mechanisms Ltd. Type CAS 2500Z 24 volt.
†† "Hellashrink" sleeving from Hellerman Ltd.

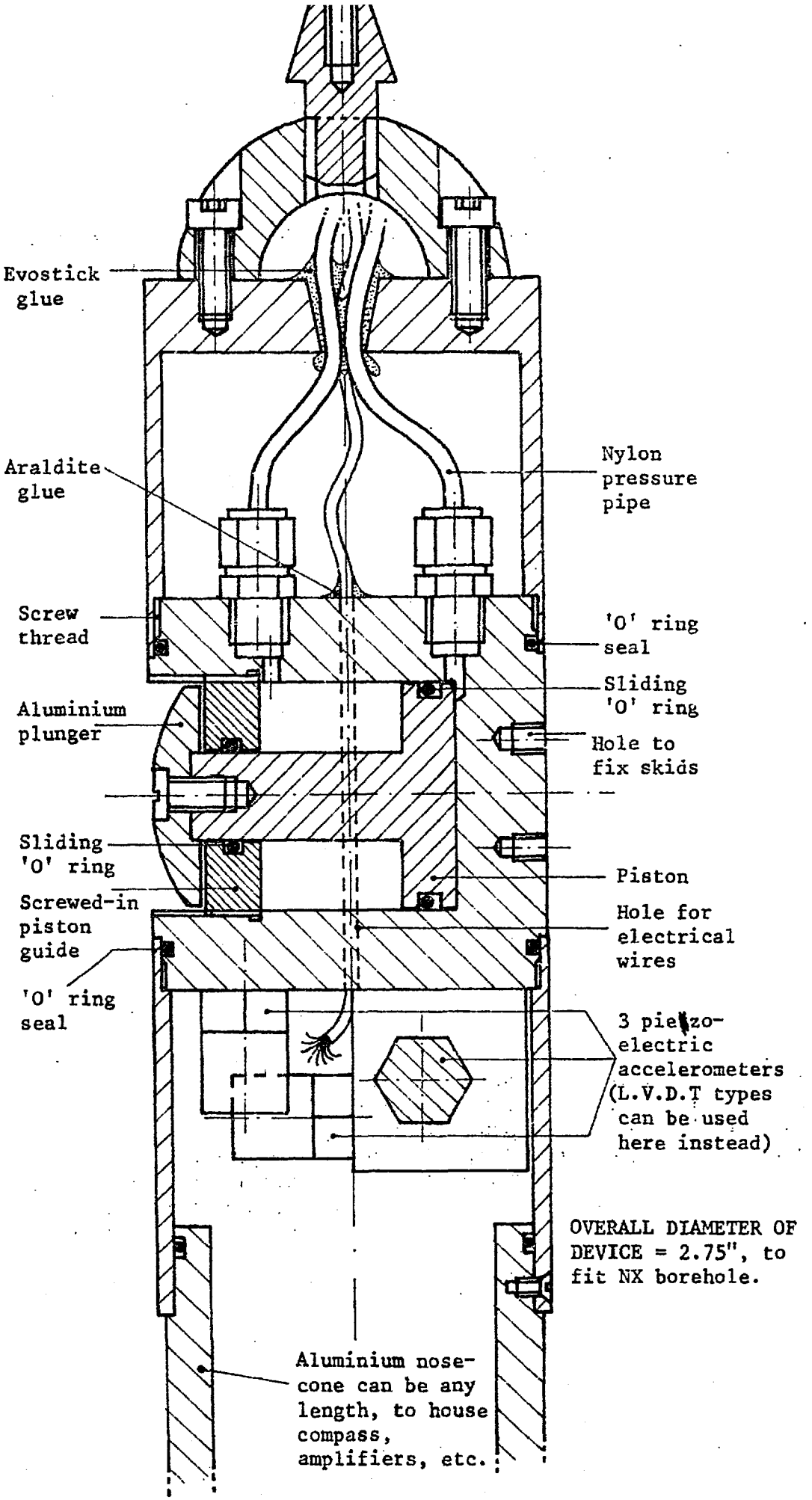

FIG. 3 SECTION THROUGH BOREHOLE ACCELEROMETER DEVICE
All materials stainless steel, except where otherwise stated. DRAWING FULL SIZE.

The Complete Instrument

The housing for the accelerometer is shown opposite in fig. 3 . There was in fact provision for a three-dimensional accelerometer array, but due to lack of tape-recorder channels, only one accelerometer was used down each hole. The whole unit was made from stainless steel, except for the nose-cone and plunger which were made from aluminium. The fixing piston could be both ejected and withdrawn by air pressure. The maximum pressure that was tried was 600 p.s.i., which corresponds to about ½ ton force exerted by the piston on the side of the borehole. The piston was in fact capable of crushing small rocks that might get wedged behind the plunger. There was provision for fixing two skids on the opposite side of the instrument from the piston, in order that the unit could be used in different-sized holes. The design hole was NX.

The cable was made up of four parts: two pressure tubes (Nylaflow nylon tube, S.W.P. 700 p.s.i.), one multi-way screened electrical cable and one stainless-steel tension wire for support. The whole group was tightly enclosed by a heat-shrinking sleeving†† which provided a tough, abrasion-resistant outer covering.

"O"-ring seals were used at all joints in the instrument casing, so that it could be used under water. The electric cable was sealed at two points with epoxy resin and "Evostick" glue.

A compass device was made, but not in fact used, since it turned out that most of the boreholes had to be cased with steel tubes to prevent collapse. However, a brief description follows, since it may be of use in other applications. In fact, the orientation was determined by reflecting the sun's rays down the borehole with a mirror to illuminate the top of the instrument, and a visual sighting obtained. The method worked well to at least 30 metres down a hole (so long as the sun was shining!).

The Remote Read-Out Compass

The requirement was that the borehole accelerometer could be orientated in a given direction with respect to the open-pit. This simplified the design of the compass unit, as the read-out could be of the "yes-no" type. In other words, when the accelerometer was pointing in the correct direction, an affirmative signal would be sent to the surface. In fact three signals were used in practice, to indicate if the accelerometer lay within three sectors, each corresponding to a different degree of precision. The first sector was easy to locate, covering a 90 degree arc about the desired direction. The second and third were progressively narrower. The construction of the unit is explained in fig. 4 . Of course, a compass orientating device is only accurate if no magnetic disturbances exist near the borehole. In an attempt to overcome these difficulties, experiments were carried out with gyroscopes, but it was concluded that a sufficiently accurate device would need to be made to a high degree of precision, rendering the cost prohibitive.

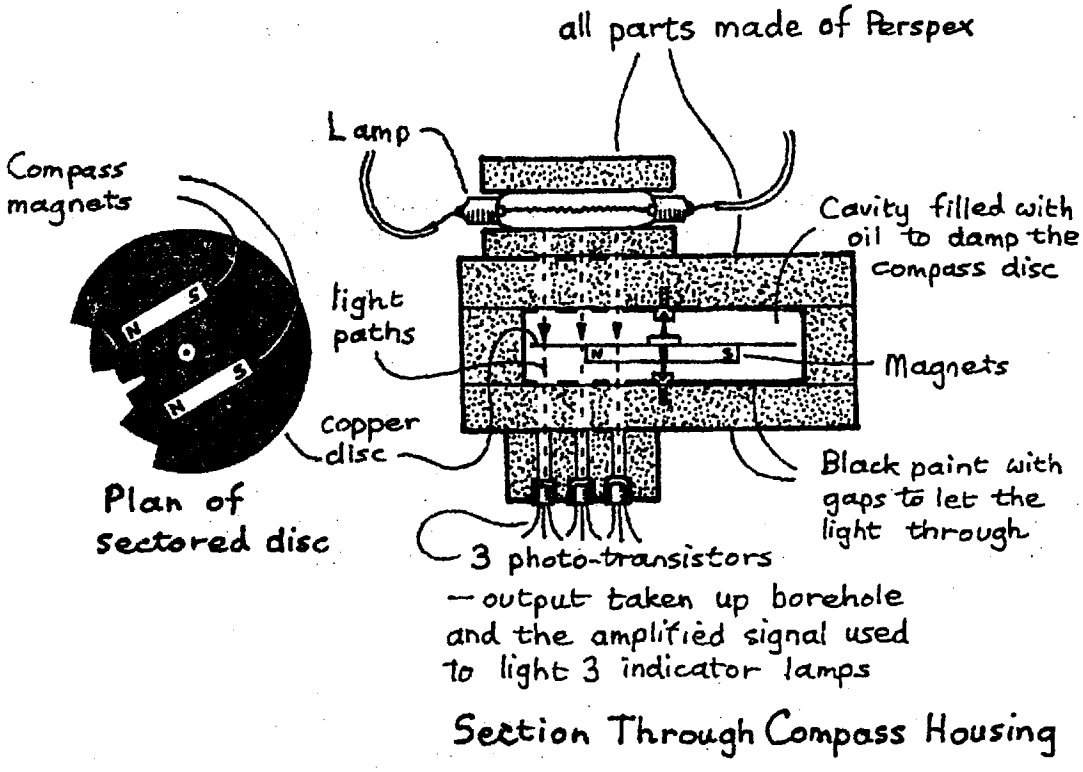

FIG. 4 THE CONSTRUCTION OF THE REMOTE READ-OUT COMPASS UNIT.

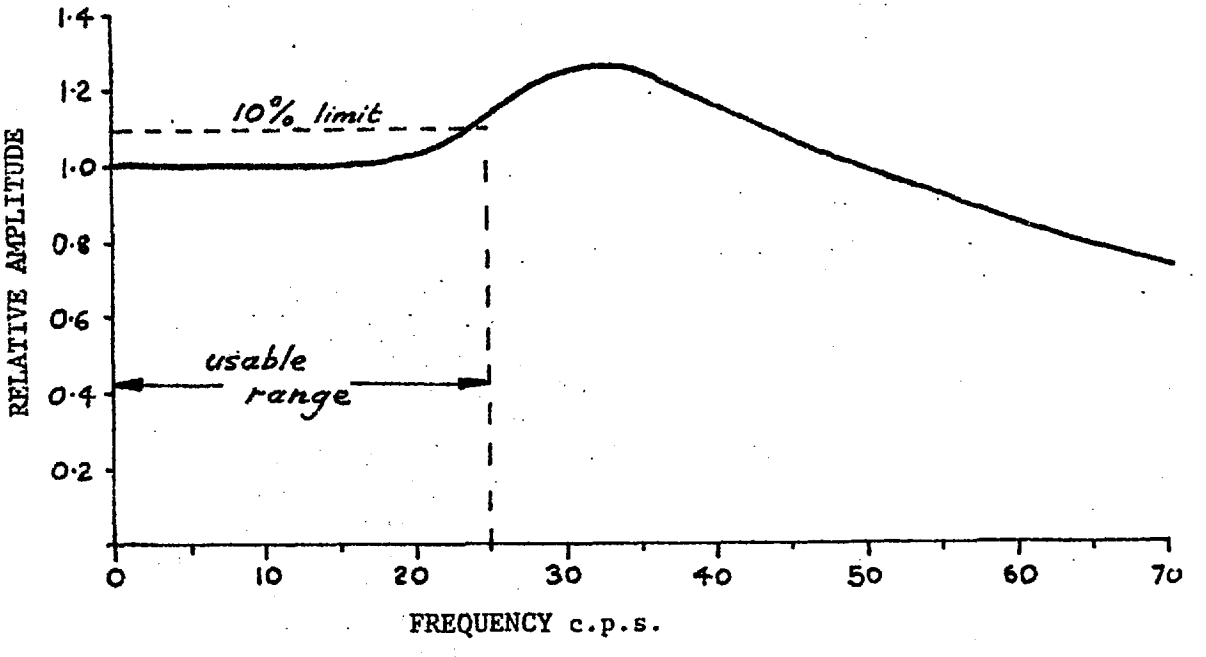

FIG. 6 FREQUENCY RESPONSE OF COMPLETE ACCELEROMETER SETUP.

Frequency Response

The whole instrument was clamped inside a hole drilled in a block of rock, and the complete block vibrated. The frequency response is given in fig. 6. The acceleration of the block was kept constant by monitoring it with a piezo-electric accelerometer which could be assumed flat up to at least 15 Kc/s (resonance= 35 Kc/s), and with a low frequency cut-off at 0.01 c.p.s.

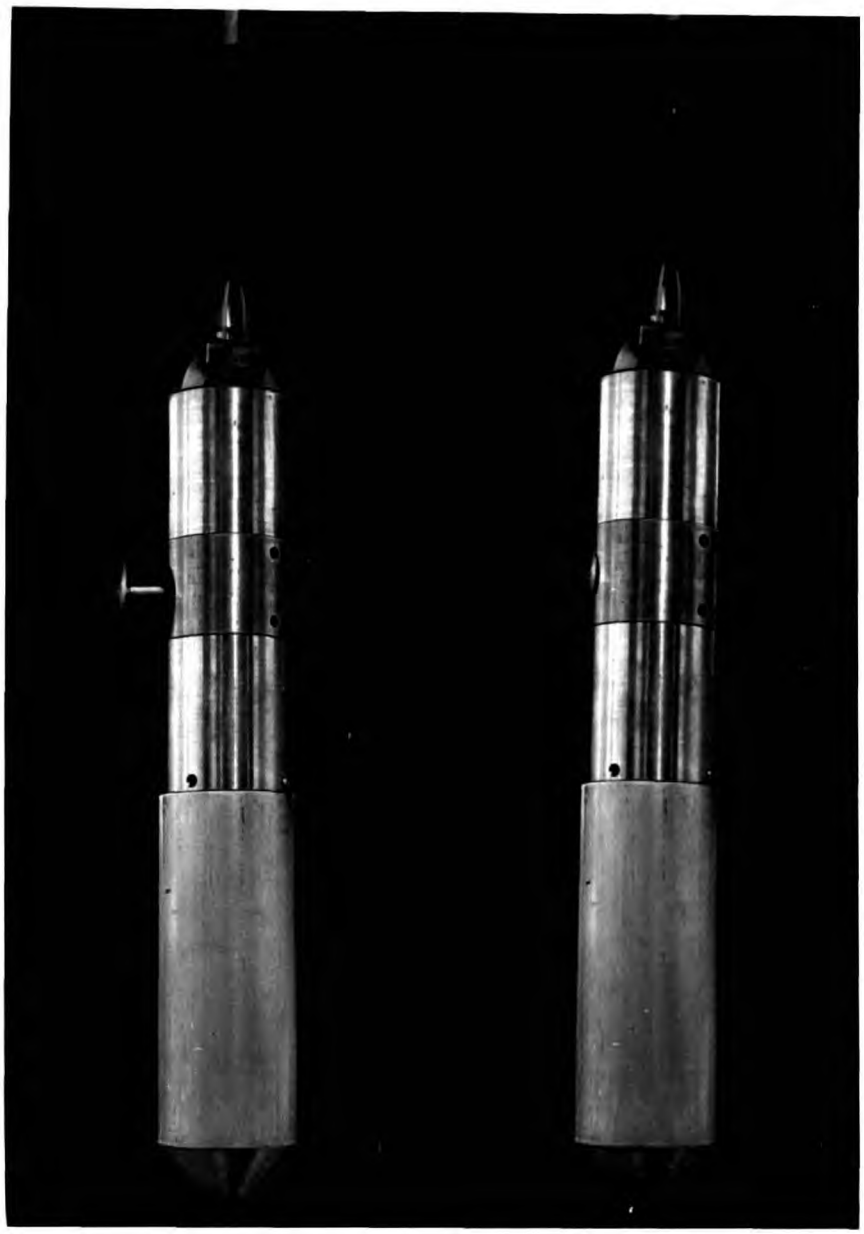

FIG. 5 THE BOREHOLE ACCELEROMETER DEVICE, WITH PLUNGER BOTH EXTENDED AND WITHDRAWN.

FIG. 7: GENERAL VIEW OF THE TRUCK IN THE FIELD

FIG. 8: TILTING TEST PERFORMED ON THE TRUCK: the photograph shows it on the point of toppling.

E. EXPERIMENTAL SET-UP

Mobile Laboratory

The truck shown in fig. 7 was acquired for exceptionally low cost, being an ex- Air Force crash rescue ambulance with four-wheel drive. It may look unstable, but in fact has a toppling angle of 35 degrees (fig. 8). The vehicle proved ideal, having high headroom, good traction and rugged construction.

Power Supplies

One of the requirements of the experiment was that the recorded frequencies should be as accurate as possible. The accuracy depends on the speed of the tape recorder motors, which in turn depends on the frequency of the mains supply. In view of this, the main power supply was an accurate solid-state inverter* producing 240 volts A.C. 300W 50 c.p.s. from 24 volts D.C., with a frequency stability of 0.1% under all conditions of load and input. Four heavy duty 6 volt lead-acid batteries provided the D.C.

Recording Equipment

In the light of previous experience, it was decided that all signals must be tape-recorded. Of course, a more direct method is to record the signals as they arrive, on some form of chart recorder, but one drawback is that vast quantities of paper are produced if the exact time of the event is unknown in advance. (In the present experiment the uncertainty was $\pm$ 20 minutes).

Due to the low frequencies being observed, an F.M. (Frequency Modulation) tape recorder was essential: this type of recorder is capable of recording a static voltage. However, F.M. recorders are expensive, and it was only possible to buy a four channel instrument**. Although the recorder was accurate when it worked, it was cheaply constructed, and could generally be relied upon to have up to two channels inoperative at any one time. With this in mind, it was only attempted to record one channel from each accelerometer unit; the accelerometers were invariably orientated horizontally, sometimes directed into the pit and sometimes at a tangent to it.

The experimental set-up is shown in fig. 9. It can be seen that batteries were used at the top of the borehole to power the demodulators, since it was found in the field that the demodulators went unstable if their power leads ran close to their output leads for some distance.

Location of Accelerometers

The Atalya open-pit is roughly in the form of an ellipse. The original idea was to have four boreholes, two on each axis of the pit close to the perimeter, and measure the accelerations at any two locations. A complete picture of the pit response

* Advance Electronics Ltd. 300W Sine Wave Inverter
**Thermionic Products Ltd. type T3000, 4 Channel F.M.

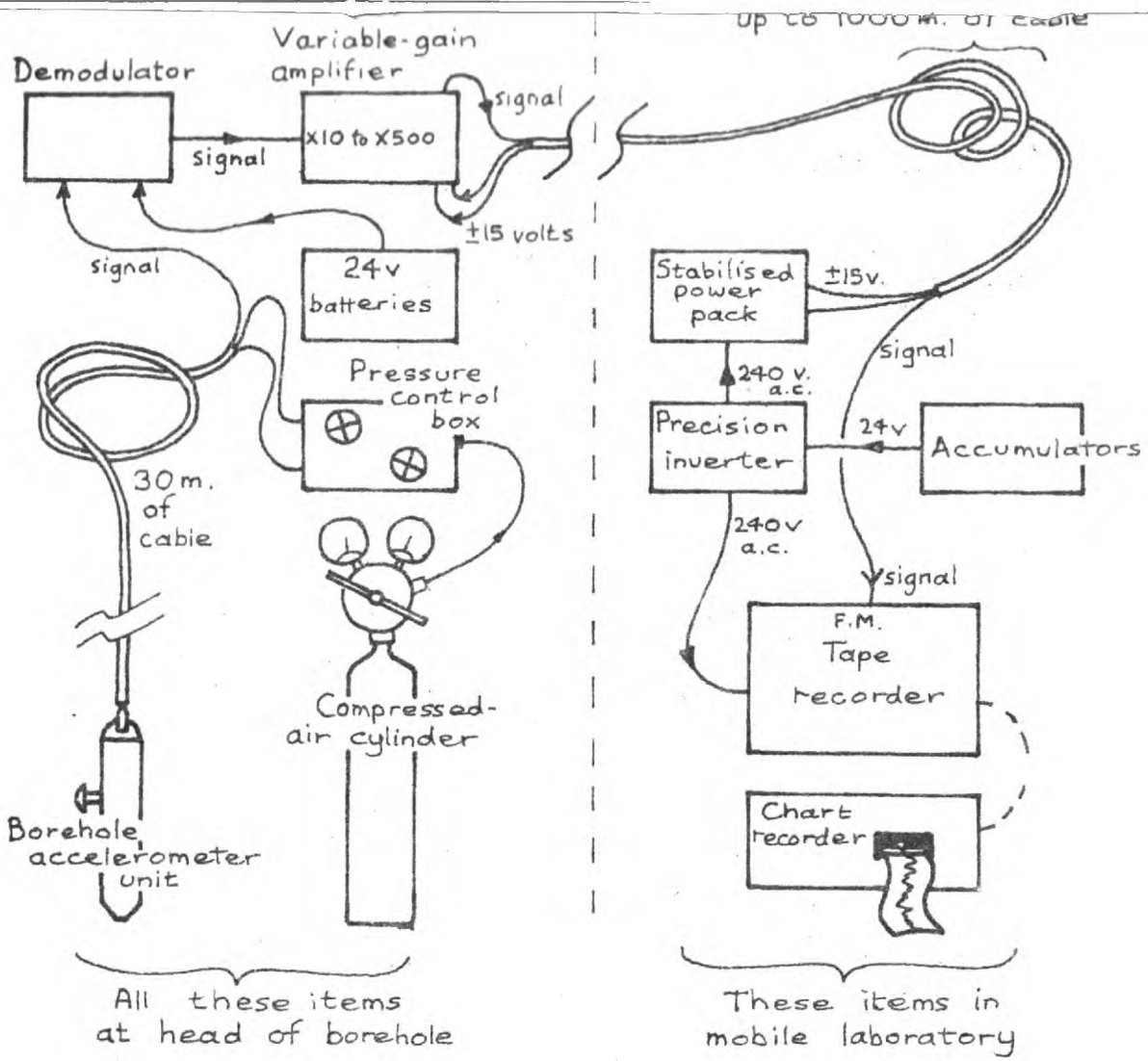

FIG. 9 DIAGRAM OF EXPERIMENTAL SETUP.

FIG. 10 EXPERIMENTAL SETUP ON SITE

could obviously not be built up from such a small number of observation points, but a considerable advantage lay in the fact that the excitation points (blasts) occurred at arbitrary points all over the pit. It was hoped that the "mode-shapes" of the pit when oscillating could be inferred by comparing the phases of the records of two accelerometers located at different points. However, a practical difficulty prevented this, as it was found that long lengths of cable picked up *magnetic* induction from nearby power lines and iron pipes, in spite of great precautions being taken over electrostatic screening. This pick-up was sufficient to swamp any signal, so that only one accelerometer could be monitored at one time, with the truck parked close by. The results were still believed to be valuable, affording a practical comparison, both quantitative and qualitative, with the results from both the model and computer studies. The quantities which could be compared were: predominant frequencies; levels of acceleration resulting from various blasting intensities; variation of predominant frequencies with depth of blast in pit; phase relationship between various frequencies; decay factor of oscillations.

Due to the slowness of the drilling crew, only three boreholes were completed on time. The location of these holes is shown in fig. 11, as are the location of the blasts that were monitored. The numbers correspond to the records discussed later on. The depth of the boreholes was 30 metres, but the accelerometers were positioned at varying depths (usually 15m), due to various circumstances.

Geology

Obviously the optimum geological environment for the present experiments would be an infinite half-space containing one rock type with uniform properties at all points within the mass. Any departure from uniformity in terms of varying rock types, or layering, may result in reflections, or other effects, which would tend to obscure the geometric effects of the open-pit. Unfortunately the Rio-Tinto area is complicated by a number of different rock types, but these are well-defined, so hopefully the reflection effects may be distinguished from the geometric effects. The geology of the area is shown in fig. 12, and a cross-section of the rock surrounding the open-pit in fig. 13. These maps are taken from D. William's' paper (ref.1). It can be seen that there are two main types (porphyry and slate), and bands of these run in an East-West direction. Fig. 12 only shows the local region around the pit, but in fact the bands extend in a similar fashion to at least five pit diameters on either side. Another prominent feature is the fault running roughly North-South; this dips steeply to the East. The reason for the Mine's existence is the large deposit of Pyrites located at the contact between slate and porphyry.

It would seem likely that any reflection of dynamic waves from the pit would most probably arise from one or other of the slate/porphyry contacts to the North or South of the pit. The fault would probably not give rise to any significant reflection of long waves, since the lengths of slate/porphyry contact are only short.

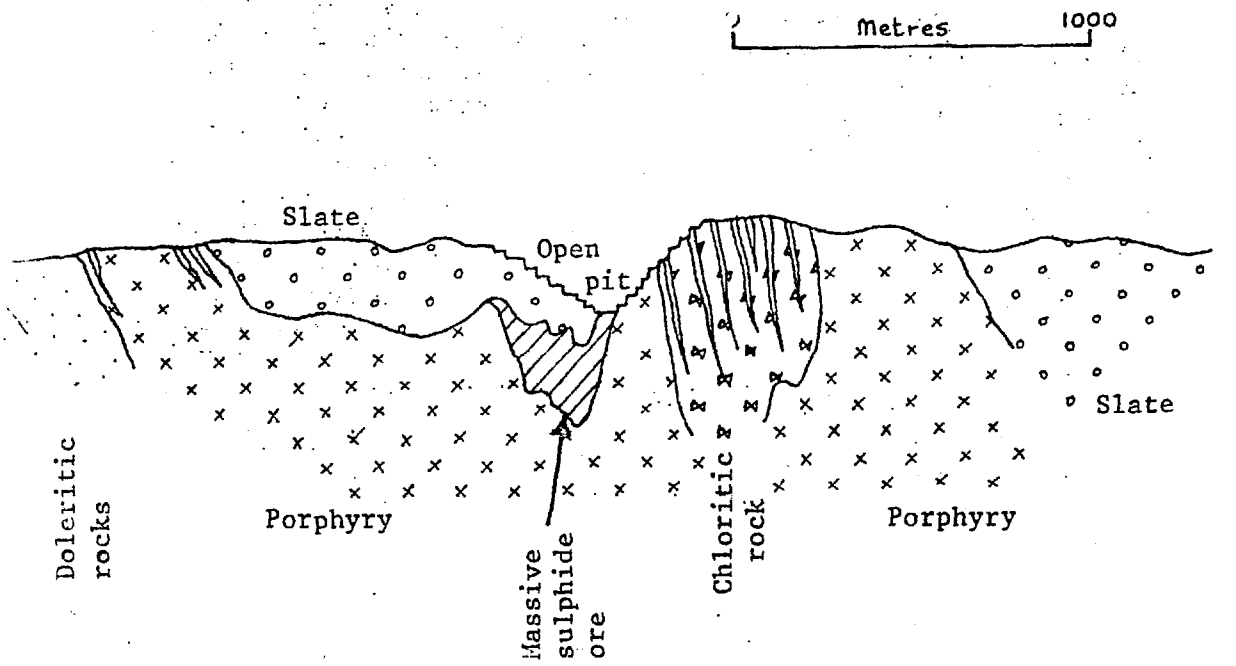

FIG. 13: GEOLOGICAL SECTION ALONG LINE A-B OF FIG. 12

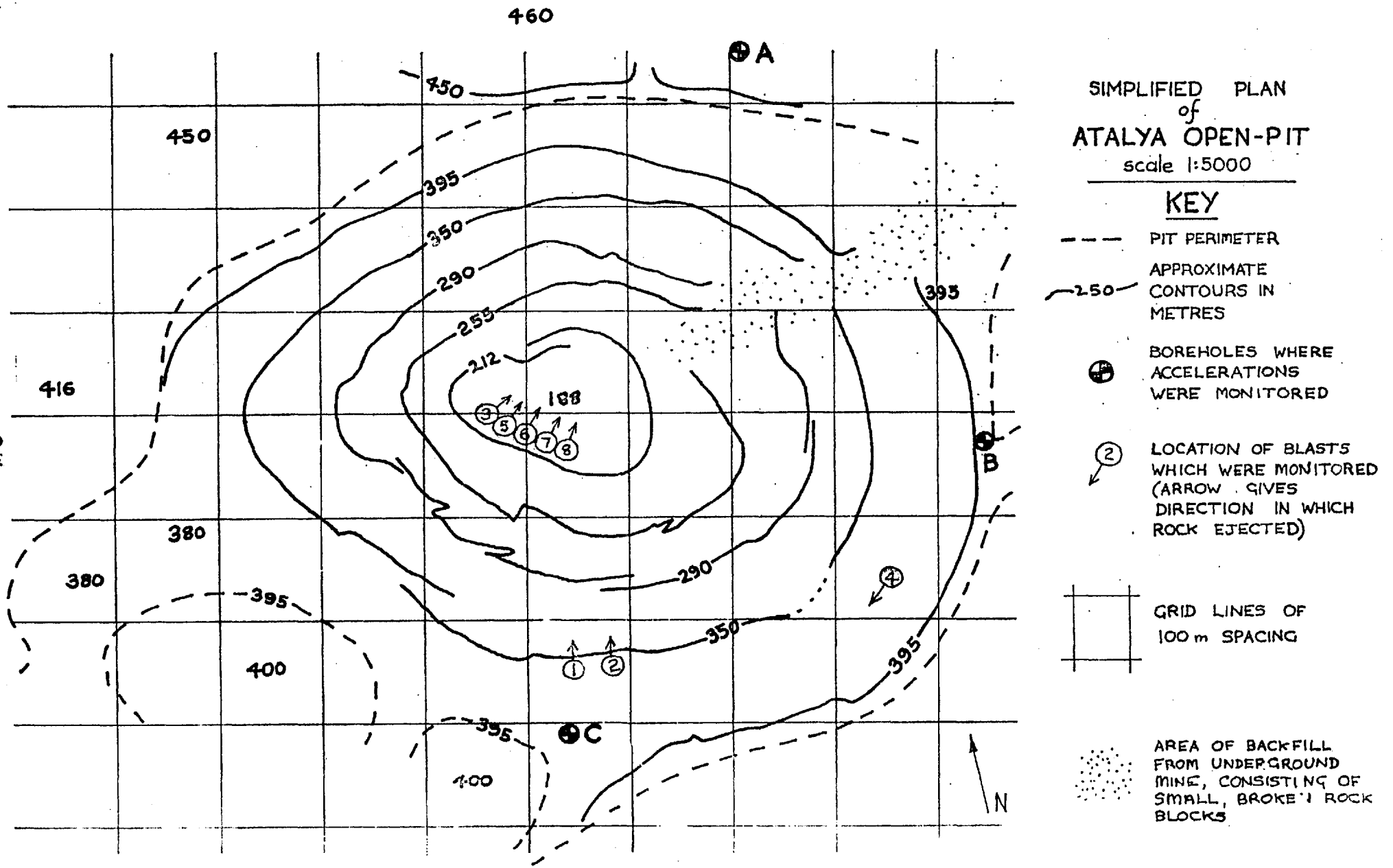

FIG. 11: PLAN OF ATALYA OPEN-PIT

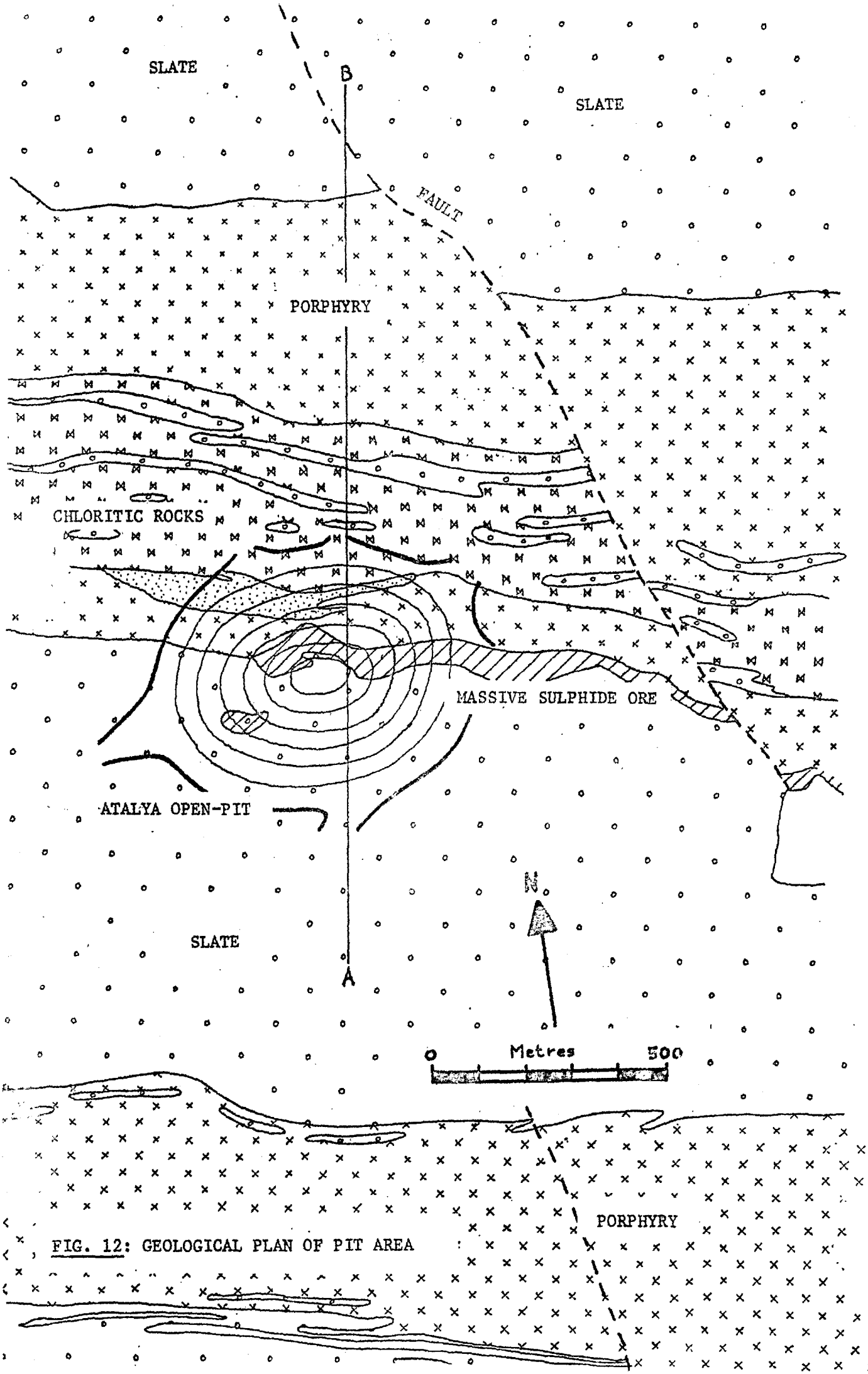

FIG. 12: GEOLOGICAL PLAN OF PIT AREA

F. RESULTS

Nature of Blasting at Atalya

Blasting occurred every day at Atalya, but there were two types of blast, only one of which was really useful for the present experiment. The useful blasts were designed to remove substantial parts of benches, and generally involved several thousand tons of rock. They were set off electrically, and usually incorporated several delays between sets of shot holes. The quantity of rock removed was accurately known since the rotary-drilled holes were carefully positioned so that the volume of rock could be calculated to ensure that the correct quantity of explosive would be used. The other type of blast was used for tidying-up purposes and breaking up ore. The holes were percussion-drilled at essentially arbitrary locations, the explosive being set off with Cordite fuses having no delays. Unfortunately, there was generally only one of the large type of blast per day, and sometimes none.

A large number of small blasts were let off deep down in the pit for the purpose of removing ore. The location of these blasts was not known accurately; therefore the positions given for the deep events on fig. 11 are only approximate.

The records given here represent only about half the events recorded, since duplication occurred when a number of events came from the same location; also for some records there were factors which threw doubt on their validity, such as electrical noise. As a matter of interest it was found that if two blasts were let off very close together, and monitored at the same point, the two records were almost identical.

Frequency Analyses and Integration of Records

In four cases, the acceleration records were integrated to give velocity and displacement curves, and full frequency analyses were performed on the records.

The acceleration records were converted into digital form for use in a computer by means of a digitizing table and card punch. The accuracy of this method was assessed by comparing the computer plots from several digitizations of the same record. The differences were found to be negligible in comparison with the other errors about to be discussed. Given an acceleration record, it is extremely difficult to say exactly where the zero line lies, especially if there is some background noise. Even a very small error in the zero level will be amplified out of all proportion when the acceleration record is integrated twice to give displacement. A similar effect occurs if the acceleration record has a slight overall tilt. The net result of these errors is to yield a finite value of displacement, and possibly a residual velocity, after the dynamic motion has died away. Of course there may in actual fact *be* some residual displacement after a blast, although clearly the velocity must reduce to zero. For the sake of uniformity in all the results to follow, the tilt and zero level of the acceleration records were adjusted so that the final values of displacement and velocity were zero. In some cases this leads to strange-shaped velocity and displacement curves, but attention should be focussed on the high-frequency components, since the low-frequency components will be

F. RESULTS

Nature of Blasting at Atalya

Blasting occurred every day at Atalya, but there were two types of blast, only one of which was really useful for the present experiment. The useful blasts were designed to remove substantial parts of benches, and generally involved several thousand tons of rock. They were set off electrically, and usually incorporated several delays between sets of shot holes. The quantity of rock removed was accurately known since the rotary-drilled holes were carefully positioned so that the volume of rock could be calculated to ensure that the correct quantity of explosive would be used. The other type of blast was used for tidying-up purposes and breaking up ore. The holes were percussion-drilled at essentially arbitrary locations, the explosive being set off with Cordite fuses having no delays. Unfortunately, there was generally only one of the large type of blast per day, and sometimes none.

A large number of small blasts were let off deep down in the pit for the purpose of removing ore. The location of these blasts was not known accurately; therefore the positions given for the deep events on fig. 11 are only approximate.

The records given here represent only about half the events recorded, since duplication occurred when a number of events came from the same location; also for some records there were factors which threw doubt on their validity, such as electrical noise. As a matter of interest it was found that if two blasts were let off very close together, and monitored at the same point, the two records were almost identical.

Frequency Analyses and Integration of Records

In four cases, the acceleration records were integrated to give velocity and displacement curves, and full frequency analyses were performed on the records.

The acceleration records were converted into digital form for use in a computer by means of a digitizing table and card punch. The accuracy of this method was assessed by comparing the computer plots from several digitizations of the same record. The differences were found to be negligible in comparison with the other errors about to be discussed. Given an acceleration record, it is extremely difficult to say exactly where the zero line lies, especially if there is some background noise. Even a very small error in the zero level will be amplified out of all proportion when the acceleration record is integrated twice to give displacement. A similar effect occurs if the acceleration record has a slight overall tilt. The net result of these errors is to yield a finite value of displacement, and possibly a residual velocity, after the dynamic motion has died away. Of course there may in actual fact *be* some residual displacement after a blast, although clearly the velocity must reduce to zero. For the sake of uniformity in all the results to follow, the tilt and zero level of the acceleration records were adjusted so that the final values of displacement and velocity were zero. In some cases this leads to strange-shaped velocity and displacement curves, but attention should be focussed on the high-frequency components, since the low-frequency components will be

largely a function of the integration process. In fact it was found that the effect of altering the zero and tilt of the acceleration records was to modify only the region of the frequency plots from zero to one cycle per second.

The frequency analyses were performed by numerically evaluating the Fourier Transform of the records, i.e:

$$F(\omega) = \int_{-\infty}^{+\infty} e^{-i\omega t} f(t)\, dt$$

where ω ($= 2\pi f$) is the angular frequency
$F(\omega)$ is the Fourier Transform
$f(t)$ is the amplitude of the wave as a function of time.

In practice the transform was evaluated in two parts:

$$F(\omega) = \int_{-\infty}^{+\infty} \cos(\omega t) f(t) dt - i \int_{-\infty}^{+\infty} \sin(\omega t) f(t) dt$$

$$= A - iB$$

The magnitude of the spectrum was then given by:

$$f(\omega) = \sqrt{A^2 + B^2}$$

The phase is

$\Phi(\omega) = \tan^{-1}(-\frac{B}{A})$, but this was not plotted as it was not considered sufficiently relevant.

The number of frequency steps used in the numerical integration was 500, and the number of time steps between 400 and 600 depending on the length of the record.

On The Interpretation of Spectrum Plots

It is not strictly necessary to perform a frequency analysis for acceleration, velocity and displacement records, since they are all related. Consider an acceleration of f with an angular frequency of ω.

let $f = a \sin(\omega t)$

$v = -\frac{a}{\omega} \cos(\omega t)$, integrating

and $d = -\frac{a}{\omega^2} \sin(\omega t)$

$$\boxed{\hat{d} = \frac{\hat{v}}{\omega} = \frac{\hat{f}}{\omega^2}}$$, where ^ denotes peak values

Thus the velocity spectrum is just the acceleration spectrum divided by ω, and the displacement spectrum is the acceleration spectrum divided by ω^2. In other words the lower frequencies are progressively accentuated in the velocity spectrum, and even more so in the displacement spectrum. The phase spectra of velocity and acceleration have constant differences of 90° and 180° respectively from the phase spectrum of displacement.

If the time record lasts T seconds, then there is generally a peak in the frequency curve at $f = \frac{1}{T}$ (i.e. at a very low frequency). This peak can be entirely unrelated to the blasting waves if the record contains some d.c. level due to, say, poor integration. In practice this means that no importance should be attached to the spectrum below about 1 c.p.s. if the results are to be meaningful.

The Blast Records

On the following pages are set out the records derived from a number of blasts. The table below gives some relevant information about each blast, and the location of the accelerometers.

Blast No.	location of blast.	location of accelerometer.	size of blast	Delays
1	S. slate	A	750 m^3 of rock	none, but blast fired electrically
2	S. slate	B	Unknown, but similar to Blast 1	?
3	Bottom of Pit	C	very small	none
4	S.E. slate	B	22,000 m^3 of rock	9 delays ~0.13 sec.
5	Bottom of Pit	C	very small	none
6	"	C	"	"
7	"	C	"	"
8	"	A	"	"

NOTE: Only the final part of Blast 4 is shown, as the tape-recorder saturated for the first part. The full record is given at the bottom of the page. For this blast the displacement curve was considered meaningless, due to the omission of half the record; hence it was not printed.

BLAST 1

Fig. 14 : DISPLACEMENT, VELOCITY AND ACCELERATION, WITH ASSOCIATED FREQUENCY SPECTRA.

NOTE: DISPLACEMENT RECORD UNRELIABLE

BLAST 2

Fig. 15 VELOCITY AND ACCELERATION, WITH ASSOCIATED FREQUENCY SPECTRA

BLAST 3

Fig. 16 : DISPLACEMENT, VELOCITY AND ACCELERATION, WITH ASSOCIATED FREQUENCY SPECTRA.

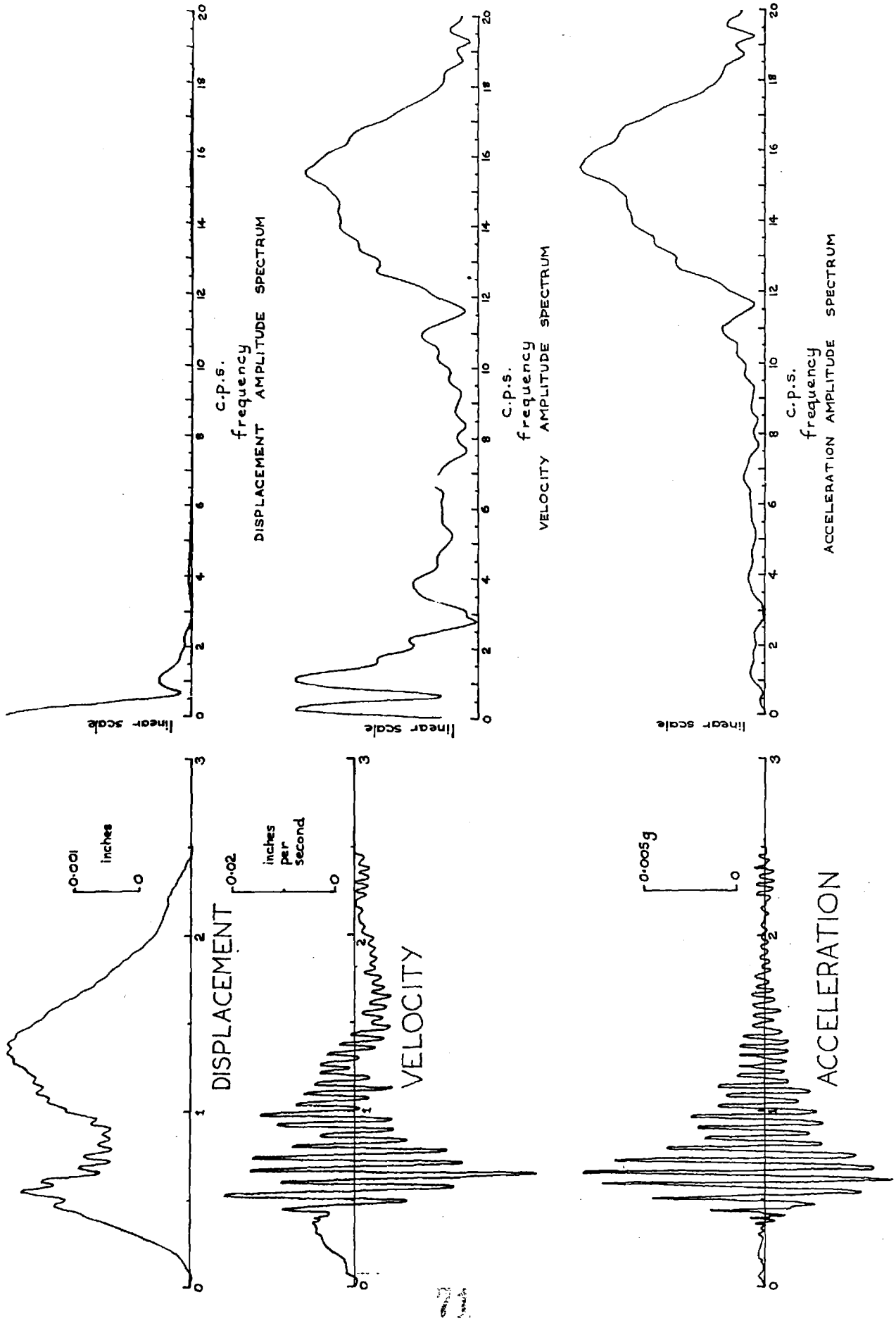

BLAST 4

Fig. 17 : VELOCITY AND ACCELERATION, WITH ASSOCIATED FREQUENCY SPECTRA.

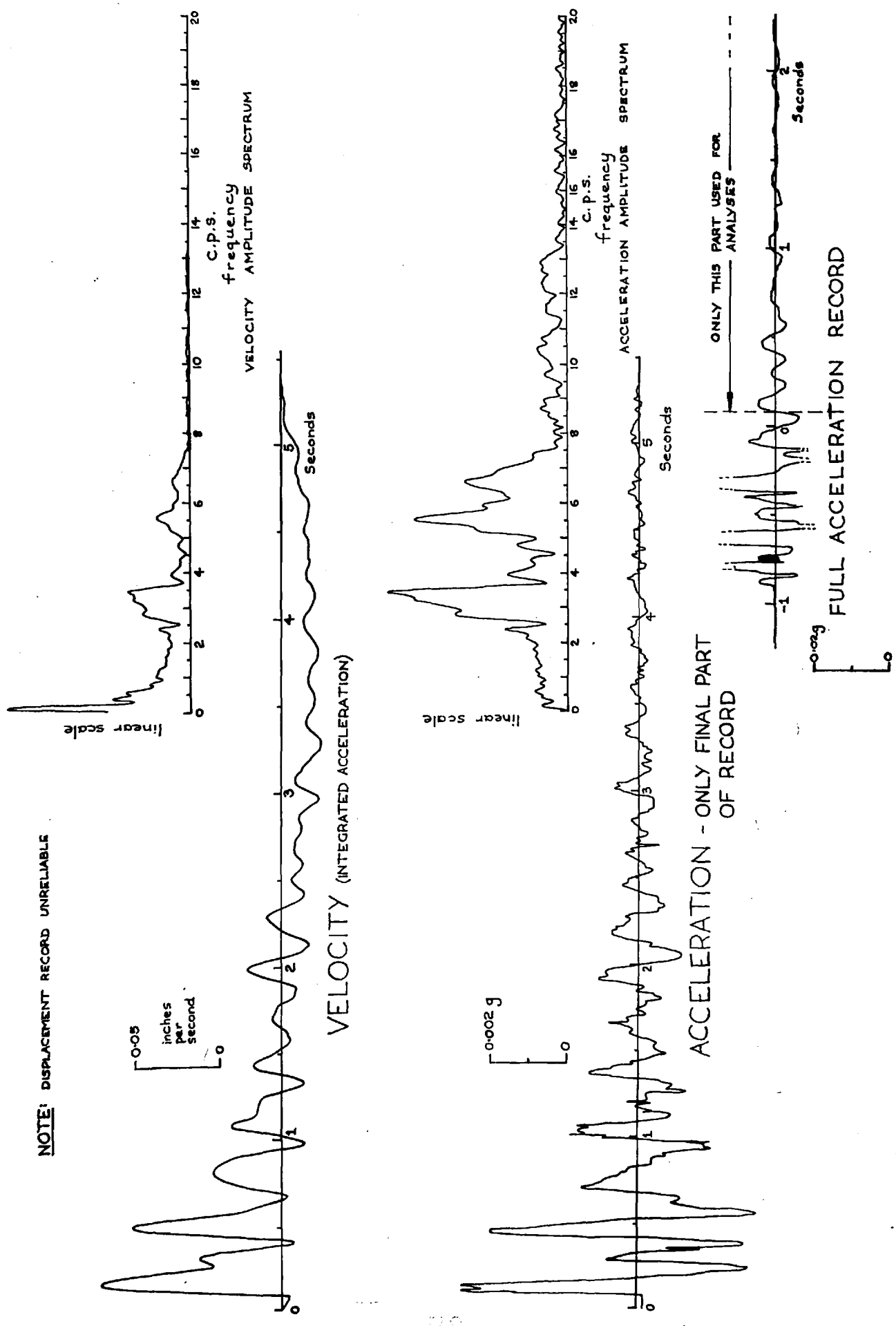

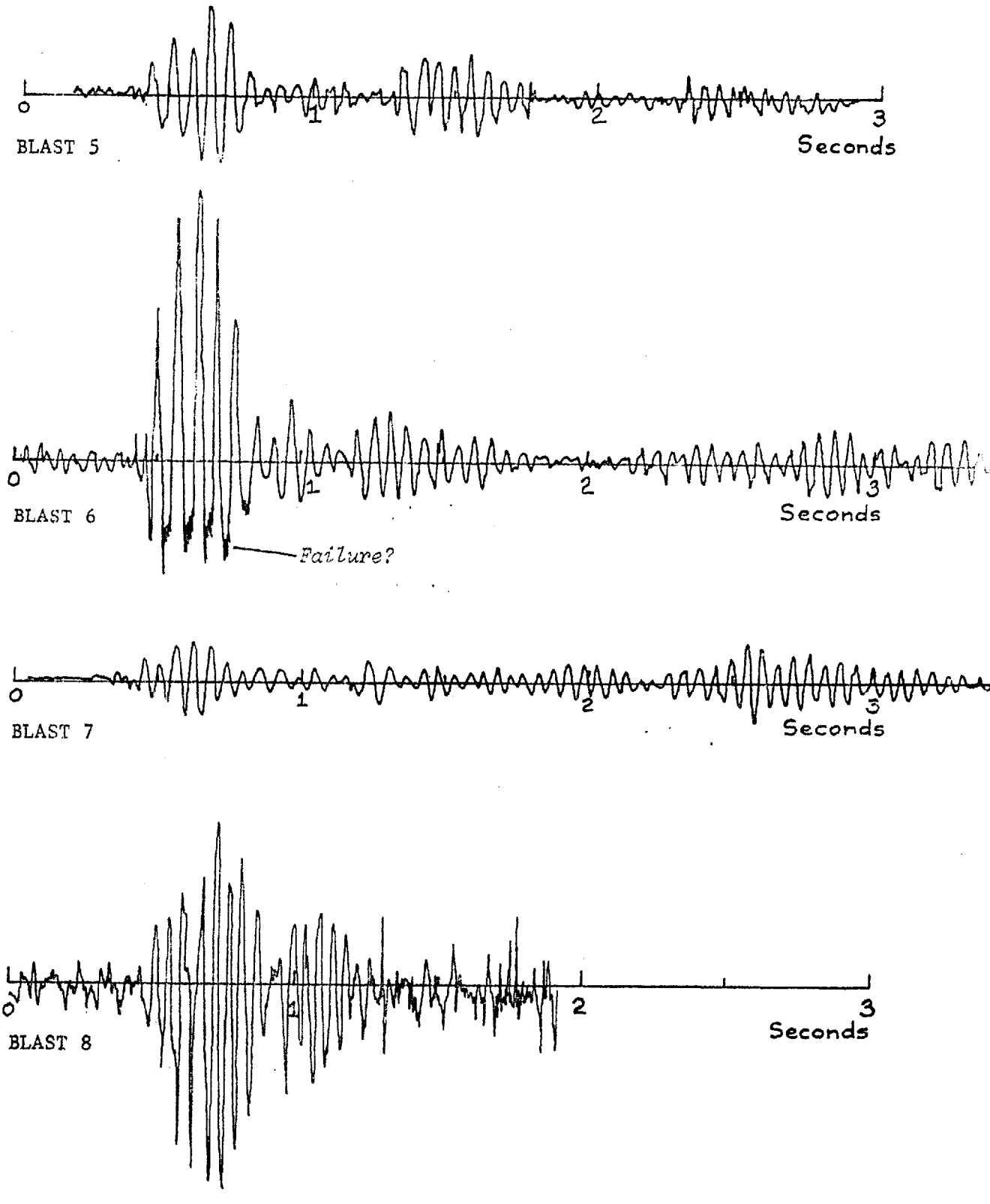

FIG. 18: SOME FURTHER BLAST RECORDS

Interpretation of Results

General Remarks

A fact which immediately stands out is the large variation in frequency which is evident throughout the records. The higher frequencies seem to come from blasts deep down in the pit, which may possibly be explained by the smaller dimensions of the base of the pit, compared with the periphery. Alternatively, the fact that all the deep blasts were very small and set off with no delays by Cordite may be a relevant factor. Whatever the detailed reason it is generally true that high frequencies are associated with small dimensions and low frequencies with large, assuming a common velocity. The most likely form of wave to be generated in the vicinity of a surface excavation is the Rayleigh wave, as was shown in Chapter 2. Hence a reasonable figure for the wave velocity may be assumed. Combining this with the observed frequencies will give an approximate estimate of the dimensions involved, and what mode of oscillation is most likely. Of course it must be bourne in mind that the velocity of Rayleigh waves will alter when propagating around a curved surface: a reasonable estimate of the velocity may be made on the results from Appendix II. Another confusing factor is the fact that distinct frequencies might be contributed by reflections from nearby geological discontinuities.

A further general observation is that the levels of accelerations are surprisingly low considering the enormous volume of rock removed by a typical blast. Accelerations were commonly recorded of a few milli - g (0.001 g), reaching possibly 30 mg for the largest blast (22,000 cu. m. of rock).

The decay factor of the recorded oscillations is another noteworthy feature. In the case of the largest blast (no. 4) the detectable vibrations continued for at least five seconds after the blast. Assuming a wave speed of 2000 m/sec (a low estimate) the waves would have travelled more than six miles in those five seconds if allowed to propagate in a straight line. The fact that they were largely confined to a structure with a principal dimension of one third of a mile indicates the existence of an efficient mechanism for trapping energy.

Speed of Waves

It is extremely difficult to estimate the velocity of long-period waves near the surface of the earth. In the case of the Atalya pit, there are a number of ways in which figures may be obtained. The most direct source is a seismic survey carried out by a Spanish firm to determine the "rippability" of the rock (an index which may be correlated with ease of mechanically "ripping" the rock). The seismic traverses (up to 60m long) were carried out along a bench about a third of the way down the pit. The tests were all in the

slate, and seemed to indicate an upper, low velocity, layer with a wave speed of 1000 m/sec, and a high-velocity layer at a depth of 5 m, with a speed of 3000 m/sec. It is not clear what type of wave was being propagated. Barton & Ross-Brown (Ref. 2) performed some tests with a commercial instrument consisting of a sledge-hammer coupled to a micro-switch, and an electronic counter. The ground was struck by the sledge-hammer, and the counter started by the micro-switch. The counter was then stopped by a signal of sufficient strength derived from a geophone located some distance from the sledge-hammer. The range of recorded velocities was from 200 m/sec to 2000 m/sec in the slate and 4000 m/sec to 6000 m/sec in the porphyry. Some of the records show the velocity *decreasing* with the distance between source and pick-up, which is difficult to understand. Barton & Ross-Brown also measured the longitudinal wave speed of small, intact samples in the laboratory, giving velocities of 4000 to 6000 m/sec. The velocities may also be calculated from the elastic "constants" of small samples.

However, the difficulty with all these methods is that they are on a small scale, wheras the velocity is required for a sample of several thousand feet long (since that is the length of the waves being propagated). There is no reason to believe that small-scale near-surface tests will give the correct velocity figures. It is also highly doubtful whether static tests will enable the velocity to be computed accurately, particularly in the case of a rock like slate with considerable hysteresis (which slope is the correct one?). In view of the difficulties, an intelligent guess was made, giving a P-wave speed of 3,500 m/sec, an S-wave speed of 2000 m/sec and a Rayleigh wave speed of 1800 m/sec..

Frequencies

Referring to the records, figures 14 to 18, it should be remembered that the region below 1 c.p.s. on the spectrum plots was considered meaningless (see paragraph on frequency analysis). A prominent frequency on most of the plots occurs just above 1 c.p.s., say 1.1 c.p.s. This can be seen most clearly in the velocity spectra. The peak may possibly correspond to the fundamental circulating Rayleigh-wave mode of oscillation:

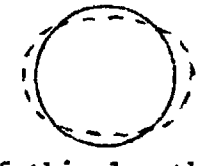

It appears that waves of this length propagate with about half the speed of plane waves, say 1000 m/sec (see Appendix II).

Hence, $\lambda f = 1000$

$2\lambda = 2\pi r$ for mode shown above

thus $\lambda = \pi.350$

$$f = \frac{1000}{\pi.350}$$

$$\doteq \underline{1 \text{ c.p.s.}}$$

Hence the peak at around 1 c.p.s. may be due to surface waves circulating near the rim of the pit. It should also

be possible for similar waves to circulate at any depth, but the preferred location is likely to be near the rim since there the radiation will only be in one direction, namely downwards.

Another powerful peak occurs in Blast 3, and also in Blasts 5,6,7,8, although no frequency plots are given for the last four. The peak is rather broad, centred around 15 to 16 c.p.s. It is interesting to note that this frequency is exclusive to those blasts fired near the floor of the pit. Could it be due to the floor of the pit oscillating in a fundamental mode?

The dimensions of the floor are rather variable, but 100 m is a rough average.

$$\frac{\lambda}{2} = 100$$

$$\lambda f = 1800 \text{ m/sec}$$

$$\therefore f = \frac{1800}{200}$$

$= 9$ c.p.s., which is rather too low to satisfactorily explain the effect. Perhaps the frequency is due to waves trapped in the ore chimney at the base of the pit. The ore is very dense and stiff compared with the surrounding rock, and may trap energy.

Blasts 1 and 2 yield a common frequency, namely 7.5 c.p.s. This frequency appears to be associated with the pit slopes, since both blasts occurred at the top of the south slope, although the monitoring points were different. It is interesting to compare Blast 8 with Blast 1, since both these blasts have a common monitoring point, the north borehole (A). Thus the observed frequencies, being very different, are seen to be a function of the source rather than the monitoring point.

Blast 4 is something of an anomaly in that it contains two distinct frequencies which are absent from other records. The blast was unusual in that it was tangential to the pit perimeter, whilst the all other blasts were normal to the perimeter. Hence unusual modes might have been excited. Chapter 5, on numerical methods, may be able to throw some more light on this question. It should be remarked here that Blast 4 was spread out over a long delay period of greater than 0.1 seconds. Thus the spectrum cannot be expected to contain much amplitude above $1/0.1 = 10$ c.p.s., which is confirmed by the records.

Blasts 5 to 8 show further bursts of oscillations after the initial vibrations have died down. There seems to be a prominent one with a delay of about one second. These could be due to reflections from geological discontinuities, or may result from groups of high-frequency waves circulating the free surface of the pit.

Reflections

It is difficult to assess the effects of geological structures external to the pit. The nearest discontinuity is about 700m to the south of the pit. Assuming a surface wave of 1800 m/sec the time for a round trip would be approximately 0.8 seconds, which may affect the lower frequencies of the spectrum plots, and in particular may be responsible for the 1.1 c.p.s. peak noted previously. However it is inconsistent with the fact that the peak is completely absent from the Blast 4 records. It is difficult to believe that external reflections play much part in the response measured, since the major function of a remote discontinuity would be to produce effects common to all plots. This fact is not evident, the records being largely functions of the local positions of the blasts within the pit.

Amplitudes of Motion

It is unfortuate that the initial part of Blast 4 is missing, due to the tape-recorder saturating. However it is clear that the low-frequency component could have reached at least 30mg. It is shown in Chapter 6 that the impulse (=mv =pt) given to the rock is the relevant factor in assessing the low-frequency motion. Blast 1 and Blast 4 can be compared on this basis.

Blast 1: 750 m^3 of rock, 1mg max. acceleration.
Blast 4: 22000 m^3 of rock, 30mg max. acceleration.

$$\frac{\text{Impulse 1}}{\text{Impulse 4}} = \frac{22000.\rho v}{750.\rho v} = \frac{29}{}$$, assuming the same velocity and density.

$$\frac{\text{Accel. 1}}{\text{Accel. 4}} = \frac{30}{}$$

The correlation is interesting, although clearly generalisations cannot be made on two observations.

The actual impulse given to the rock can be calculated if the rock ejection velocity is known. Petkof et al (Ref.3) determined this velocity for a number of rock types and situations. The velocities varied from 2 m/sec to 25 m/sec. If a value of 10 m/sec is assumed, the momentum of the rock in the Blast 4 is:

$$M = \text{Volume}.\ \rho\ .\ v$$
$$= 22000\ .\ 3X10^3\ .\ 10 \quad \text{(using densities given in Ref. 2)}$$
$$\simeq \underline{7X10^7}\ \text{Kg.m.sec}^{-1}$$

Assuming a delay factor in blasting of a total of 0.1 seconds, the force becomes:

$$P = \frac{\text{momentum}}{\text{time}}$$
$$= 7X10^8 \text{ Newtons}$$
$$\simeq 7X10^7 \text{ Kg force}$$
$$\simeq 70{,}000 \text{ Tons}$$

NOTE: this calculation is only valid if most of the explosion pressure is dissipated in accelerating the rock blocks, and not in actually breaking the rock. This condition is likely to exist in most open-pits, where the free surface is very broken.

The ratio of long-period accelerations to the impulse supplied by the blast can be estimated:

30mg was produced by $7X10^{7}$ Kg.m.sec^{-1}

$$\frac{\text{Accel.}}{\text{Impulse}} \simeq \frac{4X10^{-7}}{} \text{ milli-g per Kg.m/sec}$$

This figure will be compared with the computer simulation, in Chapter 6.

Another interesting calculation can be performed as a result of an experiment performed by a colleague at the same time. (see Ref. 4). A thin-walled steel cylinder containg oil was grouted into a borehole located near the accelerometer borehole. The long-period pressure fluctuations were found to be about 7 p.s.i. for Blast 4. Assuming that the device measured the total direct rock stress existing at that point, the fluid pressure can be related to the particle velocity:

$p = \rho c v$ (see Chapter 6)

$v = \frac{p}{\rho c}$

$\rho = 3X10^{3}$ Kg/m^{3}

$p = 7$ p.s.i. $= \frac{7X10^{3}}{1.42}$ Kg/m^{2}

$c = 3{,}500$ m/sec (pressure-wave vel.)

$$v = \frac{7 \cdot 10^{3} \cdot 9.81}{1.42 \cdot 3 \cdot 10^{3} \cdot 3500}$$

$\simeq 5X10^{-3}$ m/sec

$= 5X10^{-1}$ cm/sec

$\simeq$ 0·2 inches/sec

This figure correlates very well with the velocity records given in Fig.17.

Decay Factors

It is important to consider decay factors since these determine how "active" a particular mode is. The less decay a mode exhibits, the more it will amplify motion of the relevant frequency derived from, say, an earthquake. An overall value from all the records seems to be: the oscillations decay to about a half in three cycles. From the frequency plots, the magnification factor of a number of the oscillation modes varies from 2 to 4. This means that if the

pit was exposed to a source of waves, some frequencies might be amplified up to 4 times, assuming that the coupling with the pit was of the correct form.

Conclusions

It would appear that an open-pit is capable of trapping vibrational energy of certain frequencies. This fact means that when excited by a sudden blasting force, the pit radiates those frequencies slower than others, which allows distinct oscillations to be observed. The decay factor of the oscillations is such that the motion of an incident wave-train (e.g. earthquake) may be amplified up to four times, if the pit is excited in an efficient manner.

A tentative figure has been derived expressing the magnitude of acceleration resulting froma blast involving a given mass of rock.

REFERENCES
Chapter 4

1. WILLIAMS, D. "The Geology of the Rio Tinto Mines, Spain" Transactions Inst. Min. & Met. V. XLIII April 1934.

2. ROSS-BROWN, D.M., BARTON, N.R. "Rock Mechanics Considerations & the Stability of the Opencast Mines at Rio Tinto, Spain". Rock Mechanics Research Report. N°. D.7. Imperial College. Sept 1969.

3. PETKOF, B., ATCHISON, T.C., DUVALL, W.I. "Photographic Observation of Quarry Blasting" U.S. Bureau of Mines, Report of Investigations N°. 5849 1961.

4. SHARP, J.C. "Fluid Flow Through Fissured Media". PhD Thesis, London University (Imperial College), May 1970.

* * * * * * *

Chapter 5

Chapter 5: NUMERICAL METHODS

A. PREAMBLE

B. GENERAL CALCULATION PROCEDURE USED

PART 1: Elastic Response of an Open-Pit

A. STATEMENT OF PROBLEM

B. CHOICE OF METHOD

C. TO ILLUSTRATE SOME CHARACTERISTICS OF DYNAMIC RELAXATION

- Time Increment
- Density of Mesh
- Damping
- Non-Linear Stress Wave Propagation
- Tensile-Bar Failure

D. SOME PROBLEMS ENCOUNTERED

- Reflections From Boundaries
  - *Graded Net*
  - *Damping*
  - *Special Boundary Conditions*
- Erroneous Oscillations

E. RESULTS FROM THE DYNAMIC PROGRAMS

- Two-Dimensional Plane Strain Dynamic Program
  - *Frequencies*
  - *Resonance Magnification*
- Two-Dimensional Circular Hole
- Full 3-Dimensional Dynamic Program
- Observations and Conclusions

PART 2: Further Computer Methods

A. DISCUSSION

B. STATIC STRESS ANALYSIS

- Stress-Loaded Underground Opening
- Plane-Strain Self-Weight Model
- 3-Dimensional Axi-Symmetric Gravity Model

C. UBIQUITOUS JOINT ANALYSIS

D. DISCRETE JOINT ANALYSIS

- The joint as A Boundary Condition
- Examples
- Conclusions

E. PROGRESSIVE FAILURE IN A BLOCKY SYSTEM

- Discussion

A. PREAMBLE

At the present time computers seem to be regarded as a mixed blessing in the Rock Mechanics field. In the early days it was common for some people to regard anything produced by a computer as the truth, irrespective of how it was arrived at, and what data was used. Fortunately this era has largely passed, leaving us with a doubtful addition to the English language: "GIGO" (Garbage In, Garbage Out). If anything, the swing at present is to the other extreme, characterised by the view that computers are unnecessary because most practical calculations can be done on the back of an envelope. This is a difficult argument to refute, since a good deal of what is useful in Rock Mechanics *can* be done on the back of an envelope.

Why then should computers be used?

A power ful application is the use of the computer in a semiqualitative way, to find out how a complex system will react to changes in various parameters. Once the "behaviour - pattern" of the system has been understood, simple hand calculations may be made for real cases. The computer methods presented in this Chapter are intended to be viewed in this light, rather than be regarded as accurate numerical solutions to particular physical problems. In any event, in the Rock Mechanics field there can be so much uncertainty in the numerical values given to the paramenters governing the problem, that a good deal of human judgement still needs to be exercised. The computer can guide this judgement by showing what outcomes result from a particular set of well-defined assumptions, no matter whether they completely model a physical problem or not, so long as the assumptions made are well understood.

This Chapter is divided into two Parts. The first Part is concerned with trying to understand how an open-pit embedded in the surface of an elastic half-space reacts to dynamic stimulii of various forms. The calculation method used is Dynamic Relaxation, which is a finite-difference solution of the separated stress-strain and equilibrium equations, where each iteration represents a small, fixed time increment. The second Part of the Chapter is concerned with several ideas which were followed up, suggested by the dynamic studies, but not directly concerned with dynamics. The main topics are static stress solutions, inclusion of joints and simulation of a blocky rock mass.

Both parts of the Chapter use a calculation method which is common to both, and is described below.

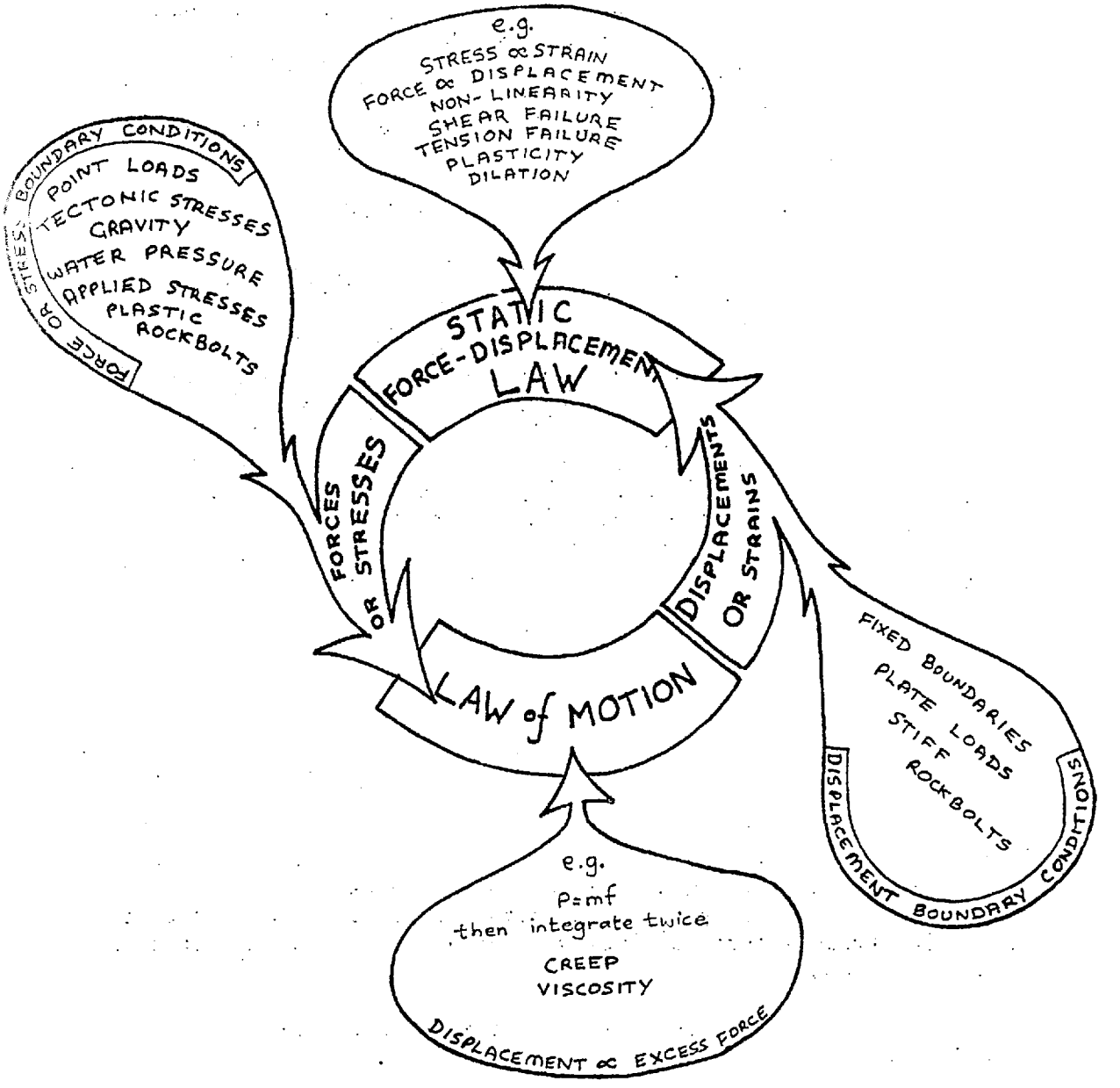

FIG.1: GENERAL CALCULATION CYCLE USED

B. GENERAL CALCULATION PROCEDURE USED

The method was suggested by, and is a generalisation of, Dynamic Relaxation (Otto, Cassel & Hobbs, ref. 1). It is a cyclic calculation in which one cycle advances time by one increment. The cycle is shown in fig. 1.

Assume initially that a set of displacements exist for each element in the calculation area. Forces, or stresses, can then be calculated from the displacements by some static law(s) relating the forces or stresses between elements to their relative positions in space.

A complete set of forces now exists for each element in the calculation net. Equilibrium of the forces acting on each element is now considered. If there is an excess force, in some direction, on the element, its resultant motion is computed according to some law of motion. This part of the calculation cycle causes time (or its equivalent) to be advanced by one increment. At the end of the time increment, there will be a complete set of displacements for each element, so that the calculation can return to the first part of the cycle.

In Dynamic Relaxation, the two stages in the calculation are supplied by the finite-difference approximations to the separated stress-strain and dynamic equilibrium equations.

However, in general, any laws can be used for either stage in the cycle. For instance in the first stage, any static stress-strain law may be used: non-linear, hysteretic, "failing" etc. There are in practice limitations on the nature of the laws used, concerned with the numerical stability of the calculations. These limitations do not impose very serious restrictions on the problems that can be tackled, and they will be discussed more fully in the Sections concerned. The second stage in the calculation cycle may use any law which relates the motion of an element to the forces acting on it. Examples of such laws: P=mf, viscosity ($p \propto v$), creep.

Since the programmes are written in terms of the separated equations, boundary conditions of both the displacement type and the force/stress type may be applied with ease.

The calculation procedure outlined above would seem to have useful application to many rock mechanics problems. Whereas Dynamic Relaxation allows the calculation of the static or dynamic stress distribution in an elastic, continuous, linear medium, it should also be possible, using the general method, to study the equilibrium conditions and progressive failure mechanisms in a non-linear, inelastic and discontinuous medium.

The question must arise as to what relationship the present method bears to the Finite Element method. Of course, both methods set out to solve the same equations, but the difference comes both in the discretization of the continuum, and also in the

precise method of solving the large number of simultaneous equations. However there is no sharp dividing line between the two methods; if rectangular elements are used in Finite Elements and a relaxation method used to solve the equations, the two methods become almost identical. The reason for choosing Dynamic Relaxation instead of Finite Elements for investigating the dynamics of open-pit mines will be discussed in the following Part.

PART 1

PART ONE

A. STATEMENT OF PROBLEM

It is useful to know, as far as stability is concerned, the magnitudes and locations of movements occurring as a result of a blast or earthquake of given size or location. The "natural" frequencies of the pit are also of interest, since the motions in an earthquake wave may be amplified if the wave contains a predominance of similar frequencies. In connection with this effect, it is also necessary to know the decay factor of the oscillations; i.e. how powerful the resonance is.

In any numerical idealisation of an infinite continuum, it is necessary to limit the distance to which the calculations can be extended, due to the finite storage of computers; in other words an artificial boundary must be introduced. In order to accurately model a particular problem, it must be possible to demonstrate that the boundary has little effect on the response of the pit.

Furthermore, a numerical method relies upon approximating a continuum to a number of discrete elements or meshes. The calculated response characteristics of the model must be shown to be sensibly independent of the discretisation used.

It should be noted that any elastic three-dimensional dynamic analysis will yield a large volume of information, namely the complete time history of motion in three dimensions at a large number of points within the solid. Unfortuately, conventional stability calculations are unlikely to be able to use the abundance of information. In view of this some way must be found of presenting the data in simplified form so that the essential features can be appreciated quickly.

B. CHOICE OF METHOD

In the past ten years, the Finite Element method has come to be widely used for both dynamic and static problems. It was originally developed to serve the aircraft industry, so that structures with complex shapes and varying material properties could be modelled easily. The drawback with the existing finite difference methods was that, being based on a regular grid, they could only be used to model complex boundary shapes by firstly finding a mathematical function to roughly fit the boundary, then transforming the co-ordinates of the grid to conform to the chosen function. Alternatively a stepped boundary could be used. The finite element method, on the other hand, calculates the individual stiffness (in the form of a matrix) of each element as determined by its shape and properties. Thus elements of any reasonable shape may be used. The equations for each element are then linked with those of its neighbours, by considering equilibrium and compatibility. The complete set of simultaneous equations for the whole body may then be solved by direct substitution, inversion of the matrix, or relaxation.

Nevertheless, a finite difference method was used in the present work. The major reason for this was as follows: the problem of an open-pit vibrating in a semi-infinite continuum is dominated by its infinite nature. Any method which seeks to impose artificial boundaries, must affect the results to some extent. To minimise this, the boundaries should be made as distant as possible, which may be achieved by using the greatest number of elements which can be accommodated within the computer storage. The Finite Element method is generally wasteful of storage, particularly in three dimensions, since the elements are numbered arbitrarily, giving a sparse matrix for storing inter-element stresses and displacements. In other words, a large number of locations in the matrix are unused due to the large jumps in numbering occurring between neighbouring elements. In the finite difference method, each element, or mesh, is specified, not by a single number, but by its co-ordinates (I,J,K) in space. Thus all storage locations may be used. For example, using a 60K storage computer, 5,000 three-dimensional elements may be used with finite differences, whilst Finite Elements can rarely achieve a tenth of this figure. It may be argued that progressively larger elements may be used with Finite Elements to extend the boundary. Unfortunately in dynamics the element sizes need to be a good deal smaller than the smallest wavelength to be propagated (e.g. a tenth). If a wave intercepts an element of similar, or larger, dimensions than its wavelength, reflection occurs since the element cannot transmit it faithfully.

The geometry of the boundaries in the present work was not complex - a conical pit in the surface of a flat half-space. Hence the ability of Finite Elements to model complex shapes was not required.

An advantage of Finite Elements is that, being a matrix method, the eigenvalues corresponding to any true modes of resonance can easily be found. However in the present application

there are no true resonances, so the method is inapplicable.

An endearing feature of finite difference programs is that they are generally much simpler than Finite Element programs, and therefore less prone to error and easier to de-bug. A typical finite-difference program in three dimensions may use 3 or 4 pages of computer paper, whilst 3D Finite Element programs commonly cover 10 or 15 pages. Furthermore, a finite difference program generally needs no data, whilst the Finite Element program needs many data cards to give information about the shape and location of each element. All of which means that it takes far less effort to carry the cards over to the computer room if finite differences are used.

The finite difference method used here was Dynamic Relaxation (Ref. 1). The method was originally developed for static analyses, but is used here in the full dynamic form. The separated equations are used, each iteration representing a fixed time increment.

A real-time calculation method was employed, since it was necessary to know the response to arbitrary waveforms. Also it was envisaged that the inclusion of failure mechanisms would be made possible by simply allowing certain parameters to alter as time progressed. This would seem to be more realistic than the current Finite Element technique, in which a complete elastic stress analysis is done, then various parameters altered according to the outcome, and a further complete analysis done, and so on. Similar arguments may be used to show that D.R. should be much more economical when dealing with non-linear problems than F.E.

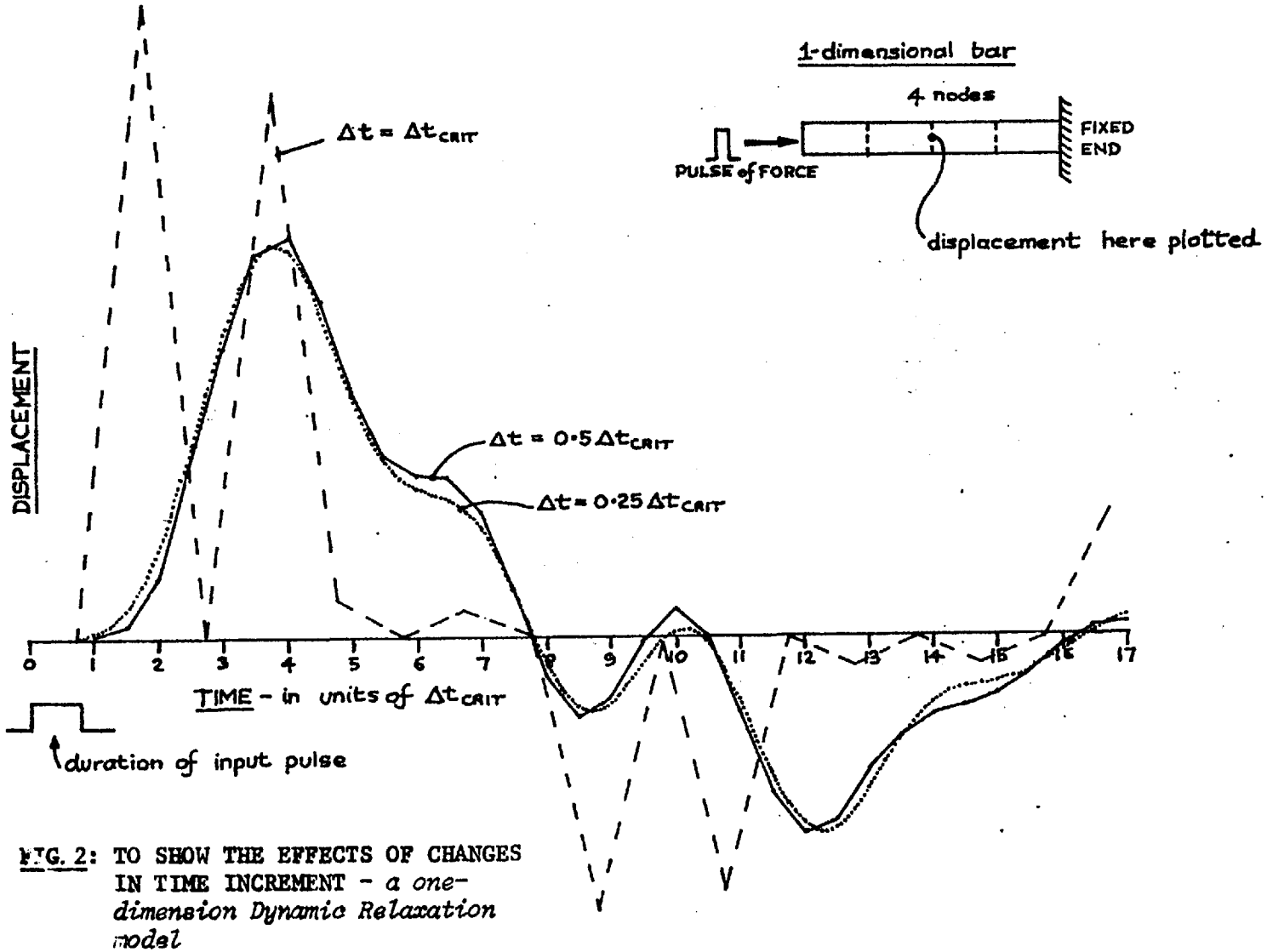

FIG. 2: TO SHOW THE EFFECTS OF CHANGES IN TIME INCREMENT - *a one-dimension Dynamic Relaxation model*

C. TO ILLUSTRATE SOME CHARACTERISTICS OF DYNAMIC RELAXATION

An excellent description of Dynamic Relaxation is given in the paper by Otter, Cassell and Hobbs (Ref. 1). This paper contains a lucid account of the use of the method in solving one-, two- and three-dimensional static problems. There seems to be no merit in trying to improve upon their paper here.

In order to apply Dynamic Relaxation to true dynamic problems, the damping is set to a low value, or zero. This Section records some of the characteristics peculiar to the dynamic version of the method.

Time Increment

The value used for the time increment is important in view of the numerical stability of the calculations. An intuitive way of viewing the situation is as follows: an elastic wave spreads out from an excitation point with a maximum speed of V_p, where V_p is the compressional wave speed. However the fastest speed that the computer program can communicate between one part of the mesh and another is one mesh-length per iteration period. If this speed is less than the compressional-wave speed, the program will tend to be unstable, since it cannot correctly follow the physical process. A more rigorous treatment is mentioned in the paper by Otter et al, and the formula for time increment is as follows:

$$\Delta t \leqslant \frac{1}{c}\left\{\left(\frac{1}{\Delta x_1}\right)^2 + \ldots\ldots\ldots \left(\frac{1}{\Delta x_m}\right)^2\right\}^{-\frac{1}{2}}$$

For m cartesian co-ordinates.

where $\Delta x_1 \ldots\ldots \Delta x_m$ are the respective mesh lengths,

and c = compressional wave speed.

In one dimension this simplifies to

$$\Delta t \leqslant \frac{\Delta x}{c}$$

$$\leqslant \Delta x\sqrt{\frac{\rho}{E}}$$

It is interesting to compare this formula to the one derived in the section of the Chapter on the Block Model (page 118):

$$\Delta t < 2\sqrt{\frac{m}{s}}$$

Figure 2 shows the effects of changing Δt in a simple 4 - node one-dimensional case. Clearly if Δt is set to Δt_{crit} $(= \Delta x\sqrt{\rho/E})$, the calculation becomes very inaccurate, but $0{\cdot}5\Delta t_{crit}$ gives a reasonable value. In all cases to follow, the solutions were checked by varying Δt.

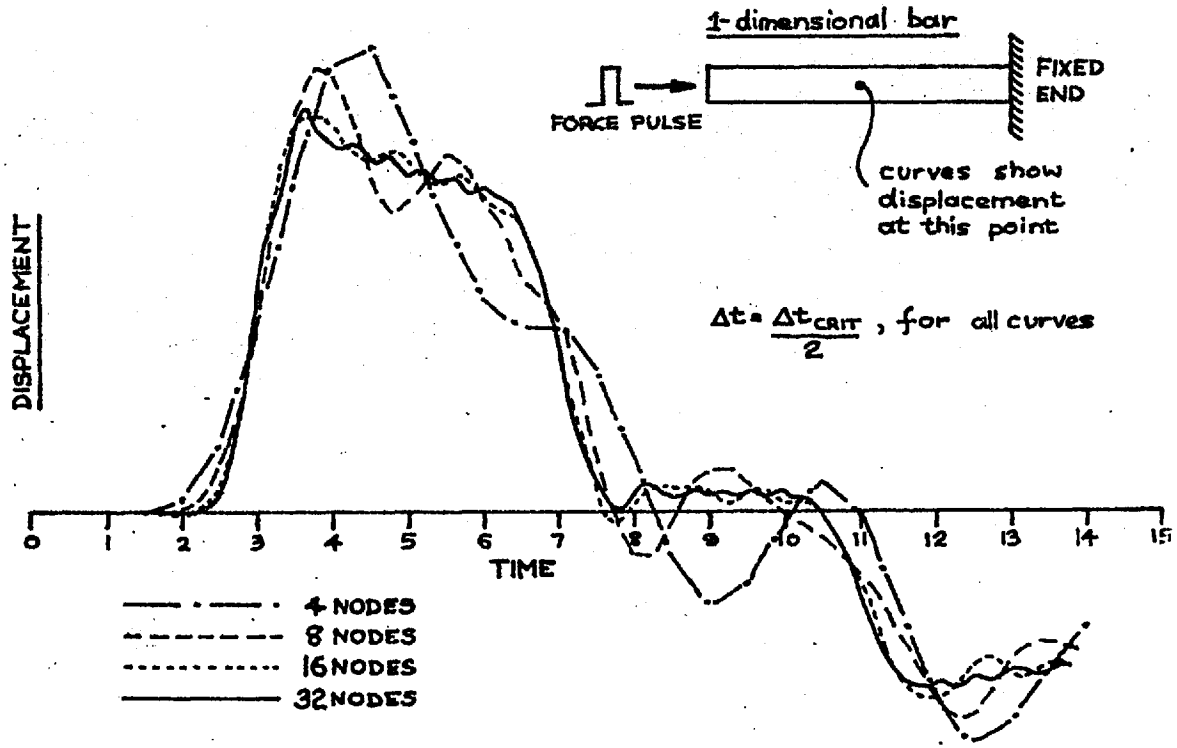

FIG. 3: TO SHOW THE EFFECTS OF CHANGES IN MESH SIZE

Density of Mesh

In the static case, the mesh is chosen fine enough so that rapid changes in stresses (or displacements) are modelled accurately. The dynamic requirements are more severe, since the fluctuations in stress become more and more rapid (with respect to distance) as the frequency increases. Thus in general, the higher the frequency of excitation, the more nodes are needed per unit length. The problem may also be stated in terms of wavelength: the mesh size should be much smaller than the shortest wavelength to be propagated.

Tests were carried out, using the same program as for the Δt tests, but this time keeping $\Delta t/\Delta t_{crit}$ constant, and varying the number of nodes in the bar (keeping the actual bar length constant). The results for four different mesh sizes are shown in Figure 3. It can be seen that some error is introduced even with 16 nodes. The main error is with the high frequency response. Since the excitation is a short pulse, the response of the bar should be almost a square-wave. The curves for small numbers of nodes are unable to follow the rapid changes in slope present in the true response. A feature which is immediately noticed is the rapid oscillations superimposed on the true response. The frequency of these oscillations increases as the node spacing decreases. Since Δt also decreases with node size, the oscillation period for all the curves is roughly constant if it is expressed as a fraction of Δt. The period is approximately $7\Delta t$ to $8\Delta t$, = 3·5 to $4\Delta t_{crit}$.

The theoretical period may be deduced from the difference equations used in the Dynamic Relaxation method. The equations are identical to those for a discrete mass-spring system:

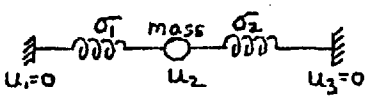

Assuming only one degree of freedom (i.e. all displacements are zero except one), the equation of motion used in Dynamic Relaxation (see Ref 1, page 636) is:

$$\dot{u}_2^{(1)} = \dot{u}_2^{(0)} + \frac{(\sigma_2^{(0)} - \sigma_1^{(0)})\Delta t}{\rho \Delta x}$$ (assuming no damping)

The equivalent acceleration is:

$$\frac{(\sigma_2^{(0)} - \sigma_1^{(0)})}{\rho \Delta x}$$

But the stress-strain law in difference form is:

$$\sigma_1^{(0)} = \frac{E}{\Delta x}\left(u_2^{(0)} - u_1^{(0)}\right) = \frac{E u_2^{(0)}}{\Delta x}$$

$$\sigma_2^{(0)} = \frac{E}{\Delta x}\left(u_3^{(0)} - u_2^{(0)}\right) = -\frac{E u_2^{(0)}}{\Delta x}$$

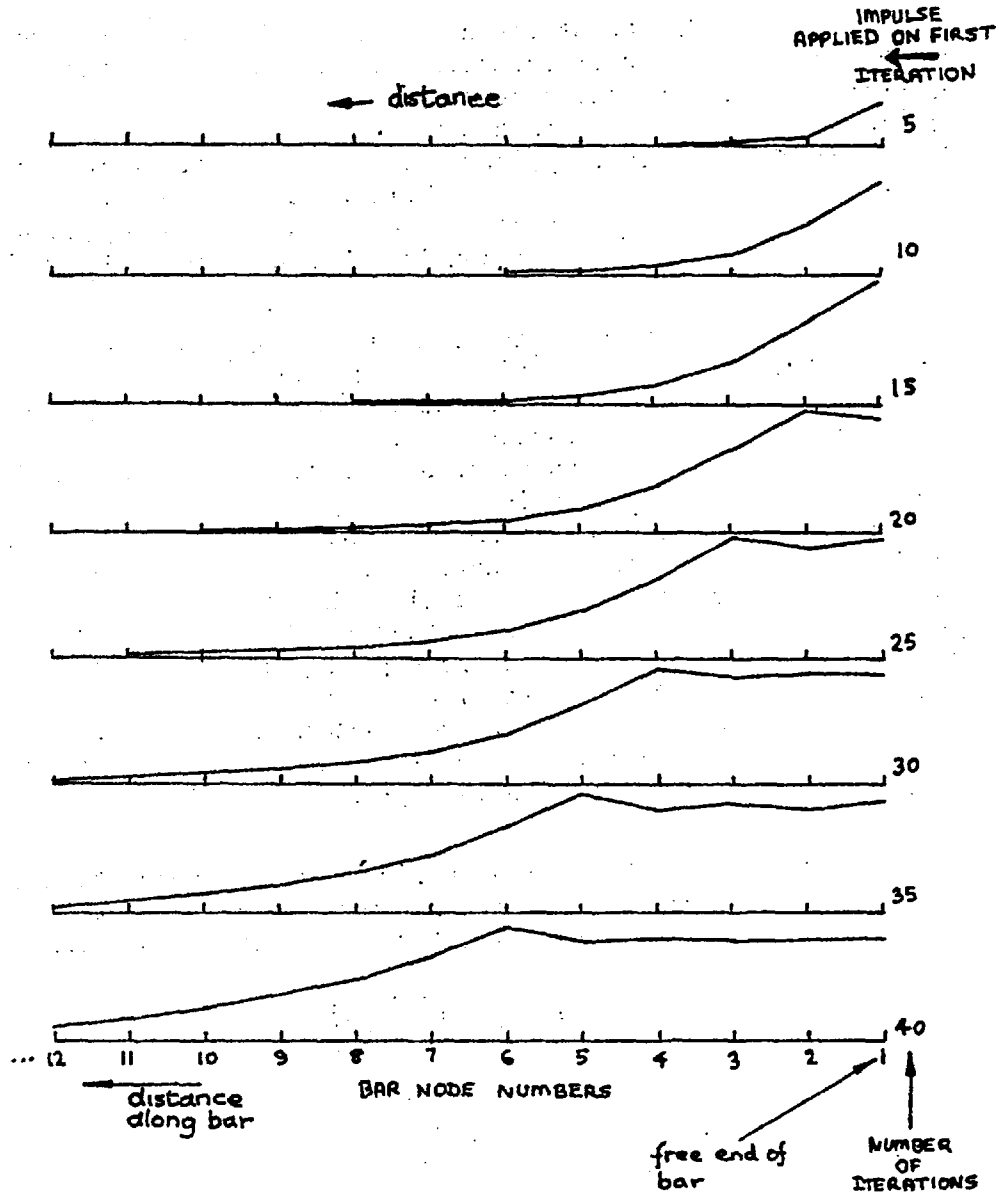

FIG. 4: THE DISTRIBUTION OF DISPLACEMENT ALONG A BAR AT REGULAR TIME INTERVALS - square root stress-strain law.

Acceleration, $a_2^{(o)} = -\frac{2Eu_2^{(o)}}{\rho\Delta x}$

$$\therefore -\frac{a_2^{(o)}}{u_2^{(o)}} = \frac{2E}{\rho\Delta x^2}$$

, which is the defining equation for simple harmonic motion, giving

$$\omega^2 = \frac{2E}{\rho\Delta x^2}$$

The period, $T = \frac{2\pi\Delta x}{\sqrt{2}}\sqrt{\frac{\rho}{E}}$

$$= \sqrt{2}\pi\Delta x\sqrt{\frac{\rho}{E}}$$

But $\Delta t_{crit} = \Delta x\sqrt{\frac{\rho}{E}}$

$$T = \sqrt{2}\pi\Delta t_{crit}$$

$$\approx 4.45\,\Delta t_{crit}$$

This value is of the same order as that found above. The general conclusion may be drawn that the application of impulsive loads to a finite difference net will excite individual nodes to oscillate at their natural frequencies. Furthermore, the propagation of waves containing higher frequencies is not possible in an assemblage of such elements.

Damping

In the static case, damping is necessary to cause the stresses and displacements to converge to steady values. It takes the form of viscous stresses applied to all nodes, relative to inertial space. The magnitude of damping is calculated (in Ref. 1) by considering what viscous stresses would be necessary to critically damp the lowest mode of oscillation of the complete system being modelled. This may not be the optimum method of applying damping. Since the lowest mode of resonance depends on the particular system being modelled, it may be better to critically damp the *highest* modes, i.e. the natural frequencies of individual meshes. This method is particularly advantageous if a non-uniform mesh size is used (e.g. axi-symmetric net), since the damping needed is a function of mesh length. If an overall damping factor is used, some parts will be over-damped, and some under-damped.

The critical damping factor for a mass-spring system is $2\sqrt{sm}$ (see "Block Program - *damping*" in this Chapter), where s is the stiffness and m the mass. Refering to the previous paragraph ("Density of Mesh"), the equivalent mass is seem to be $\rho\Delta x$ and the equivalent stiffness $\frac{2E}{\Delta x}$

Thus the damping factor $(= \frac{\text{stress}}{\text{velocity}}) = 2\sqrt{2E\rho}$

But damping per unit length is required for D.R.

Thus $K_{crit} = \frac{2\sqrt{2E\rho}}{\Delta x}$ (= stress/velocity per unit length)

This method of calculating critical damping factor was used in all the following examples. Of course "Δx" is replaced

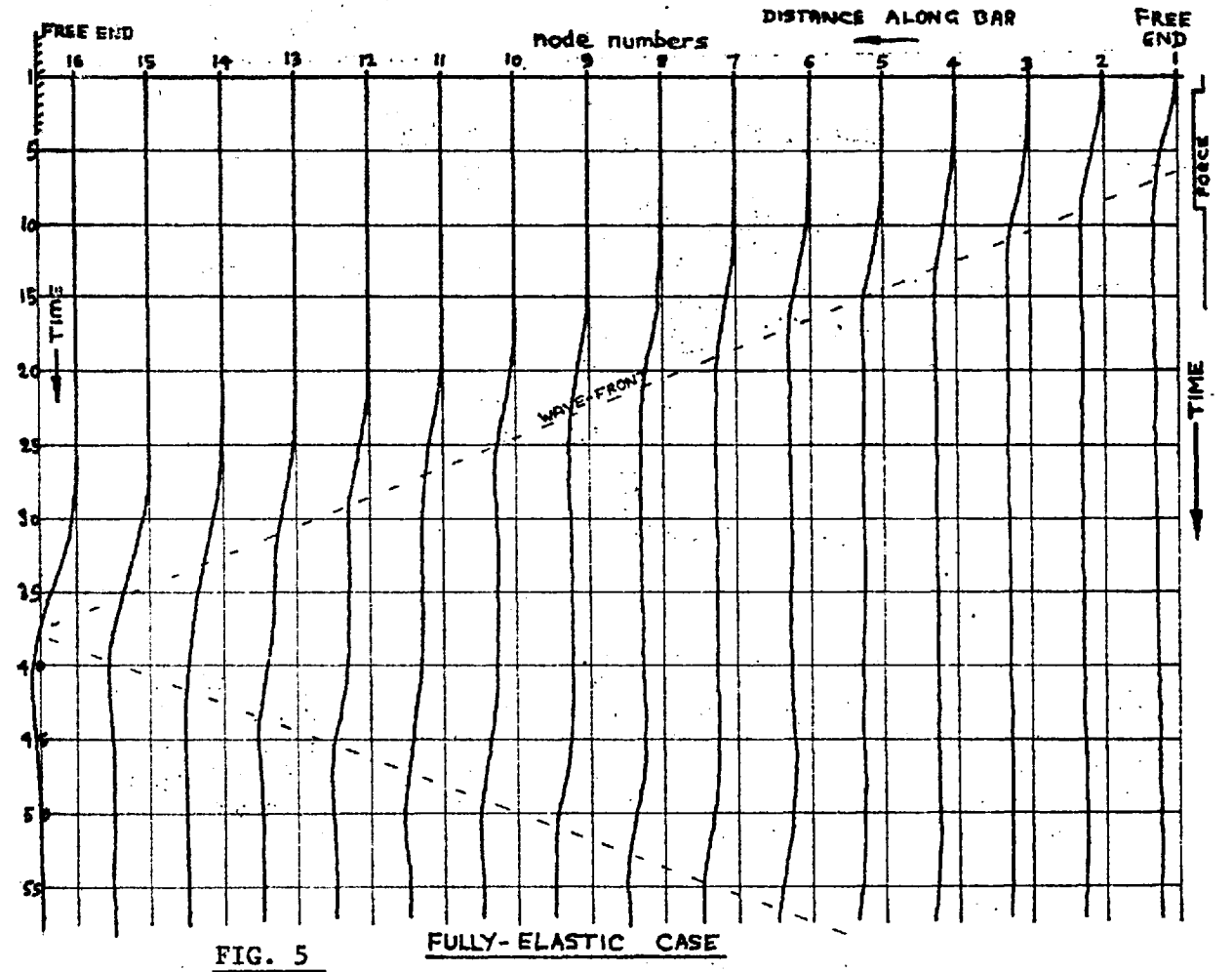

FIG. 5 FULLY-ELASTIC CASE

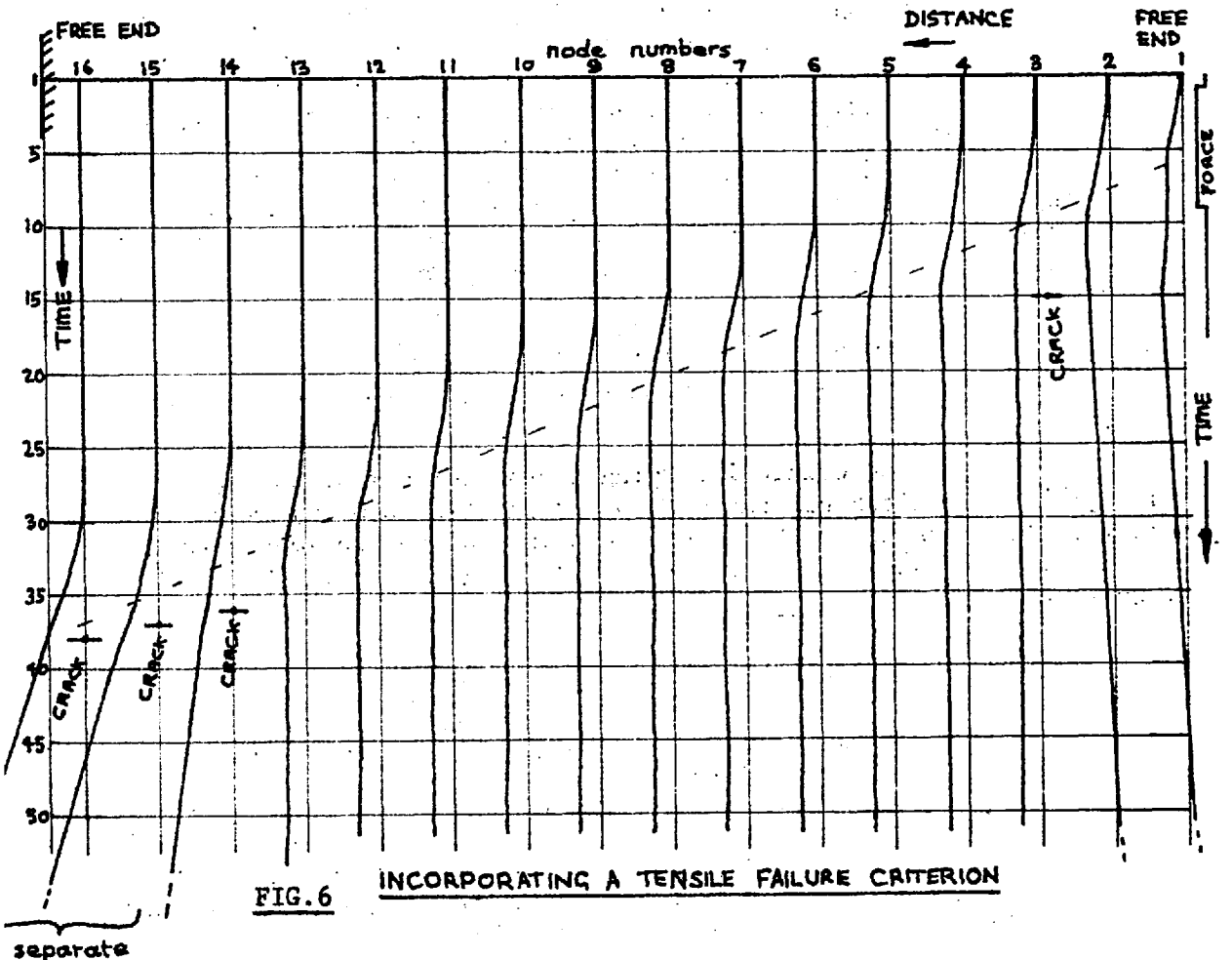

FIG.6 INCORPORATING A TENSILE FAILURE CRITERION

FIGS. 5 & 6: VARIATION WITH TIME OF DISPLACEMENTS AT ALL POINTS ALONG A BAR, with and without tensile failure.

by the mesh length appropriate to the location being considered.

Non-Linear Stress Wave Propagation

Whilst it is not strictly relevant, it is interesting to record the results of using a non-linear stress-strain law in the one-dimensional program described earlier. Instead of the law $\sigma = E\varepsilon$, the square-root law $\sigma = E.\text{sign}(\varepsilon).\sqrt{\varepsilon}$ was used, representing a material which becomes softer with increasing stress:

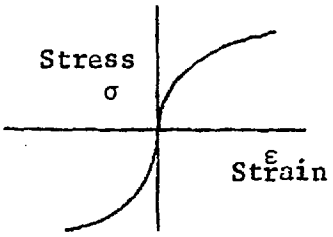

The distribution of particle displacement along the bar was plotted out (Figure 4) at regular time intervals, after exciting one end of the bar with an impulsive stress. The plot shows that the wave-form is the direct opposite of a shock-wave: i.e. small stresses propagate quickly due to the high initial slope of the stress-strain law, whilst large stresses propagate slower as the curve becomes less steep. Thus a long tail is propagated *ahead* of the main pulse.

Tensile-bar Failure

A well-known cause of rock breakage by blasting is the tensile stress wave generated by a compressive wave on reflection from a free face. This effect was simulated in the one-dimensional program by simply setting the stress at a point permanently to zero if a certain tensile stress was exceeded at any time. Figure 5 shows the elastic response of the bar, without tensile failure, whilst Figure 6 shows the effect of including the failure law. The displacement of each node in the bar is plotted against time. Tensile slabbing of the end of the bar can be clearly seen, the inner slab fracturing first. The outer slab acquires the greatest velocity. An interesting fact is that almost all of the momentum of the wave is carried off by the slabs, since no returning wave can be seen.

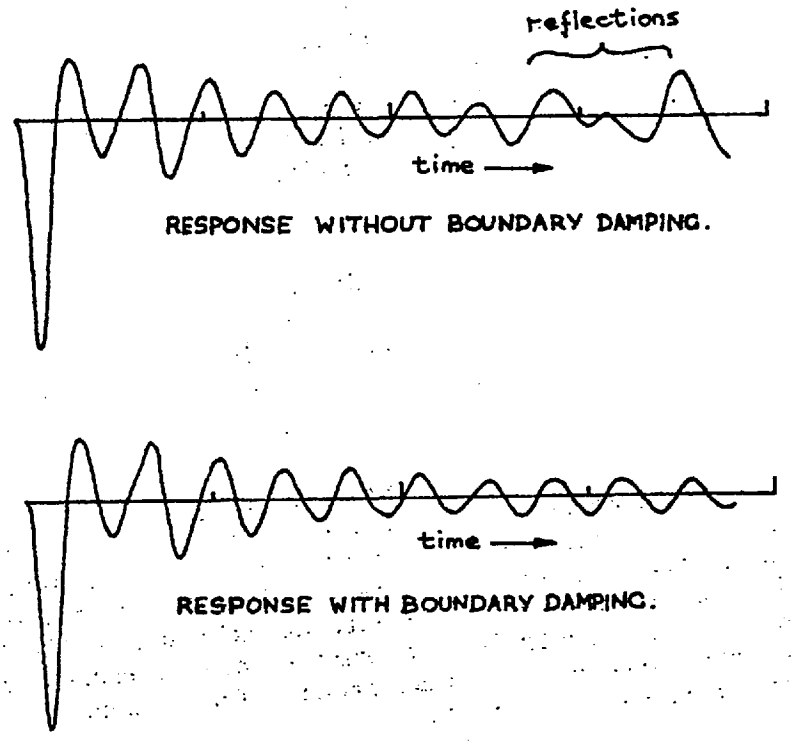

FIG. 7: VERTICAL DISPLACEMENT RESPONSE OF THE FREE SURFACE OF AN ELASTIC D.R. BLOCK DUE TO AN IMPULSIVE LOAD - with and without boundary damping.

D. SOME PROBLEMS ENCOUNTERED

Reflections From Boundaries

The biggest single problem with the Dynamic Relaxation programs was that of eliminating reflections from the boundaries of the calculation net. Clearly, if the reflections have similar amplitudes and frequencies to the desired open-pit response, no valid conclusions can be drawn regarding the response of a pit in a semi-infinite solid. Several approaches were tried in the hope of eliminating reflections. They are discussed below:

Graded Net

It is common practice in static analyses to use a fine mesh near the stress concentrations, but progressively enlarge the mesh size with distance, as the stress variations decrease. Unfortunately a dynamic wave has the property that its stress variations (in terms of distance between opposite polarities, for example) tend to remain constant no matter what the distance from the source. In order to faithfully transmit a wave with a wavelength of λ, a finite-difference grid must have a mesh size considerably smaller than λ. If a wave impinges upon a mesh with similar dimensions to the wavelength, the mesh will be unable to transmit it faithfully (one reason being that the D.R method assumes a *linear* stress variation across a mesh), and consequently some of the energy is reflected. A further part of the energy may cause the mesh to oscillate at its natural frequency (assuming the incident wave contains that frequency), which frequency is then re-radiated back in the direction of the source, further confusing the issue.

Hence graded meshes were not used.

Damping

It is of course possible to apply damping to all nodes so that reflected waves will be reduced in amplitude during their journey to and from the boundaries. With present-day computers however there is only a limited storage, so that in three-dimensions the boundaries must be placed necessarily close to the source. It was found that if an overall damping was used sufficient to reduce boundary boundary reflections, then the response of the open-pit was affected to an unacceptable extent.

An improvement was effected by damping only those nodes near the boundary, so that the pit response remained unaffected. This scheme was tried on a three-dimensional program written in cylindrical polar co-ordinates. The model was a cylindrical block of material 15 nodes high, 18 nodes radius and 8 sectors around. The sides and edges of the block were fixed and the top surface unconstrained. Figure 7 shows the vertical displacement of a point just under the surface of the block (near the centre) due to an impulsive force at that point. The top curve gives the displacement without damping, whilst the lower curve shows the effect of incorporating a 5-node band of damping at the side and bottom boundaries. The damping was graded so that the inner damping constant was low, building up to the critical value near the edge. In this way, it was hoped that reflections off an initial stiff dashpot could be avoided. Figure 7 indicates

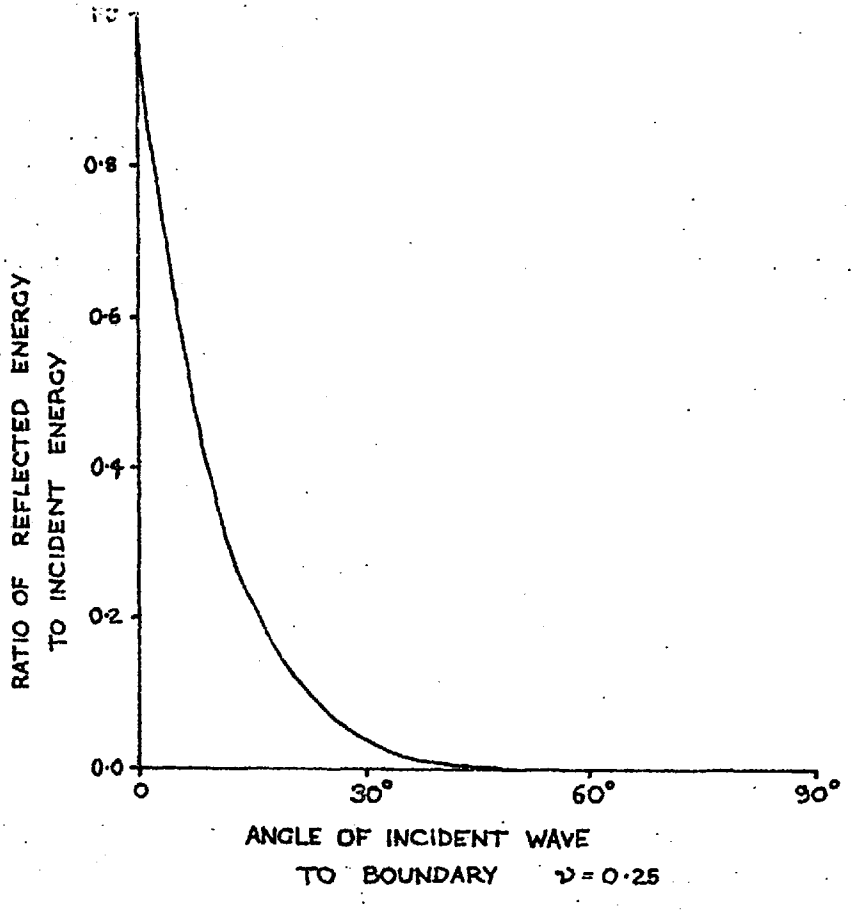

FIG. 8: TO SHOW THE EFFICIENCY OF THE CRITICAL-DASHPOT METHOD IN ABSORBING P WAVES INCIDENT ON A PLANE BOUNDARY

that a boundary damping band is useful in eliminating high-frequency waves, but when the wavelengths become longer than the dimensions of the damping band, the band becomes transparent to the wave. This point is dealt with further on in the Chapter. In almost all of the D.R. examples to follow, a boundary damping band was used.

Special Boundary Conditions

It is tempting to speculate that it might be possible to remove all the energy incident on a boundary by a numerical process operating on the boundary stresses and displacements. It may be recalled that in Chapter 2 it was mentioned that a stress wave propagated down a one-dimensional bar could be completely absorbed by a viscous dashpot with the particular damping factor of ρc , where c is the wave speed. However in two dimensions it can be shown that single-element dashpots cannot absorb all the energy of a wave impinging on a boundary with an arbitrary angle of incidence. However the method was used in a two-dimensional D.R. program and found to be effective in removing most of the energy of waves incident on the boundaries. The boundaries were arranged to be stress-free, but a viscous damping of ρc_p was applied in the normal direction, to the final node, and a damping of ρc_s in the shear direction (c_p = p wave velocity, c_s = s wave velocity). A similar method has recently been used by Lysmer and Kuhlemeyer (Ref. 5). Figure 8, which is drawn from the figure in their paper shows the reflected wave energy of a p wave as a function of the angle of incidence, using a critically-damped two-dimensional boundary. Clearly, as the angle of incidence decreases, the boundary absorption becomes less and less. This type of boundary may be useful in two-dimensional problems where the incident energy is likely to be confined to high angles. However, for the axi-symmetric case in three dimensions, some of the major modes of "resonance" of an open-pit may be ones involving circulating waves. In this case, the effective angles of incidence to the outer circumferential boundary will be zero. The critcal dashpot method will thus be ineffective in this case.

In any event, the critical dashpot method cannot fully absorb surface Rayleigh waves of an impulsive nature since the dashpot constants required vary with frequency (see Lysmer et al).

It is open to doubt whether *any* method could be used to totally simulate a truly infinite medium. Consider the following example:

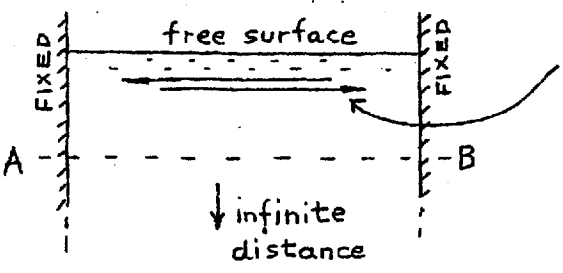

Plane Rayleigh wave being reflected back and forth between the ends, without loss of energy.

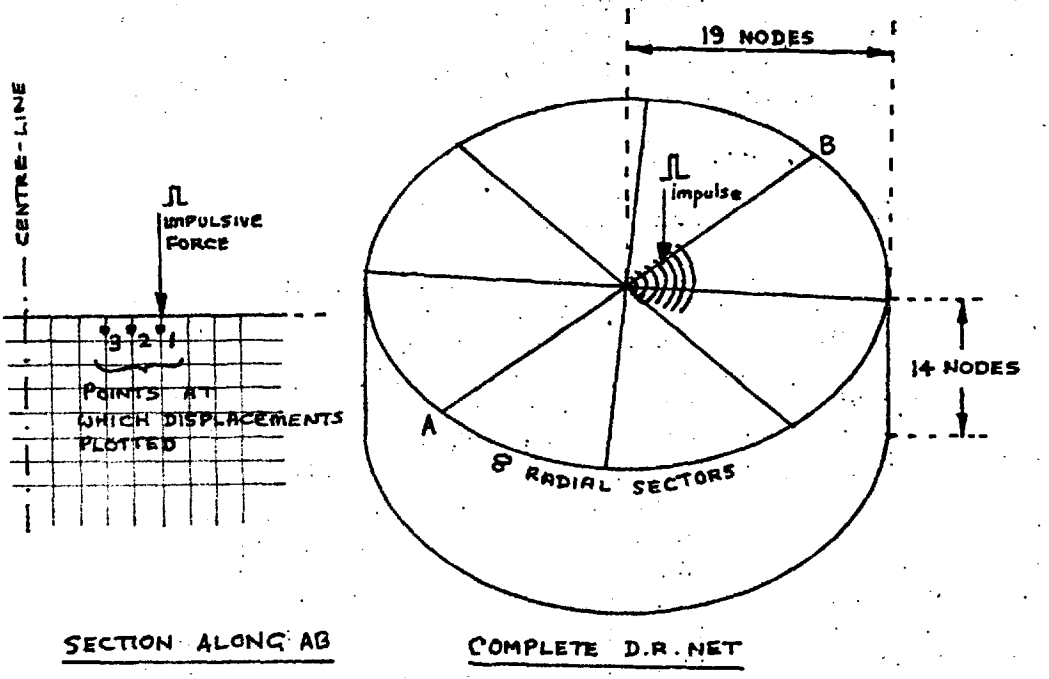

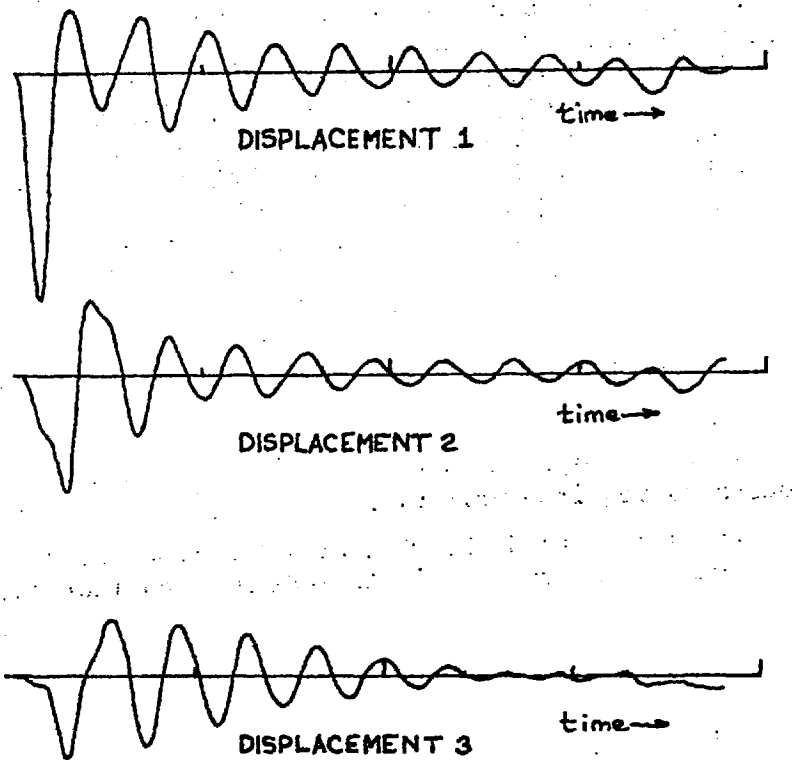

FIG. 9: VERTICAL DISPLACEMENT RESPONSES - 3D DYNAMIC RELAXATION PROGRAM

Suppose we require to simulate the infinite medium by replacing it with an artificial boundary at AB. This boundary must *not* absorb energy, since the amplitude of the wave would decrease: it must react to the wave in such a way that there is some energy flow in both directions. However it must also simulate the correct force-displacement functions of a truly infinite medium. Clearly a mechanism for merely removing energy is not good enough.

Erroneous Oscillations

It was mentioned in the previous Section (C) that individual meshes tend to oscillate at their own natural frequency, when subject to impulsive loads. This effect may hide the true response of the system under consideration. In the next Section (E) a three dimensional dynamic program is described to model an open pit in the surface of an elastic solid. This program was used, without the pit (i.e. with a flat surface) to determine the response of a flat surface to an impulsive point force. Theoretically the response should be a uni-directional pulse, with no trailing oscillations (see Chapter 2, Section D). However, the response using the D.R. program exhibited considerable oscillation after the initial impulse had died away. Figure 9 shows the vertical displacement of serveral points around the excitation point. The major oscillation frequency conforms well with that predicted by the formula $T = \sqrt{2}\,\pi\Delta x/c$ derived previously (the paragraph on Mesh Density). Δx in this case is replaced by Δz, the vertical mesh size. The curve of Displacement 1 is also seen to contain a low frequency component, which is probably the natural frequency of the circumferential mesh size, $r\Delta\theta$.

No satisfactory method was devised for dealing with oscillations of individual meshes. It is possible to apply damping to all elements, but this obscures the desired response as well. A different exciting waveform was tried, which contained little energy at the mesh frequencies, but this was only a partial success and is described in a later section. The only really satisfactory solution to the problem is to ensure that the frequencies of the open-pit are much lower than those of individual mesh oscillations so that the two are easily separable.

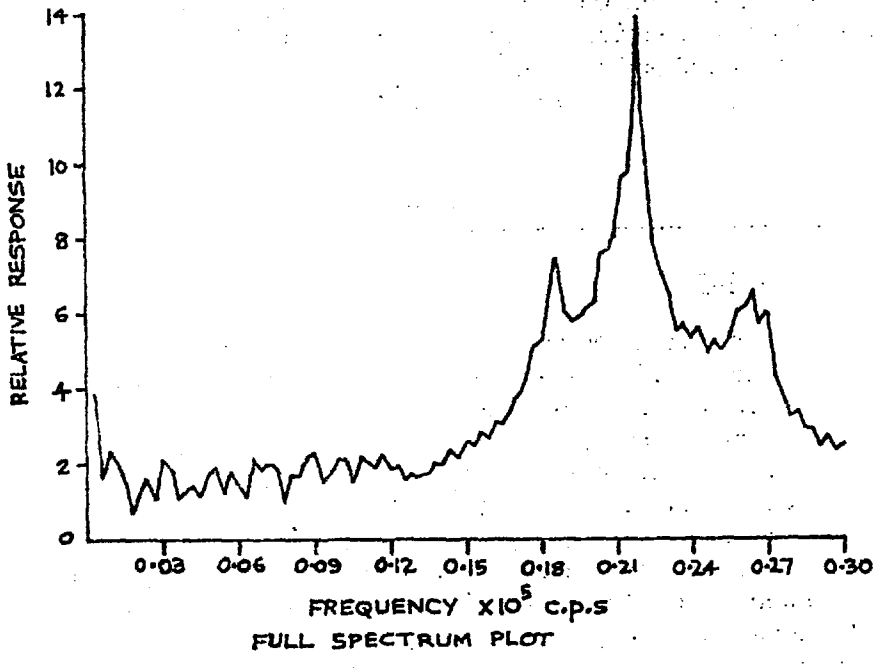

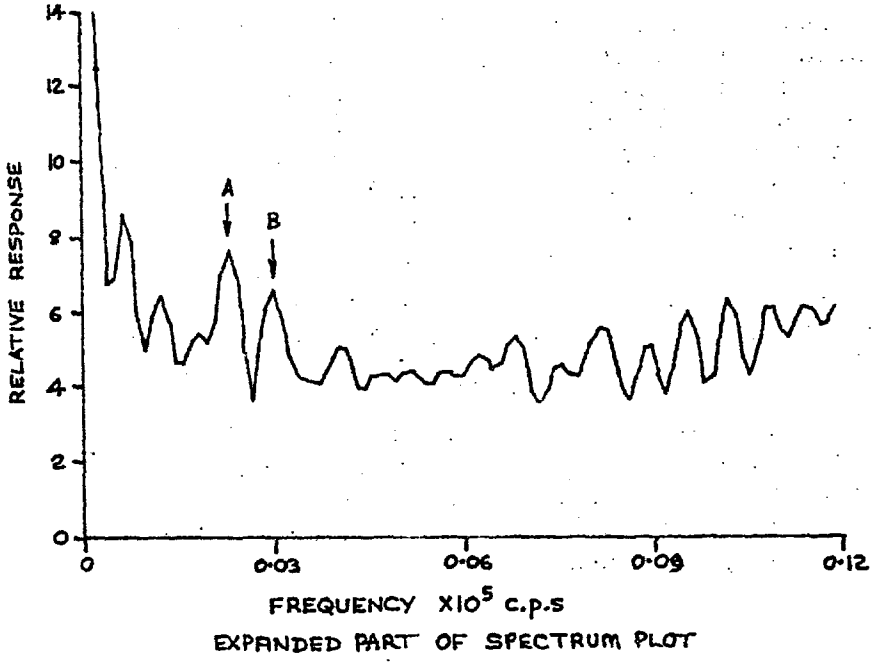

FIG. 11: FOURIER TRANSFORM OF HORIZONTAL DISPLACEMENT AT CREST OF SLOPE; Impulse excitation.

E. RESULTS FROM THE DYNAMIC PROGRAMS

The 3-dimensional problem of an open-pit vibrating was tackled in three stages:

(1) A 2-dimensional vertical slice was modelled in cartesian co-ordinates.

(2) A 2-dimensional horizontal slice was modelled in polar co-ordinates.

(3) The full 3-dimensional program was used - cylindrical polar co-ordinates.

Of course, given a large enough computer and unlimited computer time, only the 3D program need be run, but due to limitations of storage and time only a very approximate solution could be achieved with the present 3D program.

Two-Dimensional Plane Strain Dynamic Program

Due to the reasons given in the previous Section infinite boundaries could be simulated quite well by incorporating critical dashpots at the actual boundary nodes. Tests were made using this approach on a two-dimensional program, and showed that the boundary reflections could be significantly reduced - in most cases below a tenth of the incident wave. The model was as follows:

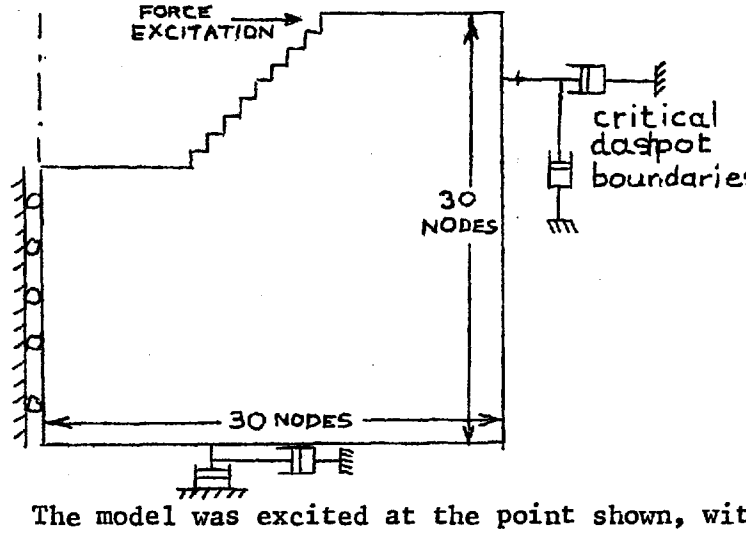

The model was excited at the point shown, with an impulsive force lasting one time increment. The time response of horizontal displacement was printed out, together with the Fourier Transform of the displacement waveform (The Fourier analysis is described in Chapter 4). The frequency response of the point at the top of the crest is given in Figure 11, to two scales. The upper curve shows a very large peak around $0{\cdot}25 \times 10^5$ c.p.s., which corresponds to the individual mesh oscillations, and has no bearing on the physical problems in hand. An expanded plot of the lower frequencies is given in the lower curve. Several peaks can be seen. In order to understand what particular modes of oscillation these corresponded to, the model was excited at the same point with a sine-wave force at the particular frequency concerned. After allowing several cycles of the excitation for the system to settle down to steady-state conditions, the motion of each node was plotted

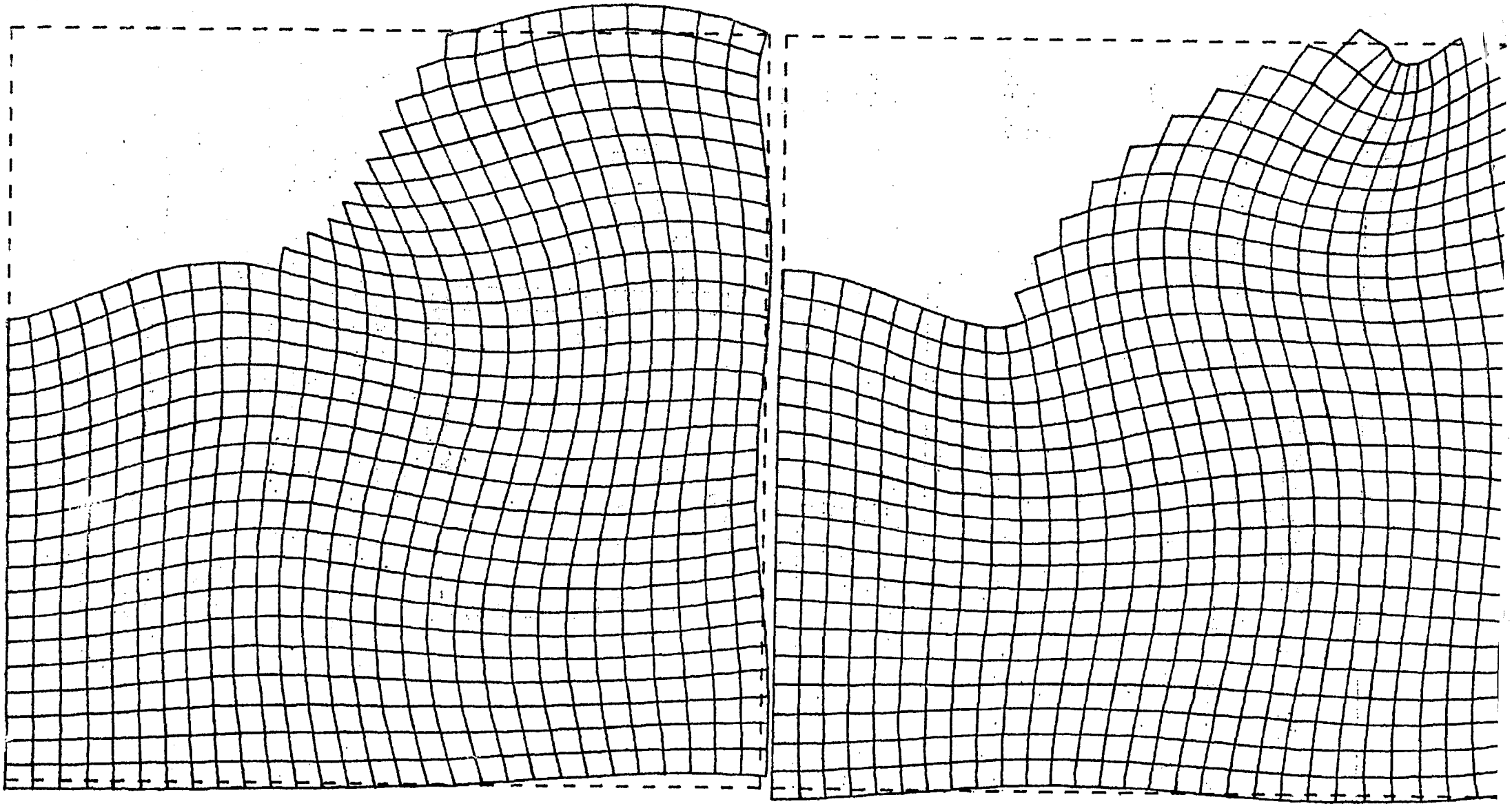

FIG. 12: EXAGGERATED DISPLACEMENT PATTERN DUE TO SINE-WAVE EXCITATION AT CREST OF SLOPE. Two instants in time are shown.

FIG. 10 : DYNAMIC DISPLACEMENT ELLIPSES

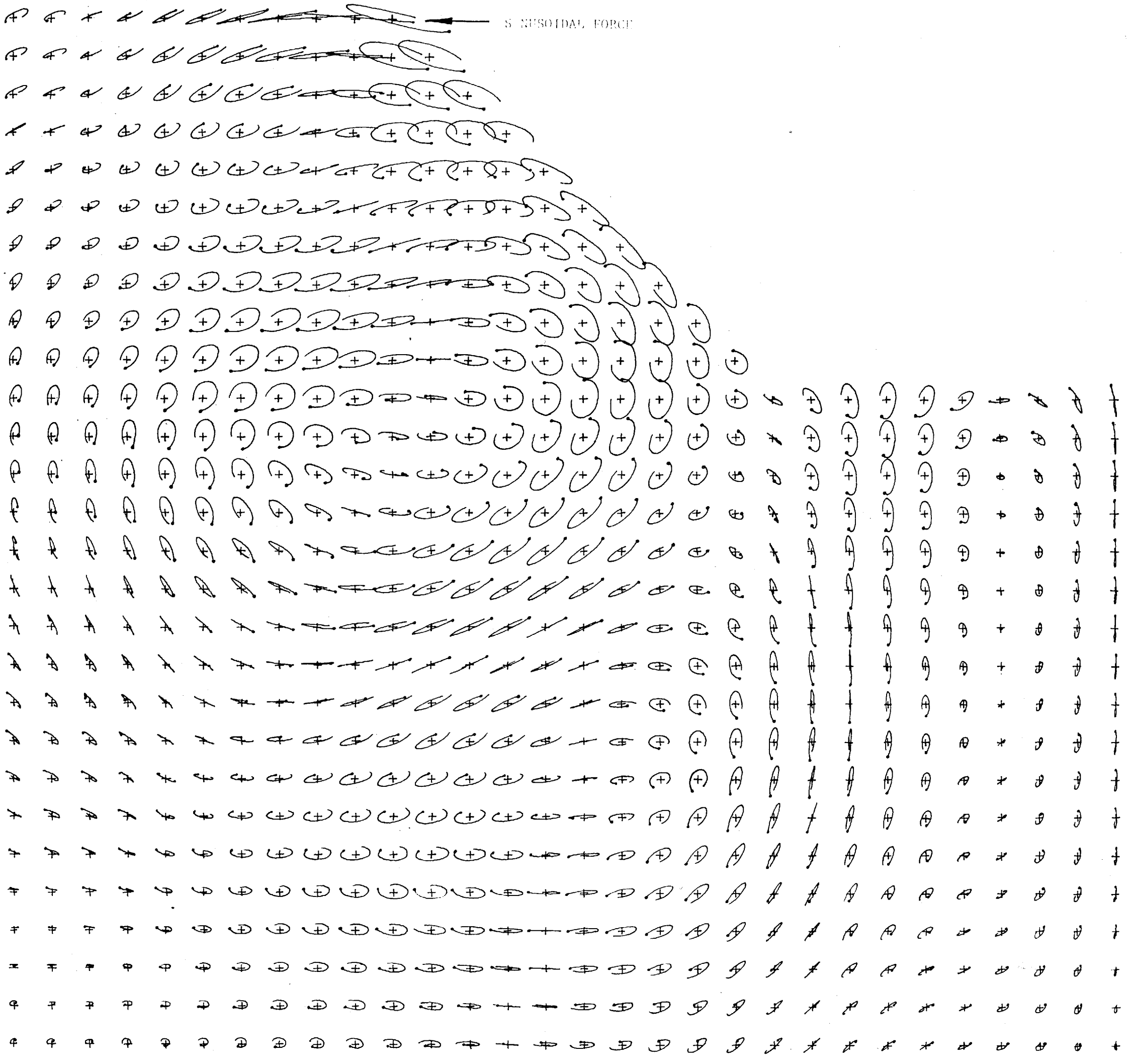

out as an ellipse. These ellipses show the locus of each point as it oscillates in two dimensions, the direction of rotation of the ellipse being shown by the dot, which is the latest point in time. The plot is given in Figure 10 (folded over). This particular plot was for an excitation frequency of $0{\cdot}03 \times 10^5$ c.p.s; i.e. the second high peak (B) in Figure 11. The plot brings out the fact that a true resonance is not possible in a non-conservative system: there are no zero-displacement points, and in general the displacement locii are ellipses, reflecting large phase differences.

An alternative way of presenting the information is shown in Figure 12, which shows two instantaneous pictures of the deformation of the model (greatly exaggerated) when excited by a sinusoidal force of 0.024×10^5 c.p.s. (peak A on Fig. 11). This diagram does not yield as much information as the ellipse plots, but it can be clearly seen that the motion involves alternate extension and contraction of the sloping face of the pit.

Frequencies

The frequencies corresponding to the peaks of Figure 11 may be normalised, by reference to the shear wave velocity (hence Rayleigh wave speed) and a dimension of the pit. The "radius", R, of the pit is taken as the distance from centre-line to crest. The data for the model is as follows:

$E = 0.362 \times 10^{11}$ N/m^2
$\rho = 0.26 \times 10^4$ Kg/m^3
$\nu = 0.2$
$\Delta X = 0.5 \times 10^{-1}$ m
$\Delta Y = 0.5 \times 10^{-1}$ m

$$\therefore \text{Shear modulus } \mu = \frac{E}{2(1+\nu)} = 0.151 \times 10^{11} \text{ N/m}^2$$

$$\text{Shear velocity } C_s = \frac{\mu}{\rho} = 2.41 \times 10^3 \text{ m/sec}$$

$$\text{"Radius" } R = 20 \times 0.5 \times 10^{-1} = 1 \text{ m}$$

$$\text{If frequency} = K.\frac{C}{R}$$

$K = \underline{0.995}$ for the first peak
and $K = \underline{1.15}$ for the second peak

Resonance Magnification

Some estimate of the pit's ability to magnify incident waves needs to be made. The ratio of the height of the first peak on Fig. 11 to the average response level is

$$\frac{7.5}{5.0} = \underline{1.5}$$

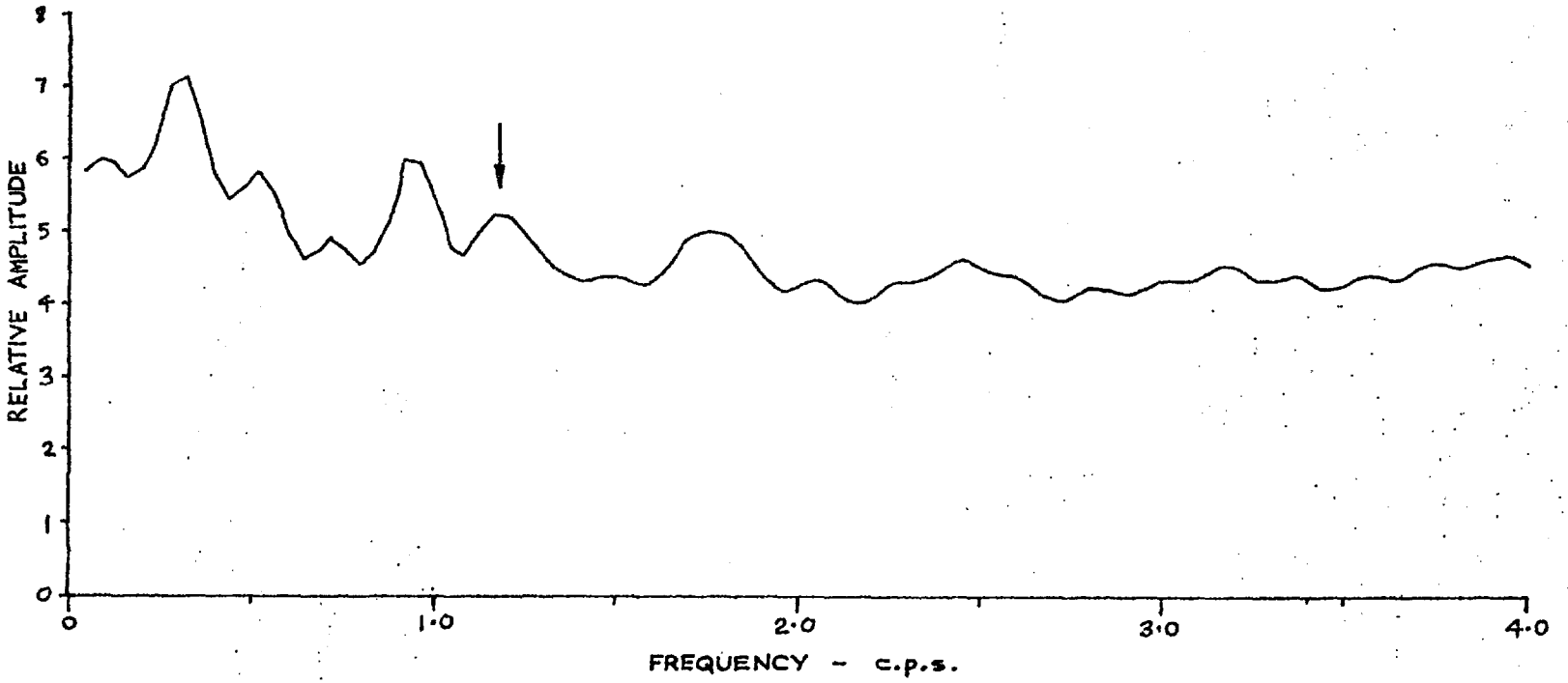

FIG. 14: SPECTRUM OF DISPLACEMENT RESPONSE OF A POINT ON THE SURFACE OF A HOLE - Radial impulse excitation at the same point.

2-Dimensional Circular Hole

The possibility that circulating waves may contribute modes of oscillation prompted the writing of a plane strain program in polar co-ordinates, to simulate the response of a 2-dimensional hole in an infinite solid. As mentioned previously, the critical dashpot method for boundary damping was considered inappropriate in this case. However, a small damping band was included at the boundary to absorb any waves approaching with normal incidence. The model used was 70 nodes from the centre to the boundary, divided circumferentially into 32 sectors, the whole 360° being modelled. The hole had a radius of 4 nodes. Thus the ratio of boundary radius to hole radius was 17·5:1, which was believed to be adequate to simulate an infinite medium.

An impulsive force was imparted to the hole boundary, and the displacements plotted out as a function of time. The plot is not included here because it is considered to be of little value since it was dominated by the individual mesh oscillations. A great many techniques were tested in order to try to eliminate these oscillations, but the best were only partial successes. For instance, an exciting waveform was used, the Fourier Transform of which cut off at a frequency just below that of the mesh oscillations. Unfortunately the exciting waveform necessary to achieve that Fourier Transform was itself highly oscillatory, which caused as much confusion as the original oscillations The only answer seems to be to dispense with the time records, and concentrate solely on the frequency plots, ignoring those frequencies corresponding to mesh oscillations.

The spectrum plot for the hole displacement is shown in Figure 14. The hole was then excited by a sinusoidal force with a frequency corresponding to a particular peak of Fig. 14. Figure 13 (located at the end of this Part, folded up) gives an ellipse plot for an exciting frequency of 1·18 c.p.s. This is rather a curious plot, since it has three positions of maximum amplitude, but at all those points the particle motion is in the same direction. However there is no corresponding motion of other points in the opposite direction. Thus all points on the surface are either moving outwards or inwards together.

Unfortunately Figure 13, and all the similar plots obtained, were largely a function of the far boundary. Remarkable as it may seem, a boundary 70 units away from a hole of 4 units affects the response to such an extent as to seriously alter the nature of the ellipse plot. This fact was determined by varying the boundary dimensions, and noting the outcome. In view of this, little reliance should be placed on the results of the program. It may be worth recording the relevant frequencies and magnification factors:

The data was:
$E = 0.3 \times 10^{11}$ N/m^2
$\rho = 0.26 \times 10^{4}$ Kg/m^3
$\nu = 0.22$
$\Delta R = 87{\cdot}5$ m

shear modulus $\mu = 0.123 \times 10^{11}$ N/m^2

$C_s = 2.175 \times 10^{3}$ m/sec

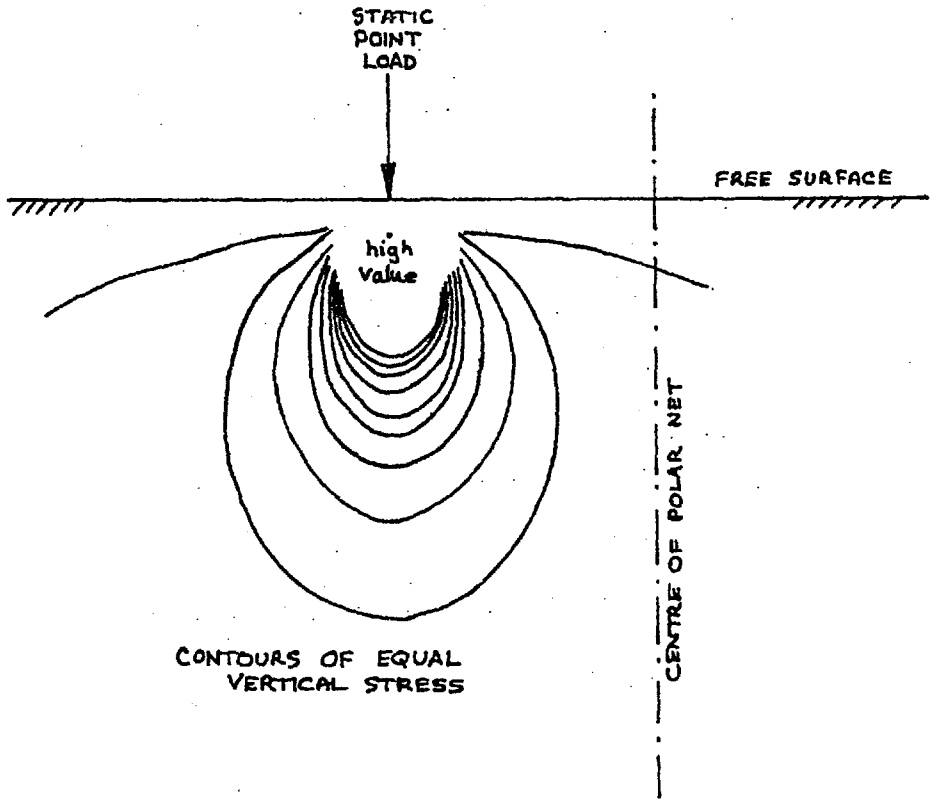

FIG. 15: STRESS CONTOURS DUE TO STATIC POINT LOAD TEST OF 3-DIMENSIONAL PROGRAM

Radius R = 87.5 X 4 = 350 m

Normalised frequency = 0.19 $\frac{C_s}{R}$ for the 1.18 c.p.s peak.

i.e. the frequency is about one fifth of that derived from the previous program for a vertical slice.

The highest "resonance" peaks were a factor of 1.25 above the general response level. This factor is likely to be in error on the high side, since the boundary has been shown to be influencing the problem.

Full Three-Dimensional Dynamic Program

A three-dimensional elastic D.R. program was written in cylindrical polar co-ordinates. A circular pit was included in the centre of the net. The model could be loaded in a fully asymmetrical fashion.

Many checks were performed on the program to ensure that it was correctly modelling the physical problem - both static and dynamic tests. Figure 15 gives the results from one such test - a point load applied near, but not at, the centre of the net, to see whether a symmetrical stress distribution would result. This provided a powerful check on the correctness of the polar equations, and the validity of the calculations performed at the centre of the net.

The centre of the polar net represents a singularity, since no finite-difference calculations can be performed there due to the vanishingly-small size of the meshes there. However, in order to perform calculations a short distance away, at the first ring of nodes, values of stress and displacement are *required to exist* at the centre node. As explained, these values cannot be found in the normal way, from the difference equations. The method of generating the required variables was to take the average of a the relevant variables existing at the closest distance out from the centre. Of course in order to arrive at the average, it was necessary to resolve the various stresses or displacements in the correct directions. In point of fact all the variables at the centre *could* be set to any value without affecting the behaviour of the complete system to any great extent. This is because the centre node represents only a very small volume in comparison to that of the whole system, so that its stresses and displacements are unable to exert much effect on the system.

The major drawback with the 3D program was that, even with 4000 or so nodes, the boundaries needed to be so close to the open-pit that all hope of eliminating or neglecting reflection effect was lost. No dynamic plots are shown, as they are almost totally dominated by the boundary effects and mesh oscillations. The only conceivable use for the program is to furnish orders of magnitude for the displacements resulting from a given impulsive force. These are likely to be higher than reality due to the reflection of energy from the boundaries. To assess the levels of displacement, the complete set of displacements was printed out for the whole system, at regular time intervals. From this

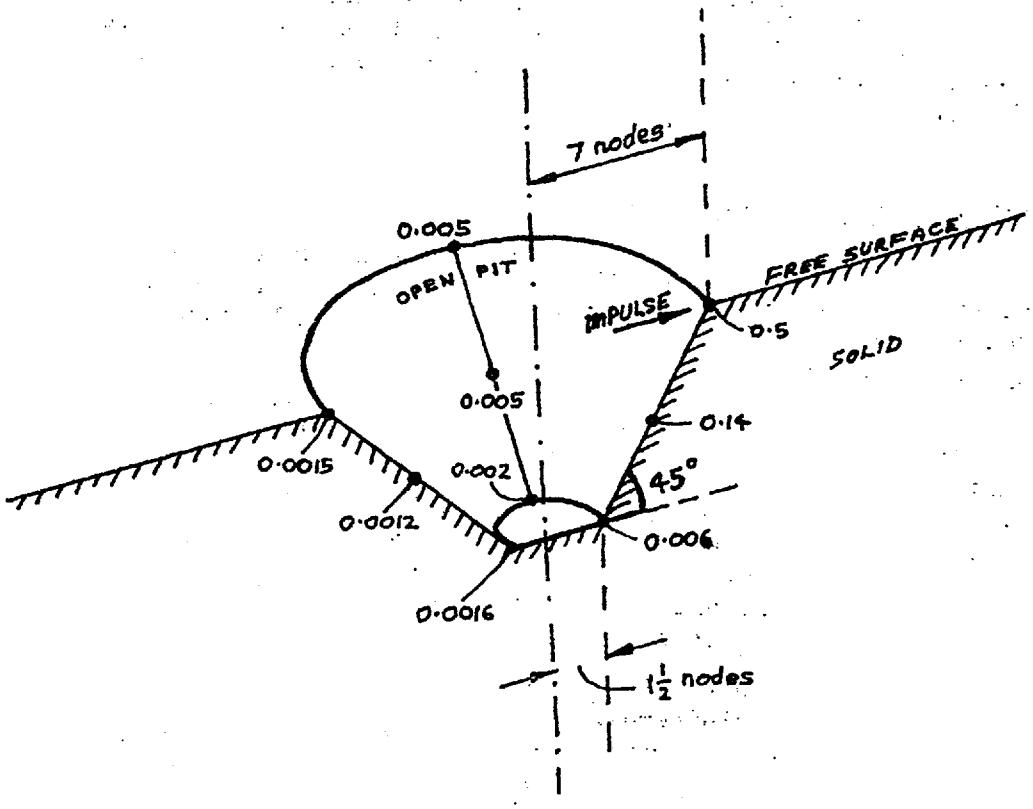

FIG. 16: VIEW OF HALF THE OPEN-PIT, SHOWING PEAK HORIZONTAL DISPLACEMENTS AT VARIOUS POINTS 3D Dynamic Relaxation program.

print-out, general conclusions could be drawn regarding the levels and locations of pit responses.

The impulse was 1 N-sec/m^2 applied to an area of 50 X 110 m^2 at the crest of the pit.

$\therefore$ Impulse = 5500 N-sec

Other Data

ΔR = 50 m
ΔZ = 50 m
$\Delta\theta = \frac{\pi}{8}$ (16 sectors)
ρ = 1.0 Kg/m^3
ν = 0.25
E = 1.0 N/m^2
angle of slope = 45^o
Radial boundary = 15 nodes
Vertical boundary = 10 nodes

The maximum displacements were always close to the pit surface. The displacements also varied depending on their location in the pit. Figure 16 gives the magnitudes of the peak displacements recorded at various locations on the surface of the pit. The units are metres, only the long-period displacements being noted. The reason for displacements being given instead of, say, accelerations is that the accelerations would be affected to a far greater extent by the high-frequency mesh oscillations.

The figures given in Fig. 16 should not be taken as representing an exact solution to the problem. They are presented only insofar as they indicate the order of magnitude to be expected and the general distribution of displacements around an open-pit.

Observations and Conclusions

An attempt has been made to simulate the response of an open-pit to impulsive excitation. Judged by the lack of unequivocal results for the problem, the attempt must be viewed as a failure. The failure was brought about by an inability to model an infinite problem with a finite number of elements. No way was found of eliminating the effects of the boundaries. Nevertheless conclusions have been drawn regarding the expected frequencies, the magnification factors of the pit and the levels of motion resulting from a given blast. These conclusions should be used with due regard to their origins.

A major point of interest is the lack of any pronounced resonance effects associated with an open-pit. In fact the resonance effects observed with the two-dimensional models should over-estimate the true magnification factors.

It is believed that the same difficulties associated with the boundary conditions and extraneous oscillations would have been met if Finite Elements had been used instead of Dynamic Relaxation.

PART 2

PART TWO

A. DISCUSSION

As mentioned earlier, a number of ideas were suggested by Dynamic Relaxation, and some of these were followed up. The results are included here for interest, even though they have no direct bearing on the main topic of the Thesis.

Dynamic Relaxation was of course developed to solve static problems. For problems involving simple geometries it is quick and efficient. However there is evidence to suggest that a static stress distribution is of little value for failure calculations in Rock Mechanics. St. John (Ref. 8) produced a number of self-weight stress distributions in continuous, homogeneous, elastic slopes by using the Finite Element method. He then resolved the stresses in the direction of a hypothetical joint set, and calculated what shear and normal stresses would exist on the joint, assuming that the joint in no way affected the stress distribution. The shear stresses were then compared with those that could be mobilised assuming a realistic Mohr-Coulomb failure law. The broad conclusion was that large parts of the slope exceeded the failure criterion, even though the geometry chosen was demonstrably stable. The answer to the paradox is that very small movements do occur on the joints, these movements completely altering the original stress distribution. The result of the slight "shuffling" of the joints is to redistribute the stresses in such a way as to make all parts of the slope stable with respect to the failure criterion. Even though static stress distributions in elastic ~~jointed~~ media have been shown to be of dubious worth, a short section of this Chapter deals with them, as a number of interesting facts emerge.

Bearing in mind the above observations, the obvious question is: "can failure mechanisms be built into the computer programs?" Some of this part deals with the varying success with which some degree of progressive failure has been incorporated into Dynamic Relaxation programs.

Even the inclusion of failing joints within an elastic continuum may not be the whole answer. When a rock mass starts to move, voids appear, point-contacts occur and all manner of discontinuous effects are manifest. It is pertinent to ask whether the concept of "stress" has any meaning under these conditions. Even the stress-distribution within two imperfectly-touching blocks pressed together is very complex, with numerous high and low spots. There is, however, one parameter that remains finite and well-defined, and that is the force between the blocks. In the final section of this Part, stresses and strains are dispensed with, and a program described which deals with the forces and displacements existing within a system of discrete blocks.

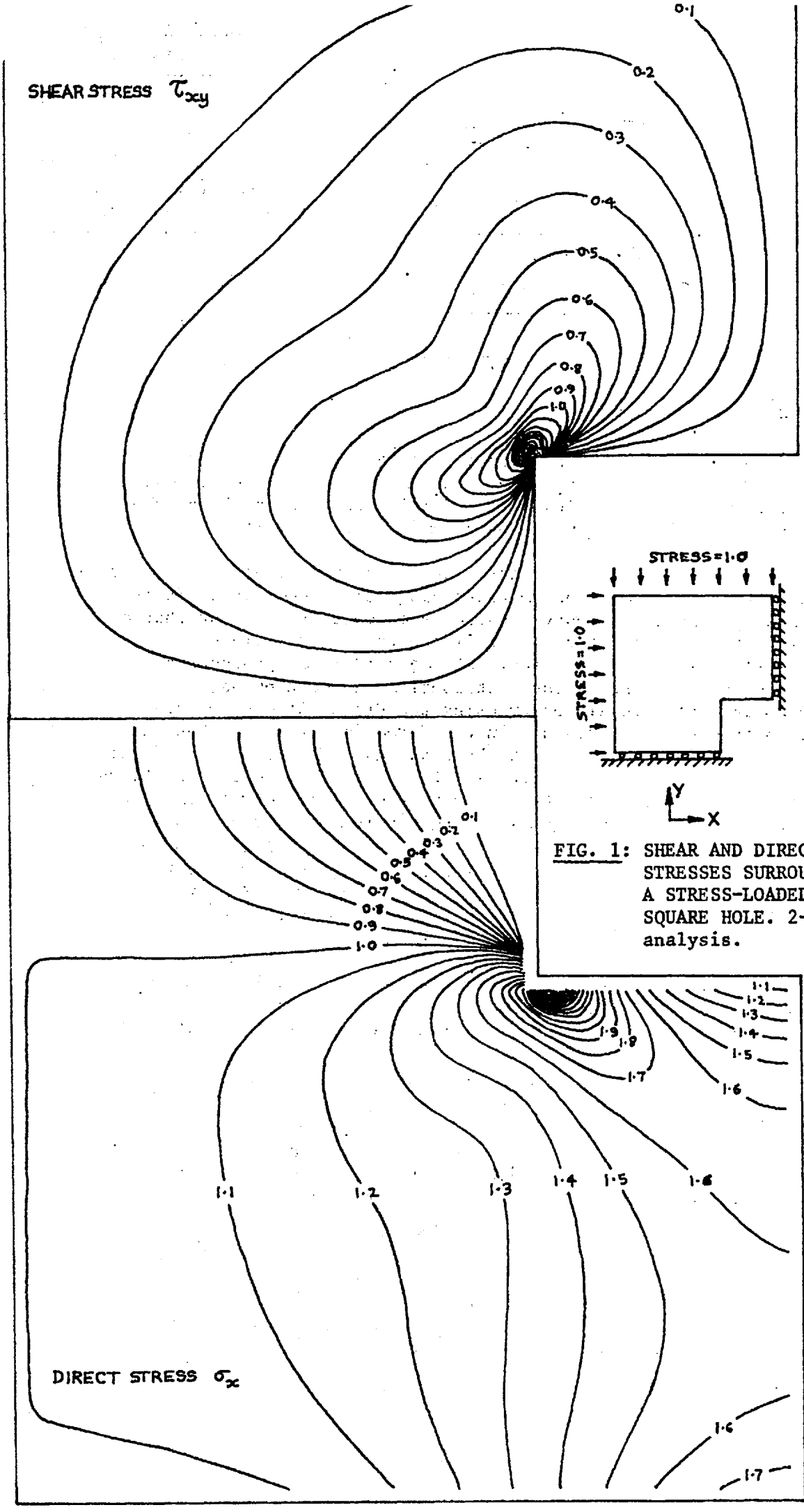

FIG. 1: SHEAR AND DIRECT STRESSES SURROUNDING A STRESS-LOADED SQUARE HOLE. 2-dim. analysis.

B. STATIC STRESS ANALYSIS

Stress-Loaded Underground Opening

A square, two-dimensional underground opening was modelled. Only a quarter-model was considered since a square hole has two-fold symmetry. The boundaries for the plot given in Figure 1 were situated at three times the hole dimension from the centre, but little change in the stresses around the hole were caused by increasing the boundaries. Stresses were applied to the boundaries, the ratio of X stress to Y stress being 1:1 in this case, although of course any stress ratio may be used. The number of nodes along one side of the quarter-hole was ten, which results in a good definition of the stresses around the opening. The displacements and stress trajectories corresponding to Figure 1 are given in Figures 2 and 3. The displacement vectors are magnified images of infinitesimal movements. The stress trajectories show the direction of the major principal stress at each point. The value of Poisson's ratio has no effect on the stress distribution since there are no displacement constraints. Similarly, the stresses are independent of the other elastic constants, such as Young's modulus.

Plane Strain, Self-Weight Model

A two-dimensional plane-strain rectangular notch cut in the free surface of an elastic gravity-loaded block was analysed. This model is included since it brings to light a number of important points about loading sequences. There are several ways of generating a stress distribution around an excavation, each of which may give a different answer. The easiest way is to simply "switch on" gravity to an existing non-stressed geometry, e.g.,

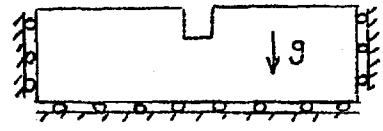

Alternatively a uniform stress field may be built up in an un-excavated model, then a portion removed to cause a redistribution of stress. In this case, attention must be paid to the constraint existing at the boundaries whilst the excavation is taking place. Clearly if the boundaries are far enough away, the boundary conditions should not affect the solution at the excavation. The present model was analysed in three stages, shown in Figure 4. For the first stage, only stresses were applied to the boundaries. In this way, any level of horizontal pre-stressing could be achieved without Poisson's ratio effects causing non-uniform stress fields as would have been the case had any displacement boundaries been used. For the second stage, the two extreme possibilities are: (a) infinitely soft boundaries (i.e. constant stress), or (b) infinitely stiff boundaries (constant displacement). In the present case, the two approaches gave almost identical results, since the ratio of boundary distance to notch size was large (12·5 : 1).

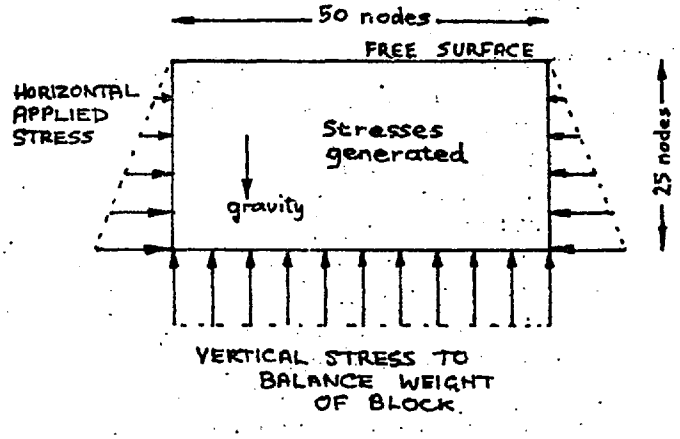

FIRST STAGE : CREATING UNIFORM STRESS FIELD

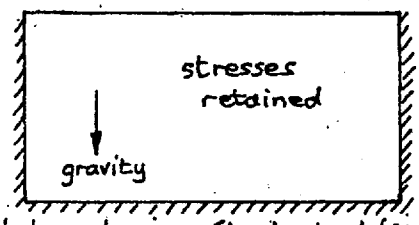

All boundaries fixed at deformed positions

SECOND STAGE : FIXING BOUNDARIES

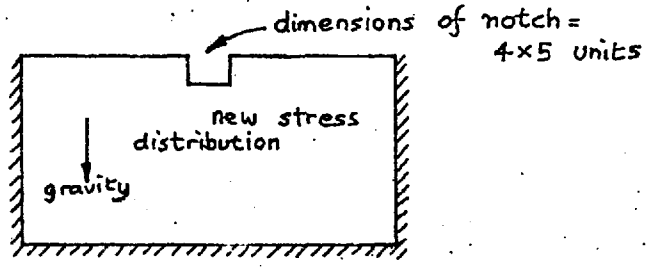

THIRD STAGE : NOTCH CUT IN FREE SURFACE

FIG. 4: STAGES INVOLVED IN LOADING A 2 - DIMENSIONAL SELF-WEIGHT NOTCH MODEL.

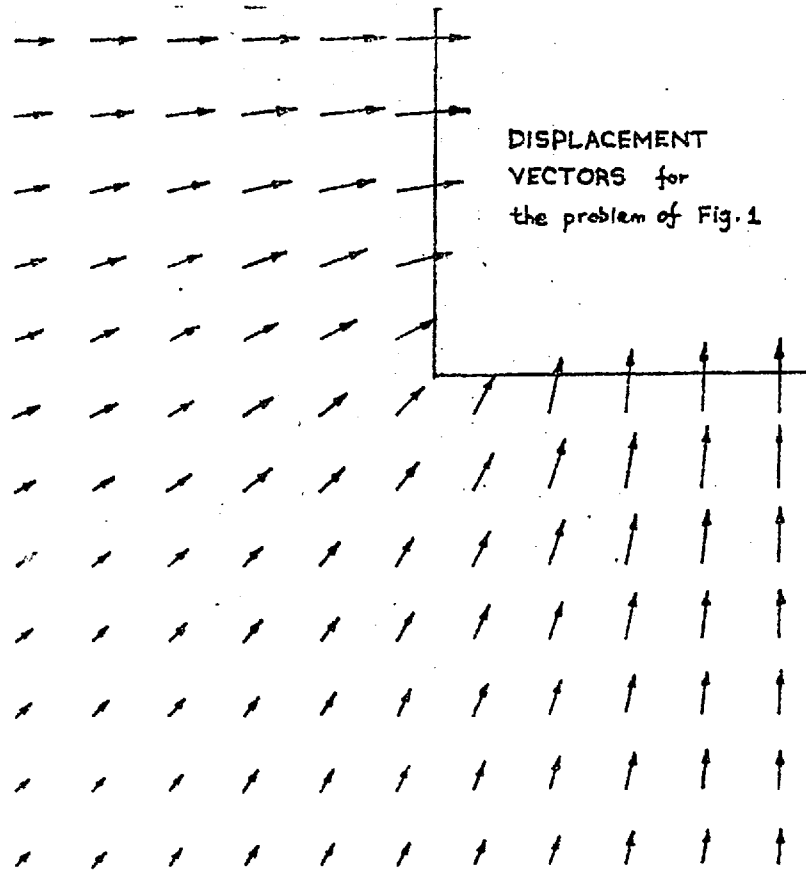

FIG. 2: DISPLACEMENTS

FIG. 3: STRESS DIRECTIONS

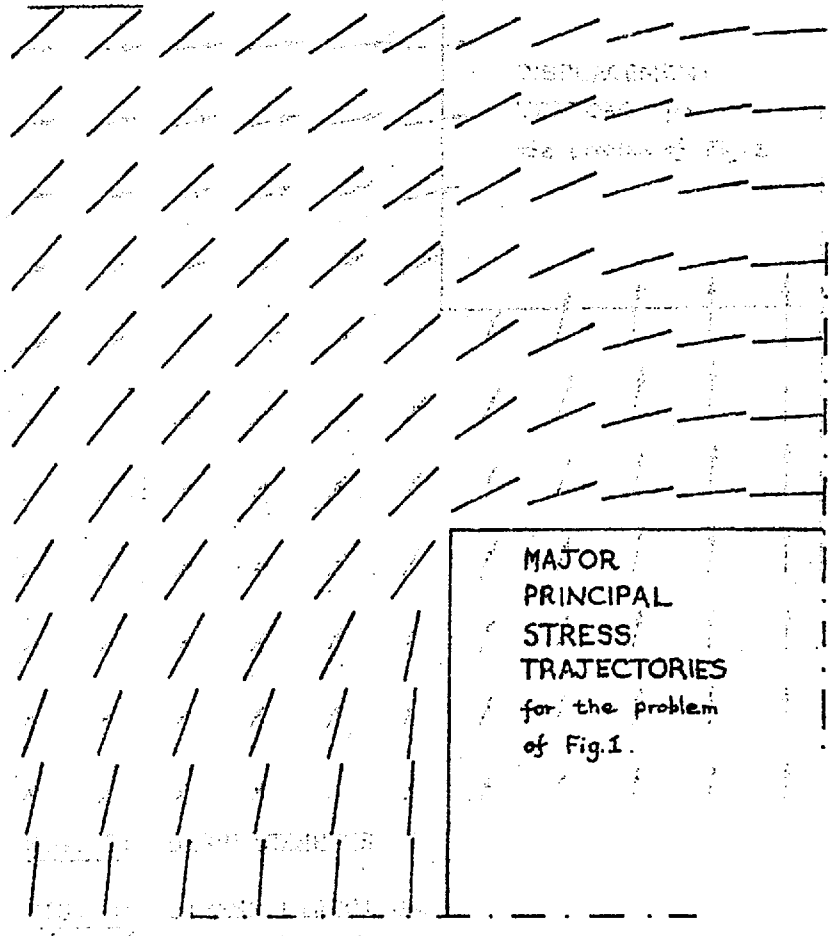

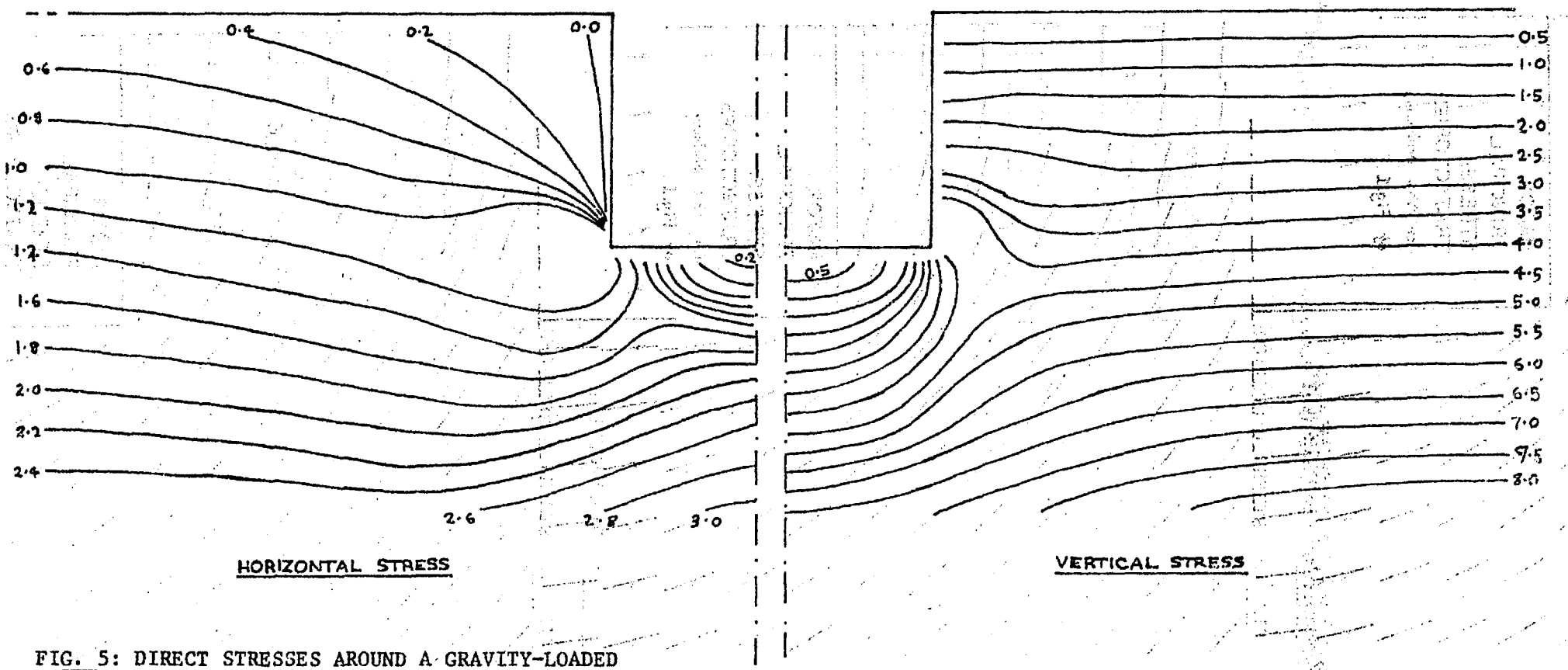

FIG. 5: DIRECT STRESSES AROUND A GRAVITY-LOADED NOTCH. Horizontal applied stress gradient is 1/3 of the vertical gradient.

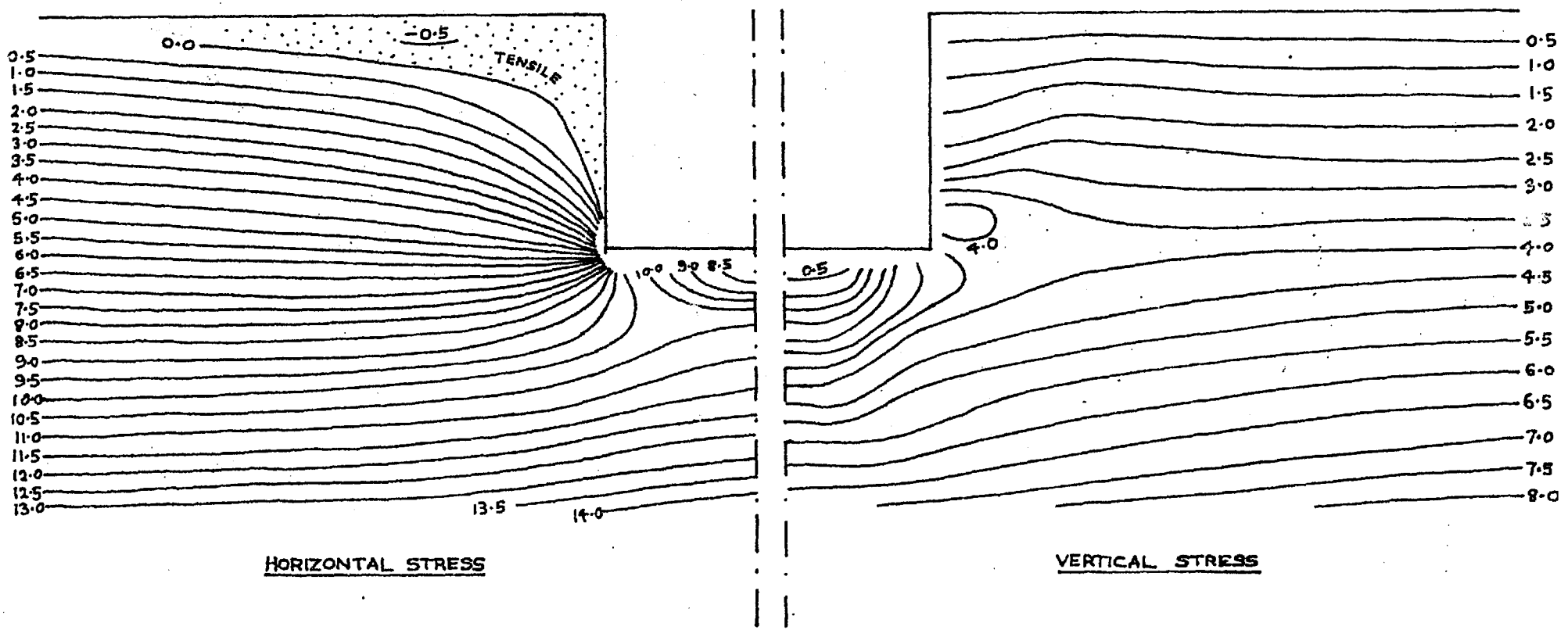

FIG. 6: AS FIG. 5, but horizontal applied stress gradient is 1·6 times the vertical gradient.

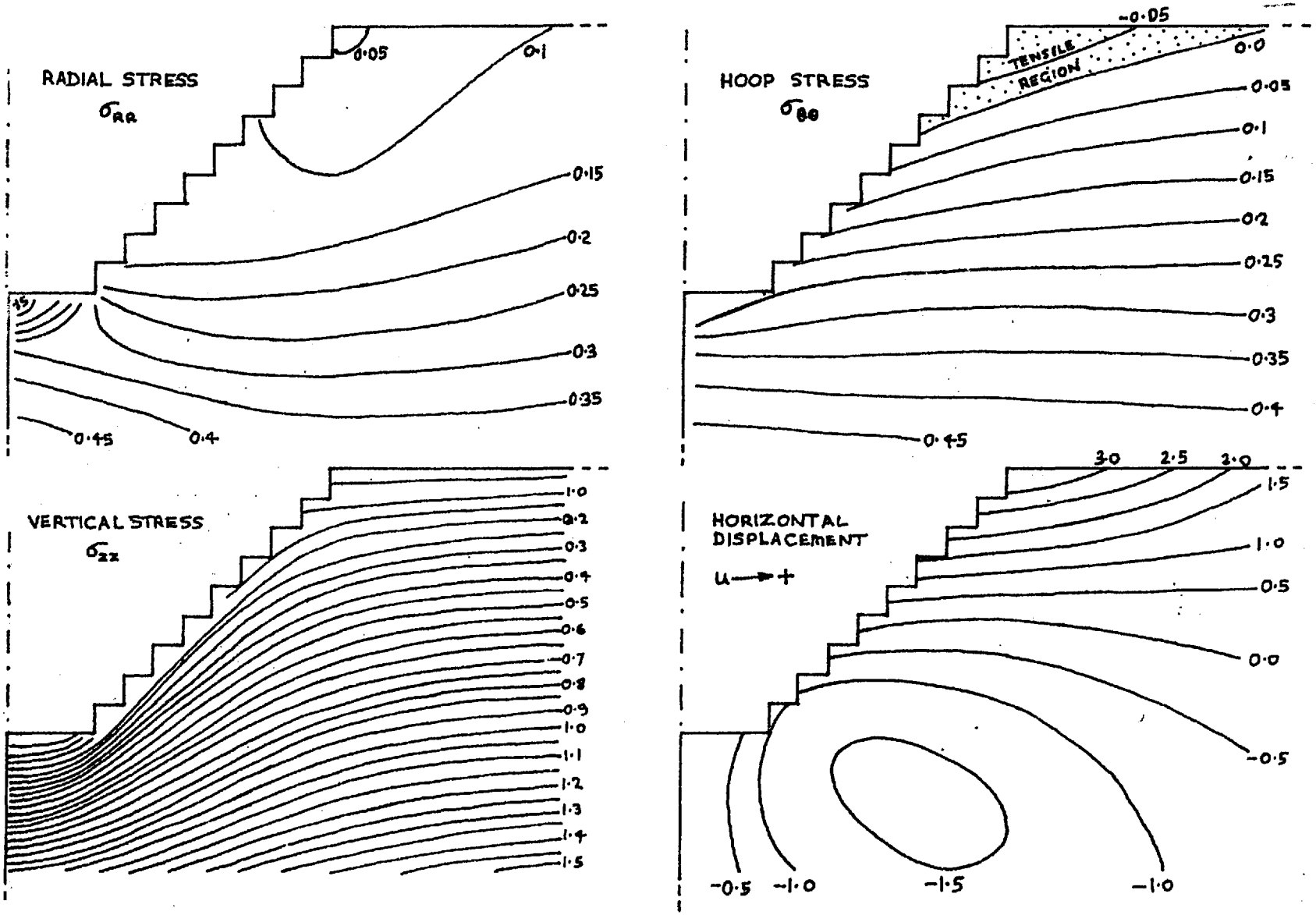

FIG. 7: STRESSES AND DISPLACEMENTS AROUND A GRAVITY-LOADED 3-DIMENSIONAL AXI-SYMMETRIC 45° PIT.

The stress plots for two different applied horizontal stress gradients are shown in Figures 5 and 6. The interesting fact is revealed that the *higher* applied stress generates the *lower* stress at the crest of the notch. In fact it is tensile. Further tests have shown that if the horizontal applied gradient is greater than about 1/3 of the vertical, a tensile region is present at the crest of a notch.

3 Dimensional Axi-Symmetric Gravity Model

The stress distribution around a circular 45° pit embedded in the surface of an elastic continuum was modelled by Dynamic Relaxation using cylindrical polar co-ordinates. Since the stress distribution must be symmetrical about the centre-line of the pit, only a single, thin sector was analysed. Only radial and vertical displacements were allowed, the circumferential displacements being set to zero. The model was as follows:

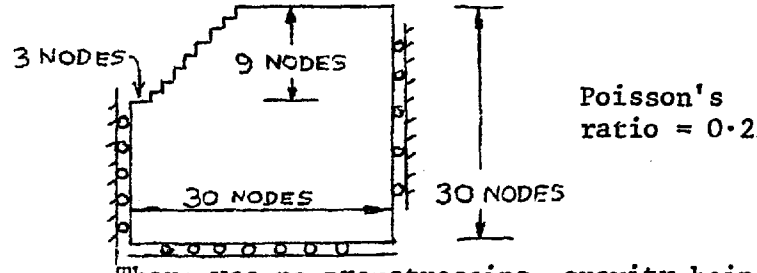

There was no pre-stressing, gravity being applied instantaneously, vertical motion only being permitted at the side boundaries, and horizontal motion at the base. As well as stresses in the plane of the wedge, the perpendicular stress (hoop stress) was also calculated, since the existence of this stress is often assumed in comparing the stability of a curved pit with a linear one. Three direct stresses are plotted in Figure 7, together with the horizontal displacement.

The most prominent features are: (a) the large reduction in radial stress just behind the pit slope (c.f. the plane strain notch) and (b) the tensile region of hoop stress. This last observation is interesting in view of the common assumption that a circular pit is stabilised by a *positive* hoop stress existing behind the slopes. The displacement plot is consistent with the negative hoop stress, since the top part of the slope is observed to move outwards, thus tending to increase the circumference of the pit. Tension is naturally generated due to the increased circumferential length.

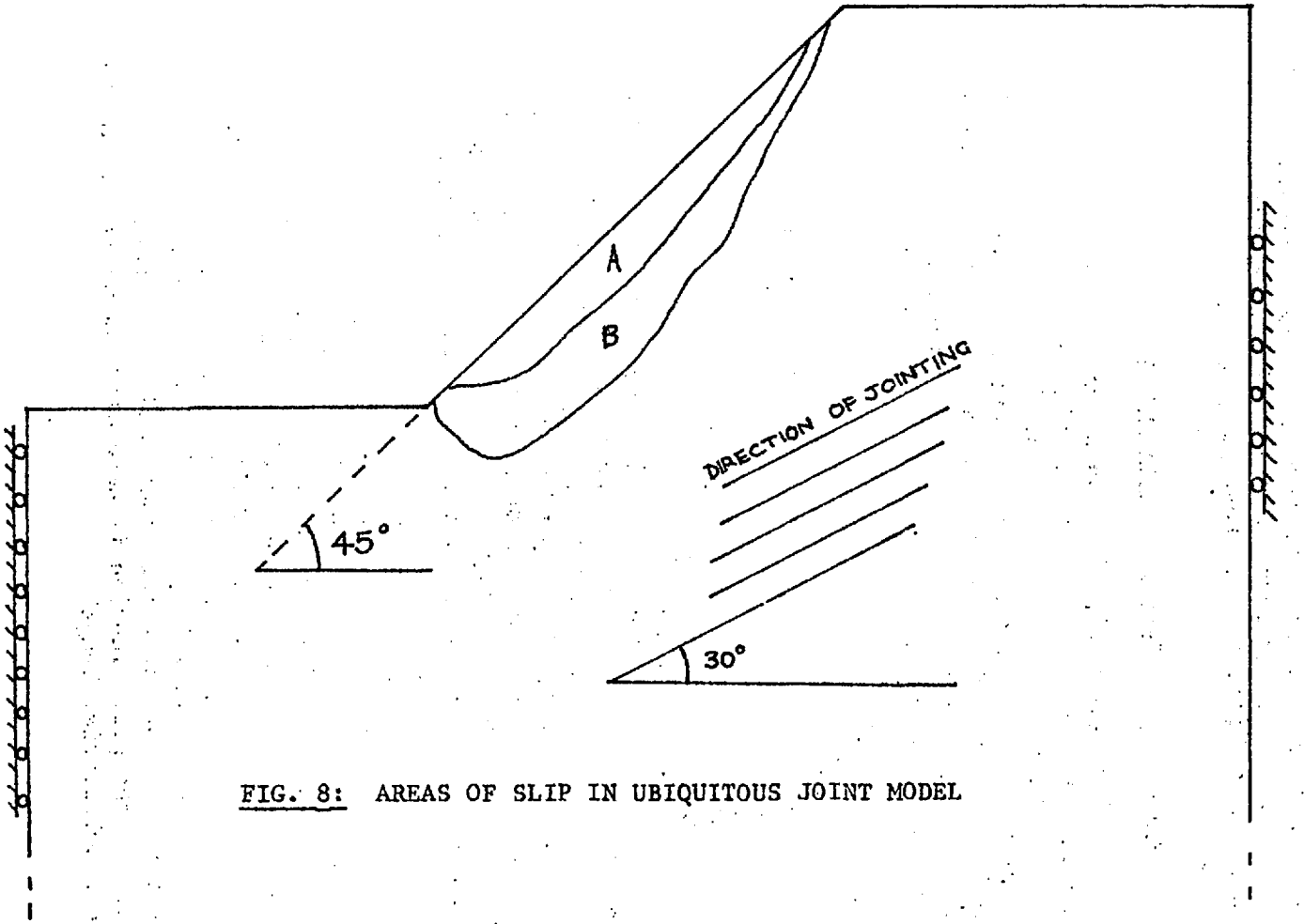

FIG. 8: AREAS OF SLIP IN UBIQUITOUS JOINT MODEL

C. UBIQUITOUS JOINT ANALYSIS

One way of modelling a heavily-jointed medium is to regard the joints as existing at all points within the continuum. The joints may be thought of as altering the material properties of the solid in an anisotropic fashion. This approach was tried with Dynamic Relaxation, the jointing procedure being incorporated in the stress-strain section of the program (i.e. the static part of the cycle). The steps were as follows:

1. Stress-stain calculations performed as standard program. Resultant stresses resolved to give normal and shear stresses in assumed joint direction.

2. Joint shear stress compared with normal stress to test for slip, i.e. if $\tau > c + \mu\sigma$. If slip indicated, shear stress set to $\mu\sigma r$, where r is the residual fraction of peak stress.

3. New joint stresses resolved back to X-Y co-ordinates for inclusion in the next iteration cycle.

Of course, the steps must be modified if a point is *already* slipping, in which case the cohesion, c, is ignored, and r set to 1. The program allows points to return to elastic conditions if the joint shear stress falls below the value necessary for slip. A disadvantage of the method is that, using the interlaced net of Dynamic Relaxation, the X-Y stresses must be averaged between nodes to give the total stress at a point, before resolving in the joint direction. An averaging process must then be used again to return to X-Y stresses. This procedure alone introduces errors.

Where a small amount of slip was necessary, the program appeared to work satisfactorily. Region A on Figure 8 shows the area initially exceeding the failure criterion. After a number of iterations, this area had spread, and then stabilised, after covering a total area of A + B. In passing, it is interesting to note that the elastic analysis of the slope shows that there is a "failing" area even though the physical situation is clearly highly stable.

Unfortunately, when fairly large amounts of slip were necessary, the program went unstable, even though the physical system should have been stable. The precise reason for this is uncertain, but it may be connected with the fact that large stress gradients are observed to develop in a particular area that is slipping. In fact, the stresses at adjacent nodes are often of opposite sign. This may explain the instability, since the finite difference method is based on the assumption of continuous variation of stress between nodes.

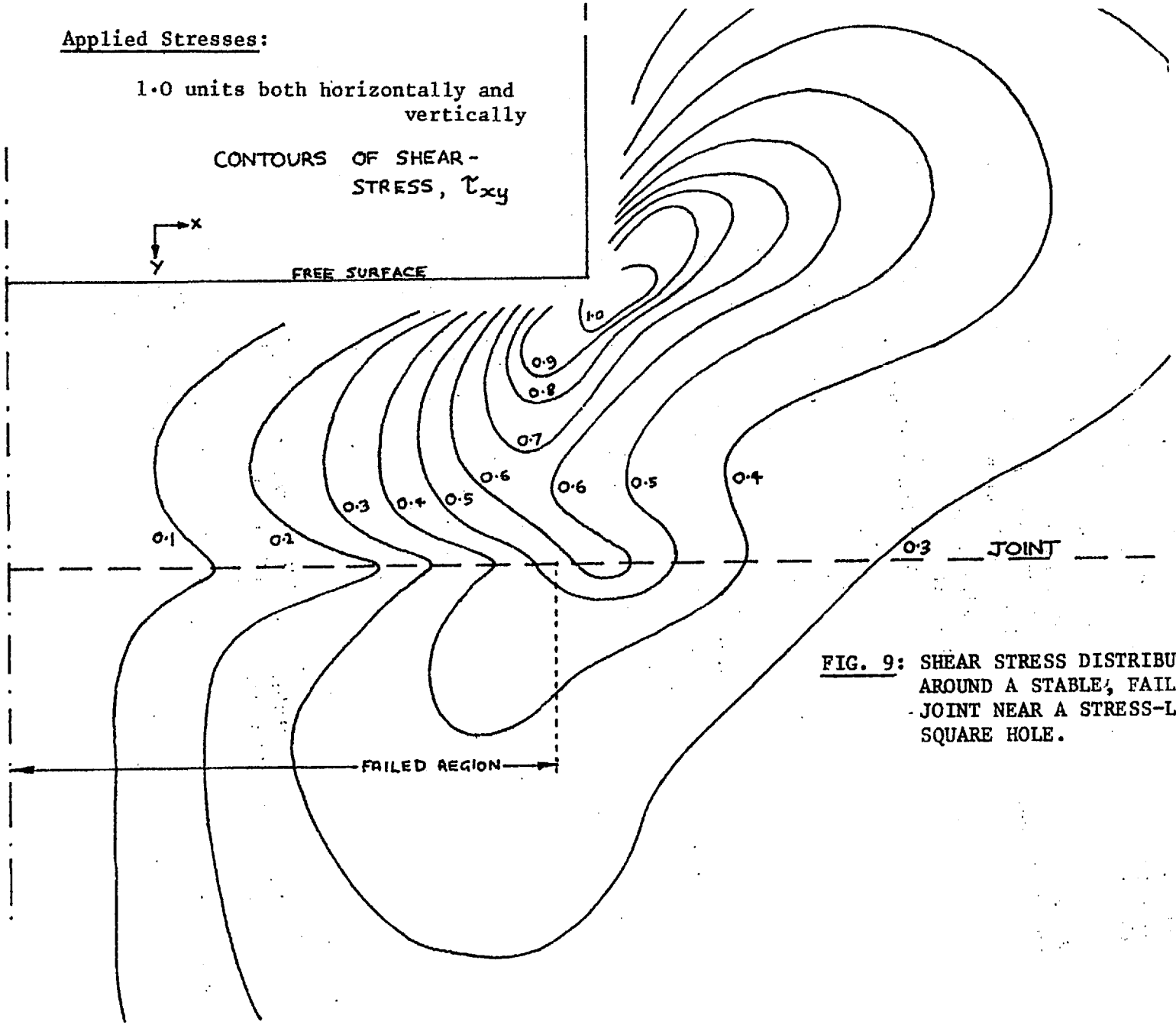

FIG. 9: SHEAR STRESS DISTRIBUTION AROUND A STABLE, FAILED JOINT NEAR A STRESS-LOADED SQUARE HOLE.

D. DISCRETE JOINT SYNTHESIS

As mentioned in the Discussion, an elastic solution to a stress problem may give misleading results if used to predict stresses in a discontinuous rock mass. This is due to the fact that the joints are able to shear, and to open up, causing the stress distribution to be entirely altered. It was considered useful to try to include the effects of one or more failing joints in the static elastic Dynamic Relaxation program. At about the same time a number of people were trying to achieve similar objects using Finite Elements, notably Goodman (Ref. 4). Goodman includes a "joint" by modelling it as a thin element, of nominally zero width, which can alter its properties depending on the level of applied stress - it can have elasto-plastic characteristics. A good deal of success was achieved with this method.

The Joint as a Boundary Condition

It is believed that a more powerful method of modelling a joint is to regard it as a *boundary condition* rather than as an alteration of the local properties of the continuum. If the properties of a particular element are altered as a result of "failure", this element must be incorporated in the matrix, to be solved along with all the other "normal" elements. If the properties of several elements are very different, the matrix can become ill-conditioned and hard to solve accurately. However, modelling the joint as a boundary condition allows the properties of the elements comprising the continuum to remain unchanged. The joint manifests itself as a series of displacements and stresses prescribed at a particular boundary.

In the present work, only joints lying along the lines of the Dynamic Relaxation grid were modelled, although no doubt joints at arbitrary angles could be included, by using suitable interpolation procedures. The D.R. interlaced net ideally lends itself to the inclusion of a joint. The following diagram shows part of the net, with the position of the joint:

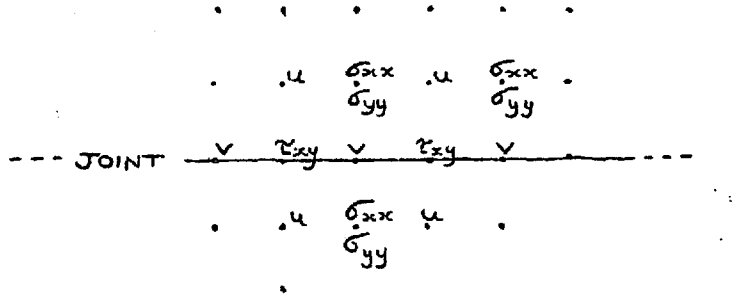

The shear stress on the joint is already located at the correct position. The normal stress is calculated at the same point by averaging the four surrounding σ_{yy} stresses. If the shear stress exceeds $c + \mu\sigma_n$ then the joint is regarded as slipping at that point, and the shear stress is set to $\mu\sigma_n r$, where r is the residual fraction of the peak stress, and c the cohesion. Naturally if the point has slipped previously, c is set to zero, and the criterion becomes $\tau_{xy} > \mu\sigma_n r$. Since σ_{yy} is continuous across the joint, it is calculated in the normal way. The displacement, u, is in general not continuous across the joint. Whilst the joint is failing, the upper u is assumed to bear no

Applied Stresses:

4·0 units horizontally
1·0 units vertically

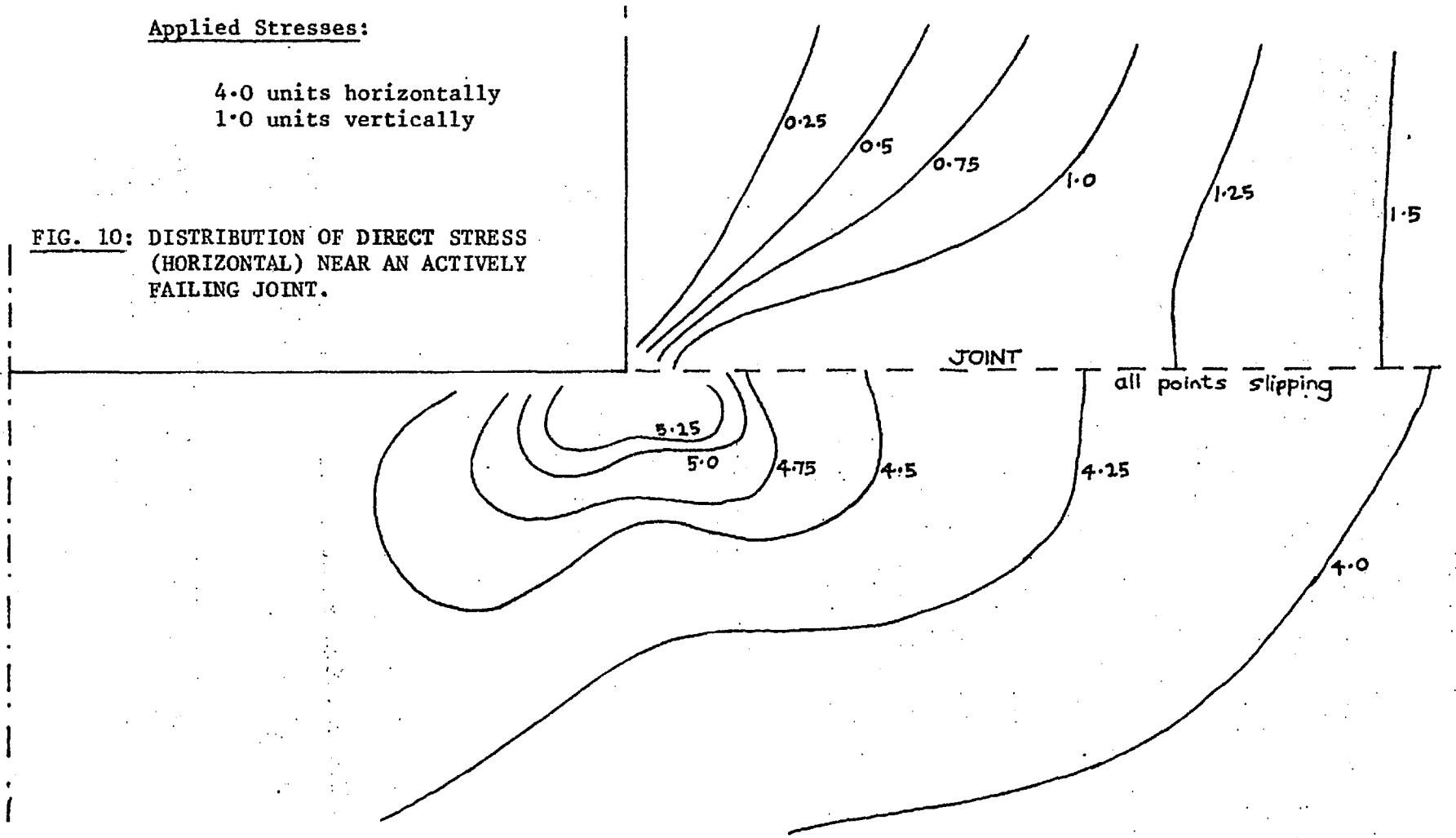

FIG. 10: DISTRIBUTION OF DIRECT STRESS (HORIZONTAL) NEAR AN ACTIVELY FAILING JOINT.

relation to the lower u, but the *change* in relative displacement across the joint is tested over each iteration period to see if the joint could support elastic conditions again. If it is able to, a fictitious relative displacement is established, to act as the datum for future elastic calculations. In view of this the actual horizontal displacements across the joint may have very different values, causing σ_{xx} in turn to be discontinuous across the joint.

The program worked well and appeared numerically stable, even with negative stiffness laws (i.e. stress falling with displacement). The Finite Element method apparently is difficult to use in that case. If the Dynamic Relaxation method is used with *stiffening* joints (rather unlikely) care must be taken to see that the Δt criterion (see Time Increment section) is obeyed, otherwise instability will result.

Examples

Two models were chosen, one of which is physically stable and the other not. The example used previously was employed - a stress-loaded square hole. A joint was inserted just below the opening (and one above, for symmetry). Clearly this joint is physically stable since it does not intersect a free surface. However, on comparing the shear and normal stresses which would exist if the joint were not present, the failure criterion is seen to be exceeded, assuming moderate friction values. The result of including the joint in the D.R. calculation is shown in Figure 9. The joint has slipped, and susequently stabilised, altering the stress distribution so that the failure criterion is not exceeded at any point. It is interesting to note that the shear stress has been *lowered* all along the failed region, but *raised* at the end of the region. The characteristics of the joint were: $\mu = 0{\cdot}7$, cohesion $= 0$, residual ratio $= 0{\cdot}7$.

The second example is of a joint intersecting the opening, forming a kind of shear-box. Physically it is to be expected that the material contained between the two joints would move continuously into the hole. This is in fact what happens in the D.R. model - the solution does not converge, and all the points along the joint slip. Figure 10 plots the horizontal stress, to illustrate the ability of the model to handle large stress discontinuities. The failing block is virtually stress-free. The characteristics of the joint were: $\mu = 0{\cdot}7$, $c = 0$, $r=1$.

Conclusions

A method has been developed to model a failing joint having general friction characteristics, including that of stress falling with displacement. Only single joints have been considered, but it is reasonable to suppose that multiple joints could be used, provided that enough D.R. nodes were used between the joints to adequately define the inter-joint elastic conditions.

E. PROGRESSIVE FAILURE IN A BLOCKY SYSTEM

Discussion

The inclusion of simple joints in an elastic continuum would seem to be a reasonable approach when the displacements are small and the jointing system is simple, e.g. a single joint set, or one possible failure mode. In many situations however, gross movements can occur, with the accompaniment of essentially *geometric* effects, such as the interlocking of rock blocks, creation of voids and staggering of joints due to gross rotation of blocks. Under these conditions, "stress" and "strain" become powerless to describe the situation since they acquire locally very large or very small values due to the voids, point contacts and large slips. The stress distribution within a rock block would appear to be largely a function of the local irregularities existing around its surface. In view of this it seems fruitless to try to assess the equilibrium of a rock block by considering its internal stress distribution. It is more profitable to observe that there are two quantities which remain finite and definable: "force" and "displacement".

This Section deals with the development of programs to simulate both equilibrium state and the progressive large-scale movements of an assemblage of blocks, in which only forces and displacements are considered. Furthermore, the intact elastic properties of the rock material are assumed to be unimportant, if the view is taken that any joint between rock blocks will be much "softer" than the intact rock; therefore any movements taking place will be associated with these soft regions. The justification for making this assumption is based upon experiments which show that rock joints are commonly soft, both in the shear and normal directions, compared with even large spans of intact rock. A typical figure is that one joint has the same compressibility (normal deflection per unit normal stress) as 40 feet of intact rock (refs. *5* and *6*). Hence it seems to be a reasonable assumption to ignore the intact properties of a highly jointed rock system, and concentrate the analysis of the joint properties.

It may be as well to pause here for a moment to examine the overall question of whether it is worth even attempting to produce complicated methods for modelling rock systems, when it is

(a) impossible to completely define the structure in a real situation,

and (b) very difficult to measure the physical properties of the rock with any precision.

It must be true that the Rock Mechanics engineer will never be able to completely predict the behaviour of a rock system: there are so many imponderables. He will always need to exercise engineering judgment. But he is not born with such judgment - it comes from observing real situations, and understanding what is happening. This understanding is helped, in a complex situation, by having a model to demonstrate clearly the major characteristics of the system. A physical model suffers from

the drawback that its parameters are generally more or less fixed, and if they are variable then they cannot be varied independently of each other. In a numerical model, all the parameters can be varied independently, so that causes and effects can be separated and a clear idea can be gained of what is important in a system.

To give a definite example, it may be useful to know what the *pre*-failure displacement pattern is, in a mine with particular joint sets. If the observed displacement pattern could be correlated with that of the numerical model, it might be possible to predict what mode of failure could occur, and under what conditions.

Another example is dilation. It is arguable just what effect the normal dilation of a joint when shearing will have on the overall failure mode. This question could be swiftly resolved by a numerical model which could vary the dilation independently of the other joint parameters.

Basic Assumptions and General Laws

It has already been mentioned that in a highly jointed rock, it may be reasonable to regard the stiffness of joints and point contacts as very low compared with that of the intact rock. In other words the intact rock may be taken as rigid. Furthermore, since the numerical model will be used to examine modes of *failure* (involving shear and tension failure), it may be postulated that the assumed laws governing the elastic stiffness of joints will play only a small part in the failure mode, provided that the laws are not too grotesque (e.g. *very* soft joints). The proof of this assumption can be easily tested, by varying the joint stiffness and noting whether the failure mode changes significantly. In view of this, the simplest possible laws may be used to describe the elastic stiffness of the joints. Of course the laws describing the shear failure of the joints should be as realistic as possible.

The reader may wonder why it is necessary to even include the elastic properties of joints in a failure model. The answer is that a *progressive* failure model is intended. For example, some parts of the system may fail, then stabilise as forces re-adjust. If only parts of the system are failing, the system is statically indeterminate - it is necessary to consider displacements in order to arrive at a complete picture of the force distribution. The reason that the method of "limit equilibrium" works, is that it assumes firstly a failure mode, then assumes that the joints comprising the mode are all failing together according to a perfectly *plastic* shear force law (i.e. shear force independent of displacement). Hence the shear forces all become known functions of normal forces, and the system becomes determinate (N equations, N unknowns). In passing, it is interesting to note that if a non-plastic shear force law is assumed, then "limit equilibrium" is powerless, as it takes no account of displacements.

In all the remainder of this Section, the elastic

laws between block are assumed to be linear. That is to say, the change in force (either shear or normal) between two blocks is assumed to be proportional to their relative change in displacement.

A simple model is considered first, in which the rigid block takes the form of a 2-dimensional ball (more correctly, a cylinder). The method is then extended to include systems of angular blocks which more nearly resemble a real rock structure. Even the ball model may be useful in modelling some soils, since several thousand balls may be dealt with using a moderately-sized computer.

Application to a System of Balls

The present program only considers a system in which all the balls have similar radii: it is a simple matter to modify it to include arbitrary dimensions. The program stores the cartesian co-ordinates of the centroid of each ball. The cycle of calculation is basically as follows:

STEP 1: Take each ball in turn, and calculate whether its circumference overlaps that of any other ball.

STEP 2: If there is an overlap between two balls then the normal force between the balls is given by:

$$F_n = C_n (2R - d)$$

where R = radius of ball,
d = distance between centroids
C_n = chosen normal "stiffness"

The shear moment between balls depends on

(a) whether the balls were touching on the previous iteration, and
(b) if they were, how much they have moved subsequently, and
(c) if slip is taking place.

If (a) is satisfied, then the shear moment is given by:

$$M = C_s (\Delta\alpha + \Delta\beta)$$

where $\Delta\alpha$ = the change in angle (radians) of the first ball during the iteration.
$\Delta\beta$ = the change in angle of the second ball,
C_s = shear "stiffness"

If the balls were not touching on the previous iteration, then M = 0 (approximately true if the iteration time is small).

The shear *force* is given by:

$$F_s = M.R.$$

If $F_s > \mu F_n$, then slip is taking place (μ = co-ef of friction).

So the revised value of F_s is given by $F_s(new) = \mu F_n.r$, where r = residual fraction of peak shear force.

Diagramatically,

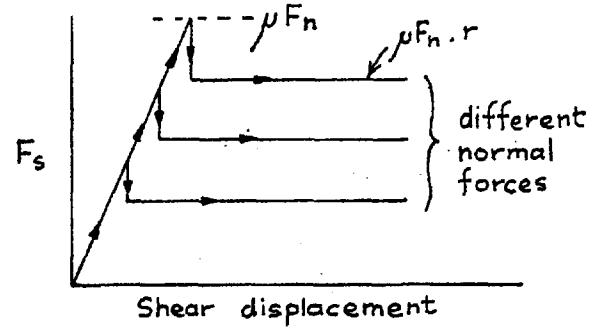

STEP 3: Add up all the moments and forces acting on each ball by resolving forces in the X and Y directions and summing.

STEP 4: Add in gravity as a downwards force on each ball.

STEP 5: Calculate the velocity of each ball in the X and Y directions, and the angular velocity:

linear velocity: $V_{new} = V_{old} + \frac{F}{m}.\Delta t$ where F = force, m = mass of ball

angular velocity: $w_{new} = w_{old} + \frac{M}{I}.\Delta t$ where M = moment, I = moment of inertia, Δt = time increment

STEP 6: Calculate the displacements from the velocities:

$d_{new} = d_{old} + V.\Delta t$ V = velocities from previous step

STEP 7: Go back to step 1.

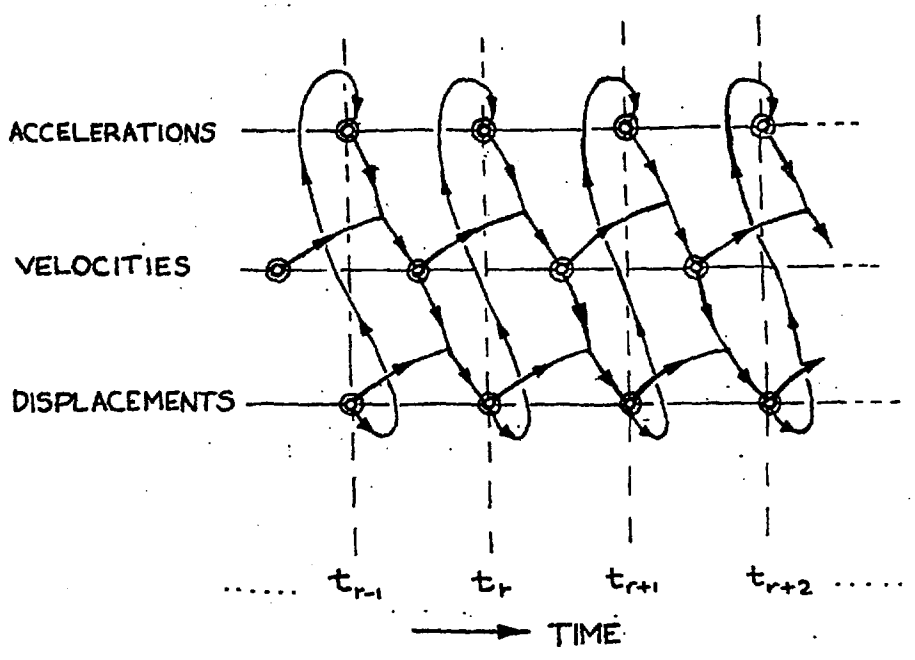

FIG. 16 TO ILLUSTRATE THE TIME INTERLACING USED IN THE BALL PROGRAM.

Interlacing Procedure for Time Integration

As with Dynamic Relaxation, the displacements, velocities and accelerations are interlaced in time to give better accuracy. Figure 16 may help to explain the sequence. Time proceeds from left to right, and the arrowed lines indicate the sequence of calculations.

The Choice of Time Increment

Clearly there must be an upper limit to the value of the time increment used in steps 5 and 6 above. If it is of a similar length to the period with which the balls naturally come into and out of contact with each other (or slip and non-slip), a severe approximation is made, since the time increment itself will tend to govern the periods of contact and non-contact. In order that the response of the ball system should be sensibly independent of the time increment, the value of the increment must be reduced until that requirement is satisfied. Quite apart from considerations of contact time, there is a further constraint on the time increment, even when balls are in permanent mutual contact. The ball system is, in essence, a large number of masses connected together by springs. Each mass will have a particular resonant frequency, dependent on the effective spring stiffness acting on it. If the time increment is greater than a certain proportion of the oscillation period, *numerical* instability will ensue, with resultant total breakdown in the process of calculation. To determine the critical value of time increment, it is necessary to write down the difference equation for a single mass-spring system in terms of, say, displacement only. Using the algorithms quoted in the calculation steps set out previously:

$$d_{r+1} = d_r + v_{r+1}\Delta t \qquad \therefore \quad v_{r+1} = \frac{d_{r+1} - d_r}{\Delta t}$$

$$d_r = d_{r-1} + v_r\Delta t \qquad \therefore \quad v_r = \frac{d_r - d_{r-1}}{\Delta t}$$

Substituting in $v_{r+1} = v_r + f_r\Delta t$, (f= acceleration)

$$\frac{d_{r+1} - d_r}{\Delta t} = \frac{d_r - d_{r-1}}{\Delta t} + f_r\Delta t$$

But, $f_r = \frac{-s.d_r}{m}$, where s is the apparent stiffness operating on mass m.

The difference equation thus becomes:

$$d_{r+1} + (\frac{s}{m}(\Delta t)^2 - 2)d_r + d_{r-1} = 0$$

The solution of this equation is detailed in several text-books (e.g. Hildebrand, Ref. 3). The nature of the solution depends on the roots of the auxhiliary equation:

$$x^2 + (\frac{s}{m}(\Delta t)^2 - 2)x + 1 = 0$$

The roots are:

$$\alpha, \beta = [-\frac{s}{2m}\Delta t^2 + 1] \pm \frac{\Delta t}{2}\sqrt{\frac{s^2}{m^2}\Delta t^2 - \frac{4s}{m}}$$

The solution is oscillatory if the roots are complex.

Let $\alpha = a + ib$ and $\beta = a - ib$ (a,b real)

In this case the general solution of the diffence equation is:

$$d_r = \rho^r(Ae^{i\phi r} + Be^{-i\phi r}) \quad \ldots\ldots \quad 1$$

where $\rho = \sqrt{a^2 + b^2}$, $\rho\sin\phi = b$ (or $\rho\cos\phi = a$)

For complex roots,

$$\frac{4s}{m} > \frac{s^2}{m^2}\Delta t^2$$

$$\therefore \Delta t < 2\sqrt{\frac{m}{s}}$$

To test whether the oscillations diverge or converge,

$$\rho = \sqrt{\left(-\frac{s}{2m}\Delta t^2 + 1\right)^2 + \frac{\Delta t^2}{4}\left(\frac{s^2}{m^2}\Delta t^2 - \frac{4s}{m}\right)}$$

$$= 1 \text{ , if } \quad \Delta t < 2\sqrt{\frac{m}{s}}$$

Thus the oscillations are stable, and correspond to the natural vibrations of the mass-spring system.

If $\Delta t > 2\sqrt{\frac{m}{s}}$, $\rho > 1$, giving diverging iterations.

Thus the overall condition for stable calculations is:

$$\boxed{\Delta t < 2\sqrt{\frac{m}{s}}}$$

The frequency of oscillation of d is affected to some extent by the value of Δt. The real time, t, is related to r by:

$$t = r\Delta t$$

$$r = \frac{t}{\Delta t}$$

Equation 1 becomes

$$d(t) = \rho^{(\frac{t}{\Delta t})}\left(Ae^{i\phi\frac{t}{\Delta t}} + Be^{-i\phi\frac{t}{\Delta t}}\right)$$

Hence the circular frequency ω is

$$\omega = \frac{\phi}{\Delta t}$$

But $\sin\phi = \frac{b}{\rho}$

$= b \quad$ (since $\rho = 1$)

$\therefore \sin\phi = \frac{\Delta t}{2}\sqrt{\frac{4s}{m} - \frac{s^2}{m^2}\Delta t^2}$

As $\Delta t \to 0$

$\sin\phi \to \Delta t\sqrt{\frac{s}{m}}$

$\therefore \phi \to \Delta t\sqrt{\frac{s}{m}}$

$\therefore \omega \to \sqrt{\frac{s}{m}}$ (i.e. the natural frequency of the mass-spring system)

If $\Delta t = 2\sqrt{\frac{m}{s}}$, the critical time increment,

$\sin\phi = 0$

$\phi = 0$

$\therefore \omega = 0$

Thus the apparent oscillation frequency decreases to zero as the time increment approaches the critical value.

FIG. 17

PROGRESSIVE FAILURE OF A SYSTEM OF CYLINDERS DUE TO GRAVITY.

$\phi = 10°$

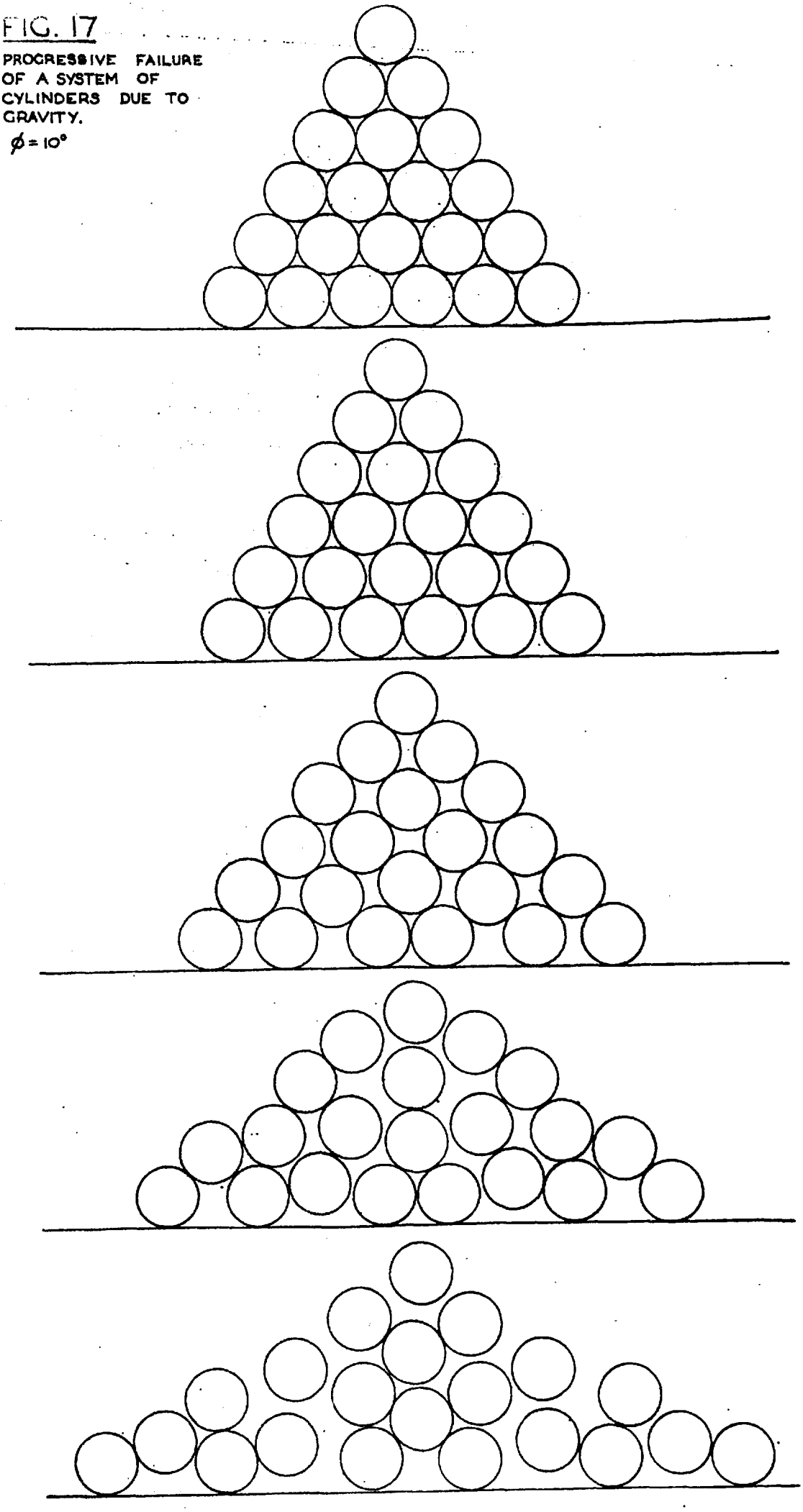

Damping

The present program is a *dynamic* one, and if no form of energy dissipation is provided, the kinetic energy derived from gravity-assisted movements will never disappear, but will oscillate forever between strain energy and kinetic energy. In other words the balls will be in constant motion. One way to damp out the vibrational energy is to include a force on the balls proportional to their absolute, or relative, velocities (i.e. a viscous force). This method is explored later on when angular block systems are considered, but in the case of the ball program, a hysteresis-type damping was used. Both the normal and shear stiffnesses were arranged to have different values depending on whether the corresponding forces were increasing or decreasing, as shown here:

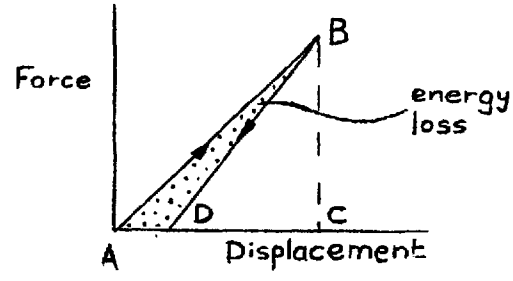

The area ABC represents the maximum strain energy, whilst ABD gives the energy lost by hysteresis. An energy ratio (area ABD ÷ area ABC) of 0.1 was found to quickly damp out oscillations.

Examples in the Use of the Ball Model

Only one example in the use of the ball model is given here, as it seems to have only a limited application in the Rock Mechanics field. A heap of balls is considered, which is then allowed to fail under its own weight. The program contains a routine for assembling the co-ordinates of the ball centroids, having specified the number of balls comprising the base and the radius of each ball. Initially it is necessary to *consolidate* the pile of balls; that is to say the balls must be allowed to settle under the action of gravity so that a force distribution is built up, as well as the displacements necessary to generate these forces. For this phase the friction was set high enough to prevent collapse. After consolidation, the friction was then given a low value, whereapon total failure ensued. The sequence of diagrams shown in fig. 17 records the subsequent positions of the balls at regular intervals after the start. The failure could, with equal ease, have been brought about by, say, removing a ball whilst keeping the friction constant.

It is interesting to note that in the later stages of failure, some of the balls appear to be suspended in mid-air. This is due to the fact that, because of their own inertia, these balls remain relatively stable when the balls below them move away.

Summary of Important Points

A method has been developed which permits the

calculation of the movements of a system of balls brought about by changes in parameters such as friction and geometry. Each ball is allowed unlimited movement, and can touch any other ball at any stage in the calculation. The method relies upon the assumption that, during progressive failure, the elastic properties of the balls play no part in the failure. In view of this, simple linear laws are used to relate the shear and normal forces between balls to changes in their slight geometrical overlap. Of course, this overlap must be made very small in relation to the radius of the balls. Under this condition the balls may be regarded as "rigid". Realistic friction laws may be used in order to study a failure process, and it should also be possible to include factors such as dilation, in which a normal force is generated as a result of shear slip on a joint.

The method of "Limit Equilibrium" has the drawback that it is necessary to select a failure mode before a stability calculation is performed. In the present method, the system automatically fails in that mode which has the lowest factor of safety. This fact may be useful in analysing complicated systems, in which the most likely mode of failure is not immediately obvious. Another advantage is as follows: whereas Limit Equilibrium may predict failure to occur in some mode, it may happen that the system will then stabilise again after only a small movement. The present method would be able to model this situation.

It is believed that the method can only be used in those situations where the average forces between blocks are of the same order as the weight of the blocks, such as in a shallow open-pit. In a deep underground mine, however, the forces are so high around the excavation that the *elastic* displacements may be of similar magnitude to the slip or tension displacements. The present numerical model may well be unrealistic in that case, since one of the basic assumptions was that the elastic displacements were very small.

The Program

A listing of one version of the ball program is given in Appendix III. It is not in the form of a "package" which can be used as a general problem-solving tool, but is more of an experimental form where the user can modify it to suit his needs. However, it is a working program, and with the data given, will yield the plots given in this section.

The program was not written with economy of execution time and storage in mind, as it was only a preliminary to the block program described later. The execution time was about 2 minutes for 2000 iterations of 21 balls, using a CDC 6600 computer, and the storage about $2N^2$, where N is the number of balls. Theeconomy in time and storage could be improved drastically by limiting the scanning of balls to those immediately surrounding the one of interest, as is done in the block program. An occasional overall scan could be used to define the area of influence of each ball.

Application to Angular Blocks

A real rock mass is often found to be divided by a number of sets of roughly parallel joints. One of these sets usually predominates, in the sense that it is more continuous than the other sets. It was thought useful to model a rock system having one set of parallel continuous joints (primary set) and another set perpendicular to the first, but completely discontinuous (secondary set):

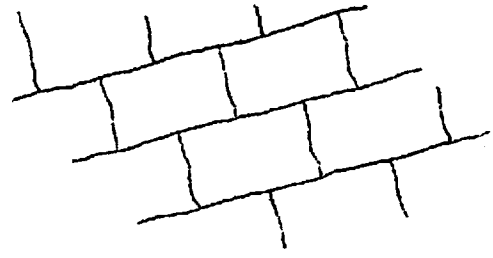

In other words, individual blocks are defined. The next few pages will be devoted to attempting to apply the principles developed for the ball program to angular blocks.

Location of forces

The first problem arises when trying to describe the contact between two blocks with their parallel faces together. In the case of the balls, a simple point contact was assumed. With two blocks in contact, it seems that the resultant force between them could act at any point along the common joint. For the purposes of the present program, it was assumed that all forces would arise at the corners of the blocks, so that in the case of a common joint, forces would act at either end.

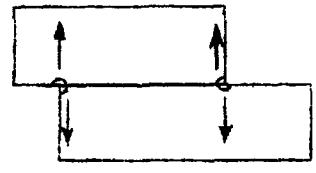

In this way an equivalent force at any intermediate point along the joint could be simulated by varying the ratio of the two end forces. The assumption may seem wild at first sight, but it must be remembered that any real surface is only likely to touch at a small number of points, possibly only two. It would seem unlikely that the precise location of these points would play much part in the macroscopic behaviour of the two blocks.

Force-Displacement Laws

In the ball program a linear law relating the force between balls to the overlap displacement was used. The contact between two blocks is more complex since the geometry of contact changes with relative block rotations:

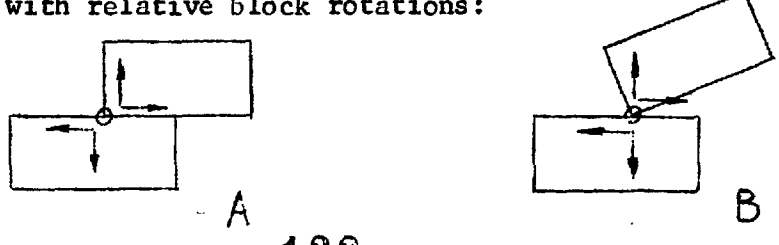

It is clear that the point contact of A will have a different stiffness from B . However, since it is assumed that the elastic displacements are so small as to play no part in failure, the present program ascribes equal stiffness (= force/displacement) to both cases.

However when the *slip* conditions of A and B are compared, it is realised that the program should take account of the different frictional properties of the two cases. This is quite easy to do as the friction can be made a function of relative angle between the blocks. Out of shear ignorance as to what this dependence was, the friction was assumed independent of angle in the examples to follow.

The force-displacement laws used in the block program are explained in the following diagrams:

Normal force:

$F_n = C_n \delta_n$

(C_n = normal stiffness)

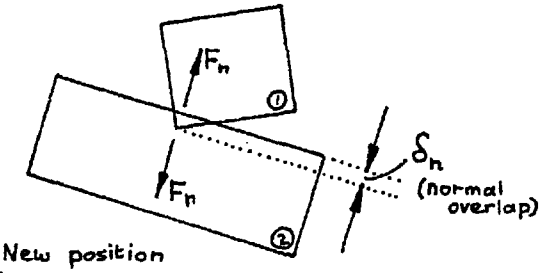

Shear force:

$F_s^{(new)} = F_s^{(old)} + C_s \delta_s$

(C_s = shear stiffness)

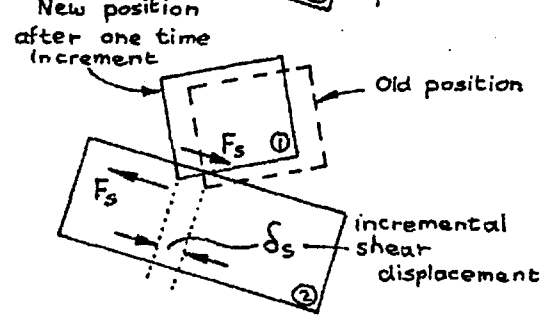

As in the ball program, shear slip occurs if

$F_s > \mu F_n$ $\qquad$ $\mu = \tan \phi$
ϕ = angle of friction.

If this inequality holds, then F_s is set to F_n.

i.e. $F_s = \mu F_n$

In general of course there will be many forces acting on each block:

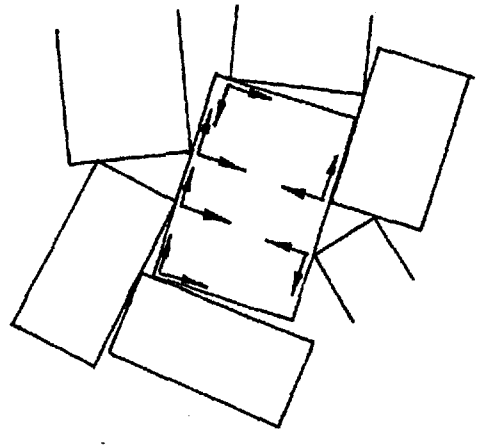

These forces are resolved into the X and Y directions, then summed into three resultants:

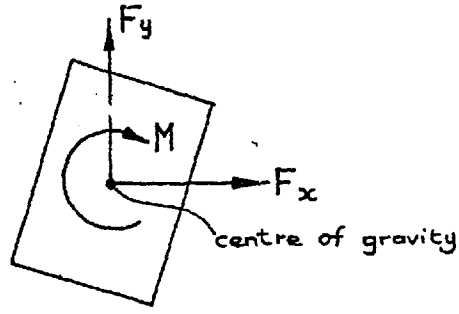

Laws of Motion

The motion of the block is then calculated according to the dynamic equations:

$$\text{velocities} \begin{cases} V_x^{(1)} = V_x^{(o)} + \frac{F_x}{m} \cdot \Delta t \\ V_y^{(1)} = V_y^{(o)} + \frac{F_y}{m} \cdot \Delta t \\ \omega^{(1)} = \omega^{(o)} + \frac{M}{I} \cdot \Delta t \end{cases}$$

(1) denotes new value

(o) denotes previous value

$$\text{displacements} \begin{cases} d_x^{(1)} = d_x^{(o)} + V_x^{(1)} \cdot \Delta t \\ d_y^{(1)} = d_y^{(o)} + V_y^{(1)} \cdot \Delta t \\ \theta^{(1)} = \theta^{(o)} + \omega^{(1)} \cdot \Delta t \end{cases}$$

The new positions of the blocks are then used to generate a new set of forces, and so on.

Damping

To reduce storage requirements, the damping used in the block program was of a viscous nature. One way of applying damping as shown below, with a dashpot to "ground" connected to each block:

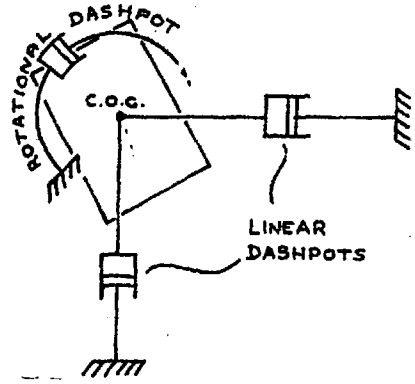

This method was not used however, since if a realistic value of dashpot constant was chosen to damp out the high frequency oscillations of the block, then the overall motion of the block became unacceptably slow.

A better method was found to be to connect a dashpot in parallel with each "spring" formed by a corner contact:

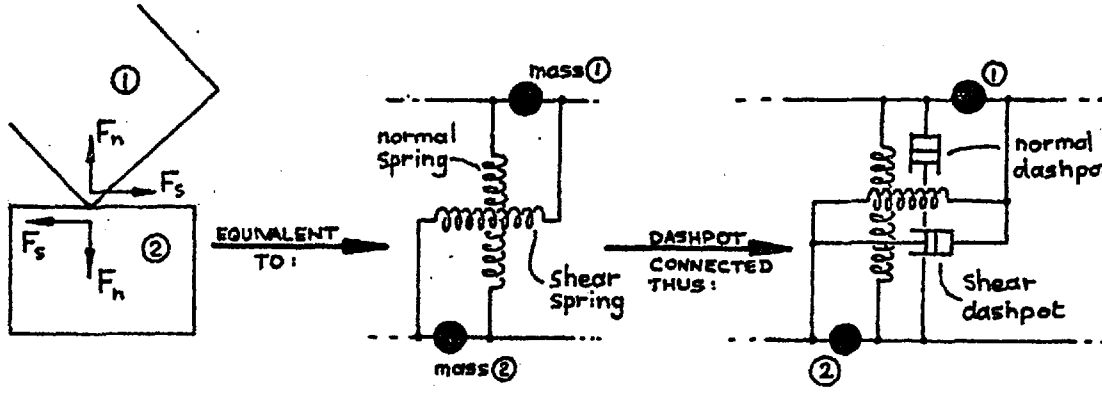

In this way the mass-spring oscillations caused by block contacts can be damped, without the gross block movements being affected. The damping constant of the dashpot was expressed as a fraction of the critical damping (= dead-beat response of the mass-spring system). The critical damping can be found by considering the differential equation of the mass-spring system:

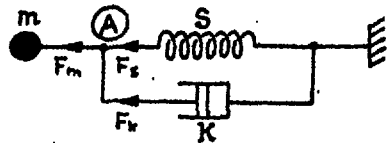

u = displacement of Ⓐ

For equilibrium at the point Ⓐ,

$$m\frac{d^2u}{dt^2} + K\frac{du}{dt} + Su = 0$$

This equation gives oscillatory u if

$$K < 2\sqrt{ms}$$

If $K = 2\sqrt{ms}$, the response is dead-beat.

In practice the value of dashpot constant was taken as some fraction of the critical value, i.e.:

$K = f.2\sqrt{ms}$ where f is the fraction of critical. In actual program the damping was applied in a rather non-rigorous fashion in order to save time and storage. It was incorporated in the force-displacement section of the program, which meant that the dashpot force was introduced at a strictly incorrect time. The time error was in fact $\Delta T/2$, where ΔT was the time

increment. Thus if ΔT was small very little error in the calculation occurred. In both the shear and normal directions the dashpot force was made proportional to the incremental displacement arising in one time increment.

$F_{dn} = C_d \delta_n$ where: F_{dn} = normal dashpot force

$F_{ds} = C_d \delta_s$ F_{ds} = shear dashpot force

δ_n, δ_s = normal and shear incremental movement

C_d = dashpot constant

These dashpot forces were added to the other forces on each block. The shear dashpot was "disconnected" if slip occurred at contact point.

In addition to the damping already mentioned it was found useful to set all block velocities (both linear and rotational) to zero at regular intervals throughout the calculations. In this way a truly static failure situation could be simulated, since the blocks were not allowed to acquire sufficient kinetic energy to change the failure mode through inertia effects.

The Program

A listing of a block program is given in Appendix III. In order to eliminate data-cards a subroutine is included, which scans through a specified rectangle of space and assembles blocks to fill the space, given the primary and secondary joint spacing and joint angle. It also numbers the blocks in a zigzag fashion (easier for plotting) and creates a matrix for each block listing the blocks near it. The main program is in fact only designed to take account of the blocks immediately surrounding a given block, in order to minimise storage and computing time. However this is not a *fundamental* limitation, and it would be an easy modification to cause the program to update the list of neighbouring blocks every so often (say 100 iterations) so that a truly infinite movement would be possible.

Routines are also included for fixing any number of blocks to provide a fixed boundary, and also for removing any number of blocks so that excavation can be simulated. As with the ball program, it is necessary to consolidate the block system so that it becomes stable under its own weight. This was usually done under low friction conditions in order to initially achieve low joint shear stresses - a condition that may occur in reality. The friction was then set to a realistic value and excavation carried out to cause failure.

The number of storage locations required by the program is about 35N where N is the number of blocks. This figure assumes that up to six blocks can touch any one block; if more touching blocks are required the storage must be increased. The calculation time is typically one minute for 1000 iterations of 90 blocks using a CDC 6600 computer. 1000 iterations is generally sufficient for one "operation" such as consolidation.

Alternative Law of Motion

It is by no means obvious that any one law of motion is more "realistic" than all others. Only one law has been considered so far, namely that of inertia. In many practical instances it is difficult to imagine that inertia can play much part in the progressive failure of a blocky structure since the movement can be so slow, possibly occupying weeks or months. It is conceivable that some sort of creep law is in operation, or maybe relief of stress due to dissipation of water held by joints.

In order to pursue this line of thought, the block program was modified to utilise a very simple law of motion - one having no direct connection with time. It will be remembered (see fig. 1) that the first part of the calculation cycle computes the equilibrium conditions of each block, yielding out-of-balance forces if the block is not in equilibrium. The simplest assumption that can be made is that the block will then move in the direction of the resultant of the forces. It is also assumed that the amount of movement is proportional to the resultant force.

i.e. $d_x^{(new)} = d_x^{(old)} + K.F_x$

$d_y^{(new)} = d_y^{(old)} + K.F_y$

$\theta^{(new)} = \theta^{(old)} + K_m.M$

where K, K_m are constants

There is of course a limit on the magnitude of K and K_m. For one degree of freedom, the above equations are of the form:

$$d_{r+1} = d_r + K.F_r$$

It will be recalled that the "elastic" equation for a single contact point was

$$F_r = -C.d_r$$

(assuming one block fixed;
d_r = overlap of the blocks,
C = stiffness)

Combining the two equations, assuming no body forces,

$$d_{r+1} = d_r(1-K.C) \quad \ldots 1$$

By definition, K.C is always positive.

If $K.C<1$, the recurrence relation will monotonically converge to the equilibrium condition, $d = 0$.

If $1<K.C<2$, convergence to zero will also occur but in an oscillatory fashion.

If $K.C.>2$, the calculation will diverge.

In practice K.C was set very much less than unity, since, as mentioned earlier, the apparent stiffness experienced by a block completely surrounded by others is much greater than the single contact stiffness. The equation 1 represents a logarithmic function (if K.C < 1) since each term will bear a constant ratio to the preceding one. Thus the law of motion considered here can be seen to be equivalent to a viscous-type resistance to motion. This is further confirmed by considering a single block, acted on by one body force (e.g. gravity). In this case the motion will be uniform since the block moves in equal steps.

It was found that in problems involving small movements, the results from using either the inertia law or the direct iteration law were very close (in the examples to be presented next, the last two plots were made using the direct iteration law).

Examples in The Use of The Block Program

Two systems were tried: a slipping model and a toppling model.

The slip model had a primary joint set inclined at 45° to the horizontal. Certain blocks were removed from the system as assembled by the computer, to give a steeply dipping free "face". A number of boundary blocks were then fixed (shown shaded in Fig. 18), and the system allowed to consolidate with low friction under gravity. However an unforeseen situation developed. As the stiffness was set to a rather low value, the bottom right-hand block was able to rotate, causing a reaction to spread up the whole *rear* face. Figure 18 shows this effect. Rather than increase the stiffness (and use more computer time), further fixed blocks were incorporated along the rear face, as shown in Figure 19, and the consolidation proved more conventional. It should be noted that Figure 19 represents a *stable* condition in which the blocks are in equilibrium under the system of forces built up between them.

The friction was then set to 43° (i.e. just enough for failure to occur) and the four fixed blocks on the left-hand side removed to expose a free face. Figure 20 shows the positions of the blocks at a particular stage during failure. The dotted lines indicate the previous consolidated state. It is interesting to note that further consolidation has taken place in the block mass below the sliding surface. This is due to the fact that the load originally taken by the four fixed blocks on the face is now transfered to the lower blocks. Some of the blocks on the sliding mass appear to be toppling as well as sliding. This is not surprising since a single square block at 45° is obviously on the point of toppling.

The second model was one of toppling, the configuration being shown in Figure 21. The consolidation in this case was straightforward, most of the movement taking place in the direction of the primary joint set. After setting the friction angle to 20°, seven blocks were removed from the right-hand face. A toppling mode of failure then ensued. It will be noted that most of the vertical joints remain closed, the relatively low friction allowing slip to occur.

Figure 23 shows the same elapsed time as Figure 22, but in this case with a friction angle of 60°. The system is still unstable, but there is much more opening-up of joints, presumably because close-contact sliding is difficult under the high friction. The necessary rotation of each block is taken up either by the stiffness of the secondary joints or in tension cracks opening along these joints.

With the same stiffness as in the previous case, the friction angle was set to 85°, resulting in a *stable* system. However, due to the unconfined nature of the rear face, gross block rotations have taken place, causing voids to open up within the block mass. The large amount of overlap present between some blocks indicates that large inter-block forces are present. It is interesting to note that the left-hand blocks have moved *uphill*. Presumably the system as a whole has moved downhill to reduce the total potential energy. Figure 25 represents the same situation, but with all joint stiffnesses multiplied by a factor of five. The same rotational tendencies are obviously present but the movements are much less.

It should be noted that in all the block plots, all displacements are shown as calculated, and not magnified as with some other methods.

Conclusions

A computer program has been developed which allows the study of progressive large-scale movements in a system consisting of numbers of rectangular blocks. Realistic friction laws may be incorporated, and the blocks are allowed unlimited movement. The technique would seem to have wide possibilities, especially as an aid to understanding the mechanisms involved in a relatively complex structure. Even the simple cases presented here have yielded some surprising results which may not have been obvious beforehand.

As in the case of the ball program, the method is not designed to be used in situations where the elastic deformations of blocks are comparable to the displacements along the joints.

An attractive possibility lies in using the program on a real-time computer with a cathode-ray tube display. A particular structure could be sketched on the screen with a light-pen, and the various parameters fed in by keyboard. The program would then display the response of the system of rock blocks to any input operation, such as excavation of blocks, inclusion of rockbolts, changes in water pressure or friction etc.

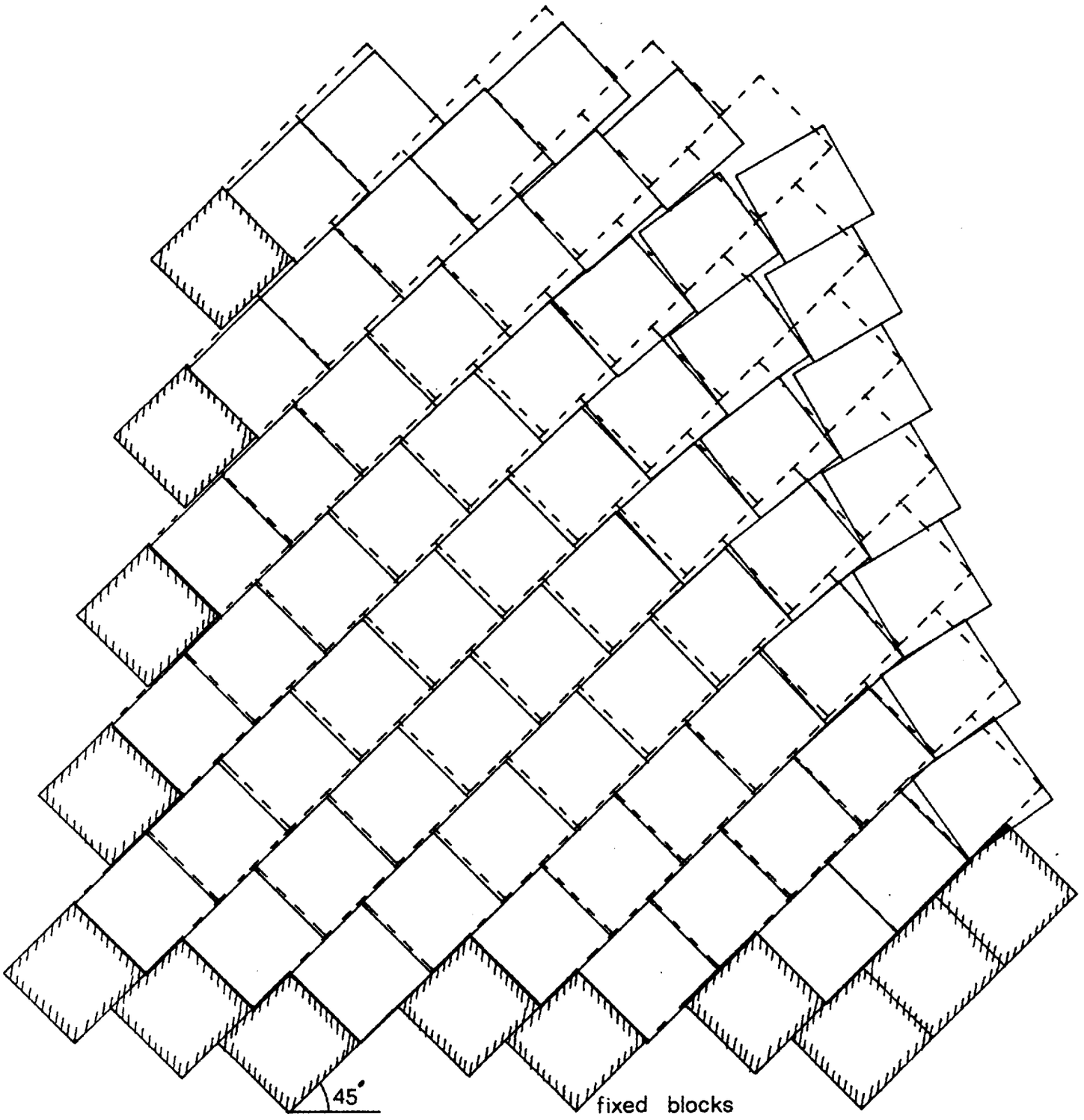

FIG. 18 : ANOMALOUS CONSOLIDATION OF SLIDING MODEL. $\phi = 1°$

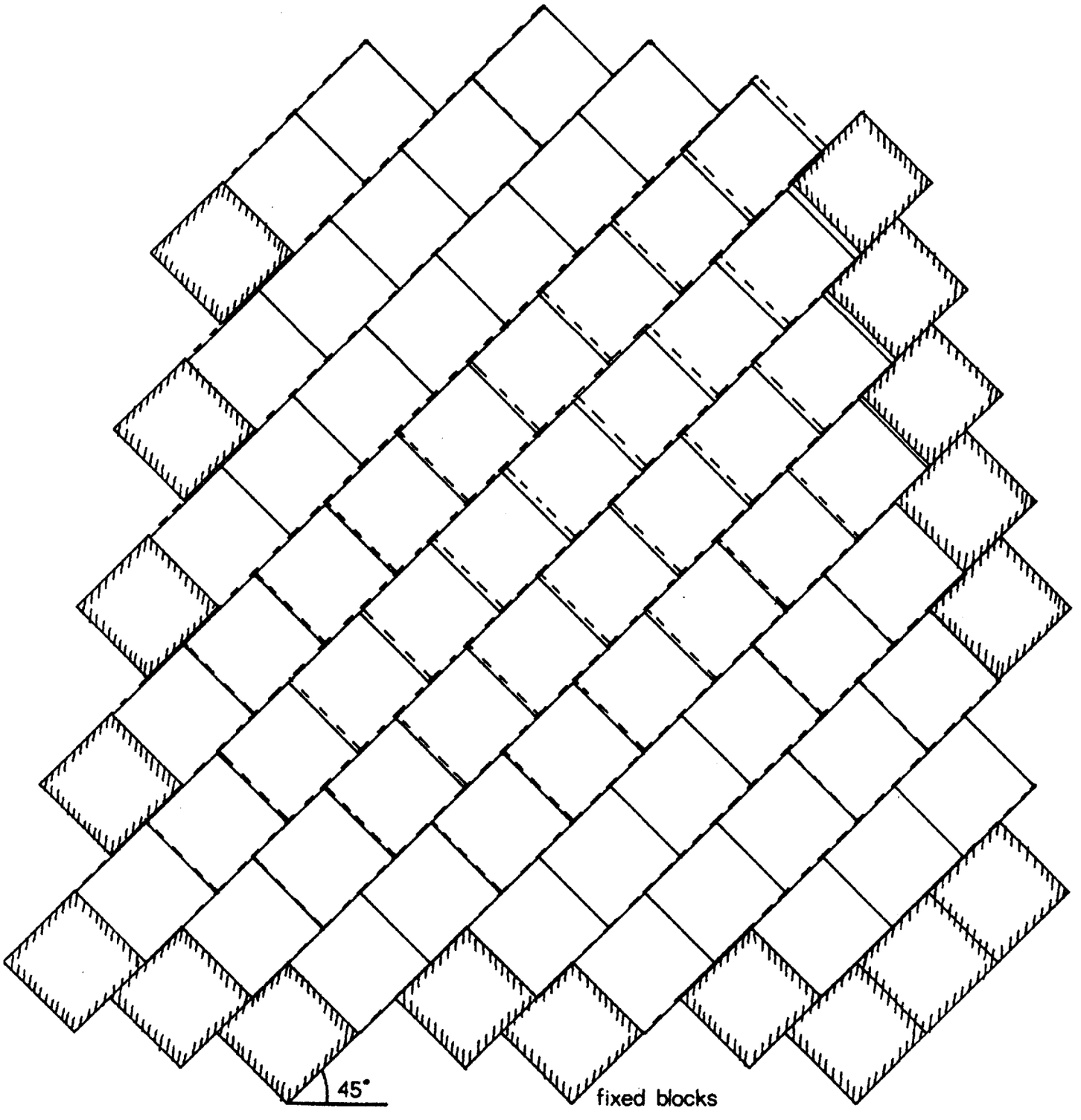

FIG. 19 : CORRECT CONSOLIDATION OF SLIDING MODEL. $\phi = 1°$

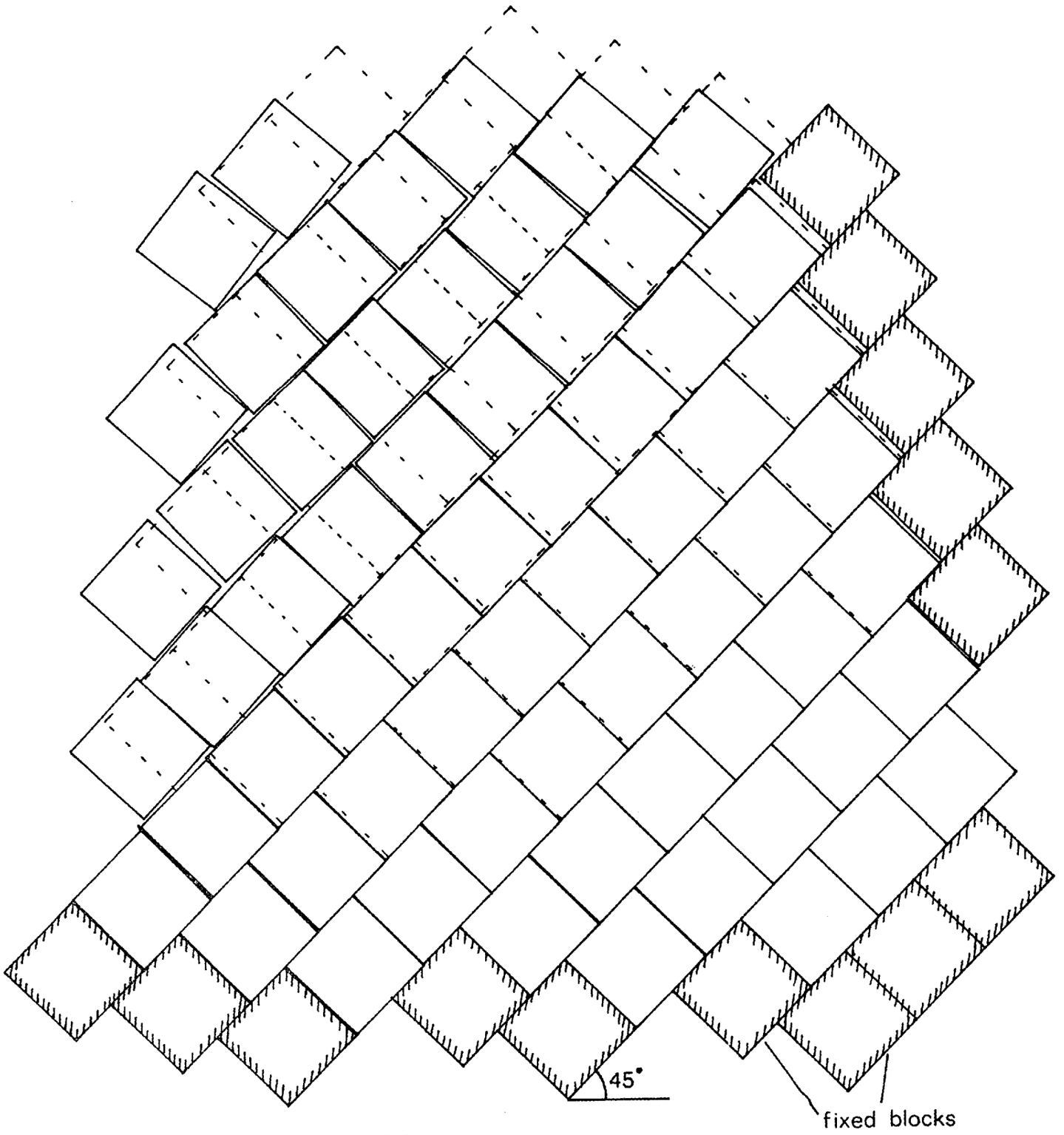

FIG. 20: PROGRESSIVE FAILURE OF SLIDING MODEL. $\emptyset = 43^{\circ}$

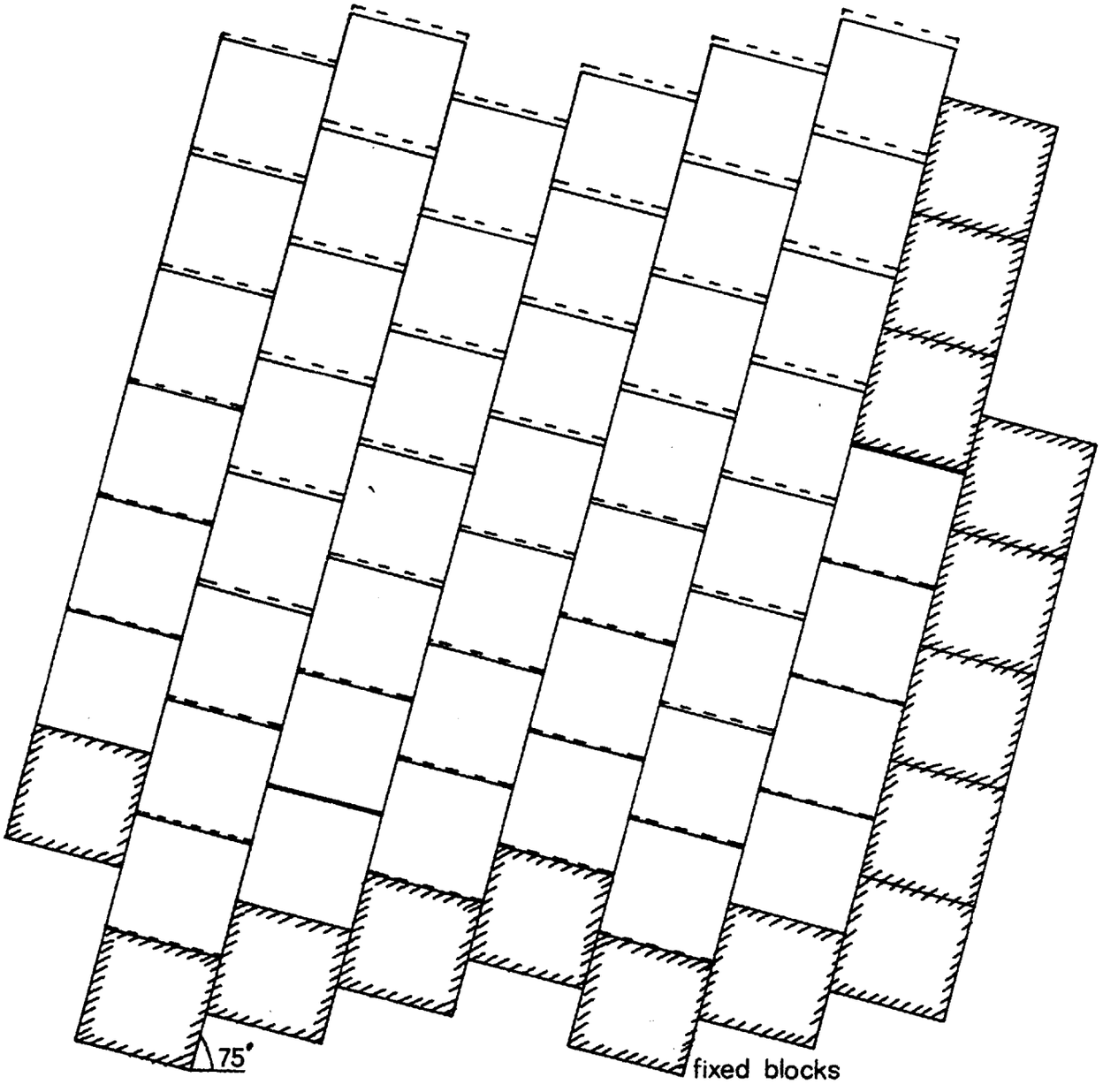

FIG. 21: CONSOLIDATION OF TOPPLING MODEL. $\phi = 1°$

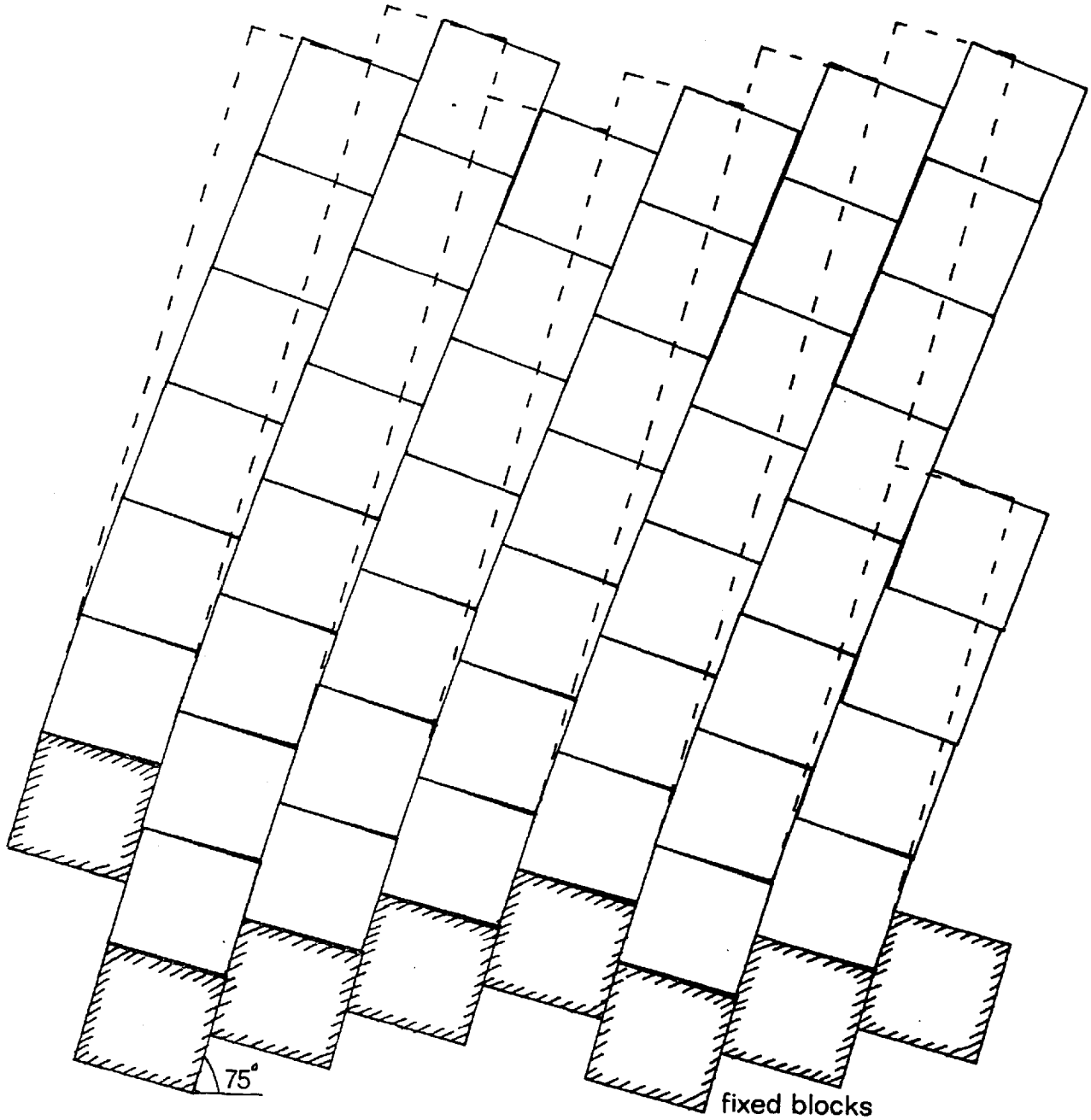

FIG. 22: PROGRESSIVE FAILURE OF TOPPLING MODEL. $\phi = 20^{\circ}$

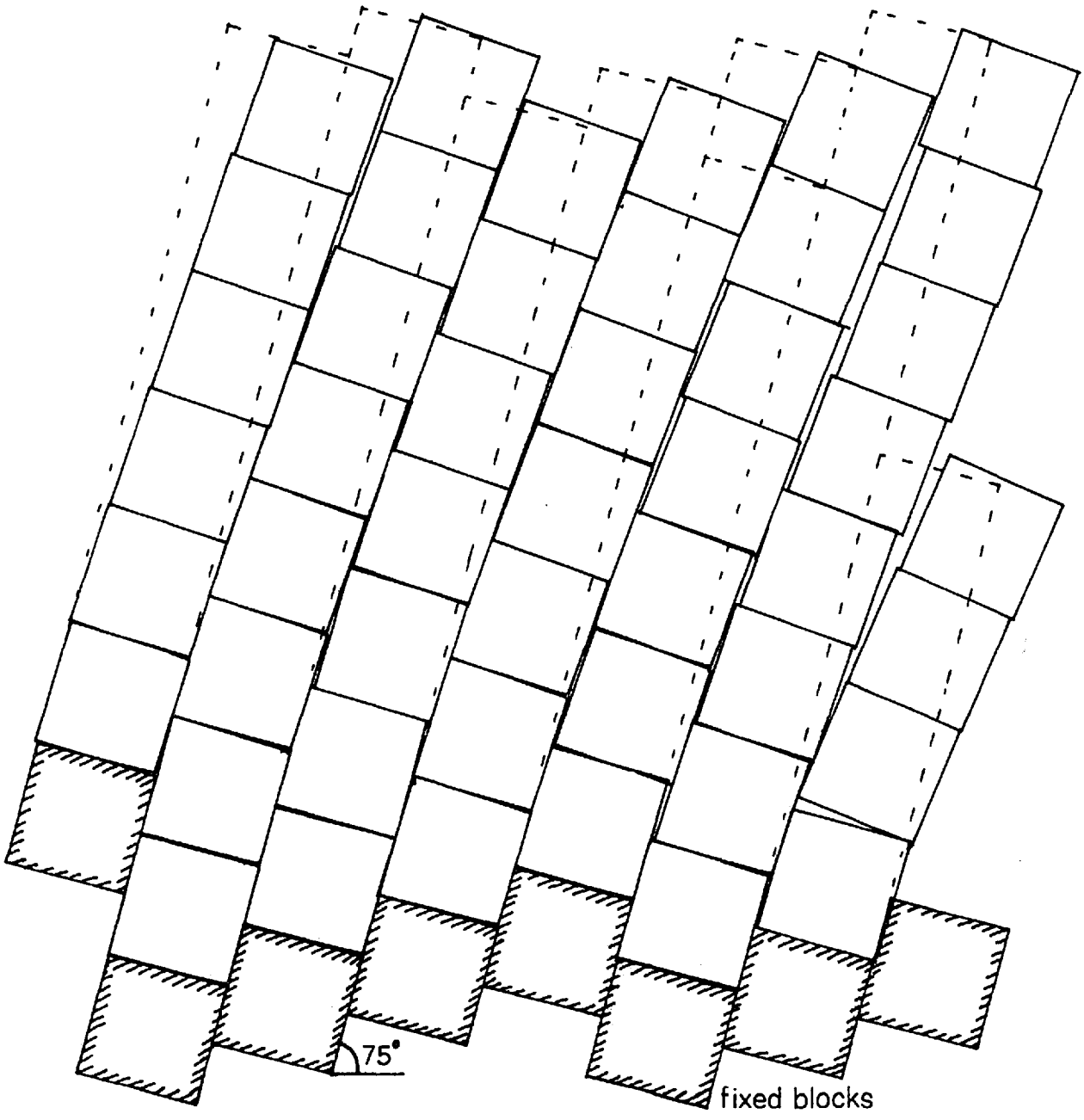

FIG. 23: PROGRESSIVE FAILURE OF TOPPLING MODEL. $\phi = 60^{\circ}$

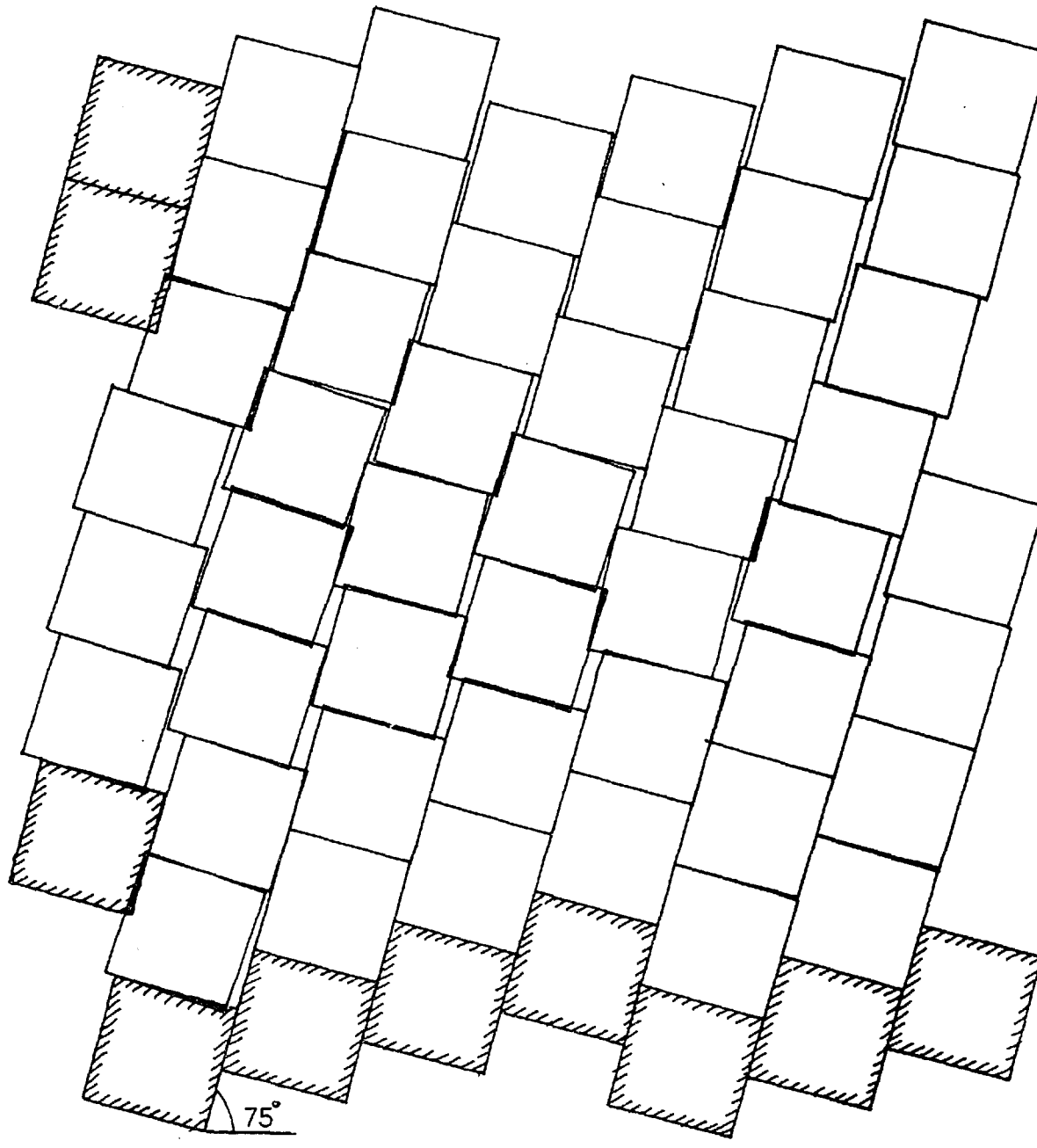

FIG. 24: STABLE CONFIGURATION OF TOPPLING MODEL. $\phi = 85^{\circ}$ low stiffness.

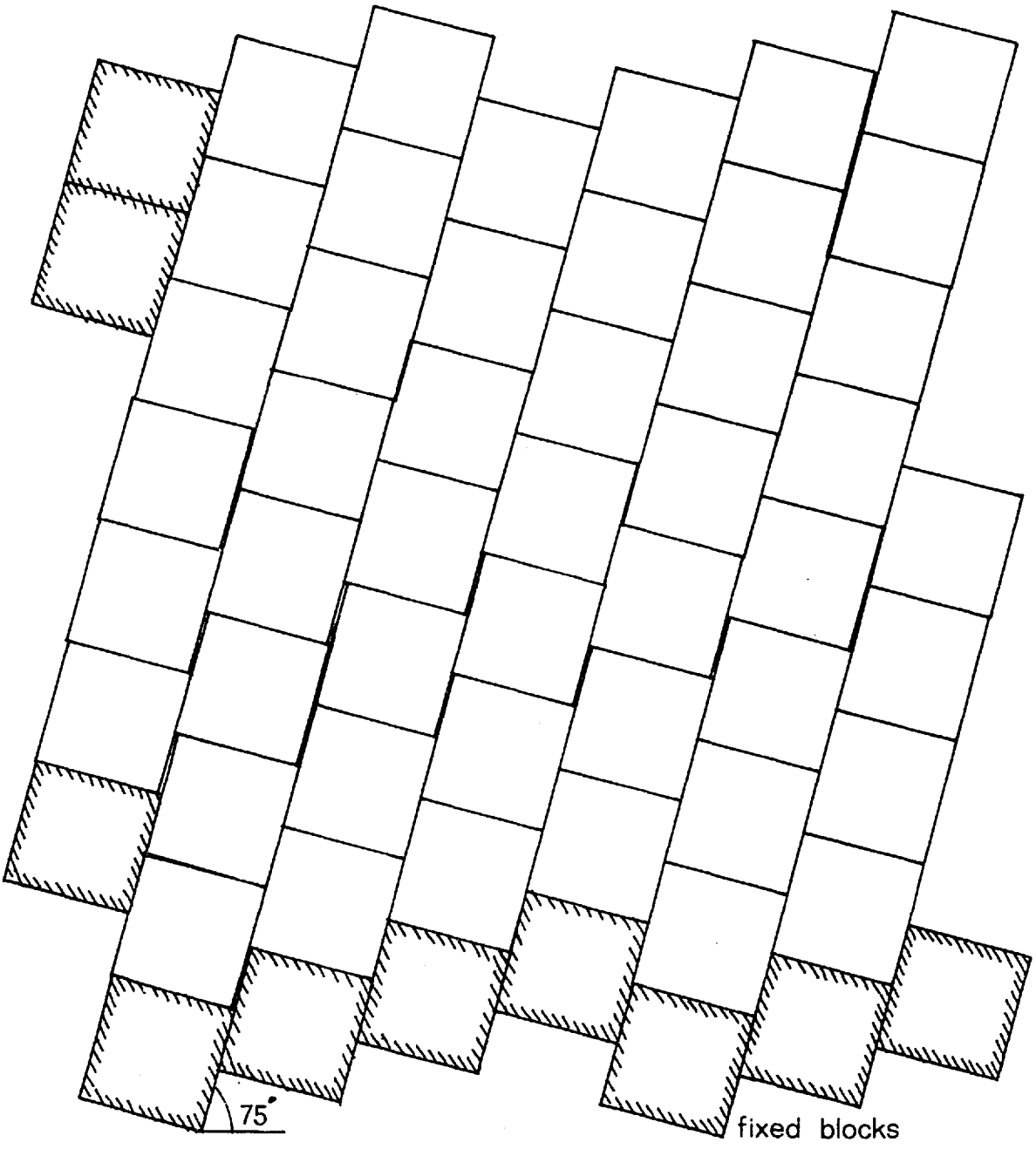

FIG. 25: STABLE CONFIGURATION OF TOPPLING MODEL. $\phi = 85^{\circ}$ high stiffness.

REFERENCES

Chapter 5

1. OTTER, J.R.H., CASSELL, A.C., HOBBS, R.E. "Dynamic Relaxation" Proc. Instn. Civ. Engrs. V 35. Dec 1966

3. HILDEBRAND, F.B. "Finite-Difference Equations and Simulations" Prentice-Hall, Inc. 1968

4. DUNCAN, J.M., GOODMAN, R.E., "Finite Element Analysis of Slopes in Jointed Rock". Report N^{O}. TE-68-1 College of Engineering, University of California, Berkeley. Feb. 1968.

5. LOUIS, C. "A Study of Groundwater Flow in Jointed Rock and its influence on the Stability of Rock Masses" Imperial College Rock Mechanics Research Report N^{O} 10. Sept 1969.

6. BARTON, N.R. Personal Communication. 1970 Imperial College

7. LYSMER, J., KUHLEMEYER, R.L. "Finite Dynamic Model for Infinite Media" Jour. E.M. Div. Proc. Am. Soc. Civ. Eng. N^{O} EM4 August 1969

8. St. JOHN, C.M. PhD. Thesis. London University (Imperial College) 1971 - to be published.

* * * * * * *

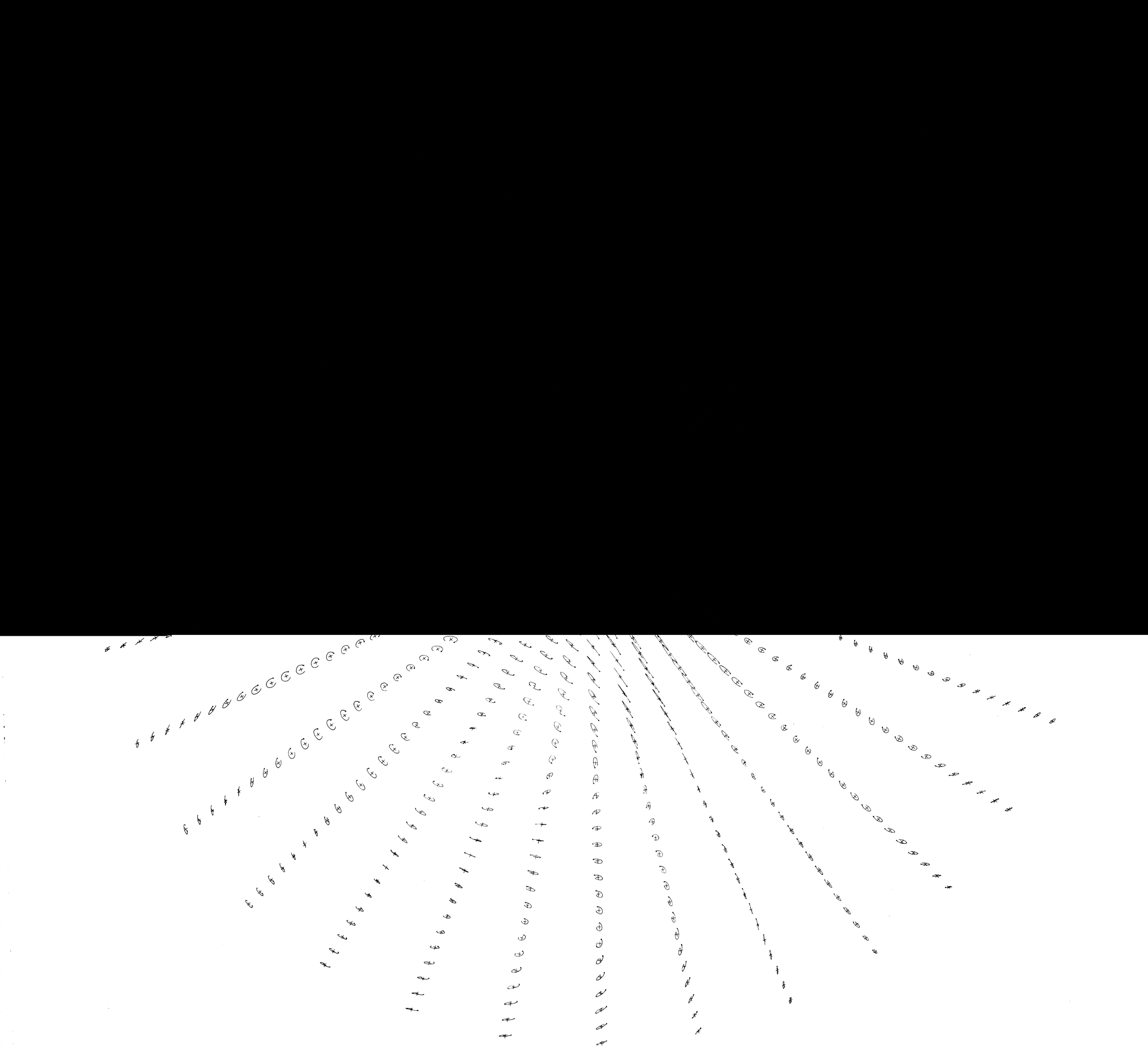

Chapter 6

Chapter 6: Elastic Generalisations and Failure Implications

A. INTRODUCTION

B. GENERAL LAWS GOVERNING LEVELS OF MOTION ACCOMPANYING BLASTING
   Dimensional Analysis
   Numerical Examples

C. FREQUENCIES AND DECAY FACTORS

D. DYNAMIC FAILURE

E. EARTHQUAKES

F. CONCLUSIONS AND SUMMARY

A. INTRODUCTION

Earthquakes and large blasts arouse concern due to the possible irreversible effects that they may cause. These effects range from total failure at one extreme, to slight irrecoverable displacement across a joint at the other. However, this Thesis has concentrated mainly on the elastic characteristics of open-pits. The reason for this is firstly that the problem is easier, and secondly that it is important to appreciate the underlying elastic response, before trying to understand how failure can occur. In this Chapter, an attempt is made to generalise the elastic results, and also to formulate some simple failure concepts.

B. GENERAL LAWS GOVERNING LEVELS OF MOTION ACCOMPANYING BLASTING

Dimensional Analysis

A good deal of knowledge concerned with the effects of various factors on the levels of motion produced by blasting may be elicited from a dimensional analysis.

As pointed out in Chapter 4 (Section C) it may be reasonable to regard a blast as equivalent to a force, of short duration, applied to a small element of the pit's surface. As far as long period motions of the pit are concerned, the important factor can be shown to be the *impulse* given to the pit surface. For instance, consider a force of magnitude F applied to the pit wall for a time t.

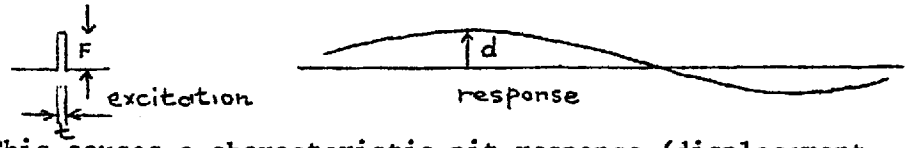

This causes a characteristic pit response (displacement, velocity or acceleration) of a particular magnitude, proportional to, say, d. Clearly, double the force would cause double the response, since a linear system is involved:

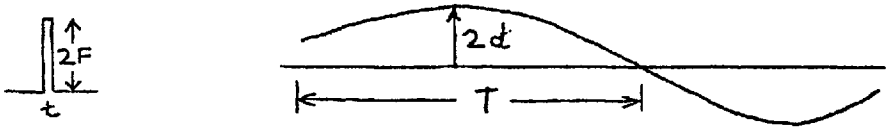

It can also be demonstrated that double the *time* will also cause double the response. That is only true however if the characteristic response is of much greater time period than the exciting force.

i.e. $T \gg t$

In that case the impulse may be regarded as two separate impulses, each of time t, each producing a response of magnitude d. Since the system is linear, the two response waveforms may be added to give the resultant. However, since the waveforms are only separated by a short time interval, they may be

regarded as occurring simultaneously, in which case the response will be double that resulting from only one impulse.

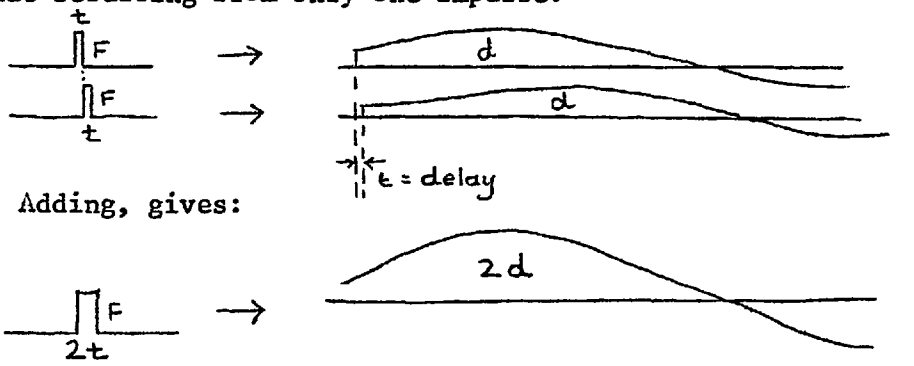

Adding, gives:

In the same way, an arbitrary excitation waveform can be broken down into a number of short impulses. Thus the response waveform will be proportional to the total area under the excitation waveform - i.e. the total impulse.

The other factors which determine the size of response to a blast were assumed to be: the elastic stiffness of the ground, the density and the size of open-pit. Since the dynamic acceleration, velocity and displacement are all of importance, each is considered in turn:

Let displacement, $d \propto I(s)^a(\rho)^b(1)^c$

where I = impulse
s = stiffness
ρ = density
1 = a dimension of the pit, assuming constant shape.

$$[L] = MLT^{-1}[ML^{-1}T^{-2}]^a[ML^{-3}]^b[L]^c$$

$1 = 1 - a - 3b + c$
$0 = 1 + a + b$
$0 = -1 - 2a$

$a = -\frac{1}{2}, \quad b = -\frac{1}{2}, \quad c = -2$

$$d \propto \frac{I}{l^2\sqrt{s\rho}} \qquad \ldots 1$$

Similarly, let velocity, $v \propto I(s)^a(\rho)^b(1)^c$

In this case it turns out that a = 0, b = -1, c = -3.

$$v \propto \frac{I}{l^3\rho} \qquad \ldots 2$$

Similarly, acceleration, $f \propto I(s)^a(\rho)^b(1)^c$

The relationship here is:

$$f \propto \frac{I}{l^4}\sqrt{\frac{s}{\rho^3}} \qquad \ldots 3$$

The above relations are only valid for pits of similar shape, and for displacements, velocities and accelerations which are generated as a result of the shape of the pit alone.

Motions which result from other factors, such as geological discontinuities, will not obey the relations.

Numerical Examples

The expressions derived above may be used to compare the results of the computer studies (Chapter 5) and the field tests (Chapter 4). From Blast 1 it was found that 750 m^3 of rock blasted off the face gave a displacement on the opposite face of approximately 0.001 inches.

Impulse = Volume X Density X velocity

$= 750 \times 3\times10^3 \times 10$

$= \underline{2.25 \times 10^7}$ N-sec

In a similar situation analysed in Chapter 5, the displacement obtained was approximately 0.15×10^{-2} m for an impulse of 5500 N-sec. Using subscript f to denote field values and c for computer values, the two results can be compared using equation 1. The displacement found from the computer study was normalised to the field data.

Thus: $$d_f = \frac{l_c^2}{l_f^2} \frac{\sqrt{s_c \rho_c}}{\sqrt{s_f \rho_f}} d_c \frac{I_f}{I_c}$$

From Ref 2 of Chapter 4, $s_f = E = 500\times10^3$ Kg_f/cm^2
$\simeq 5\times10^{10}$ N/m^2

$$\therefore d_f = \frac{2{\cdot}25\times10^7}{5500\sqrt{5\times10^{10}\times3\times10^3}} d_c$$

$= 3.3\times10^{-4}\ d_c$

But $d_c = 0.15\times10^{-2}$ m $= 0.15$ cm

$d_f = 0.5\times10^{-4}$ cm

$= \underline{0.00002 \text{ inches}}$

This figure is about fifty times smaller than the measured value. Bearing in mind that the calculated figure is likely to be on the *high* side (due to the boundary confinement and mesh oscillation), it is quite clear that a homogeneous elastic model is completely powerless to describe the field results. Some other mechanism must be responsible for the high degree with which vibrational energy is retained close to the pit. A possible explanation might be the trapping of energy within bands of rock of differing density and stiffness. This is also consistant with the low rate of decay of oscillations monitored around the pit.

C. FREQUENCIES AND DECAY FACTORS

Considering solely the frequencies associated with the shape of the pit, the requirement of similitude between pits of different size and elastic properties is that the wavelengths remain a constant proportion of a characteristic pit dimension.

i.e. $\frac{\lambda_1}{\lambda_2} = \frac{l_1}{l_2}$

But $\lambda = \frac{c}{f} = \frac{1}{f}\sqrt{\frac{s}{\rho}}$, where s = stiffness parameter, c = wave speed

$\therefore \frac{f_1}{f_2} = \frac{l_1}{l_2}\sqrt{\frac{s_1\rho_2}{s_2\rho_1}}$, where f = frequency.

Or $\frac{f_1}{f_2} = \frac{c_1}{c_2}\cdot\frac{l_2}{l_1}$

The frequencies found from both the computer and model studies may be compared on this basis.

The model frequency was 27.8 c.p.s. for what appeared to be this mode:

A similar mode in the two-dimensional Dynamic Relaxation example gave 0.93 c.p.s.

The two may be compared in terms of the plane Rayleigh wave speed:

C_m = 16.3 m/sec , R_m = 7.5 cm (m=model)

$C_c = 2.175 \times 10^3 \times 0.919$, R_c = 350 m (c=computer)

For the model, $\frac{f_m R_m}{C_m} = \frac{27.8 \times 7.5 \times 10^{-2}}{16.3}$

$= \underline{0.13}$

For the computer simulation,

$$\frac{f_c R_c}{C_c} = \frac{0.93 \times 350}{2.175 \times 10^3 \times .919}$$

$= \underline{0.16}$

There is clearly good agreement, especially bearing in mind that one result is for a two-dimensional case, and the other three-dimensional.

The decay factors found from both the computer and model studies are consistant in being very high. In other words, the frequency-dependant effects associated with the shape of the pit are very weak. The fact that the decay factors found in the field tests were much lower suggests that another mechanism was responsible for trapping vibrational energy.

Another interesting point is that although the long-period oscillations measured in the field test at different locations around the pit were of similar amplitude, the range of amplitudes found in both the computer and model studies was very great, sometimes reaching 100:1.

D. DYNAMIC FAILURE

Although this Thesis is concerned mainly with the elastic response of an open-pit, it is pertinent to consider briefly the mechanisms of dynamic failure. The simplest way of allowing for dynamic movements in a static stability analysis is to assume an additional acceleration to act (usually horizontally) on the failing mass, the magnitude of the acceleration being taken as a suitably large value depending on the expected size of the future dynamic movements. This approach is commonly refered to as a psuedo-static analysis. However, the approach may represent a rather conservative estimate, and more importantly, may obscure the true phenomena involved under dynamic loading. Newmark (Ref. 1) considered the motion of a rigid block on a horizontal plane, the plane being given a pulse of acceleration. He derived an expression for the total relative movement between block and plane due to slip along the contact. Newmark presents graphs showing the net displacements resulting from several recorded earthquakes as a function of friction value.

A similar calculation may be performed in the case of a block resting on a sloping plane, with a dynamic acceleration acting at an arbitrary angle to the horizontal:

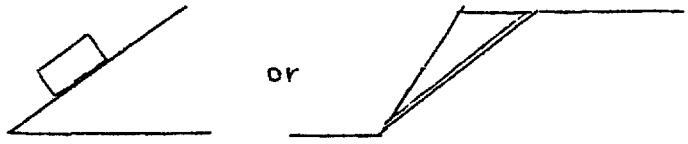

It may be assumed that slip will only take place *downhill*, in which case each dynamic pulse will cause the block to move further down the plane (provided that the dynamic acceleration is great enough). An interesting point is that the direction of acceleration to cause slip is *away* from the slope:

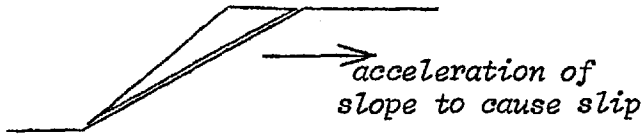

The generalised form of Newmark's equation can easily be shown to be:

$$\text{Net displacement, } \delta = \frac{V^2}{2\bar{\mu}g}\left[\frac{1}{\cos\alpha - A\sin(\alpha-\beta) - \frac{1}{\bar{\mu}}\sin\alpha} - \frac{\bar{\mu}}{A}\right]$$

The symbols are defined as follows:

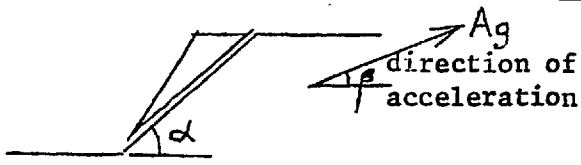

Acceleration = Ag, lasting for time t:

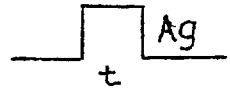

$\bar{\mu} = \frac{\text{shear force}}{\text{normal force}}$, for a rigid-plastic force-displacement relation

V = peak slope velocity = Agt

g = acceleration of gravity.

If $\alpha=0$ and $\beta=0$, the above equation reduces to Newmark's, i.e.

$$\delta = \frac{V^2}{2\bar{\mu}g}\left(1 - \frac{\bar{\mu}}{A}\right)$$

The above treatment is rather unrealistic from a rock mechanics point of view, since it is rare to find a joint possessing even approximately a rigid-plastic force-displacement characteristic. A typical rock joint might have the following shear characteristic:

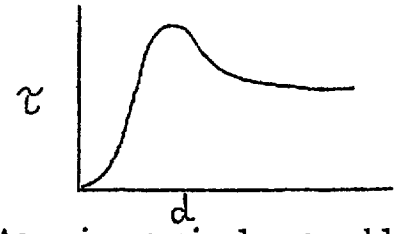

Assuming a simple, one-block failing mass, a mechanism for the long-term failure due to repeated dynamic loading might be as follows. Only the peak of the above curve is plotted, for clarity.

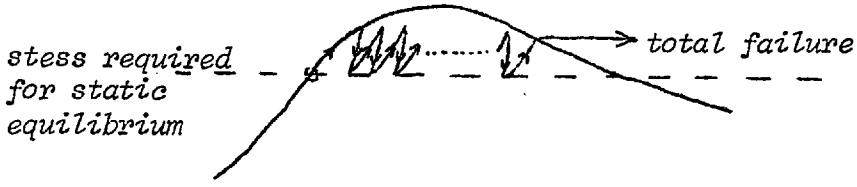

The dotted line represents the shear stress necessary for *static* equilibrium. Assuming a hysteretic behaviour resembling that shown by the arrowed line, it can be seen that initially the joint becomes stiffer, since the stress-stain curve becomes steeper. Due to the particular type of hysteresis possessed by the joint, a cumulative total displacement builds up, finally causing complete collapse. Yet the magnitude of dynamic stress at no stage was great enough to cause the factor of safety calculated by the psuedo-static approach to drop below unity. Of course, one could imagine a stress-strain law which possessed no hysteresis, but there is reason to believe that the type of law outlined above is reasonably common to rock joints.

In order to be able to calculate the effects refered to above, it is necessary to know the characteristics of a rock joint under cyclic loading conditions, as well as the dynamic

stresses induced by seismic loading. A useful formula may be derived (e.g. Kolsky, P 43; Ref. 2, Chapter 2) relating the particle velocity at a point to the dynamic stress at that point, for an unattenuated plane wave propagating through an elastic medium:

$$\sigma = \rho c v$$

where σ = stress
ρ = density of medium
c = velocity of wave propagation
v = particle velocity

In Chapter 4 (page 78) good agreement is obtained using this expression to relate stress and velocity measured for a blasting wave.

Since a blasting wave usually contains rapidly varying stress levels, the effects of fast loading on joints should be considered.

E. EARTHQUAKES

There are a number of papers which investigate the levels of motion to be expected from earthquakes of given magnitude. A clear account is given in Ref. 2, which provides the means for assessing the approximate accelerations, predominant periods, duration of shaking and time history from the magnitude of the earthquake and distance from the causative fault. As mentioned earlier in this Chapter, it is not likely that the shape of the open-pit would affect the acceleration levels to any great extent. However, there is evidence to show that the local geology will play a large part in the magnitude of response. In particular a soft surface layer may amplify the deep-level accelerations by a large factor. Ref. 3 gives an instance of surface motions being magnified by up to three times the level at 18 metres depth. Ref. 4 provides a comprehensive account of how various geological environments may alter the levels of motion experienced from an earthquake.

It may be reasonable to suppose that any failure taking place as a result of earthquake waves would be governed by essentially *static* laws of slip and fracture, since earthquake motions are relatively slow - in the range 0.1 to 10 c.p.s.

Even though an earthquake may not initiate immediate total failure it may cause irreversible displacements to take place, as described earlier, thus weakening the structure.

F. CONCLUSIONS AND SUMMARY

It would appear, from both the model studies and computer simulations presented in this thesis that the geometry of an open-pit plays very little part in the levels of motion and frequencies observed around an open-pit. A simple scaling law was derived which enabled the field results to be compared with the computer simulation. It is apparent from both the levels of motion and the decay factors that there was some mechanism at Atalya pit responsible for efficient trapping of vibrational energy. This mechanism may possibly be associated with the geological inhomogeneity present around the pit. For example it is known that a weak surface layer can amplify incident earthquake waves.

The simple dynamics of a block sliding on a sloping plane was derived, assuming a rigid-plastic friction law. However this assumption was not thought to be particularly true in many rock situations, and a mechanism was proposed to explain the cumulative displacements often observed as a result of cyclic dynamic loading. Clearly, data must be available giving the effect of cyclic loading on the shear properties of a joint, and, in the case of blasting, it is also necessary to know the effect of rate of loading.

REFERENCES

Chapter 6

1. NEWMARK, N.M. "Effects of Earthquakes on Dams and Embankments" Geotechnique V. 15, N° 2, June 1965, pp139-159

2. SEED, H.B., IDRISS, I.M., KIEFER, F.W. "Characteristics of Rock Motions During Earthquakes". Jour. Soil Mech. & Found. Div., A.S.C.E. V. 95, N° SM5, Sept. 1969, pp1199-1218.

3. YOSHIZAWA, S., TANAKA, T., KANAI, K. "Some Features of Strong Underground Earthquake Motions Computed from Observed Surface Records". Bull. E.Q. Res. Inst., Univ. of Tokyo. V 46, Part 3, May 1968.

4. BAROSH, P.J. "Use of Seismic Intensity Data to Predict the Effects of Earthquakes and Underground Nuclear Explosions in Various Geologic Settings" Geological Survey Bullctin N° 1279, U.S. Government. 1969.

* * * * *

Appendices

APPENDIX II

CIRCULATING ELASTIC WAVES AROUND THE SURFACE OF A HOLE IN AN INFINITE TWO-DIMENSIONAL CONTINUUM.

This Appendix explores the possibility that a circular hole in an infinite 2-dimensional continuum may be able to trap vibrational energy without radiating any of it into the infinite solid. Of course energy loss will occur due to internal friction. However, as reported in Chapter 2, most structures embedded in an infinite solid radiate so much energy into their surroundings that internal friction becomes unimportant. In that case, the structure can hardly be described as having a "resonance" - more of an undulating frequency response curve. If it is true that a 2-dimensional hole *can* trap all of its vibrationsl energy, a theoretically infinite resonance peak is possible.

In order to make the solution of the differential equations easier, it is necessary to make some assumptions about the nature of the circulating wave. The classic method is to separate the variables (e.g. the Pochhammer equations for a bar; see Kolsky, referenced in Chapter 2); that is to say, the variations in the components of the wave with respect to radius are assumed to be independent of the variations with respect to both time and angle around the hole. Furthermore, the wave is considered to be of one frequency, and to have existed for all time. This last requirement is not too restricting as arbitrary waveforms and time-limited waves can be dealt with by common methods once the single-frequency case has been solved. The simplest equations of displacement would seem to be:

$$u_r = U(r)\exp[i(pt + f\theta)] \quad \ldots\ldots 1$$

$$u_\theta = V(r)\exp[i(pt + f\theta)] \quad \ldots\ldots 2$$

where U(r), V(r) are (possibly) complex functions of r.

p & f are real numbers, where p=2πF
F= frequency
f= number of wavelengths around the hole.

The phase velocity, in terms of angle/second

$$= \frac{p}{f}$$

These equations represent a wave circulating around the hole, with the same angular phase velocity at any radius: in other words, the linear phase velocity tends to infinity at infinite radius. This may not be unrealistic, as it is the *group* velocity which governs the speed at which energy is transfered. The possibility of curved wave-fronts is also included in the equations if V(r) and U(r) are complex.

It might seem more logical to write the equations as a function of θr instead of just θ. However this would mean that (a) the solution would be very difficult due to the non-separated variables, and (b) the shape of the wave-front would change as the wave progressed around the hole, which is not the sort of wave

which is being looked for.

The combined elastic equations in terms of displacements are, in cylindrical polar co-ordinates:

$$\rho \frac{\partial^2 u_r}{\partial t^2} = (\lambda+2\mu)\frac{\partial \Delta}{\partial r} - \frac{2\mu}{r} \cdot \frac{\partial \omega_z}{\partial \theta} \quad \ldots\ldots 3$$

$$\rho \frac{\partial^2 u_\theta}{\partial t^2} = \frac{(\lambda+2\mu)}{r}\frac{\partial \Delta}{\partial \theta} + 2\mu \frac{\partial \omega_z}{\partial r} \quad \ldots\ldots 4$$

Where the dilation, $\Delta = \frac{\partial u_r}{\partial r} + \frac{u_r}{r} + \frac{1}{r} \cdot \frac{\partial u_\theta}{\partial \theta}$. 5

and rotation, $2\omega_z = \frac{1}{r}\left(r\frac{\partial u_\theta}{\partial r} + u_\theta - \frac{\partial u_r}{\partial \theta}\right)$. 6

Assuming plane strain, $u_z = 0$, $\frac{\partial u_r}{\partial z} = 0$ etc.

Equations 1 and 2 are then used to evaluate the differentials with respect to θ and t in 3 and 4, giving:

$$u_r = \frac{2\mu i f}{\rho p^2 r}\omega_z - \frac{\lambda+2\mu}{\rho p^2} \cdot \frac{\partial \Delta}{\partial r} \quad \ldots\ldots 7$$

and $$u_\theta = -\frac{(\lambda+2\mu) i f}{\rho p^2}\frac{\Delta}{r} - \frac{2\mu}{\rho p^2} \cdot \frac{\partial \omega_z}{\partial r} \quad \ldots\ldots 8$$

These values are then inserted in 5 and 6, differentiating where necessary, giving:

$$r^2\frac{\partial^2 \Delta}{\partial r^2} + r\frac{\partial \Delta}{\partial r} + \left(\frac{\rho p^2}{\lambda+2\mu} \cdot r^2 - f^2\right)\Delta = 0 \quad \ldots\ldots 9$$

$$r^2\frac{\partial^2 \omega_z}{\partial r^2} + r\frac{\partial \omega_z}{\partial r} + \left(\frac{\rho p^2}{\mu} r^2 - f^2\right)\omega_z = 0 \quad \ldots\ldots 10$$

The solutions to 9 and 10 are:

$$\Delta = AJ_f(jr) + BY_f(jr) \quad \ldots\ldots 11$$

$$\omega_z = CJ_f(kr) + DY_f(kr) \quad \ldots\ldots 12,$$

where f=0, or integral

Or:

$$\Delta = AJ_f(jr) + BJ_{-f}(jr) \quad \ldots\ldots 13$$

$$\omega_z = CJ_f(kr) + DJ_{-f}(kr) \quad \ldots\ldots 14,$$

where f is non-integral.

Where: $j = \frac{p}{c_1}$, $c_1 = \sqrt{\frac{\lambda+2\mu}{\rho}}$ (P wave speed)

and $k = \frac{p}{c_2}$, $c_2 = \sqrt{\frac{\mu}{\rho}}$ (S wave speed)

And A, B, C, D are functions of θ and t.

Taking the expressions for non-integral f, these can be written:

$$\Delta = [KJ_f(jr)+LJ_f(jr)]\exp(i(pt+f\theta)) \quad \ldots\ldots 15$$

and $$\omega_z = [MJ_f(kr)+NJ_f(kr)]\exp(i(pt+f\theta)) \quad \ldots\ldots 16$$

Where K,L,M,N are <u>not</u> functions of r,t or θ

Substituting 15 and 16 in 7 and 8,

$$U(r) = \frac{2\mu i f}{\rho p^2 r}[MJ_f(kr)+NJ_f(kr)] - \frac{(\lambda+2\mu)}{\rho p^2} j[KJ_f'(jr)+LJ_f'(jr)] \quad . 17$$

$$V(r) = -\frac{(\lambda+2\mu) if}{\rho p^2 r}[KJ_f(jr)+LJ_f(jr)] - \frac{2\mu k}{\rho p^2}[MJ_f'(kr)+NJ_f'(kr)] \quad . 18$$

Where $J_f'(jr) \equiv \frac{\partial}{\partial r}[J_f(jr)]$ etc.

<u>Boundary Conditions</u>

At the surface of the circular hole,

$r = a$ and $\sigma_{rr} = 0, \sigma_{r\theta} = 0$

But $$\sigma_{rr} = \lambda\Delta + 2\mu\frac{\partial u_r}{\partial r} = 0 \quad \Big\} \text{ at } r=a \quad . 19$$

And $$\sigma_{r\theta} = \mu\left[\frac{1}{r}\frac{\partial u_r}{\partial\theta} + r\frac{\partial}{\partial r}\left(\frac{u_\theta}{r}\right)\right] = 0 \quad . 20$$

Substituting from 15, 16, 17, 18,

$$0 = -\frac{2\mu f^2}{\rho p^2 a^2}[MJ_f(ka)+NJ_f(ka)] - \frac{2ijf(\lambda+2\mu)}{\rho p^2 a}[KJ_f'(ja)+LJ_f'(ja)]$$
$$- \frac{2\mu k^2}{\rho p^2}[MJ_f''(ka)+NJ_f''(ka)]$$
$$+ \frac{2(\lambda+2\mu)ijf}{\rho p^2 a}[KJ_f(ja)+LJ_f(ja)] + \frac{2\mu k}{\rho p^2 a}[MJ_f'(ka)+NJ_f'(ka)]$$
$$\ldots\ldots 21$$

And

$$0 = \lambda[KJ_f(ja)+LJ_f(ja)]$$
$$+ \frac{4\mu^2 ijf}{\rho p^2 a^2}[kaMJ_f'(ka)+kaNJ_f'-MJ_f(ka)-NJ_f(ka)]$$
$$- \frac{2\mu(\lambda+2\mu)j^2}{\rho p^2}[KJ_f''(ja)+LJ_f''(ja)]$$
$$\ldots\ldots 22$$

Since there are only two equations, but four unknowns, K,L,M,N, the positive and negative Bessel functions will be considered separately, i.e. first setting L=0 and N=0. Later on the second Bessel function alone will be considered.

Thus, set L=N=0 and equate the value of $\frac{M}{K}$ from 21 to $\frac{M}{K}$ from 22:

$$\frac{\frac{a^2\lambda\rho p^2}{(\lambda+2\mu)}J_f(ja) - 2\mu j^2 a^2 J_f''(ja)}{4\mu af\,kJ_f'(ka) - 4\mu f J_f(ka)} = \frac{aj\beta J_f'(ja) - fJ_f(ja)}{-f^2 J_f(ka) - a^2k^2J_f''(ka) + akJ_f'(ka)}$$

$$\ldots\ldots 23$$

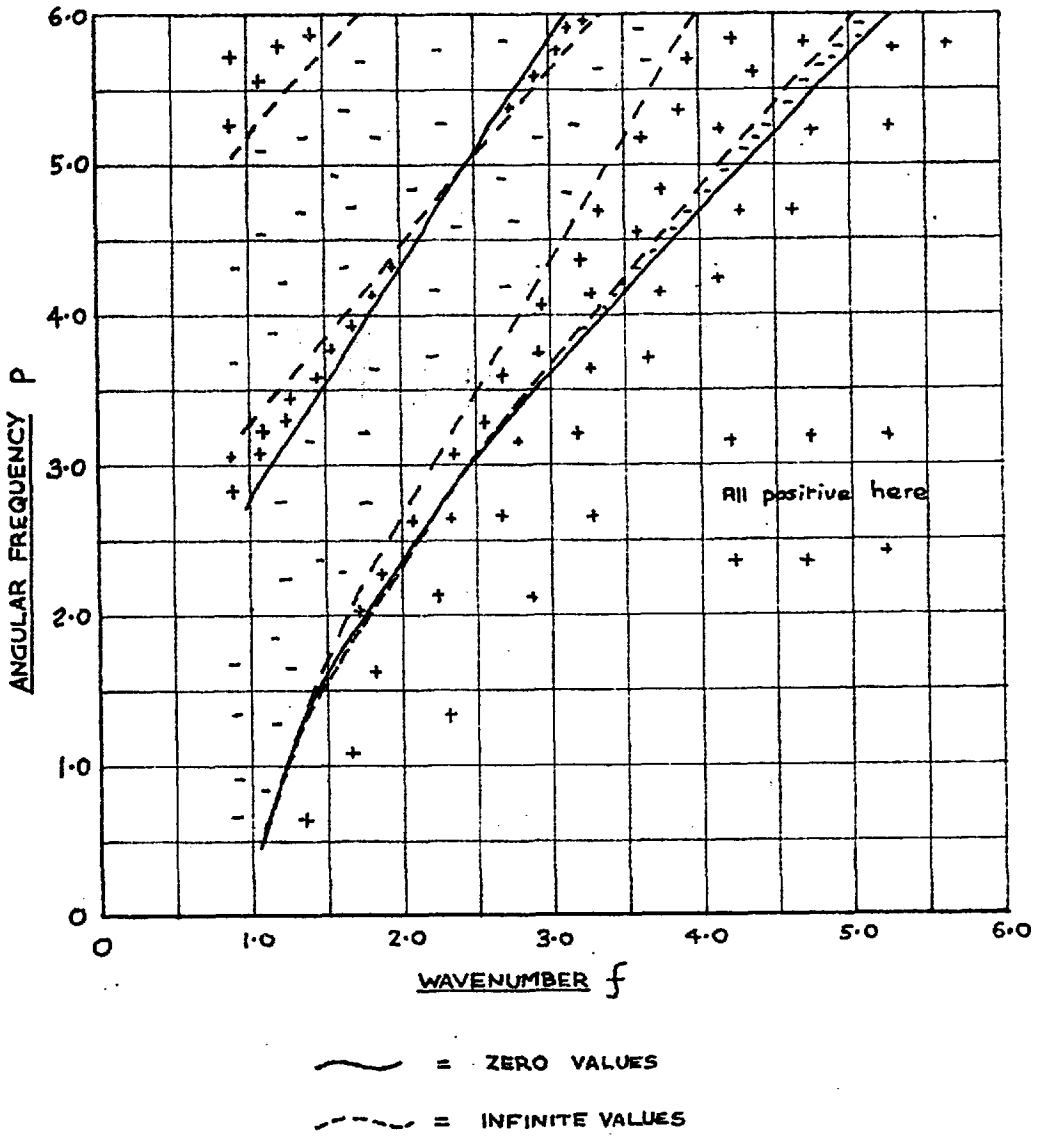

FIG. 1: MAP SHOWING LOCATION OF ZEROS AND POLES (INFINITIES) OF FREQUENCY EQUATION - using positive Bessel functions only, i.e. $J_f()$.

The above equation is the Frequency Equation, and will give, on solution, the phase velocity for any frequency or wave number.

In order to simplify calculations,

Let $\lambda = \mu = \rho = a = 1$, which means that Poisson's ratio, $\nu = 0{\cdot}25$

And P speed, $C_1 = \sqrt{3}$ $\therefore\ j = \frac{p}{\sqrt{3}}$

S speed, $C_2 = 1$ $\therefore\ k = p$

Equation 23 becomes:

$$\frac{-\frac{p^2}{3}J_f\left(\frac{p}{\sqrt{3}}\right) - \frac{2p^2}{3}J_f''\left(\frac{p}{\sqrt{3}}\right)}{4pfJ_f'(p) - 4fJ_f(p)} = \frac{\frac{pf}{\sqrt{3}}J_f'\left(\frac{p}{\sqrt{3}}\right) - fJ_f\left(\frac{p}{\sqrt{3}}\right)}{-f^2J_f(p) - p^2J_f''(p) + pJ_f'(p)}$$

.... 24

There are only two variables here. It should be remembered that the angular phase velocity = $\frac{p}{f}$.

To solve the equation, the left-hand side and the right-hand side were evaluated for various values of p and f, and subtracted. An answer of zero represents a solution to the equation.

i.e. x = LHS - RHS

A plot of the value of x is shown in Figure 1. A prominent feature is the line of zero x starting from about f = 1·2, p = 1.0. This line was followed up to f = 100, and the ratio of p/f (phase velocity) plotted in Figure 2. It can be seen that this velocity curve is asymptotic to the Rayleigh wave speed at high frequencies, which is reasonable since the curvature of the hole boundary becomes less important when the wavelength is very small compared with the radius of the hole. However, it is necessary to know whether this solution of the frequency equation corresponds to the type of wave that was looked for.

Substituting the value of M/K obtained from 22 into equation 17, and letting L=N=0, we obtain:

$$U(r) = K\left[\frac{\mu f}{2r\rho p^2}J_f(kr)\frac{\left\{2\mu j^2(\lambda+2\mu)J_f''(ja) - \rho p^2\lambda J_f(ja)\right\}}{\left\{\frac{\mu^2 f k}{a}J_f'(ka) - \frac{\mu^2 f}{a^2}J_f(ka)\right\}} - \frac{(\lambda+2\mu)}{\rho p^2}jJ_f'(jr)\right]$$

$$V(r) = -ik\left[\frac{(\lambda+2\mu)f}{\rho p^2 r}J_f(jr) + \frac{\mu k}{2\rho p^2}J_f'(kr)\frac{\left\{\rho p^2\lambda J_f(ja) - 2\mu j^2(\lambda+2\mu)J_f''(ja)\right\}}{\left\{\frac{\mu^2 f k}{a}J_f'(ka) - \frac{\mu^2 f}{a^2}J_f(ka)\right\}}\right]$$

These equations give the variations of displacements with radius, r. It is noted immediately that the two displacement components U and V are always -90° out of phase with each other.

The variations of U and V are shown in

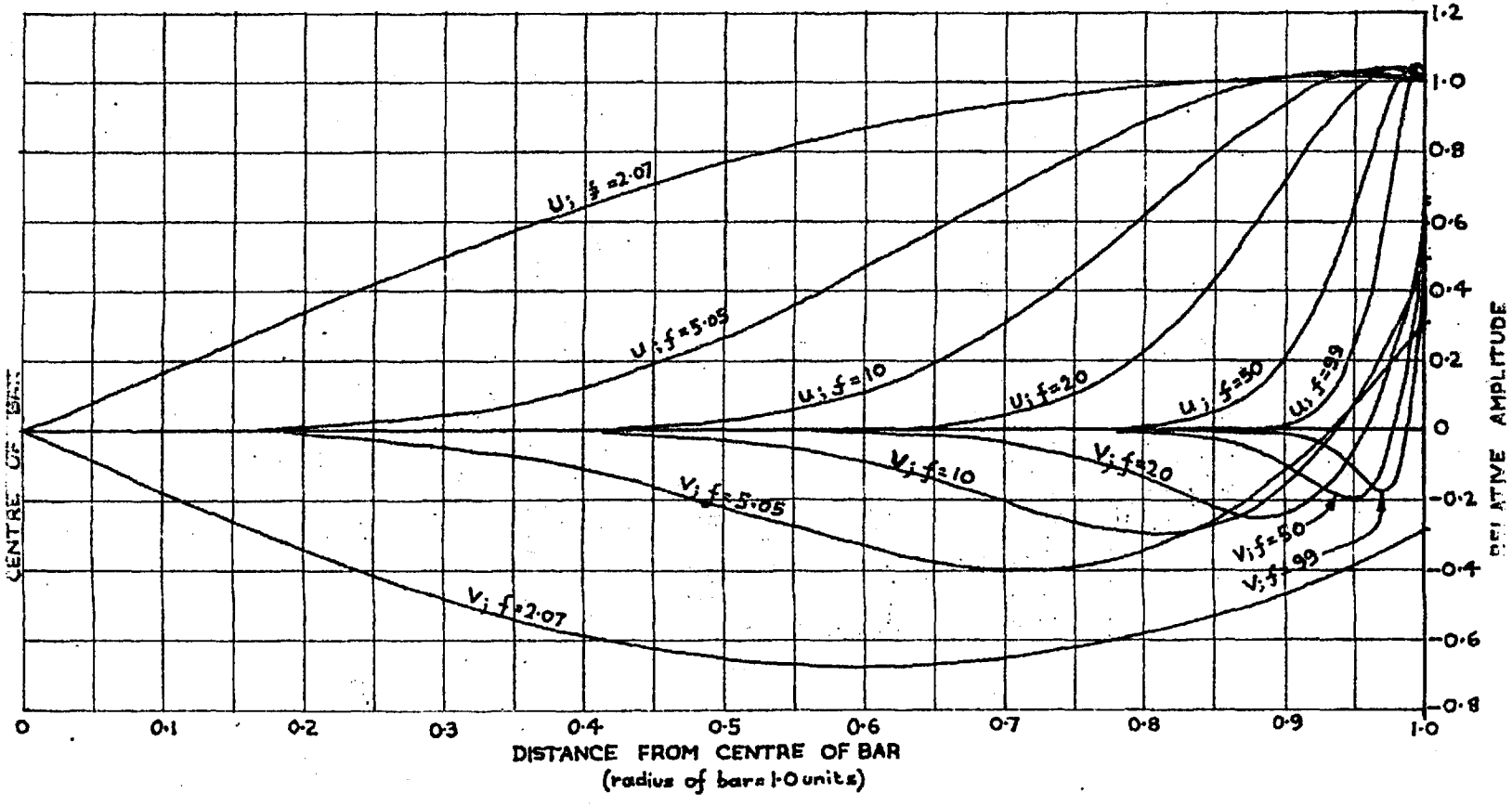

FIG: 3: VARIATIONS OF U AND V WITH RADIUS, FOR SEVERAL ROOTS OF THE FREQUENCY EQUATION (using only positive Bessel functions $J_f(\ )$).

U = displacement parallel to radii

V = displacement normal to radii

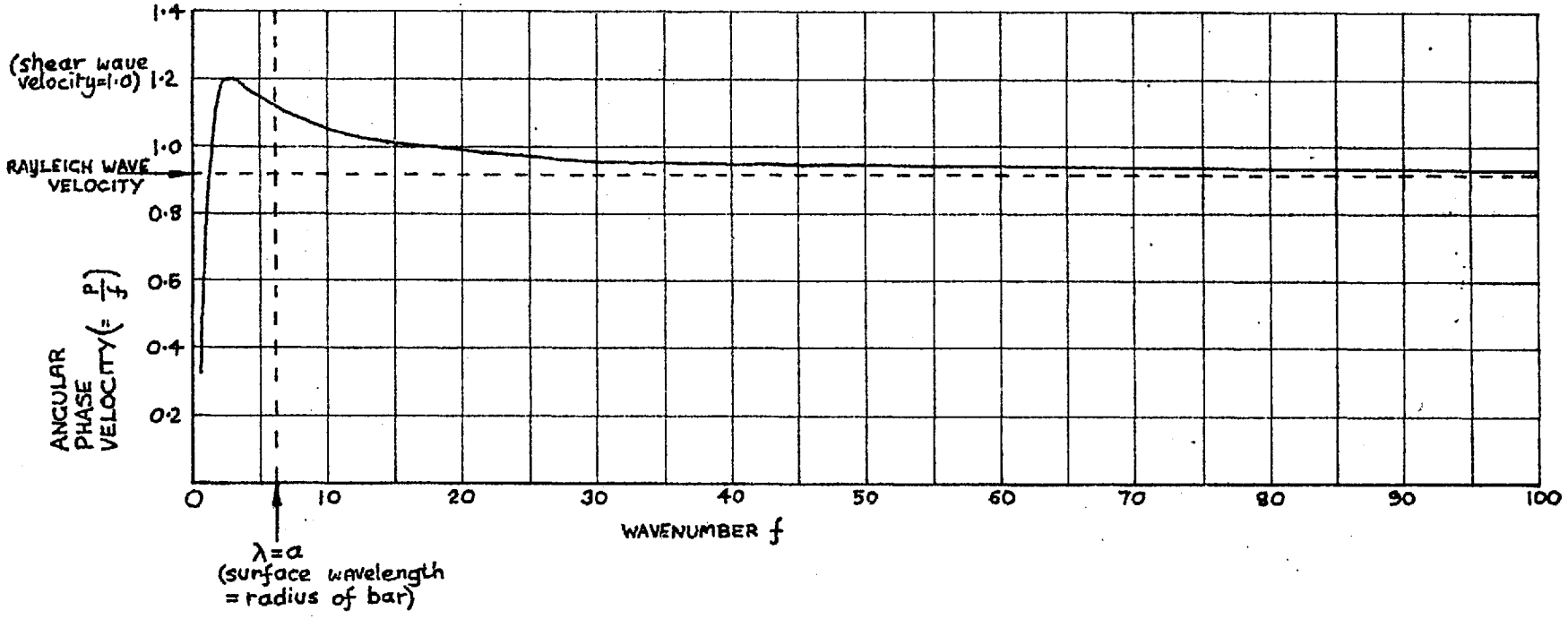

FIG. 2: PHASE VELOCITY CURVE ($\frac{p}{f}$) FOR FIRST ROOT OF FREQUENCY EQUATION (positive Bessel functions)

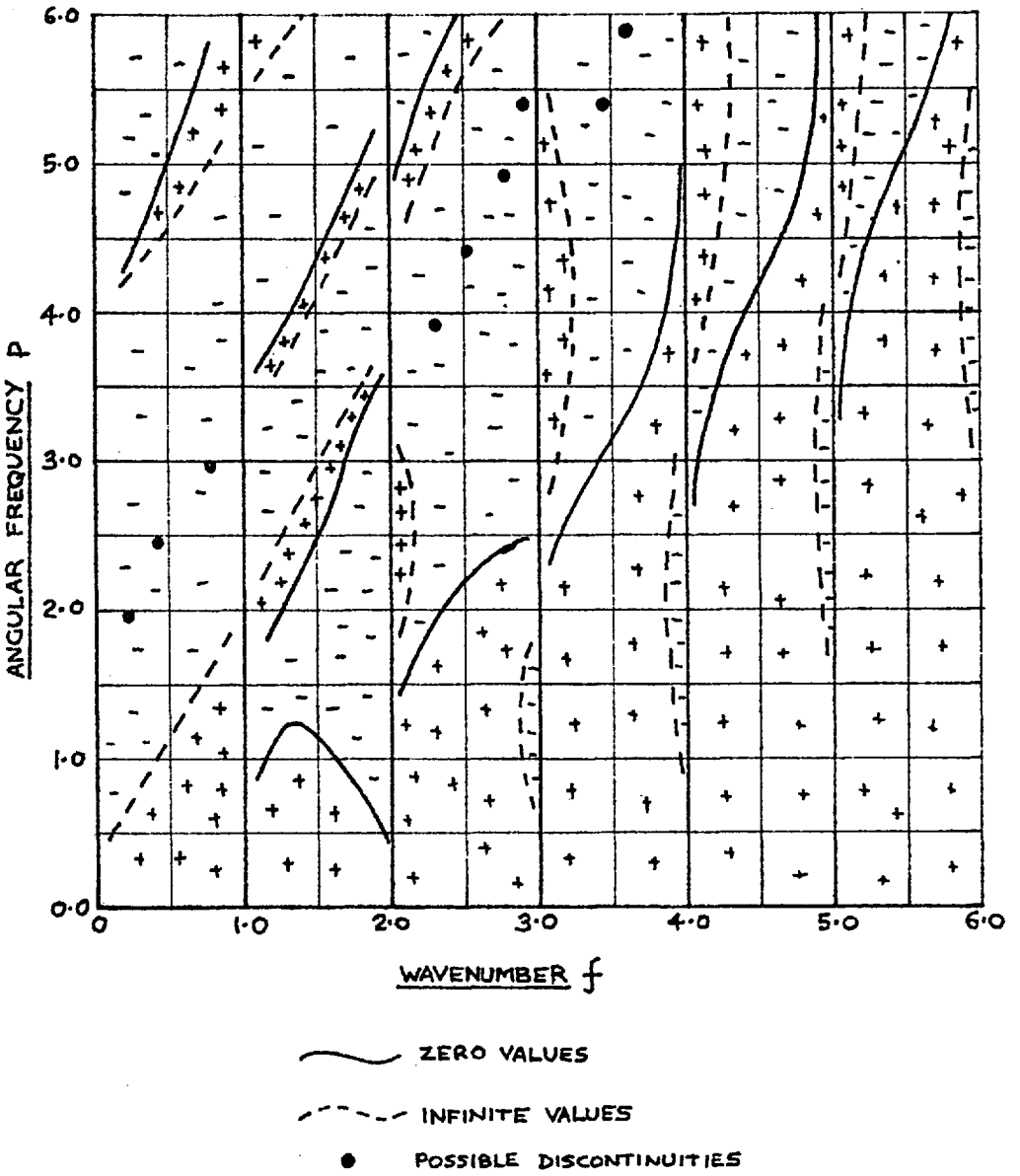

FIG. 4: MAP SHOWING LOCATION OF POLES AND ZEROS OF FREQUENCY EQUATION - using negative Bessel functions only, i.e. $J_{-f}()$.

Figure 3 for various roots of the frequency equation. The values are not plotted at greater radii than 1 since the curves quickly assume large magnitudes. In other words, the roots of the frequency equation using the positive Bessel functions yield solutions corresponding to a circulating wave *inside* a stress-free surface. That is to say, the characteristics of waves propagating around the curved surface of a bar have been found. As the frequency increases, the wave is confined more and more to the near-surface region, and a f = 99 the U and V curves are almost identical to those for a plane Rayleigh wave (see Chapter 2). At the lower end of the spectrum, the whole cross-section of the bar is in motion. It is interesting to note that the frequency of a bar in its fundamental asymmetrical radial resonance will be given by:

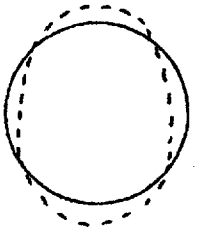

$$\omega \simeq \frac{2.36V_s}{a}$$

$$f = \frac{2.36V_s}{2\pi a}$$

where V_s = shear speed
a = radius of bar

The above frequency is in fact the lowest that can be propagated around a bar, since for lower values of f (e.g. 1.99) the U and V curves do not reduce to zero at r = 0.

Negative Bessel Functions

Since the solutions to 21 and 22 using only the positive Bessel functions did not correspond to a wave travelling around a hole, the solution was then attempted using only the negative Bessel functions. The roots of the frequency equation were evaluated as before, but substituting negative Bessel functions ($J_{-f}()$) in equation 24 instead of the positive functions. The resultant solution map is shown in Figure 4.

The map is clearly highly complex compared with Figure 1. A major feature is that singularities exist at all integral values of wavenumber, f. It seems pointless to draw a phase velocity curve, since it would be completely discontinuous. The velocities at some points examined were as follows:

f=2.1	C=0.719
f=3.5	C=0.910
f=25.5	c=0.980
f=55.5	C=0.999
f=85.5	C=1.003

These figures do not appear to be converging to the Rayleigh wave velocity of 0.919. Displacement curves were plotted for three values of f, and are given in Figures 5,6,7. The prominent feature of these curves is that they extend to a large number of wavelengths beyond the hole, with only a moderate diminution in amplitudes. They can hardly be regarded as "surface waves". Since both the velocity and form of the waves do not appear to converge, at high frequencies, to the corresponding characteristics of Rayleigh waves, it must be concluded that the waves are of a completely different *type* from Rayleigh waves. It will be recalled that the initial assumption was of a wave circulating around a

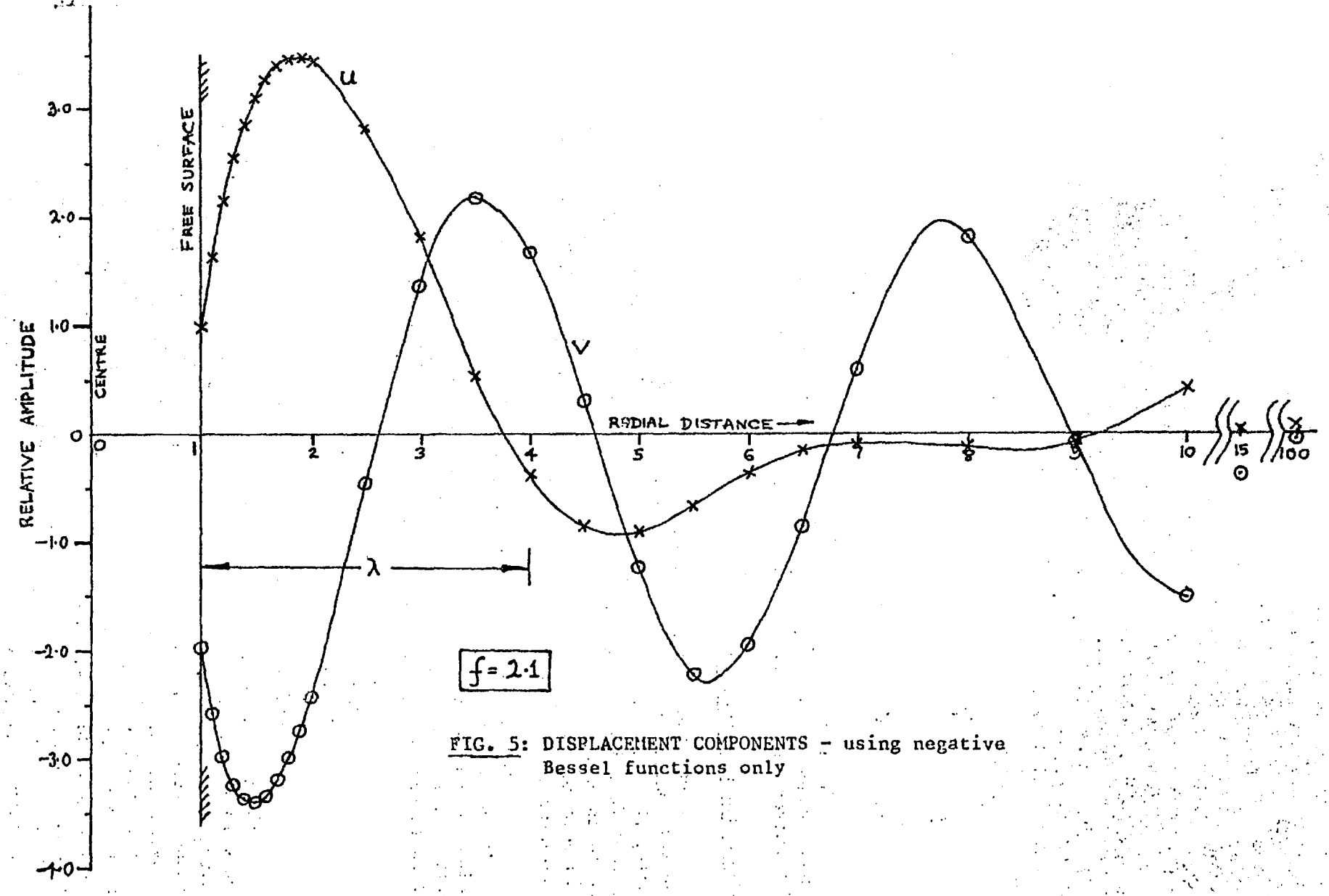

FIG. 5: DISPLACEMENT COMPONENTS - using negative Bessel functions only

FIG. 6: DISPLACEMENT COMPONENTS - using negative Bessel functions only

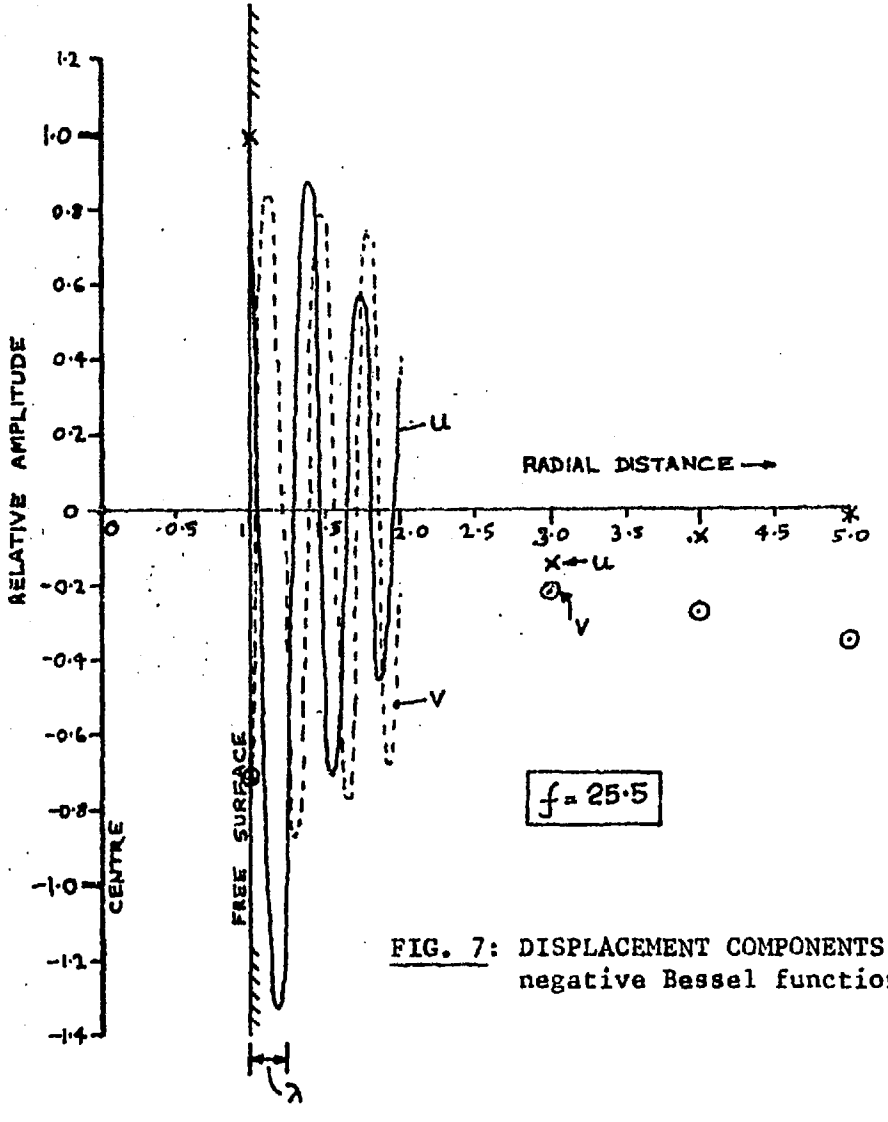

FIG. 7: DISPLACEMENT COMPONENTS - using negative Bessel functions only

hole without loss of amplitude and without change in shape. It would appear that this requirement cannot be satisfied by a simple wave confined to a surface region of comparable size to the wavelength.

It may be the case that the calculations leading to the above results were in error. This is difficult to believe however, since the same computer program was used for both the negative and positive Bessel function calculations, with only the sign of the Bessel order changed. Assuming that the calculations are correct, the solutions require that a considerable quantity of circulating energy be established extending to many wavelengths from the hole. In practice, a possible explanation of the physical process may be as follows: an initial impulse at the surface of the hole would set up waves in the solid and along the hole surface. However in order to establish the required stable circulating-wave pattern, the surface wave would radiate energy into the solid. In other words the amplitude of the surface wave would diminish until the circulating wave system required by the solution to the frequency equation was set up. This would explain the large apparent damping factor, observed in Chapter 5, for a computer model of a circular hole in a 2-dimensional solid. It would also explain why the solution was affected by the boundaries, even though these were at a considerable distance from the hole.

Since the solutions obtained have been only for non time-dependent waves, it is impossible to say what the effective rotational velocity might be for the transient waves postulated. It is likely that the speed would be a good deal slower than the shear speed - for the stable wave system the velocity falls below $0.5C_S$ in the region f = 1 to 2.

Summary

The velocity and form of waves propagating around the curved surface of a circular bar have been found. However, in the case of a circular hole in an infinite solid, the only wave found that circulates unchanged in amplitude and shape is not confined to the near-surface region of the hole. It has many concentric bands of alternate-sign components extending to many surface wavelengths from the hole. It may be possible that the energy required to establish this wave system would account for the apparent attenuation factor of surface waves spreading out from a disturbance at the surface of a hole.

APPENDIX III

COMPUTER PROGRAMS

The computer programs presented here are not "packages". They are working programs, with all the data included for successfully running them. A list of the variables, constants and subroutines is given, with their corresponding meanings and use. A competent programmer should be able to modify and adapt the programs to meet specific needs. No input specification is given, since the requirements should be clear from the examples given. In any case, the data required is minimal for the three programs (one card for the dynamic program).

3D DYNAMIC PROGRAM

Axi-Symmetric Open-Pit in the Surface of a Solid

List of Variables and Constants

MU μ L λ	Lame's constants
RR,SS,ZZ	direct stresses σ_{rr}, $\sigma_{\theta\theta}$, σ_{zz} (3D arrays)
RZ,RS,ZS	shear stresses τ_{zr}, $\tau_{r\theta}$, $\tau_{\theta z}$ "
U, V, W	velocities in r,θ and z directions
DU,DV,DW	displacements in r,θ and z directions
NA	number of nodes to radial boundary
NB	" " " " bottom "
NH	" " " for depth of pit
NW	" " " for base of pit
NR	" " sectors
ELAST	Young's modulus
POISS	Poisson's ratio
RHO	density
RDEL	length of radial mesh increment
ZDEL	length of vertical mesh increment
SDEL	angular increment
TDEL	time increment
FRAC	fraction of critical time used
ITS	number of iterations
NDAMP	number of boundary damping nodes
CRIT	fraction of critical overall damping used
CRI(I)	array of boundary damping constants
I	generally used as index for radial DO loops
J	" " " " " circumferential DO loops
K	" " " " " vertical DO loops

R1, R2 etc constants used in the stress and displacement calculations.

```
      REAL MU,L
      COMMON/BONG/ G,ITS,TDEL
      DIMENSION ONEU(16,11),TWOU(16,11),ONEV(16,11),TWOV(16,11),
     /  ONEW(16,11),TWOW(16,11)
      DIMENSION CRI(16)
      DIMENSION G(2816,12)
      DIMENSION RR(16,16,11),SS(16,16,11),ZZ(16,16,11)
      DIMENSION RZ(16,16,11),RS(16,16,11),ZS(16,16,11)
      DIMENSION  U(16,16,11), V(16,16,11), W(16,16,11)
      DIMENSION DU(16,16,11),DV(16,16,11),DW(16,16,11)
      DIMENSION R1(16),R2(16),R3(16),R4(16),R5(16)
      DIMENSION R6(16),R7(16),R8(16),R9(16),R10(16)
      DIMENSION C0(16),S1(16),C2(16),S2(16)
      EQUIVALENCE (G(1,1),RR),(G(1,2),SS),(G(1,3),ZZ),
     /            (G(1,4),RZ),(G(1,5),RS),(G(1,6),ZS),
     /            (G(1,7), U),(G(1,8), V),(G(1,9), W),
     /            (G(1,10),DU),(G(1,11),DV),(G(1,12),DW)
      REWIND 7
      READ(5,50) NA,NB,NH,NW,NR
   50 FORMAT(5I5)
C -------- DATA ----------------------------------------------------
      PI=3.1415926536
      ELAST=0.3E 11
      POISS=0.22
      RHO=0.26E 04
      RDEL=50.0
      ZDEL=50.0
      FRAC=0.9
      AMP=1000.0
      AMUL=PI/0.25
      ITS=1200
      WO=2.0*PI*2.0
      NDAMP=5
      CRIT=0.0                          Boundary damping array
      CRI(1)=4.0$CRI(2)=2.0$CRI(3)=1.0$CRI(4)=0.5$CRI(5)=0.25
C-------------------------------------------------------------------
      MU=ELAST/(2.0*(POISS+1.0))
      L =ELAST*POISS/((POISS+1.0)*(1.0-2.0*POISS))
      SPEED=SQRT((L+2.0*MU)/RHO)        P wave speed
      SHEAR=SQRT(MU/RHO)                S wave speed
      RE=NR
      SDEL=2.0*PI/RE
      RT=1.0/(ZDEL**2)+1.0/(RDEL**2)+1.0/((RDEL*SDEL/2.0)**2)
      RT=SQRT(RT)
      TDEL=FRAC/(SPEED*RT)          Calculate critical value of time increment
      ANGLE=ATAN2(ZDEL,RDEL)*180.0/3.1416
      WRITE(6,60)
   60 FORMAT(1H1)
      WRITE(6,61) NA
   61 FORMAT(21H RADIUS OF BOUNDARY =,I3,6H UNITS/)
      WRITE(6,62) NB
   62 FORMAT(20H DEPTH OF BOUNDARY =,I3,6H UNITS/)
      WRITE(6,63) NH
   63 FORMAT(15H DEPTH OF PIT =,I3,6H UNITS/)
      WRITE(6,64) NW
   64 FORMAT(24H RADIUS OF BASE OF PIT =,I3,6H UNITS/)
      WRITE(6,65) NR
   65 FORMAT(20H NUMBER OF SECTORS =,I3/)
      WRITE(6,66) ANGLE
```

```
 66 FORMAT(14H SLOPE ANGLE =,F5.1,8H DEGREES///)
    WRITE(6,67) TDEL
 67 FORMAT(17H TIME INCREMENT =,E12.4,5H SECS/)
    WRITE(6,68) FRAC
 68 FORMAT(33H FRACTION OF CRITICAL TIME USED =,F5.3/)
    WRITE(6,69) SPEED
 69 FORMAT(18H P WAVE VELOCITY =,E12.4,18H METRES PER SECOND/)
    WRITE(6,71) SHEAR
 71 FORMAT(18H S WAVE VELOCITY =,E12.4,18H METRES PER SECOND///)
    IA=NA+1$IB=NW+NH+3$IC=NW+1$ID=NW+NH+1$IE=NW+NH+2$JA=NR+1$KA=NB+1
   /$KB=NH+1$KC=NH+2$ANR=NR
    AA=L+2.0*MU
    RM=MU/RDEL
    ZM=MU/ZDEL
    DR=1.0/RDEL
    DZ=1.0/ZDEL
    DO 30 J=1,NR
    AJ=J-1
    RON=SDEL*AJ
    REG=2.0*RON
    S2(J)=SIN(REG)
    C2(J)=COS(REG)
    SI(J)=SIN(RON)                    Calculate some of the constants to be used
 30 CO(J)=COS(RON)
    DO 1 I=2,IA
    R1(I)=I-1
    R1(I)=R1(I)*RDEL
    R2(I)=R1(I)-0.5*RDEL
    R3(I)=MU/(R1(I)*SDEL)
    R4(I)=MU/(2.0*R1(I))
    R5(I)=MU/(R2(I)*SDEL)
    R6(I)=1.0/(R1(I)*SDEL)
    R7(I)=1.0/(2.0*R1(I))
    R8(I)=1.0/(R2(I)*SDEL)
    R9(I)=1.0/R2(I)
    R10(I)=1.0/(2.0*R2(I))
  1 CONTINUE
    DO 250 I=2,IA
    DO 250 K=1,KA
    CRITT=CRIT
    IF(I.LE.IA-NDAMP.AND.K.LE.KA-NDAMP) GO TO 248   Decide where the
    IF(IA-I.LE.KA-K) GO TO 247                      damping matrix is
    CRITT=CRI(KA+1-K)                               located
    GO TO 248
247 CRITT=CRI(IA+1-I)
248 DAMPU=CRITT*SQRT((L+2.0*MU)*RHO)/RDEL           The damping is
    DAMPV=CRITT*SQRT((L+2.0*MU)*RHO)/(R2(I)*SDEL)   considered
    DAMPW=CRITT*SQRT((L+2.0*MU)*RHO)/ZDEL           separately for the
    D1U=1.0/(RHO/TDEL+DAMPU/2.0)                    3 dimensions
    D2U=RHO/TDEL-DAMPU/2.0
    D1V=1.0/(RHO/TDEL+DAMPV/2.0)
    D2V=RHO/TDEL-DAMPV/2.0
    D1W=1.0/(RHO/TDEL+DAMPW/2.0)
    D2W=RHO/TDEL-DAMPW/2.0
    ONEU(I,K)=D1U*D2U
    TWOU(I,K)=D1U
    ONEV(I,K)=D1V*D2V
    TWOV(I,K)=D1V
    ONEW(I,K)=D1W*D2W
```

```
      TWOW(I,K)=D1W
  250 CONTINUE
      WRITE(6,249) NDAMP
  249 FORMAT(//* DAMPING MATRIX, BAND =*,I4,* UNITS WIDE*/)
      DO 251 K=1,KA
  251 WRITE(6,252) (ONEV(I,K),I=2,IA)
      WRITE(6,253)
  253 FORMAT(//)
  252 FORMAT(16E7.1)
      DO 254 K=1,KA
  254 WRITE(6,252) (TWOV(I,K),I=2,IA)
      WRITE(6,253)
C--------- INITIALIZE ARRAYS ----------------------------------------
      DO 2 K=1,KA
      DO 2 J=1,NR
      DO 2 I=1,IA
      RR(I,J,K)=SS(I,J,K)=ZZ(I,J,K)=RZ(I,J,K)=RS(I,J,K)=ZS(I,J,K)=
     / U(I,J,K)=V(I,J,K)=W(I,J,K)=DU(I,J,K)=DV(I,J,K)=DW(I,J,K)=0.0
    2 CONTINUE
      KK=0
C--------- START MAIN ITERATION LOOP --------------------------------
      DO 21 N=1,ITS
      TI=N
      T=TI*TDEL      "real" value of time
      DO 10 J=1,NR
      JJ=J-1
      JJJ=J+1
      IF(J.EQ.1) JJ=NR
      IF(J.EQ.NR) JJJ=1
C -------- CALCULATE DIRECT STRESSES ------------------------------
      DO 3 K=2,KA
      M=2
      IF(K.LE.KB) M=IB-K  - to define the pit geometry
      DO 3 I=M,IA
      DUDIF=(DU(I,J,K)-DU(I-1,J,K))/RDEL
      DVDIF=(DV(I,J,K)-DV(I,JJ,K))/(SDEL*R2(I))
      DWDIF=(DW(I,J,K)-DW(I,J,K-1))/ZDEL
      DUSUM=(DU(I,J,K)+DU(I-1,J,K))/(2.0*R2(I))
      RR(I,J,K)=AA*DUDIF+L*(DUSUM+DVDIF+DWDIF)
      SS(I,J,K)=AA*(DUSUM+DVDIF)+L*(DUDIF+DWDIF)
      ZZ(I,J,K)=AA*DWDIF+L*(DUDIF+DUSUM+DVDIF)
    3 CONTINUE
      IF(NW.EQ.0.AND.NH.EQ.0) GO TO 35
C--------- HORIZONTAL SURFACES, ZZ=0 --------------------------------
      DO 4 I=2,NW
    4 ZZ(I,J,KB)=-ZZ(I,J,KC)
      DO 5 I=ID,IA
    5 ZZ(I,J,1)=-ZZ(I,J,2)
C--------- 'SLOPE' STRESS-FREE CONDITIONS ---------------------------
      DO 6 K=2,KB
      I=IE-K
      ZZ(I,J,K)=-ZZ(I,J,K+1)
    6 RR(I,J,K)=-RR(I+1,J,K)
      GO TO 56
   35 CONTINUE
      DO 55 I=2,IA
   55 ZZ(I,J,1)=-ZZ(I,J,2)
   56 CONTINUE
C--------- SHEAR STRESS, RZ -----------------------------------------
```

```
      DO 7 K=2,NB
      M=2
      IF(K.LE.KB) M=IE-K
      DO 7 I=M,NA
      RZ(I,J,K)=(DU(I,J,K+1)-DU(I,J,K))*ZM
     /          +(DW(I+1,J,K)-DW(I,J,K))*RM
    7 CONTINUE
C--------- SHEAR STRESS, RS ----------------------------------------
      DO 8 K=2,KA
      M=2
      IF(K.LE.KB) M=IB-K
      DO 8 I=M,NA
      RS(I,J,K)=(DU(I,JJJ,K)-DU(I,J,K))*R3(I)
     /          -(DV(I+1,J,K)+DV(I,J,K))*R4(I)
     /          +(DV(I+1,J,K)-DV(I,J,K))*RM
    8 CONTINUE
C--------- SHEAR STRESS, ZS ----------------------------------------
      DO 9 K=2,NB
      M=2
      IF(K.LE.KB) M=IB-K
      DO 9 I=M,IA
      ZS(I,J,K)=(DV(I,J,K+1)-DV(I,J,K))*ZM
     /          +(DW(I,JJJ,K)-DW(I,J,K))*R5(I)
    9 CONTINUE
C--------- END OF J LOOP -------------------------------------------
   10 CONTINUE
C-------- DYNAMIC INPUT -------------------------------------------
      IF(T.GT.0.5) GO TO 121   In this case, a cosine pulse is used
      ARG=AMUL*(T-0.25)
      RR(8,1,2)=AMP*(1.0+COS(ARG))-RR(9,1,2)
  121 CONTINUE
C--------- CENTRE CALCULATIONS,RS AND RZ ---------------------
      DO 12 K=KC,KA
      XXSUM=YYSUM=XYSUM=YZSUM=XZSUM=0.0
      DO 11 J=1,NR
      JJJ=J+1
      IF(J.EQ.NR) JJJ=1
      SSAV=(SS(2,J,K)+SS(2,JJJ,K)+SS(3,J,K)+SS(3,JJJ,K))/4.0
      RRAV=(RR(2,J,K)+RR(2,JJJ,K)+RR(3,J,K)+RR(3,JJJ,K))/4.0
      SUM=(RRAV+SSAV)/2.0
      DIF=(RRAV-SSAV)/2.0
      XXSUM=XXSUM+SUM+DIF*C2(J)-RS(2,J,K)*S2(J)
      YYSUM=YYSUM+SUM-DIF*C2(J)+RS(2,J,K)*S2(J)
      XYSUM=XYSUM+DIF*S2(J)+RS(2,J,K)*C2(J)
      XZSUM=XZSUM+RZ(2,J,K)*CO(J)
      YZSUM=YZSUM+RZ(2,J,K)*SI(J)
   11 CONTINUE
      DO 12 J=1,NR
      RS(1,J,K)=(0.5*(XXSUM-YYSUM)*S2(J)-XYSUM*C2(J))/ANR
      RZ(1,J,K)=(XZSUM*CO(J)+YZSUM*SI(J))/ANR
   12 CONTINUE
C-------------------------------------------------------------------
      DO 17 J=1,NR
      JJ=J-1
      JJJ=J+1
      IF(J.EQ.1) JJ=NR
      IF(J.EQ.NR) JJJ=1
C--------- RADIAL VELOCITY AND DISPLACEMENT, U AND DU --------------
      DO 14 K=2,KA
```

```
      M=2
      IF(K.LE.KB) M=IE-K
      DO 14 I=M,NA
      U(I,J,K)=U(I,J,K)*ONEU(I,K)      Velocities derived
     /  +TWOU(I,K)*((RR(I+1,J,K)-RR(I,J,K))*DR
     /           +(RS(I,J,K)-RS(I,JJ,K))*R6(I)
     /           +(RZ(I,J,K)-RZ(I,J,K-1))*DZ
     /     +(RR(I+1,J,K)+RR(I,J,K)-SS(I+1,J,K)-SS(I,J,K))*R7(I))
      DU(I,J,K)=DU(I,J,K)+U(I,J,K)*TDEL   Displacements derived from
   14 CONTINUE                                          velocities
C--------- CIRCUMFERENTIAL VELOCITY AND DISPLACEMENT, V AND DV ------
      DO 15 K=2,KA
      M=2
      IF(K.LE.KB) M=IB-K
      DO 15 I=M,IA
      V(I,J,K)=V(I,J,K)*ONEV(I,K)          Velocities
     /  +TWOV(I,K)*((RS(I,J,K)-RS(I-1,J,K))*DR
     /           +(SS(I,JJJ,K)-SS(I,J,K))*R8(I)
     /           +(ZS(I,J,K)-ZS(I,J,K-1))*DZ
     /     +(RS(I,J,K)+RS(I-1,J,K))*R9(I))
      DV(I,J,K)=DV(I,J,K)+V(I,J,K)*TDEL      Displacements
   15 CONTINUE
C--------- VERTICAL VELOCITY AND DISPLACEMENT, W AND DW ----------
      DO 16 K=1,NB
      M=2
      IF(K.LE.NH) M=IE-K
      DO 16 I=M,IA
      W(I,J,K)=W(I,J,K)*ONEW(I,K+1)          Velocities
     /  +TWOW(I,K+1)*((RZ(I,J,K)-RZ(I-1,J,K))*DR
     /           +(ZS(I,J,K)-ZS(I,JJ,K))*R8(I)
     /           +(ZZ(I,J,K+1)-ZZ(I,J,K))*DZ
     /     +(RZ(I,J,K)+RZ(I-1,J,K))*R10(I))
      DW(I,J,K)=DW(I,J,K)+W(I,J,K)*TDEL      Displacements
   16 CONTINUE
C--------- END OF J LOOP -----------------------------------------
   17 CONTINUE
C--------- CENTRE CALCULATION, DU --------------------------------
      DO 19 K=KC,KA
      SUMX=0.0
      SUMY=0.0
      DO 18 J=1,NR
            JJ=J-1
      IF(J.EQ.1) JJ=NR
      DVAV=(DV(2,JJ,K)+DV(2,J,K))/2.0
      SUMX=SUMX+DU(2,J,K)*CO(J)+DVAV*SI(J)
   18 SUMY=SUMY-DU(2,J,K)*SI(J)+DVAV*CO(J)
      DO 19 J=1,NR
      DU(1,J,K)=(SUMX*CO(J)-SUMY*SI(J))/ANR
   19 DV(1,J,K)=(SUMX*SI(J)+SUMY*CO(J))/ANR
      KK=KK+1
      IF(KK.LT.10) GO TO 25
      KK=0
   25 CONTINUE     Write selected displacements onto disc for later plotting
      WRITE(7) DU(8,1,2),DU(9,1,2),DU(8,5,2),DU(8,9,2),
     /         DW(2,1,7),DW(2,1,8),DW(9,1,1),DW(10,1,1),
     /     DW(11,1,1),DW(9,5,1),DW(9,9,1),DU(1,1,8)
      IF(DU(4,1,2).GT.10.0) GO TO 48   Trap if program goes unstable
C--------- END OF MAIN LOOP --------------------------------------
   21 CONTINUE
```

```
 48 CONTINUE
    REWIND 7
    DO 22 I=1,N
    READ(7) (G(I,J),J=1,12)      Read displacements into array G with time
 22 CONTINUE                     as the first argument (I)
    DO 491 I=1,N,4
491 WRITE(6,80) I,(G(I,J),J=1,10)
    IF(N.NE.ITS) STOP
    SIZE=0.0
    DO 492 I=1,N
    ABF=ABS(G(I,4))
    IF(ABF.GT.SIZE) SIZE=ABF
492 CONTINUE
    DO 493 J=1,12                Alter magnitudes of displacements
    DO 493 I=1,N                 for convenient plotting
493 G(I,J)=G(I,J)/SIZE
    WRITE(6,494) SIZE
494 FORMAT(//15H SCALE FACTOR =,E12.4/)
    CALL START   - Calcomp initiation
    CALL CURVE   - Subroutine plots the curves of displacement
    CALL ENPLOT  - Calcomp termination
 81 FORMAT(1H1)
 83 FORMAT(///)
 82 FORMAT(8E12.4)
 80 FORMAT(I5,10E12.4)
 70 FORMAT(I4,10E12.4)
 72 FORMAT(9E12.4)
 74 FORMAT(I5)
    STOP
    END
```

```
    SUBROUTINE CURVE   Plots out curves of displacement, together with
    DIMENSION G(2816,12)                                  axes
    COMMON/BONG/ G,ITS,TDEL
    DX=0.3937079
    D=2.33
    XC=5.0*DX
    YC=1.0
    TIC=0.04
    D2=2.0*D
    D10=10.0*D
    HMAX=D-0.1
    CALL PLOT(0.1,D,-3)
    B=ITS
    NTIME=2.0*B*TDEL
    NN=NTIME+1
    TIME=FLOAT(NN)/2.0
    XMAX=TIME*XC
    XINC=XMAX/FLOAT(NN)
    XSHIFT=XMAX+0.5
    DO 2 NUM=1,12
    I=1
    J=2
    XT=0.0
    CALL PLOT(0.0,0.0,3)
    DO 4 M=1,NN
    XT=XT+XINC
    CALL PLOT(XT,0.0,2)
    YT=TIC*FLOAT(I)
    CALL PLOT(XT,YT,2)
```

```
      CALL PLOT(XT,0.0,2)
      K=J
      J=I
      I=K
    4 CONTINUE
      X1=TDEL*XC
      Y1=G(I,NUM)*YC
      IF(ABS(Y1).GT.HMAX) Y1=HMAX*Y1/ABS(Y1)
      CALL PLOT(X1,Y1,3)
      DO 1 N=2,ITS
      AN=N
      X=AN*TDEL*XC
      Y=G(N,NUM)*YC
      IF(ABS(Y).GT.HMAX) Y=HMAX*Y/ABS(Y)
      CALL PLOT(X,Y,2)
    1 CONTINUE
      IF(NUM.EQ.6) GO TO 3
      CALL PLOT(0.0,D2,-3)
      GO TO 2
    3 CALL PLOT(XSHIFT,-D10,-3)
    2 CONTINUE
      RETURN
      END
```

```
15    10     6     2    16          DATA
```

The data here is for a 6 units high, 2 units wide (base width) pit in the surface of a solid whos boundaries are 15 units horizontally from the centre, and 10 units vertically from the surface. There are 16 radial segments.

BALL PROGRAM

A Program to assemble a pile of cylinders, consolidate them and then allow them to fail, if the particular friction chosen will allow.

List of Variables and Constants

FN(I,J)	normal force between ball I & ball J
M(I,J)	moment between balls I & J
FXSUM(I)	total X force on ball I
FYSUM(I)	total Y force on ball I
MSUM(I)	total moment on ball I
U(I)	X velocity of ball I
V(I)	Y velocity of ball I
W(I)	angular velocity of ball I
DU(I)	X co-ordinate of ball I
DV(I)	Y co-ordinate of ball I
DDU(I)	incremental X displacement in one iteration.
DDV(I)	incremental Y displacement in one iteration
GAMMA(I)	incremental angle in one iteration
XC,YC	arrays storing co-ordinates for plotting a circle
NBASE	number of balls comprising the base of the pile
NBALL	total number of balls
ITS	number of iterations
N	iteration counter
ELOSSN	specific energy loss in normal direction
ELOSSM	specific energy loss in shear direction
TDEL	time increment
C1	normal stiffness
C3	shear stiffness
D	diameter of ball
R	radius of ball
MU	friction coefficient
PHI	friction angle in degrees
DUDIF	relative X distance between centroids of two balls
DVDIF	" Y " " " " "
Z	absolute distance between centroids
G	acceleration due to gravity
MASS	mass of ball
RHO	density

```
      REAL MASS,MU,MOI,M,MSUM
      DIMENSION FN(22,22),M(22,22),FXSUM(22),FYSUM(22),MSUM(22),
     / V(22),U(22),W(22),DDV(22),DDU(22),GAMMA(22)
      COMMON DU(22),DV(22),XC(31),YC(31),DX,NBALL
      CALL START
      READ(5,51) ITS,NBASE,ELOSSN,ELOSSM
      READ(5,52) TDEL,RHO,C1,C3,R,MU
      S3=SQRT(3.0)*5.0/100.0
      DX=0.3937079
      TDEL=TDEL/2.0
      MASS=0.01*RHO*3.142*(R**2)
      MOI=MASS*(R**2)/2.0
      A1=TDEL/MASS
      A2=TDEL/MOI
      EM=1.0/(1.0-ELOSSM)
      EN=1.0/(1.0-ELOSSN)
      D=2.0*R
      G=9.81
      PHI=10.0*2.0*3.142/360.0
      SLIP=ATAN(PHI)
      STV=R-S3
      NM=1
      BIT=-R
      DO 22 J=1,NBASE          -  Assemble pile of balls
      JK=NM
      LM=NM+NBASE-J
      BIT=BIT+R
      STU=BIT
      STV=STV+S3
      DO 21 I=JK,LM
      NM=NM+1
      DU(I)=STU
      STU=STU+D
      DV(I)=STV
   21 CONTINUE
   22 CONTINUE
      NBALL=NM-1
      WRITE(6,65) NBALL,ELOSSN,ELOSSM,TDEL,RHO,C1,C3,R,MU
      NN=NBALL+1
      ORIGY=2.0*DX
      ORIGX=10.0*DX
      ANGL=0.0
      DAN=2.0*3.142/30.0
      DO 20 I=1,31             -  Generate co-ordinates for plotting
      ANGL=ANGL+DAN                balls
      XC(I)=DX*COS(ANGL)
      YC(I)=DX*SIN(ANGL)
   20 CONTINUE
      DO 7 J = 1,NN
      DO 8 I = 1,NN
      FN(J,I)=0.0
    8 M(J,I)=0.0
      FXSUM(J)=0.0
      FYSUM(J)=0.0
      MSUM(J)=0.0
      V(J)=0.0
      U(J)=0.0
      W(J)=0.0
      DDV(J)=0.0
```

```
      DDU(J)=0.0
    7 GAMMA(J)=0.0
      KK=0
      LL=0
      DV(NN)=-R
      DO 4 N = 1,ITS
      IF(N.GE.100) MU=SLIP
      DO 3 J = 1,NBALL
      DU(NN)=DU(J)
      GAMMA(NN)=-DDU(J)/R
      K=J+1
      DO 2 I= K,NN
      DUDIF=DU(J)-DU(I)
      DVDIF=DV(J)-DV(I)
C ---------- IS BALL(I) TOUCHING BALL(J) ------------------
      IF(ABS(DUDIF)-D) 23,1,1
   23 IF(ABS(DVDIF)-D) 24,1,1
   24 Z=SQRT(DUDIF**2+DVDIF**2)
      IF(Z.GE.D) GO TO 1
      DUDIF=DUDIF/Z
      DVDIF=DVDIF/Z
      DDVDIF=DDV(I)-DDV(J)
      DDUDIF=DDU(I)-DDU(J)
C ---------- CALCULATE NORMAL FORCE FN(J,I) ---------------
      DFN=C1*(DDVDIF*DVDIF+DDUDIF*DUDIF)
      IF(DFN.LT.0.0)DFN=DFN*EN
      FN(J,I)=FN(J,I)+DFN
      IF(FN(J,I).LT.0.0) GO TO 1
C ---------- CALCULATE MOMENT M(J,I) ----------------------
      THETA=(DDVDIF*DUDIF-DDUDIF*DVDIF)/D
      DM=-C3*(GAMMA(J)+GAMMA(I)-THETA)
      IF(DM.LT.0.0.AND.M(J,I).GT.0.0.OR.DM.GT.0.0.AND.M(J,I).LT.0.0
     1  DM=DM*EM
      M(J,I)=M(J,I)+DM
C ---------- CALCULATE SHEAR FORCE FT ---------------------
      FT=M(J,I)/R
C ---------- IS SLIP TAKING PLACE -------------------------
      FF=MU*FN(J,I)
      ABFT=ABS(FT)
      IF(ABFT-FF)6,6,5
    5 SGNFT=FT/ABFT
      FT=SGNFT*FF
      M(J,I)=R*FT
    6 CONTINUE
C ---------- CALCULATE FORCE COMPONENTS FX, FY ------------
      FX=FN(J,I)*DUDIF-FT*DVDIF
      FY=FN(J,I)*DVDIF+FT*DUDIF
      FXSUM(J)=FXSUM(J)+FX
      FYSUM(J)=FYSUM(J)+FY
      MSUM(J)=MSUM(J)+M(J,I)
      FXSUM(I)=FXSUM(I)-FX
      FYSUM(I)=FYSUM(I)-FY
      MSUM(I)=MSUM(I)+M(J,I)
      GO TO 2
    1 FN(J,I)=0.0
      M(J,I)=0.0
    2 CONTINUE
      FYSUM(J)=FYSUM(J)-MASS*G
C ---------- INTEGRATE ACCELERATIONS TO FIND DISPLACEMENTS --
```

Slip conditions after 100 iterations

Inclusion of hysteresis in normal force law.

Inclusion of hysteresis in shear force law.

Gravity force

```
      V(J)=V(J)+A1*FYSUM(J)
      U(J)=U(J)+A1*FXSUM(J)
      W(J)=W(J)+A2*MSUM(J)
      DDV(J)=V(J)*TDEL
      DDU(J)=U(J)*TDEL
      GAMMA(J)=W(J)*TDEL
      DV(J)=DV(J)+DDV(J)
      DU(J)=DU(J)+DDU(J)
      FXSUM(J)=0.0
      FYSUM(J)=0.0
      MSUM(J)=0.0
    3 CONTINUE
      LL=LL+1
      KK=KK+1
      IF(KK.LT.200) GO TO 4      -  To initiate a plotting sequence
      KK=0                             every 200 iterations.
      IF(N.NE.1200) GO TO 90
      ORIGY=-52.0*DX
      ORIGX=30.0*DX              -  To reset plot origin after
   90 CONTINUE                         reaching top of page.
      WRITE(6,61) N, (DU(J),J=2,20,2)
      WRITE(6,62) (DV(J),J=2,20,2)
      WRITE(6,62) (W(J),J=2,20,2)
      CALL PLOT(ORIGX,ORIGY,-3)
      ORIGY=13.0*DX
      ORIGX=0.0                  -  Origin shift.
      CALL BALL
    4 CONTINUE
      CALL ENPLOT(10.0)
   50 FORMAT(10F5.4)
   51 FORMAT(2I5,2F5.1)
   52 FORMAT(6E10.4)
   61 FORMAT(I5,10E12.4)
   62 FORMAT(5X,10E12.4)
   63 FORMAT(3I5)
   64 FORMAT(20X,11I2)
   65 FORMAT(1H1,I10,8E12.4////)
      STOP
      END
      SUBROUTINE BALL            -  To plot out pile of balls.
      COMMON DU(22),DV(22),XC(31),YC(31),DX,NBALL
      H1=-7.0*DX
      H2=17.0*DX
      CALL PLOT(H1,0.0,3)
      CALL PLOT(H2,0.0,2)
      DO 2 J=1,NBALL
      DO 1 I=1,31
      II=2
      IF(I.EQ.1) II=3
      X=20.0*DX*DU(J)+XC(I)
      Y=20.0*DX*DV(J)+YC(I)
      CALL PLOT(X,Y,II)
    1 CONTINUE
    2 CONTINUE
      RETURN
      END
 2000     6   0.1   0.5
0.5000E-031.0000E 012.0000E 030.5000E 010.5000E-011.0000E 01
```

The above data draws out ten pictures representing the progressive failure of a pile of 21 balls, with a friction angle of 10 degrees.

BLOCK PROGRAM

The program assembles enough blocks to fill a given boundary rectangle. The primary and secondary joint spacings need to be specified, as well as the primary joint angle. A plot of the block system may be obtained by a call to HEAP, which will also print out the identification number on each block if requested. Blocks may be removed by calling REMOVE. The fixed blocks are read in from the main program. The dynamic iteration procedure may then start, assuming realistic data has been specified. All block velocities may be set to zero at any time by calling ZERO.

List of Variables, Constants and Subroutines

DU(I)	X co-ordinate of centroid of block I
DV(I)	Y co-ordinate of centroid of block I
ALF(I)	angle of major axis of block I to horizontal (radians)
U(I)	X velocity of block I
V(I)	Y velocity of block I
W(I)	angular velocity of block I
A(I)	half the major lenth of I
B(I)	half the minor length of I
AMASS(I)	mass of block I
DAMP(I)	damping constant for I
AMOI	moment of inertia of I
G(I) Q(I)	constants used in integration
XSUM(I)	total X force on block I
YSUM(I)	total Y force on block I
SUMM(I)	total moment (clockwise) on I
FT(I,K)	shear force of contact K of block I
D(I,K)	shear displacement of contact K of block I
YAB(I,K)	normal displacement of contact K of block I
NEXT(I,J)	list of 6 (J=1,6) nearby blocks to I
CO(I)	cosine of block angle
SI(I)	sine of block angle
LX(I)	=1 if block I fixed horizontally (0 if not)
LY(I)	=1 " " " " vertically "
LR(I)	=1 " " " " rotationally "
IMAX	total number of blocks
IBB	used to stop program if only initial plot needed
TDEL	time increment
RHO	density of block (the third dimension is set to 0.01)
ITS	number of iterations
N	iteration counter
CRIT	proportion of critical damping used
CN	normal stiffness
CT	shear stiffness
AMMO	friction angle
NREC	printout cycle
NBLK	number of the block whos displacements printed out
FRIC	coefficient of friction
MM	counts the "stages" in the whole procedure

SUBROUTINE BLOCK - assembles and numbers a system of blocks. Read in Y boundary, X boundary, angle of pri. joint set,

primary joint spacing and secondary joint spacing

SUBROUTINE HEAP(I,J) - plots out blocks; I = colour of pen, J = option (given on program - page 7)

SUBROUTINE ZERO(IMAX) - sets all velocities to zero

SUBROUTINE REMOVE - removes specified blocks. Read in total number of blocks to be removed; then read in the particular blocks.

```
      DIMENSION XSUM(100),YSUM(100),SUMM(100),U(100),V(100),
     /  W(100),DU(100),DV(100),ALF(100),G(100),Q(100),
     / DAMP(100),AMASS(100),A(100),B(100),CO(100),SI(100),
     / FT(100,8),D(100,8),NEXT(100,6)
      DIMENSION YAB(100,8)
      DIMENSION LX(100),LY(100),LR(100)
      DIMENSION NX(100),NY(100),NR(100)
      COMMON DU,DV,IMAX,ALF,A,B,NEXT
      COMMON/PPP/LX,LY,LR
      COMMON/ZRO/U,V,W
      CALL BLOCK              - Subroutine to assemble block system
      DO 691 I=1,IMAX
      XSUM(I)=0.0
      YSUM(I)=0.0
      SUMM(I)=0.0
      U(I)=0.0
      V(I)=0.0
      W(I)=0.0
      LX(I)=0
      LY(I)=0
      LR(I)=0
      NX(I)=0
      NY(I)=0
      NR(I)=0
      DO 692 K=1,8
      FT(I,K)=0.0
      D(I,K)=0.0
  692 YAB(I,K)=0.0
  691 CONTINUE
      READ(5,501) NHOR                - Read in which blocks are to
      READ(5,302) (NX(L),L=1,NHOR)      be fixed
  302 FORMAT(2014)
      DO 303 L=1,NHOR
      J=NX(L)
  303 LX(J)=1                 Horizontal
      READ(5,501) NVER
      READ(5,302) (NY(L),L=1,NVER)
      DO 305 L=1,NVER
      J=NY(L)                 Vertical
  305 LY(J)=1
      READ(5,501) NROT
      READ(5,302) (NR(L),L=1,NROT)
      DO 307 L=1,NROT
      J=NR(L)
  307 LR(J)=1                 Rotational
      WRITE(6,302) (NX(L),L=1,NHOR)
      WRITE(6,302) (NY(L),L=1,NVER)
      WRITE(6,302) (NR(L),L=1,NROT)
      CALL REMOVE             - Remove those blocks which are not needed
      CALL START(2)           - Calcomp initiation
      CALL HEAP(2,0)          - Plots out initial position of blocks
      READ(5,501) IBB
  501 FORMAT(I5)
      IF(IBB.EQ.0) STOP
C+++++++++++++ DATA ++++++++++++++++++ ++++++++++++++++++++++++++++++++
      TDEL=0.00009
      RHO=10.0
      PI=3.14159265
      ITS=450
```

```
      CRIT=0.6
      CN=2.0
      CT=2.0
      AMMO=1.0        - Initial friction angle, for consolidation
      NREC=10
      NBLK=11
       MM=0
 1000 CONTINUE
C ++++++++++++++++++++++++++++++++++++++ ++++++++++++++++++++++++++++++
      ONK=AMMO*PI/180.0
      FRIC=SIN(ONK)/COS(ONK)
      DO 43 I=1,IMAX
      AMASS(I)=0.01*RHO*A(I)*B(I)*4.0          - Mass of each block
      AMOI=(A(I)**2+B(I)**2)*AMASS(I)/3.0      - Moment of inertia
      DAMP=2.0*CRIT*SQRT(CN*AMASS(I))/TDEL
      G(I)=TDEL/AMASS(I)
      Q(I)=TDEL/AMOI
   43 CONTINUE
      KK=0
      DO 100 N=1,ITS     - Start main iteration loop
      KK=KK+1
      DO 45 I=1,IMAX
      SI(I)=SIN(ALF(I))
   45 CO(I)=COS(ALF(I))
      DO 30 I=1,IMAX     - Scan through the blocks
      K=1
      BS=B(I)*SI(I)
      BC=B(I)*CO(I)
      AS=A(I)*SI(I)
      AC=A(I)*CO(I)
      DO 20 M=1,4        - M = 1,2,3,4 corresponds to the 4 corners of
      GO TO (1,2,3,4) M                                  each block
    1 X=DU(I)+BC+AS
      Y=DV(I)+BS-AC
      GO TO 15
    2 X=DU(I)-BC+AS
      Y=DV(I)-BS-AC
      GO TO 17
    3 X=DU(I)-BC-AS
      Y=DV(I)-BS+AC
      GO TO 18
    4 X=DU(I)+BC-AS
      Y=DV(I)+BS+AC
      GO TO 21
   15 J=NEXT(I,1)
      IF(J.EQ.0) GO TO 53
      SII=CO(J)
      COO=-SI(J)
      AA=B(J)
      BB=A(J)
      GO TO 50
   16 J=NEXT(I,2)
      IF(J.EQ.0) GO TO 53
      SII=SI(J)
      COO=CO(J)
      AA=A(J)
      BB=B(J)
      GO TO 50
   17 J=NEXT(I,3)
```

The co-ordinates of the block corners are generated

The nearby blocks are located, and their relevant faces and angles defined

```
      IF(J.EQ.0) GO TO 53
      SII=SI(J)
      COO=CO(J)
      AA=A(J)
      BB=B(J)                                  continuing the scan through nearby
      GO TO 50                                 blocks - 6 in all
   18 J=NEXT(I,4)
      IF(J.EQ.0) GO TO 53
      SII=-CO(J)
      COO=SI(J)
      AA=B(J)
      BB=A(J)
      GO TO 50
   19 J=NEXT(I,5)
      IF(J.EQ.0) GO TO 53
      SII=-SI(J)
      COO=-CO(J)
      AA=A(J)
      BB=B(J)
      GO TO 50
   21 J=NEXT(I,6)
      IF(J.EQ.0) GO TO 53
      SII=-SI(J)
      COO=-CO(J)
      AA=A(J)
      BB=B(J)
   50 CONTINUE
      XDIF=X-DU(J)
      YDIF=Y-DV(J)
      YOB=YAB(I,K)
      XR=YDIF*SII+XDIF*COO                     - Local X and Y co-ordinates of
      YIB=ABS(-XDIF*SII+YDIF*COO)              block I corner relative to block J
      IF(YIB.GE.AA.OR.ABS(XR).GE.BB) GO TO 52      centroid
      FNO=CN*(AA-YIB) -                        Detects whether the two
      FN=FNO                                   blocks are touching
      IF(YOB.NE.0.0) FN=FNO+DAMP(I)*(YOB-YIB) - Damping applied to
      YAB(I,K)=YIB                             normal contact
      DD=D(I,K)
      D(I,K)=XR
      SHIFT=D(I,K)-DD
      F=FT(I,K)+CT*SHIFT  - Shear force calculated
      FF=F+DAMP(I)*SHIFT  - Damping applied to shear contact
      SMAX=FRIC*FNO
      ABF=ABS(F)
      IF(ABF.LE.SMAX) GO TO 51        - Is the contact slipping?
      F=SMAX*ABF/F                    - If it is, calculate the new shear
      FF=F                                                          force
      GO TO 51
   56 FF=0.0
      F=0.0
   51 CONTINUE
      XD=X-DU(I)
      YD=Y-DV(I)
      XT=YD*SII+XD*COO
      XN=XD*SII-YD*COO
      HOR=-FN*SII-FF*COO  - Calculate the horizontal and vertical
      VER=FN*COO-FF*SII     components of forces derived above
      XSUM(I)=XSUM(I)+HOR
      YSUM(I)=YSUM(I)+VER - Add them to those already present
```

```
      XSUM(J)=XSUM(J)-HOR
      YSUM(J)=YSUM(J)-VER
      SUMM(I)=SUMM(I)-FN*XT+FF*XN
      SUMM(J)=SUMM(J)+FF*AA+FN*XR
      FT(I,K)=F
      GO TO 53
   52 FT(I,K)=0.0
      D(I,K)=0.0
      YAB(I,K)=0.0
   53 CONTINUE
      K=K+1
      GO TO (20,16,20,18,20,19,20,15,20) K
   20 CONTINUE
      YSUM(I)=YSUM(I)-AMASS(I)*9.81
   30 CONTINUE
      DO 32 I=1,IMAX
      IF(LX(I).EQ.0) U(I)=U(I)+XSUM(I)*G(I)
      IF(LY(I).EQ.0) V(I)=V(I)+YSUM(I)*G(I)
      IF(LR(I).EQ.0) W(I)=W(I)-SUMM(I)*Q(I)
      DU(I)=DU(I)+U(I)*TDEL
      DV(I)=DV(I)+V(I)*TDEL
      ALF(I)=ALF(I)+W(I)*TDEL
      YSUM(I)=0.0
      XSUM(I)=0.0
      SUMM(I)=0.0
   32 CONTINUE
      IF(DU(37).LE.0.01?1) GO TO 104
      IF(KK.LT.NREC) GO TO 100
      KK=0
      WRITE(6,64) N,DU(NBLK),DV(NBLK),ALF(NBLK)
  100 CONTINUE
      MM=MM+1
      GO TO(101,102,103,104) MM
  101 CALL ZERO(IMAX)
      GO TO 1000
  102 CALL ZERO(IMAX)
      CALL HEAP(4,1)
      CALL REMOVE
      AMMO=43.0
      GO TO 1000
  103 CONTINUE
      ITS=500
      GO TO 1000
  104 CONTINUE
      CALL HEAP(1,1)
      CALL ENPLOT
      STOP
   64 FORMAT(I5,3F10.7)
      END
```

Running total of X and Y forces on blocks I and J calculated. Also the total moment

This statement controls which contact is to be dealt with next.

- Gravity added in

The X, Y and rotational velocities are calculated if the block is not fixed

The displacements are calculated

Forces set to zero

- Stops the program when a particular displacement has occurred

This next section allows various factors to be varied as the program proceeds

- Subroutine to set all block velocities to zero
- Plotting routine
- Remove blocks to cause failure to start
- Set new friction angle

- Plot

```
      SUBROUTINE BLOCK
      DIMENSION THET(100),A(100),B(100),NEXT(100,6)
      DIMENSION XG(100),YG(100)
      DIMENSION YU(6),XU(6),YD(6),XD(6)
      COMMON XG,YG,IMAX,THET,A,B,NEXT
   50 FORMAT(F10.4)
      PI=3.14159265
      READ(5,50) YMAX
      READ(5,50) XMAX
      READ(5,50) ALF
```

A subroutine to assemble a system of blocks

- Position of Y boundary
- Position of X boundary
- Angle of primary joint set to horizontal

```
      READ(5,50) P          - Spacing of primary joints
      READ(5,50) S          - Spacing of secondary joints
           ANG=ALF*PI/180.0
      PI2=PI/2.0
      PI4=PI/4.0
      BB=XMAX+2.0*P
      C=-2.0*P
      YP=P*COS(ANG)
      XP=P*SIN(ANG)
      XS=S*COS(ANG)
      YS=S*SIN(ANG)
      YS2=YS/2.0
      XS2=XS/2.0
      IF(ANG.GT.PI2) GO TO 20
      I=1
      IF(ANG.GT.PI4) GO TO 80
      X=S/2.0
      Y=YMAX-P/2.0
      GO TO 81
   80 X=P/2.0                    The area defined by YMAX and XMAX is
      Y=YMAX-S/2.0               filled with blocks in a zigzag fashion,
   81 CONTINUE                   starting in the top left-hand corner.
      XG(I)=X
      YG(I)=Y
      IF(ANG.LT.PI4) GO TO 2
      GO TO 5
    6 Y=Y-YP-YS2
      X=X+XP-XS2
      IF(Y.LT.C.OR.X.GT.BB) GO TO 30
    1 CONTINUE
      IF(Y.LT.0.0.OR.X.LT.0.0) GO TO 2
      Y=Y-YS
      X=X-XS
      GO TO 1
    2 Y=Y+YS
      X=X+XS
      IF(Y.LT.0.0.OR.X.LT.0.0) GO TO 2
      IF(Y.GT.YMAX.OR.X.GT.XMAX) GO TO 3
      I=I+1
      YG(I)=Y
      XG(I)=X
      GO TO 2
    3 Y=Y-YP+YS2
      X=X+XP+XS2
    4 CONTINUE
      IF(Y.GT.YMAX.OR.X.GT.XMAX) GO TO 5
      Y=Y+YS
      X=X+XS
      GO TO 4
    5 Y=Y-YS
      X=X-XS
      IF(Y.GT.YMAX.OR.X.GT.XMAX) GO TO 5
      IF(Y.LT.0.0.OR.X.LT.0.0) GO TO 6
      I=I+1
      YG(I)=Y
      XG(I)=X
      GO TO 5
   20 CONTINUE
   30 CONTINUE
```

```
      IMAX=I
      DO 21 I=1,IMAX
      THET(I)=ANG
      A(I)=S/2.0
   21 B(I)=P/2.0
      WRITE(6,52) IMAX
   52 FORMAT(//19H NUMBER OF BLOCKS =,I5//)
      DO 103 I=1,IMAX
      DO 103 K=1,6
  103 NEXT(I,K)=0
      DEL=P/100.
      DO 102 I=1,IMAX
      YU(1)=YG(I)+YS+DEL
      YD(1)=YG(I)+YS-DEL
      XU(1)=XG(I)+XS+DEL
      XD(1)=XG(I)+XS-DEL
      YU(2)=YG(I)-YP+YS2+DEL
      YD(2)=YG(I)-YP+YS2-DEL
      XU(2)=XG(I)+XP+XS2+DEL
      XD(2)=XG(I)+XP+XS2-DEL
      YU(3)=YG(I)-YP-YS2+DEL
      YD(3)=YG(I)-YP-YS2-DEL
      XU(3)=XG(I)+XP-XS2+DEL
      XD(3)=XG(I)+XP-XS2-DEL
      YU(4)=YG(I)-YS+DEL
      YD(4)=YG(I)-YS-DEL
      XU(4)=XG(I)-XS+DEL
      XD(4)=XG(I)-XS-DEL
      YU(5)=YG(I)+YP-YS2+DEL
      YD(5)=YG(I)+YP-YS2-DEL
      XU(5)=XG(I)-XP-XS2+DEL
      XD(5)=XG(I)-XP-XS2-DEL
      YU(6)=YG(I)+YP+YS2+DEL
      YD(6)=YG(I)+YS2-DEL
      XU(6)=XG(I)-XP+XS2+DEL
      XD(6)=XG(I)-XP+XS2-DEL
      DO 102 J=1,IMAX
      DO 102 K=1,6
      IF(YG(J).GT.YD(K).AND.YG(J).LT.YU(K)) GO TO 101
      GO TO 102
  101 IF(XG(J).GT.XD(K).AND.XG(J).LT.XU(K)) GO TO 100
      GO TO 102
  100 NEXT(I,K)=J
  102 CONTINUE
      DO 104 I=1,IMAX
  104 WRITE(6,105) I,XG(I),YG(I),(NEXT(I,K),K=1,6)
  105 FORMAT(I5,2F10.6,6I4)
  107 CONTINUE
      RETURN
      END
```

This section locates six nearby blocks for each block, and records their number in NEXT(I,K)

```
      SUBROUTINE HEAP(IPEN,ISWITCH) - To plot out the blocks
      DIMENSION DU(100),DV(100),ALF(100),A(100),B(100),NEXT(100,6)
      COMMON DU,DV,IMAX,ALF,A,B,NEXT
      COMMON/PPP/ LX,LY,LR
      DIMENSION LX(100),LY(100),LR(100)
      F=75.0
      CALL PEN(IPEN)  - Written for a "Kingmatic" plotter with 4 pens
      DO 1 I=1,IMAX
      IF(ISWITCH.EQ.2) GO TO 3
```

```
      IF(DU(I).GT.1.0) GO TO 1
      IF(LY(I).EQ.1.AND.ISWITCH.EQ.1) GO TO 1
    3 CONTINUE
      SI=SIN(ALF(I))              If ISWITCH = 0  all blocks plotted
      CO=COS(ALF(I))                           1  all plotted except fixed
      BS=B(I)*SI*F                                          blocks
      BC=B(I)*CO*F                             2  all blocks plotted and
      AS=A(I)*SI*F                                          numbered
      AC=A(I)*CO*F
      UC=DU(I)*F
      VC=DV(I)*F
      X1=UC+BC+AS
      Y1=VC+BS-AC
      X2=UC-BC+AS
      Y2=VC-BS-AC
      X3=UC-BC-AS
      Y3=VC-BS+AC
      X4=UC+BC-AS
      Y4=VC+BS+AC
      CALL PLOT(X1,Y1,3)
      CALL PLOT(X2,Y2,2)
      CALL PLOT(X3,Y3,2)
      CALL PLOT(X4,Y4,2)
      CALL PLOT(X1,Y1,2)
      IF(ISWITCH.NE.2) GO TO 1
      AI=I
      CALL NUMBER(UC,VC,0.1,AI,0.0,-1)
    1 CONTINUE
      RETURN
      END
```

```
      SUBROUTINE ZERO(IMAX)   - This subroutine sets all velocities to zero
      DIMENSION U(100),V(100),W(100)
      COMMON/ZRO/U,V,W
      DO 1 I=1,IMAX
      U(I)=0.0
      V(I)=0.0
    1 W(I)=0.0
      WRITE(6,60)
   60 FORMAT(/27H ALL VELOCITIES SET TO ZERO/)
      RETURN
      END
```

```
      SUBROUTINE REMOVE       - This subroutine removes specified blocks
      DIMENSION LIST(100)
      COMMON DU,DV,IMAX,ALF,A,B,NEXT
      COMMON/PPP/LX,LY,LR
      COMMON/ZRO/U,V,W
      DIMENSION DU(100),DV(100),ALF(100),A(100),B(100),NEXT(100,6)
      DIMENSION U(100),V(100),W(100),LX(100),LY(100),LR(100)
      READ(5,50) N   - number to be removed
   50 FORMAT(I5)
      READ(5,51) (LIST(I),I=1,N)     - list of blocks
   51 FORMAT(20I4)
      DO 1 I=1,N
      J=LIST(I)
      DU(J)=1000.0
      DV(J)=1000.0      - Removed to a great distance !
      U(J)=0.0
      V(J)=0.0
      W(J)=0.0
```

```
      LX(J)=1
      LY(J)=1
      LR(J)=1
      DO 1 K=1,6
      NEXT(J,K)=0
      WRITE(6,60) N
   60 FORMAT(/I5,16H BLOCKS REMOVED-)
      WRITE(6,51) (LIST(I),I=1,N)
      RETURN
      END
```

```
0.10
0.10
45.0
0.01
0.01
   18
   8  16  20  38  40  64  65  83  84  94  95  96  97  90  76  74  54
   18
   8  16  20  38  40  64  65  83  84  94  95  96  97  90  76  74  54
   18
   8  16  20  38  40  64  65  83  84  94  95  96  97  90  76  74  54
   15
   1   2   3   4   5   6   7  17  18  19  39  28  52  53  75
   51
    4
   8  16  20  38
```

Data

In this case it is for a 45° sliding model of 97 blocks.

51

51

these numbers cut off in printing

NOTE: In general, it is necessary to do a preliminary run, plotting out all blocks with numbers, so that on subsequent runs it will be known which number corresponds to which block.